Diploma Thesis

Introducing *N*-heterocyclic carbene-based self-assembled monolayers into biomimetic membranes

Conducted at the

Institute of Applied Synthetic Chemistry

TU Wien

Research group

Molecular Chemistry and Chemical Biology

Under supervision of

Univ. Ass. Dipl.-Ing. Dorian Bader
Projektass. (FWF) Dipl.-Ing. Dr.techn. Brigitte Holzer

by

Lavinia Klement

[redacted]

Vienna 2023

Table of contents

Abstract

Alterations in membrane functions are associated with a wide range of human diseases such as cancer or neurogenerative diseases. Due to their complexity in structure and function of cell membranes, biomimetic model systems have been created that preserve the basic structure of the lipid bilayer but simplify the system so that the roles of the individual components and isolated processes can be assessed. Artificial membranes find applications in various scientific fields such as catalysis, synthesis of new materials, biopharmaceutics, drug delivery, antimicrobial activity or the design of bioelectronic devices.[1,2]

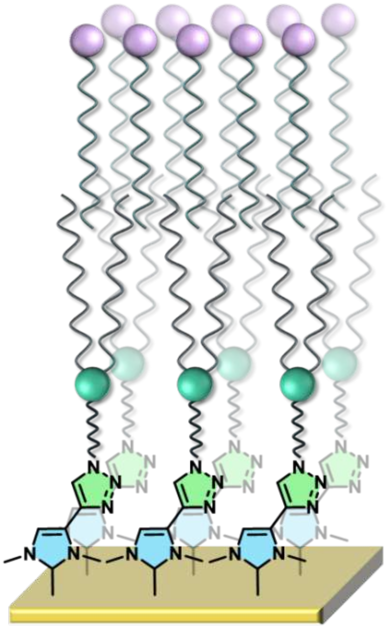

Figure 1: NHC-based tBLM on gold

This work aims toward the design, synthesis and analysis of *N*-heterocyclic carbene (NHC)-based tethered bilayer lipid membranes (tBLM) on gold substrates (Figure 1). Compared to current tethered lipid bilayers, which have well known disadvantages regarding stability, bilayer mobility and applicability to integrate membrane proteins,[3–5] NHC-based lipid analogues provide a new platform of tethered bilayer lipid membranes. Using NHCs as anchor groups allows the formation of self-assembling monolayers (SAMs), with an optimized surface density and higher mobility compared to thiol-based systems. The formation of the SAM is pursued applying a mild method using triflate precursors without the need of inert conditions and strong bases to immobilize NHCs on the gold surface. Optimization of the surface density is realized by the incorporation of NHC-based spacer molecules, different NHC-systems (imidazolium- or benzimidazolium) with varying *N,N*-disubstitution or multidentate anchor groups. Optical and electrochemical read-outs *via* electrochemical impedance spectroscopy (EIS) using NHC-based tBLMs are presented and compared with current thiol-tethered lipid bilayers.

To prove the applicability of these NHC-based tBLMs, a potassium-ion transporting nanopore, valinomycin, is incorporated in the synthesized bilayers and probed to record the activity of a single ion-specific transporter. Additional studies using NHC-based bilayer systems with a range of membrane proteins could enhance the field of bioelectronics.

Kurzfassung

Veränderungen der Membranfunktionen sind mit einer Vielzahl menschlicher Erkrankungen wie Krebs oder neurogenerativen Erkrankungen verbunden. Aufgrund der Komplexität der Struktur und Funktionsweise von Zellmembranen wurden biomimetische Modellsysteme geschaffen, die die Grundstruktur der Lipiddoppelschicht bewahren, aber das System vereinfachen, sodass die Rolle der einzelnen Komponenten und isolierte Prozesse betrachtet werden können. Künstliche Membranen finden Anwendung in verschiedenen wissenschaftlichen Bereichen wie Katalyse, Synthese neuer Materialien, Biopharmazeutika, Arzneimittelabgabe, antimikrobielle Aktivität oder Design bioelektronischer Geräte.[1,2]

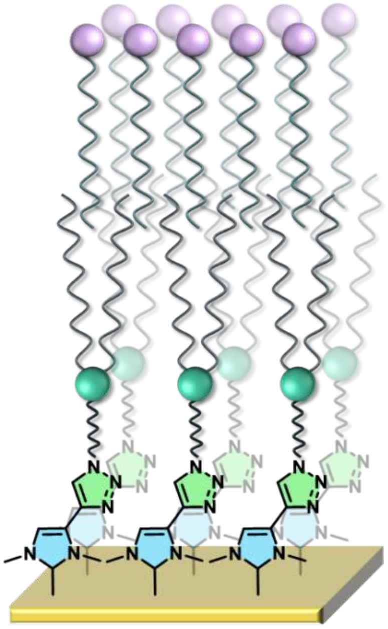

Abbildung 1: NHC-basierte tBLM immobilisiert auf einem Gold Substrat

Diese Arbeit hat das Ziel, oberflächenverankerte Lipidmembranen (tBLMs) auf Goldsubstraten basierend auf *N*-heterocyclischen Carbenen (NHCs) zu designen und synthetisieren (Abbildung 1). Verglichen mit literaturbekannten Doppelschicht-Systemen, die bekannte Nachteile bezüglich Stabilität, Mobilität und Probleme bei der Anwendung haben,[3–5] bieten NHC-basierte Lipid-Analoga eine neue Plattform für oberflächenverankerte Lipid Membranen. Die Verwendung von NHCs als Ankergruppen ermöglicht die Bildung von selbstorganisierenden Monoschichten (SAMs) mit optimierter Oberflächendichte und höherer Mobilität verglichen mit Thiol-basierten Systemen. Die Bildung der SAMs wird mit einem milden Verfahren realisiert, bei dem Triflat-NHC-Vorstufen auf der Goldoberfläche immobilisiert werden. Eine Optimierung der Oberflächendichte wird durch den Einbau von NHC-basierten Spacermolekülen, unterschiedlichen NHC-Systemen (Imidazol- oder Benzimidazol-basiert) mit variierender *N,N*-Disubstitution oder mehrzähnigen Ankergruppen realisiert. Optische und elektrochemische Auslesungen mittels elektrochemischer Impedanzspektroskopie (EIS) unter Verwendung von NHC-basierten tBLMs werden vorgestellt und mit aktuellen Thiolat-gebundenen Lipiddoppelschichten verglichen.

Um die Anwendbarkeit dieser NHC-basierten tBLMs zu zeigen, wird eine Kaliumionen-transportierende Nanopore, Valinomycin, in die synthetisierten Doppelschichten eingebaut und analysiert, um die Aktivität eines einzelnen Ionentransporters aufzuzeichnen. Zusätzliche Studien unter Verwendung von NHC-basierten Doppelschichtsystemen mit einer Reihe von Membranproteinen könnten das Gebiet der Bioelektronik erweitern.

Abbreviations

AC	alternating current
ACN	acetonitrile
AFM	atomic force microscopy
ATP	adenosine triphosphate
BLM	bilayer (black) lipid membrane
CA	contact angle
CuAAC	copper catalyzed azide alkyne cycloaddition
CV	cyclic voltammetry
DCM	dichloromethane
DHDG	dihexadecyl glycerol
DMAP	dimethylamino pyridine
DMF	dimethylformamide
DPG	diphytanyl glycerol
DPPC	1,2-dipalmitoyl-*sn*-glycero-3-phosphocholine
DPTL	2,3-di-*O*-phytanyl-*sn*-glycerol-1-tetraethylene glycol-d,l-α-lipoic acid ester lipid
EDC	1-ethyl-3-(3-dimethylaminopropyl)carbodiimid
EEC	equivalent electrochemical circuit
EIS	electrochemical impedance spectroscopy
EtOAc	ethyl acetate
EtOH	ethanol
KOtBu	potassium-tert-butanolate
LC/MS	liquid chromatography/mass spectrometry
MeOH	methanol
NBS	*N*-bromosuccinimide
NHC	*N*-heterocyclic carbene
NEt_3	triethylamine
NMR	nuclear magnet resonance spectroscopy
OMs	mesyl
OTf	triflate
PC	phosphatidylcholine
PE	petroleum ether
PEA	phosphatidylenolamine
PEG	polyethylene glycol
PPh_3	triphenylphosphine
PS	phosphatidylserine
pTsCl	*p*-toluene-sulfonyl chloride
QCM	quartz crystal microbalance
RSE	rapid solvent exchange
SAM	self-assembled monolayers
sBLM	supported bilayer lipid membrane
SPR	surface plasmon resonance spectroscopy
STM	scanning tunneling microscopy
SUV	small unilamellar vesicles
TBAI	tertbutyl ammonium iodide
tBLM	tethered bilayer lipid membrane
THF	tetrahydrofuran
TLC	thin layer chromatography
TMS	trimethylsilane
XPS	X-ray photoelectron spectroscopy

1 Schemes

1.1 Phytanoyl imidazolium-based anchor lipids

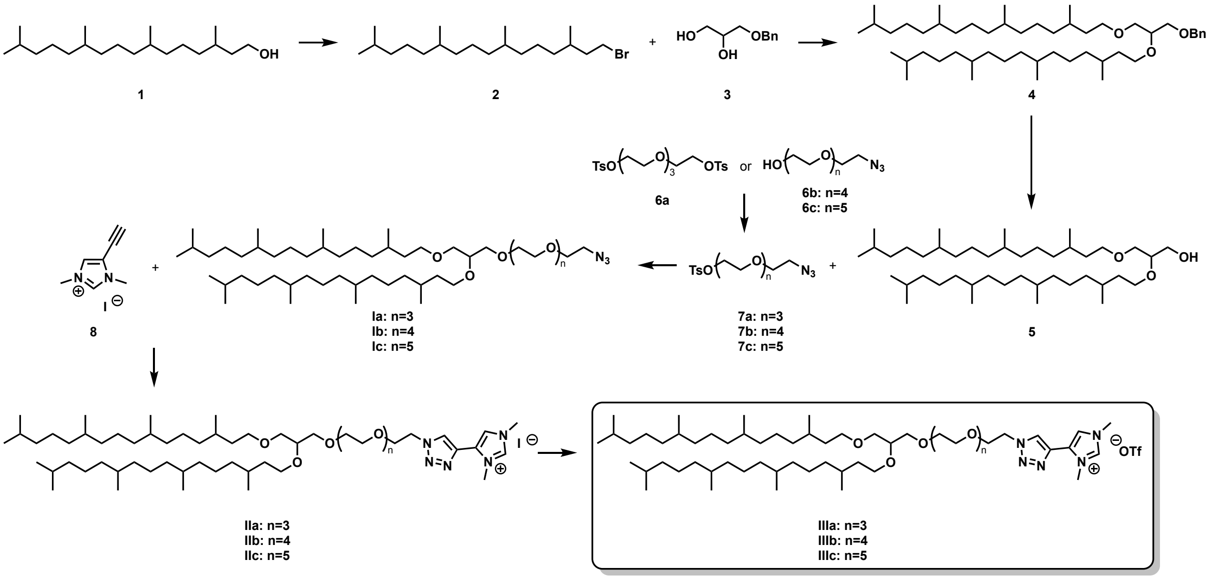

1.2 Dihexadecyl imidazolium-based anchor lipids

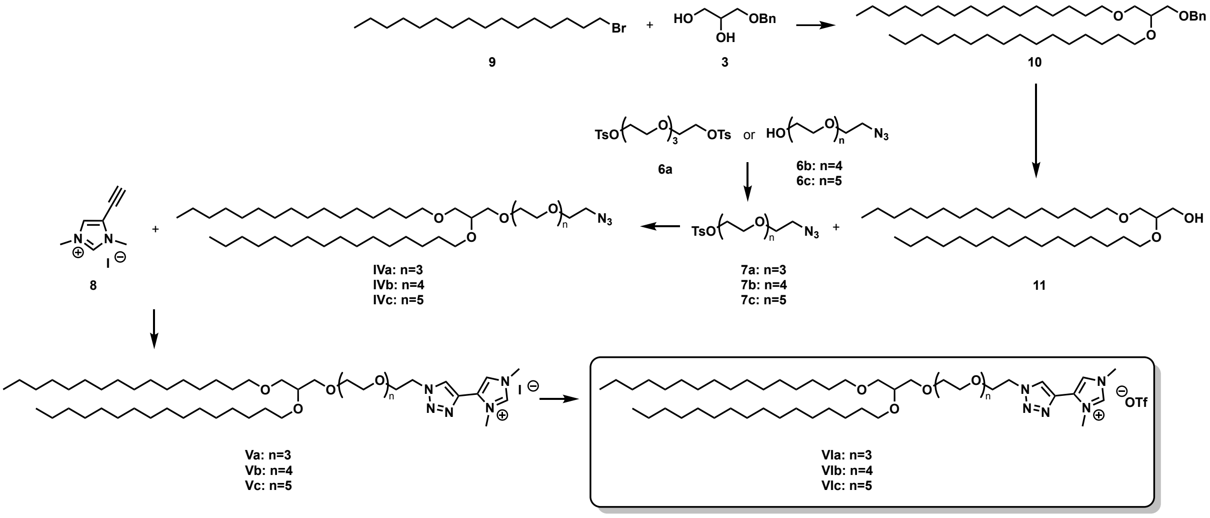

1.3 Anchor groups

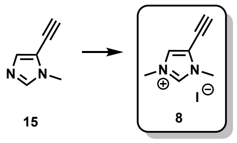

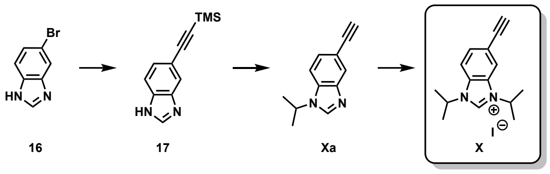

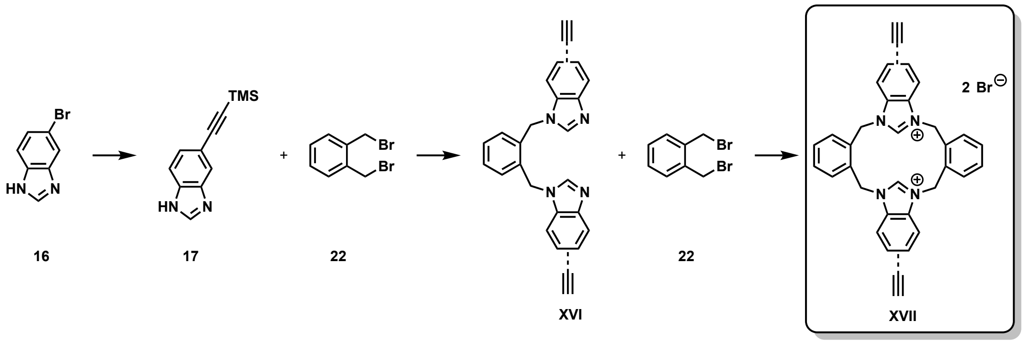

1.4 Phytanoyl benzimidazolium-based anchor lipids

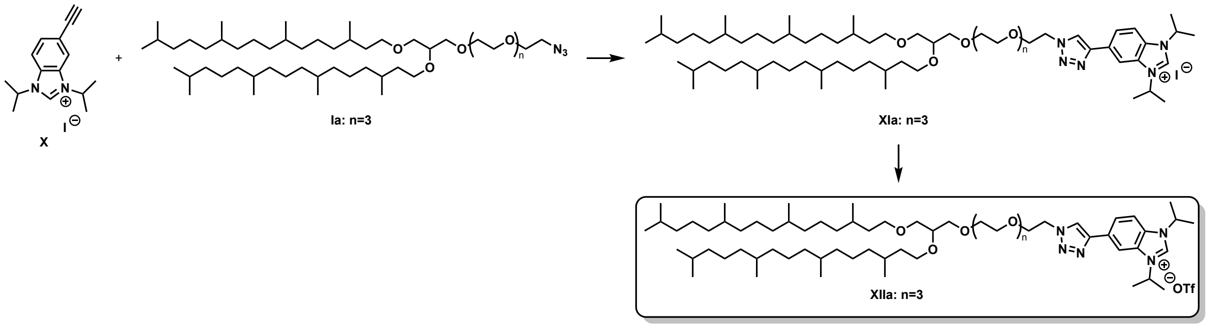

1.5 Imidazolium-based spacer molecule

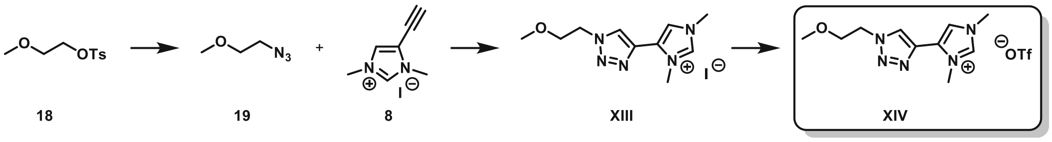

1.6 Imidazolium-based outer leaflet

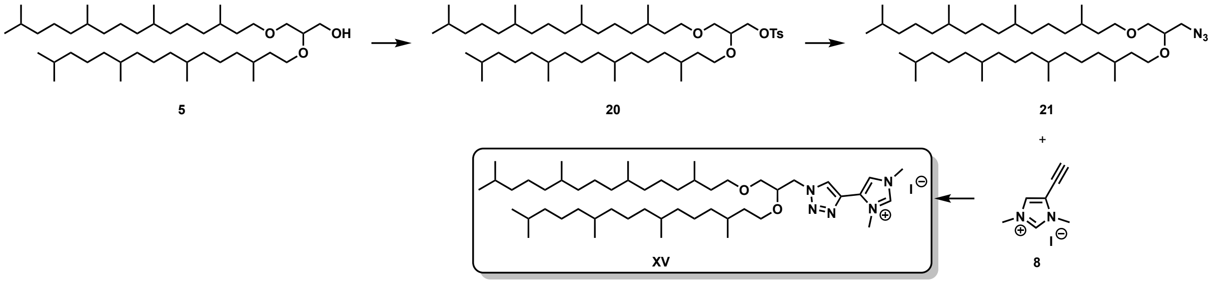

1.7 Thiol-based reference systems

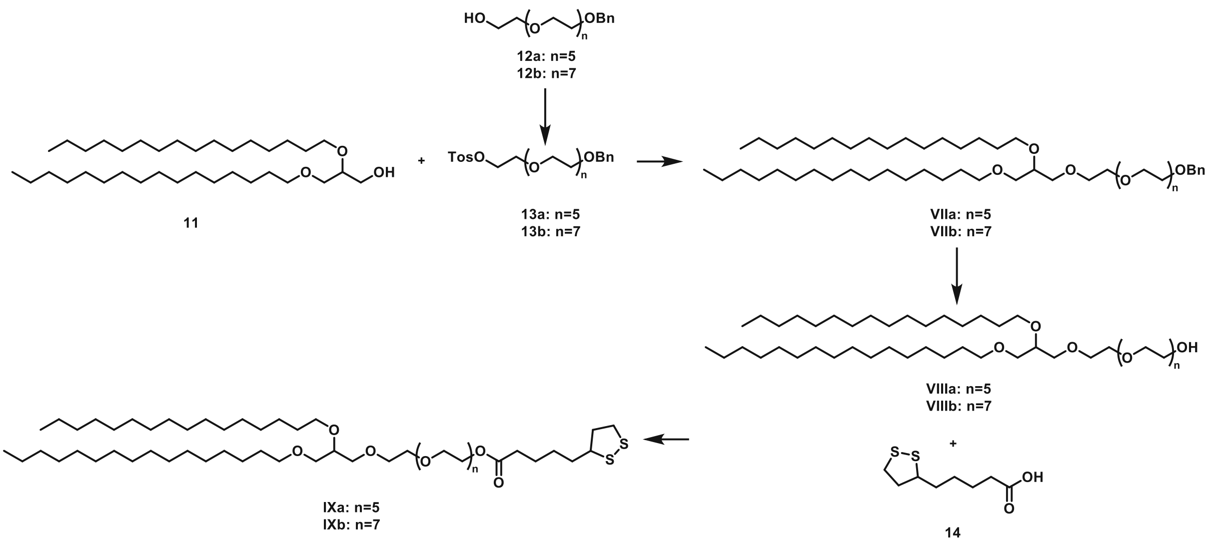

2 General part

2.1 Introduction

Lipids are essential building blocks of life being the principal component of biological membranes. They exhibit amphiphilic, highly diverse structures with a variation of polar headgroups and hydrophobic backbones.[6] The tendency of lipid molecules to self-assemble into closed structures in an aqueous environment is the physical basis for membrane formation in the development of cellular life. Biological membranes are an excellent example of highly complex molecular assemblies whose structure and function cannot be determined by the genome alone, posing challenges to science.[7] Gram-negative bacteria, for example, are asymmetric. The outer leaflet is composed of a lipopolysaccharide while their inner leaflet consists of about 25 phospholipid types.[8]

Biomembranes are present in every form of life and are capable to incorporate transmembrane ion conducting channels, signaling receptors, active/passive transporters, metabolic enzymes, anchorages for the intracellular cytoskeleton and extracellular matrix, cell-cell recognition, intercellular junctions as well as energy production as depicted in Figure 2.[7]

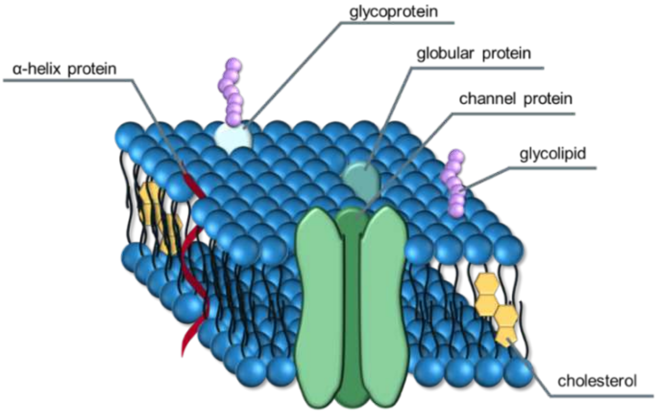

Figure 2: Structure and components of a cell membrane

2.1.1 The fluid mosaic model of cell membranes

In 1972 Jonathan Singer and Garth Nicolson proposed the dynamic and fluid nature of biological membranes in their fluid mosaic model.[9,10] According to the model, lipids and proteins can diffuse laterally through the membrane. Phospholipids can also spin around their head-to-tails axis. These types of movements create a fluid, dynamic membrane which surrounds cells and organelles.[9] The bulk of phospholipid is organized as a discontinuous fluid bilayer, whereas a small fraction of lipid may interact specifically with membrane proteins. Therefore, the fluid mosaic structure is formally a two-dimensional oriented solution of integral proteins or lipoproteins in the viscous phospholipid bilayer solvent.[10]

2.1.2 Composition and distribution of biological membranes

Generally, biomembranes consist of a bilayer of lipid molecules. Besides the lipids, membrane proteins and sugars are also key components of the structure.[9] The molecular composition of lipids, proteins, and sugars in biological membranes is highly complex, with highly diverse molecular and supramolecular structures that differ in physical properties and biological functions. Lipids for example show remarkable structural diversity, such as variable chain length and headgroups as well as modifications with sugar residues and other functional groups of different biosynthetic origin.[7] Figure 3 shows the three types of lipid structures in biological membranes, namely phospholipids, glycolipids and sterols.

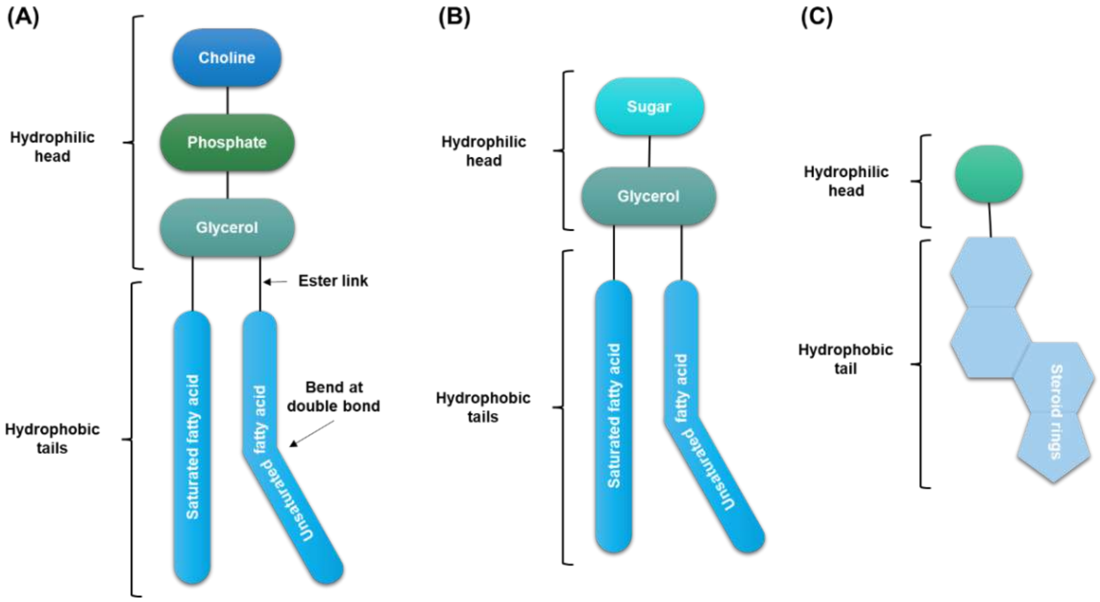

Figure 3: Schematic representation of the three membrane lipids: **(A)** phospholipids, **(B)** glycolipids and **(C)** sterols

Phosphatidylcholine (PC) (Figure 3 A) contains two fatty acid chains linked to a glycerol and a phosphate with a choline group attached to the phosphate group. Serine and ethanolamine could replace the choline in this position, forming phosphatidylserine (PS) and phosphatidylethanolamine (PEA). Glycolipids (Figure 3 B) consists of two fatty acid chains linked to a glycerol unit that is connected with a sugar such as glucose. Sterol (Figure 3 C) contains a hydroxyl group as hydrophilic head group and four-ring steroid structure.[9]

In most mammalian cells, the outer leaflet of the plasma membrane is mainly containing PC and sphingomyelin, whereas PS and PEA are found on the inner leaflet.[9]

2.1.3 Membrane proteins

Without membrane proteins, the phospholipid membrane would present an impermeable barrier, and the cell would not be able to communicate with its neighbors, transport nutrients into or out of the cell, or respond to external stimuli. Both unicellular and multicellular organisms require membrane proteins to allow vital processes. It is crucial that the right substances enter cells (e.g., nutrients) and the right substances are transported out of them (e.g. toxins). Membrane proteins can be constructed of α-helices or β-barrels. β-barrels often function as pores with hydrophobic amino acids facing out of the bilayer.[9]

For molecules there are several ways to cross biological membranes, depending on their concentration on either side of the membrane, their size and charge. Small molecules like water can simply diffuse through the membrane without assistance. However, diffusion is not possible for larger molecules or charged molecules. Ions can move through channels by a passive transport process, where they travel from an area of high concentration to an area of low concentration. This process requires channel or carrier proteins but no additional energy input. Active transport moves molecules against concentration gradients and requires energy input, which is obtained from adenosine triphosphate (ATP), light or from the downhill movement of a second type of molecule or ion within the same transporter (Figure 4).[9]

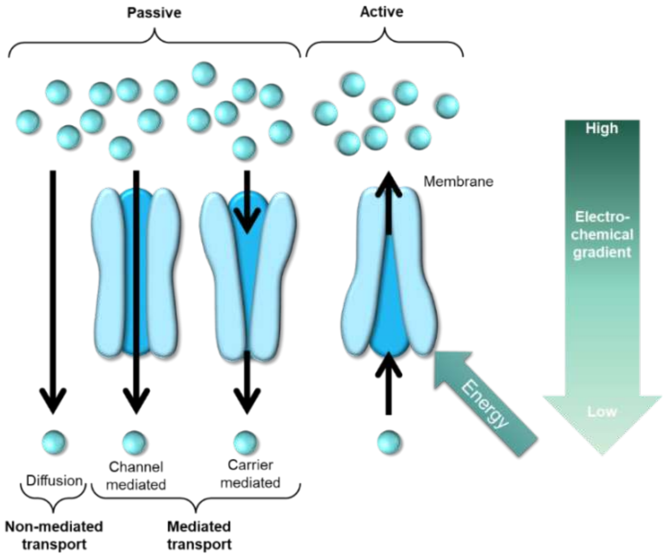

Figure 4: Passive and active transport and different types of membrane proteins involved in those processes

2.1.4 Cholesterol in lipid bilayers

Although cholesterol does not form bilayers itself, it is a very important component of the cell membrane and is nonhomogeneously distributed with higher concentration in the plasma membrane and lower concentrations in intracellular organelles.[11]

Cholesterol has a structural and regulatory role in membranes by maintaining proper fluidity and rigidity of the membrane. The hydroxyl group on cholesterol interacts with the polar head groups of the phospholipids and sphingolipids, while the bulky steroid and hydrocarbon chain are inserted in the membrane together with the hydrophobic fatty-acid chain of the lipids.[11]

2.2 Model membrane systems

Even within eukaryotic cells, the composition of biofilms varies widely, and their organization must be dynamic to mediate and regulate conformational changes, signaling, trafficking, and recognition.[12] Alteration in membrane functions are associated with a wide range of human diseases such as cancer or neurodegenerative diseases. That lead to the idea that lipid components of the plasma membrane can be selectively modified to alter the composition and structure of double lipid membranes.[13]

Because natural membranes play such an important role, and because they are so complex, many different model systems have been created that preserve the basic structure of the lipid bilayer but simplify the system so that the roles of the individual components can be assessed and its organization and dynamics can be visualized.[12] A large number of different model membrane systems have been developed in the past few years that reduce the natural complexity of the cell membrane, while providing an easily accessible experimental platform. These systems are able to mimic essential structural and chemical aspects of a lipid bilayer membrane and include model membrane systems shown in Figure 5 such as black lipid membranes (BLMs), solid supported bilayer lipid membranes (sBLMs) as well as tethered bilayer lipid membranes (tBLMs).[14]

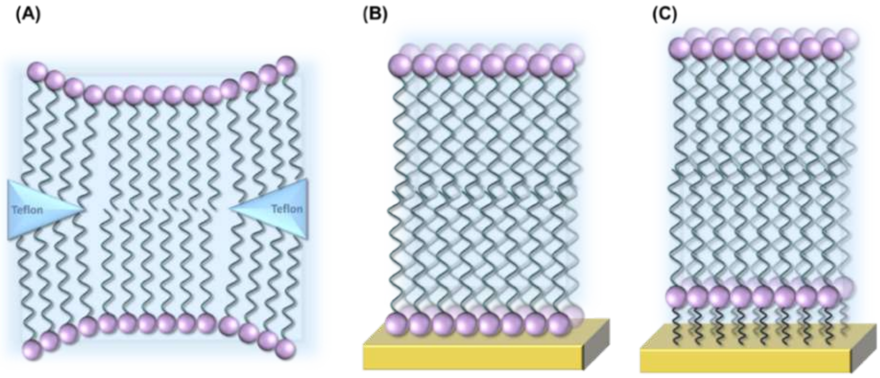

Figure 5: Model membrane systems: **(A)** black lipid membrane (BLM), **(B)** solid supported bilayer lipid membrane (sBLM) and **(C)** tethered bilayer lipid membrane (tBLM)

2.2.1 Application of model membrane systems

Biomimetic membrane systems should provide a simplified system for investigation of the membrane while maintaining fundamental membrane characteristics such as fluidity and electrical sealing properties.[15] Artificial membranes find applications in various scientific fields such as catalysis, synthesis of new materials, biopharmaceutics, drug delivery, antimicrobial activity or the design of bioelectronic devices.[1,2] They also allow the systematic study of fundamental processes at lipid bilayer interfaces, such as the membrane protein function, cell-cell signaling or protein-membrane interactions.[15] Supported bilayers allow for example the analysis of binding kinetics of a drug binding to the membrane using surface plasmon resonance spectroscopy (SPR).[16]

Especially tBLMs are considered as a comprehensive experimental platform for membrane biosensors. They have been studied in several applications ranging from antigen and antibody binding, applications as biosensors and energy-generating devices.[15]

2.2.2 Black lipid membranes

Black lipid membranes or bilayer lipid membranes (BLMs) shown in Figure 5 **A** are typically spread across a Teflon aperture with a diameter of a few 100 µm possessing excellent sealing properties about $100\ M\Omega \cdot \mathrm{cm}^2$ which results in very low leakage of background currents.[17,18] However, they remain intact for only a few hours which makes them unsuitable for long-term studies.[17] Additionally, their architecture limits the number of analytical characterization tools to only electrical and some optical methods.[17]

BLMs can be prepared *via* two different preparation methods. By using the so-called solvent containing membrane method, the lipid is dissolved in organic solvents such as decane. In the solvent-free method, lipids are spread with an organic solvent on top of the aqueous buffer.[18]

Current research is concentrating on improving the stability of BLMs by using different porous supports, for example nanoporous materials, such as anodized alumina to fabricated silicon devices with customized properties.[19]

2.2.3 Solid supported bilayer lipid membranes

Solid supported bilayer lipid membranes (Figure 5 **B**) consist of a lipid bilayer that is directly placed on a solid support such as gold, silicon, mica or glass.[14,17] Compared to black lipid membranes, sBLMs allow the use of a wider range of analytical techniques such as surface plasmon resonance of atomic force microscopy (AFM) to study membrane proteins. The solid substrate also causes a higher stability of the model membrane. However, a bilayer floating on a solid support is still relatively unstable and makes long-time measurements very difficult. The small amount of space underneath the membrane also hinders protein incorporation. Incorporated proteins may come in contact with the solid support and are very likely to lose their function due to denaturation.[14] This problem can be overcome by placing some type of cushion between membrane and substrate.[19] To prevent contact of the incorporated proteins with the solid surface a polymer cushion can be used to support the membrane. However, some polymer properties such as morphology, swelling behavior or thickness may be challenging to control. Additionally, the polymer reduces the properties of the supporting material which makes them unsuitable for electrochemical studies.[17]

2.2.4 Tethered bilayer lipid membranes

As an extension to sBLMs, so called tethered bilayer lipid membranes (Figure 5 **C**) have been developed. They have been introduced with the aim to obtain a lipid bilayer system with high electrical sealing properties and high stability that avoids direct contact between the bilayer lipid membrane and the solid support.[17]

Tethered bilayer lipid membranes consist of an anchor lipid in the inner leaflet and a phospholipid in the outer leaflet of the membrane,[17] as depicted in Figure 6. In this model system, the inner leaflet is covalently anchored to a solid substrate *via* an anchor group. A significant advantage of the covalent bond between anchor and substrate is, that such an approach inhibits detachment which may be a problem for the physisorbed membranes, e.g. under the influence of electric fields.[20] Generally, tBLMs show an improved stability compared to black lipid membranes or regular sBLMs.[19]

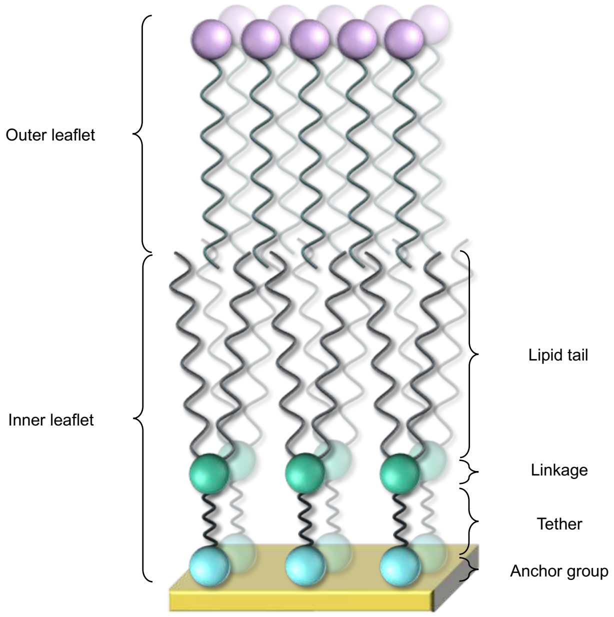

Figure 6: Schematic composition of tethered bilayer lipid membranes containing a phospholipid in the outer leaflet and an anchor lipid in the inner leaflet

In fully tethered BLMs, the inner layer consists only of anchoring lipids. This often results in membranes with excellent electrical sealing properties, ideal for electrochemical studies. A large number of different substances has been developed in the past few years as anchoring lipids which usually consists of a lipid (hydrophobic) tail that is connected through a linkage with the tether unit. The tether builds the hydrophilic part together with the anchor group, which binds the lipid to a substrate.[17]

To increase the hydration of the sub-membrane reservoir and to facilitate the incorporation of proteins into the double layer, sparsely tethered bilayer lipid membranes have been developed that use either a larger anchoring group (self-diluting anchor, Figure 7 right) or a smaller spacer molecule mixed with the anchor lipid as shown in Figure 7, middle. These architectures result in a significantly reduced density of the monolayer.[17] When using a mixture of anchor lipids and spacer molecules, the sub-membrane hydration can be increased while the sealing properties of the membrane are reduced. By modifying the anchor group, the sealing properties of the double layer remain high while the sub-membrane hydration is also increased.[21,22]

It could be shown, that in a fully tethered membrane, peptides were not able to incorporate into the bilayer. Whereas, in the sparsely tethered system, peptides were able to insert into the bilayer to form pores.[23] In general, ion transporters and ion channels are incorporated more effectively with improved function in a sparsely tethered BLM.[17]

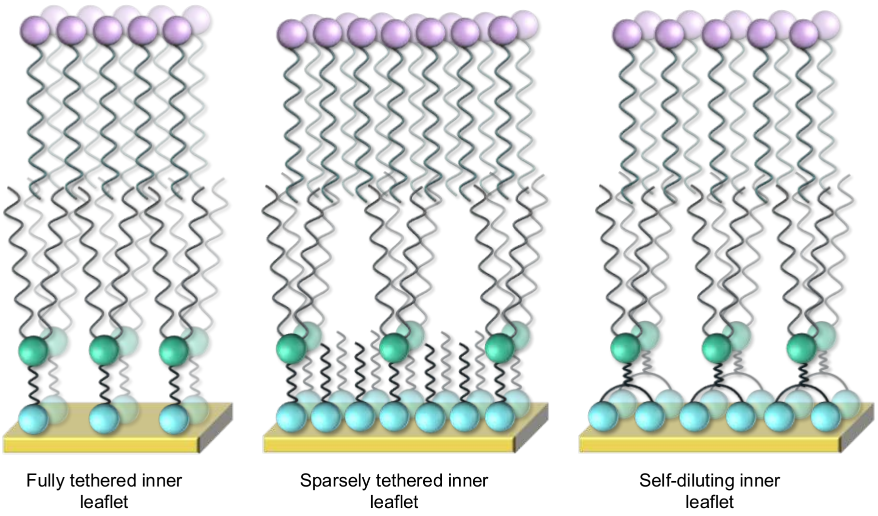

Figure 7: Comparison of different tethered membrane architectures

The structure of anchor lipid monolayers that are bound to the solid surface strongly affects the functional properties of tBLMs. The formation of the bilayer consists of a two-step process, starting with the deposition of an anchoring self-assembled monolayer (SAM) followed by the double layer formation, which will be described in chapter 2.3.[24]

2.3 Double layer formation of tBLMs

The formation of the bilayer can be realized by two different methods, namely rapid solvent exchange (RSE) or vesicle fusion as shown in Figure 8.[19]

RSE is one of the most widely used methodologies to form tBLMs. Therefore, the previously functionalized solid substrate is treated with an ethanolic solution of the outer leaflet lipid. After a short incubation time, solvent is exchanged to aqueous solution within a few seconds which leads to a spontaneous formation of the double layer. RSE bilayers are proven to exhibit excellent electrical sealing properties. The formation process is fast, but the real-time monitoring of the bilayer formation is impossible. Additionally, RSE allows limited phospholipid compositions because it requires lipids forming tBLM to be soluble in the exchangeable solvent, which is not always possible.[25]

By using the vesicle fusion method, various lipid compositions, including proteasomes and membranes derived from cells may be fused to the functionalized substrate. Generally, aqueous suspensions of small unilamellar vesicles (SUVs) are utilized to accomplish the bilayer. It has also been shown that vesicles can be fused to sparsely tethered lipid membranes. Typically, techniques such as SPR or quartz crystal microbalance (QCM) are utilized for monitoring the bilayer formation.[25]

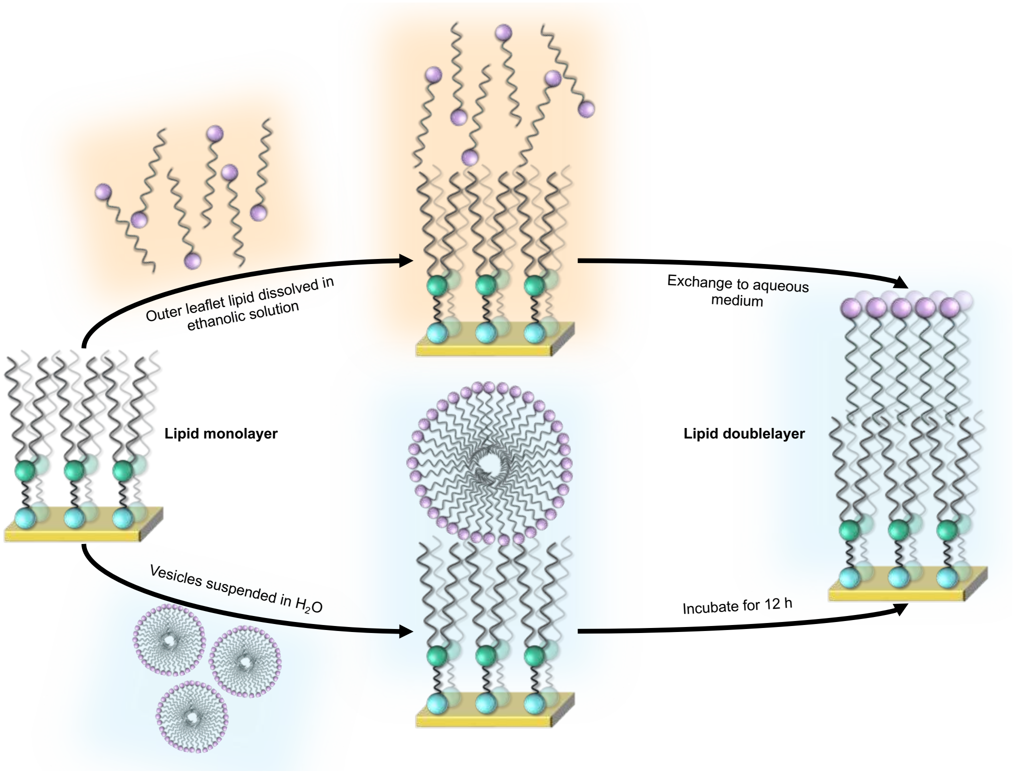

Figure 8: Formation of a lipid double layer *via* rapid solvent exchange (top) or vesicle fusion (bottom)

2.4 Monolayers of biomimetic membranes

In literature most reports on the formation of inner leaflets are on thiol-based SAMs that are grafted to metal surfaces, in most cases, gold.[24] Polyethyleneglycol (PEG) modified thiols are mainly utilized as anchor lipids as they prevent nonspecific adsorption of proteins and cells to the formed thin film.[26,27]

In 2003 Schiller et al. have successfully reported the synthesis of an anchor lipid 2,3-di-*O*-phytanyl-*sn*-glycerol-1-tetraethylene glycol-D,L-α-lipoic acid ester lipid (DPTL).[28] DPTL consists of two phytanyl chains, a tetraethylenglycol tether and a lipoic acid anchoring moiety as depicted in Figure 9.

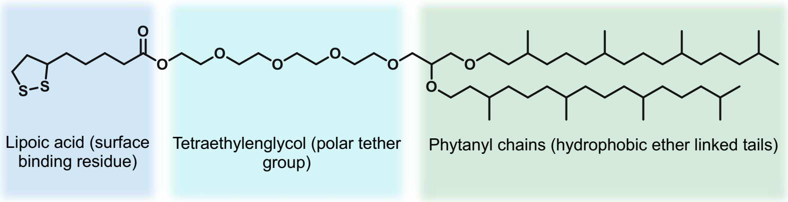

Figure 9: Chemical structure of DPTL

2.4.1 Thiol-based SAMs

SAMs are classified according to their binding ligand anchor groups. Thiolates have been the standard binding group for decades. Thiol-based SAMs were first reported 30 years ago, and since then these structures have been well studied for a variety of applications. However, their oxidative and thermal instability are well-known. These disadvantages hinder their widespread commercial application.[29]

Sulfur has a high affinity for binding gold atoms. Thiolate-SAMs on gold surfaces can be formed by using monothiols (RSH), thioethers (RSR) or disulfides (RSSR), where R is an aryl or alkyl group. Figure 10 shows a simplified standard model of a thiol-based SAM.[29,30] The S-Au bond has low polarization and thus is very stable when stored in ultra-high vacuum and in the dark.[29]

Figure 10: Example for a thiol-based SAM on gold

Although thiol-based SAMs on gold surfaces are oxidatively and thermally unstable, no truly general alternative to these ligands has been found. To avoid degradation in air at room temperature, these SAMs must be stored in ultrahigh vacuum in the absence of light. Various attempts to improve the stability by adding longer chain thiols, additives, or using polydentate thiol-based ligands did not yield to a more dramatic effect regarding stability of the SAM.[29] Bürgi et al. reported, that mixed alkanethiolate SAMs undergo phase segregation into domains, implying some mobility of the thiolates on the gold surface as well.[31] Furthermore, according to Salvarezza and co-workers, the chemical instability is the most serious problem and is the reason for the limited possible applications for thiol-based SAMs.[32]

2.4.2 *N*-Heterocyclic Carbene (NHC)-based SAM

Due to the above mentioned disadvantages of thiol-based SAMs, new systems like *N*-heterocyclic carbenes (NHCs) have gained high interest in the past few years.

Typically, carbenes are very reactive, but *N*-heterocyclic carbenes are stabilized by two adjacent heteroatoms next to the carbene carbon. NHCs can bind to gold forming stable Au-

NHC bonds, which are twice the strength of the Au-S bond in molecular complexes,[29] so NHC-metal interactions are predicted to be strong and unreactive. Additionally, NHCs are synthetically versatile due to their compatibility with various organic functional groups.[33] Therefore, NHCs are a potential alternative to thiol-based SAMs.[29] In Figure 11 a schematic structure of a NHC-based SAM is shown. In addition to the covalent bond between the gold atom and carbon, there are effective Van-der-Waals interactions between the alkyl side chains and the metal surface, which also leads to bond strengthening.[34] Changing the *N,N*-substituents has an impact on both steric and electronic properties of the SAM. Crudden et al. reported, that small *N,N*-substituents are crucial for a dense packing of the SAM.[29] According to Bakker et al., *N,N*-disubstituents have an effect on the orientation of the SAM on the substrate. They reported that an imidazolium-based system with *N,N*-dibutyl substituents lays flat on the gold surface whereas the corresponding *N,N*-dimethyl and *N,N*-diisopropyl systems form monolayers, that are facing away from the surface.[35]

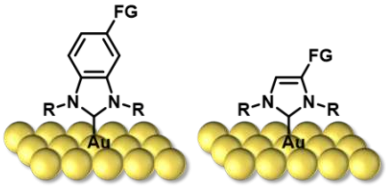

Figure 11: Schematic structure of NHC-based SAMs

Compared to thiol-based SAMs, NHC-based SAMs are stable in air and aqueous environments, so they can be stored for a long time without special conditions. However, the preparation of free NHCs usually has to be done in an inert atmosphere and deprotonated with strong bases such as NaH and KOtBu, as shown in Figure 12. This method can lead to contamination of the metal surface and excludes the use of base-labile functional groups. An alternative was recently discovered by the Crudden group, using bicarbonate salts single-source imidazolium derivatives as a starting material. The bicarbonate anion can act as a base to deprotonate the imidazolium cation to form a carbene. The only byproducts of this reaction are water and carbon dioxide.[36]

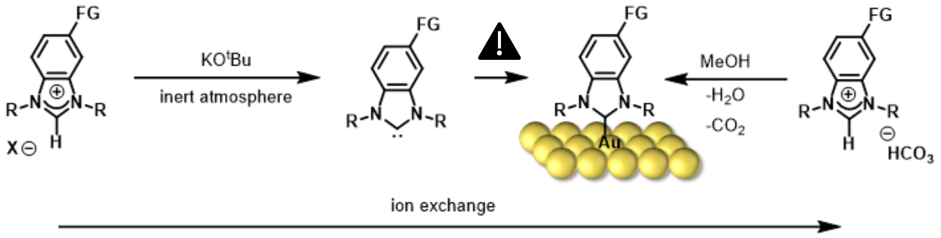

Figure 12: Possible pathways towards the formation of an NHC-based SAM on a gold surface

To obtain the desired hydrogen carbonate precursor, an ion exchange from the NHC precursor halide salt has to be done, as shown in Figure 12. The precursor can then be applied to the clean gold surface where carbene formation and subsequently surface coordination occurs.[36]

Due to the intermediate carbene formation, inert conditions are needed which makes the use of bicarbonate masked NHCs unpractical. As expected, high-quality SAMs from the bicarbonate masked NHCs cannot be obtained due to contamination challenges of ions from NHC precursors and intermediate formation of a free carbene.[33,37] However when using another mild base such as mesyl or triflate as counterion, and addition of $KHCO_3$ as a weak base, a concerted mechanism was reported, in which the base, the imidazolium salt and the substrate react simultaneously with the substrate without the involvement of a free carbene.[37] Therefore, mesyl- [OMs] or triflate- [OTf] masked NHCs seem to be resulting in a better alternative to the bicarbonate salts. The simple and mild conditions of the monolayer formation, this method allows the incorporation of a variety of functional groups.[33] The triflate salts can as well be obtained *via* an ion exchange reaction of the corresponding NHC-halide precursor. Choi et al. have previously shown the successful formation of high-quality SAMs using [OMs] masked NHCs.[33]

2.4.3 Mobility of NHCs on gold surfaces

The self-assembly of NHCs on metal surfaces is an important prerequisite in the formation of SAMs. However, a mechanism by which these NHCs extract a gold atom from the surface and build an NHC-gold adatom complex has been discovered. This complex shows high surface mobility with a ballbot-type motion.[38] That leads to the problem, that individual SAM units can move on the surface and they do not stay at a specific point.

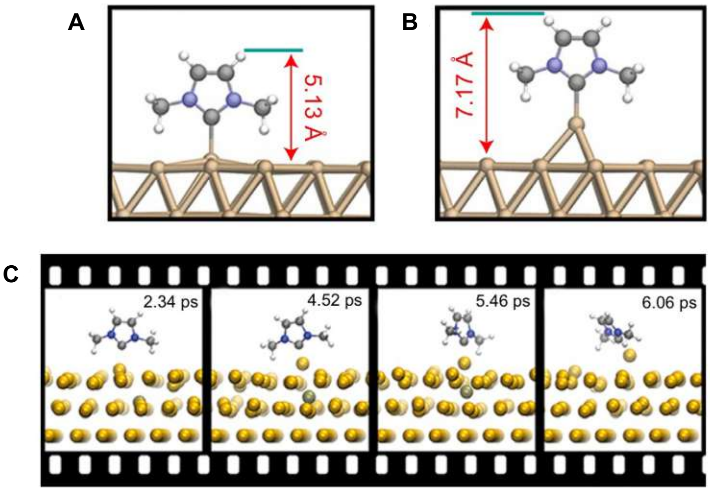

Figure 13: Geometric structures of IMe on Au(111) without (**A**) and with (**B**) an additional Au adatom as determined from DFT optimization. **C**: Snapshots from a CP–MD simulation of IMe on Au(111) illustrate the extraction of an Au atom from the top layer and the migration of an Au atom in the second layer (dark-shaded ball).[38]

After some time, the high mobility of these SAM units would lead to the destruction of the microstructures. In addition, the mobility leads to close packing, which affects the applications of SAM-modified surfaces. Photoswitches, for example, which typically need a lot of space can suffer loss of efficiency with the resulting close packing.[39,40]

However, when applying NHC-based SAMs as monolayers for biomimetic membrane, some mobility may be beneficial for the double layer formation and stability.[9,10]

2.4.4 NHCs in lipid biology

NHCs have recently gained great interest in lipid mimetics due to their synthetic accessibility and structural tunability. The Glorius group has developed a new class of imidazolium-based lipid analogs that resemble natural lipids in their amphiphilic structure. Those structures can easily be tuned and derivatized for a variety of purposes with regard to the investigation, modification and manipulation of biological membranes.[6] It was shown, that imidazolium salts bearing long alkyl chains in the backbone in position 4 and 5 (Figure 14 A) are able to behave as natural lipids by forming a stable mixed film with membrane lipids and thus may insert into the biological membrane of pro- and eukaryotes. It has also been reported that these lipids possess significant antitumor activity and cellular toxicity when using shorter alkyl chains (Figure 14 B).[41,42] Furthermore, they proved that C_{15}-IM itself forms uni- and multilamellar bilayer membranes, which are in a gel of liquid-crystalline membrane state at room temperature in the presence of a physiological buffer.[43]

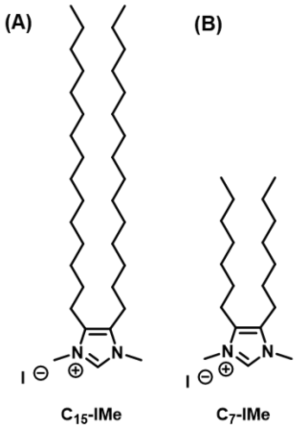

Figure 14: Chemical structure of imidazolium-based lipid analogs

Another study by Matos et al. shows, that imidazolium-based cholesterol analogs CHIM and CHIM-L (Figure 15) exhibit cholesterol-like behavior and integrate into biological membranes and living cells, and can be specifically labeled without perturbing its cholesterol-like membrane integration and partitioning.[44]

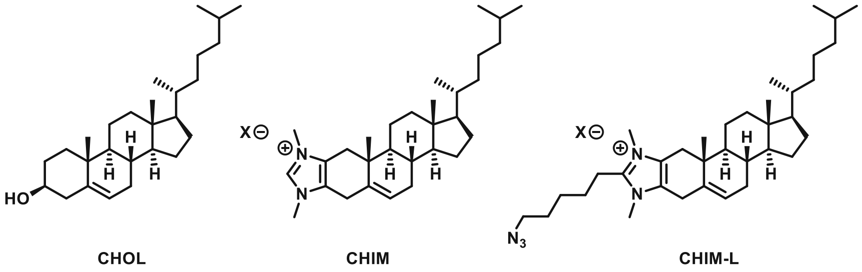

Figure 15: Imidazolium-based cholesterol lipid analogs CHIM and CHIM-L (X=Cl, I)

2.5 Motivation and thesis goals

2.5.1 Design and synthesis of NHC-based anchor lipids

Since thiol-based SAMs lack in thermal and long-term stability, NHCs are a feasible alternative for several applications. Crudden et al.[29] and Nguyen et al.[45] have already successfully immobilized modifiable NHCs on gold surfaces. This work intends to incorporate NHC-based monolayers as inner leaflet structures for tBLMs. Using NHC based inner leaflets in tBLM aims for (i) higher stability, (ii) high mobility and (iii) tunable surface density of the tethered lipid membrane to (iv) incorporate functional membrane proteins.

Since most reports on tBLMs are based on DPTL anchor lipids, this molecule will be used as a reference system. In this work, the main goal is to incorporate NHC-based anchor lipids into biomimetic membranes. These anchor groups have shown high surface mobility due to the formation of NHC-gold adatom complexes, that can move on the surface.[38] It is assumed that a higher surface mobility may be beneficial for the double layer formation and membrane properties. *N,N*-disubstitution of bench-stable imidazolium or benzimidazolium triflate-salts using different alkyl (methyl, isopropyl, ...) or the application of cyclic multidentate NHCs, as shown in Figure 16(A), will be applied to optimize and tune the stability and the surface density of the formed NHC system. To connect the NHC-precursor with the tether group, copper-catalyzed azide alkyne cycloaddition (CuAAC) will be performed.

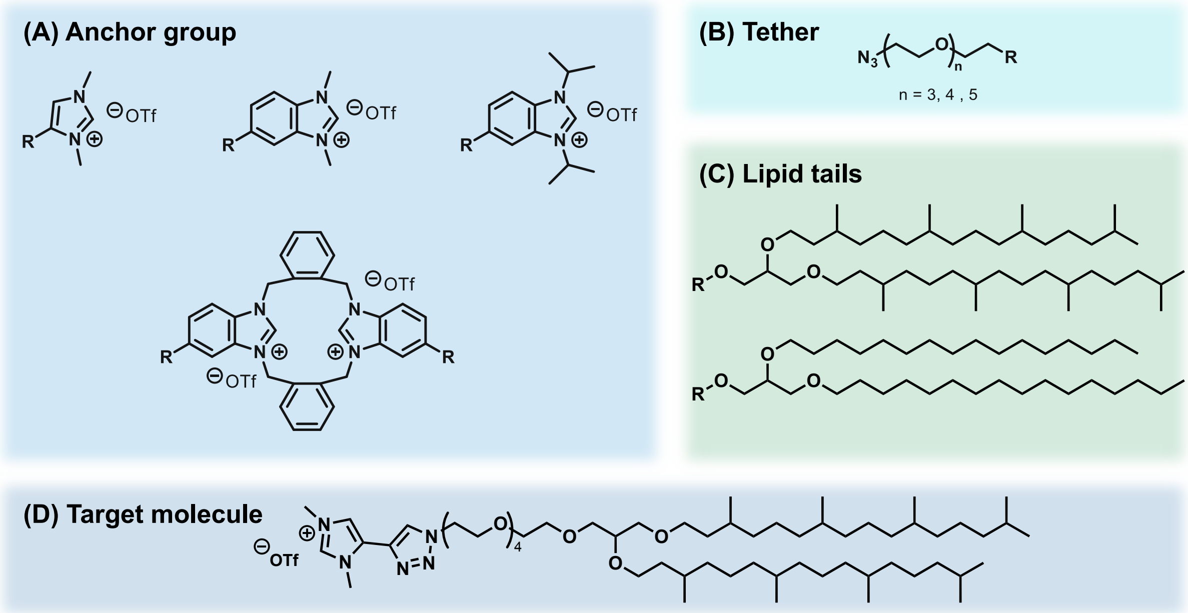

Figure 16: Molecular components of the anchor lipids: (A) anchor group, (B) tether group with different chain lengths and (C) lipid tails. (D) Exemplarily target molecule DPGPEG$_4$-Im

Polyethylene glycol (PEG)-based tether molecules (Figure 16(B)) provide a hydrophilic layer between the membrane and the substrate. Additionally, they are known to suppress nonspecific binding of proteins and decouple the artificial membrane from the gold surface.

Variation of the tether length will (i) compensate for surface roughness effects, and (ii) optimize sub-membrane hydration, while (iii) keeping membrane defects at a minimum.

For the lipid tail, phytanyl chains will be used. Earlier studies showed, that single hydrophobic chain molecules do not guarantee a stable insertion of molecules into a lipid membrane.[28] Therefore, the difference between branched phytanyl chains and unbranched hexadecyl chains will be analyzed. Variation of the lipid tail will allow optimization of the membrane composition and stabilization of specific membrane proteins. The hydrophilic and hydrophobic parts of the molecule will be connected *via* a glycerol subunit, creating diphytanyl glycerol (DPG, Figure 16 (C), top) and dihexadecyl glycerol (DHDG, Figure 16 (C), bottom). Connecting the molecular components *via* state-of-the-art chemistry operations, leads to an exemplarily target molecule (Figure 16 (D)) that can be used as inner leaflet structure for tethered bilayer lipid membranes.

However, for protein incorporation, a fully tethered BLM on a solid support is not well suited, since there is very little space underneath the membrane for sub-membrane hydration that may hinder incorporation and function of the protein. To allow a more flexible layer, sparsely tethered systems will be used. Therefore, an NHC-based spacer molecules has to be synthesized and incorporated into the monolayer as depicted in Figure 17.

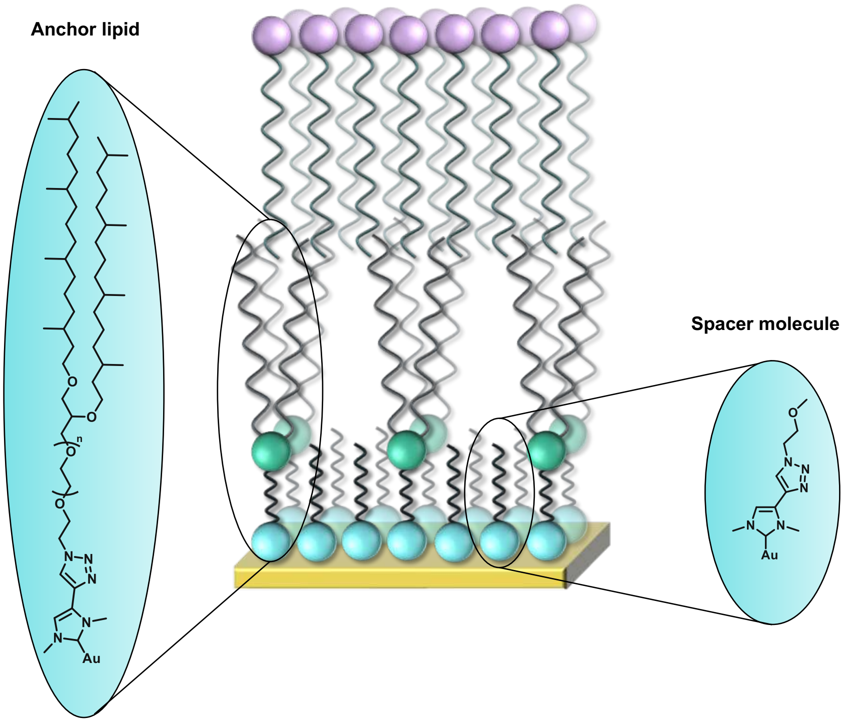

Figure 17: Anchor lipid and spacer molecule of a sparsely tethered bilayer lipid membrane

With the spacer molecule in hand, a mixed monolayer can be realized with different compositions of anchor lipid and spacer. The aim is to compare a fully tethered system with various compositions of sparsely tethered systems, to show the effect of the surface density of the monolayer on the membrane properties. Additionally, multidentate NHC-rings will be used as anchor group as another method to dilute the surface.

2.5.2 Immobilization and characterization of NHC-based tBLMs

The immobilization of the synthesized NHC-precursors will be realized by using (benz)imidazolium triflate precursors for the traceless formation of homogenous films. Therefore, the corresponding halide salts will be synthesized followed by a subsequent ion exchange to obtain the triflate precursors.

The binding strength of the Au/NHC bond in tBLMs is of significant interest regarding the stability of the membrane and will be compared to the thiol-based reference system DPTL. To analyze the successful formation of the monolayer, optical readouts such as contact angle measurements will be performed. Additionally, the electrochemical stability of the monolayers will be analyzed using cyclovoltammetry (CV). Furthermore, X-ray photoelectron spectroscopy (XPS) measurements will be done to gain insight into structural properties of the formed monolayer.

The obtained tethered materials will be further converted into tBLMs aiming for subsequent optimization of the artificial membranes regarding high electrical impedance, low capacitance as well as high fluidity and high sub-membrane hydration. For this purpose, electrochemical impedance spectroscopy (EIS) is a commonly used method.

2.5.3 Application of NHC-based tBLMs

To show that the synthesized compounds can be used as biomimetic membranes, membrane proteins shall be incorporated into the systems. In this context, it is assumed that the stabilization of membrane proteins may benefit from the high fluidity of the formed tBLMs. In this study, a potassium ion transporting peptide, valinomycin (Figure 18), will be incorporated in the bilayer as biological nanopore for single-molecule analysis. SPR studies can be used to gain both quantitative and qualitative data on molecular interactions of incorporated ion channels with the formed artificial membrane.

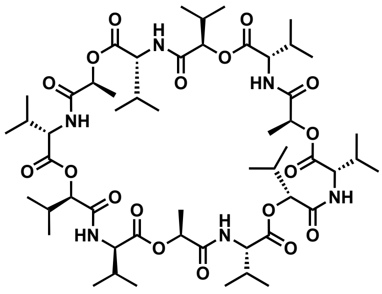

Figure 18: Chemical structure of valinomycin

3 Special part

3.1 Results and discussion

3.1.1 Synthesis of NHC-based anchor lipids

To synthesize the precursors of the anchor lipids, state-of-the art chemistry was applied. The retrosynthetic approach towards an exemplary anchor lipid is shown in Scheme 1. All the synthetic steps can be applied for similar structures, when using a different anchor group (e.g., disubstituted benzimidazolium) or other lipid tail (hexadecyl-tail).

For the last synthetic step, an ion exchange is needed, to obtain the corresponding triflate salt of the anchor lipid.

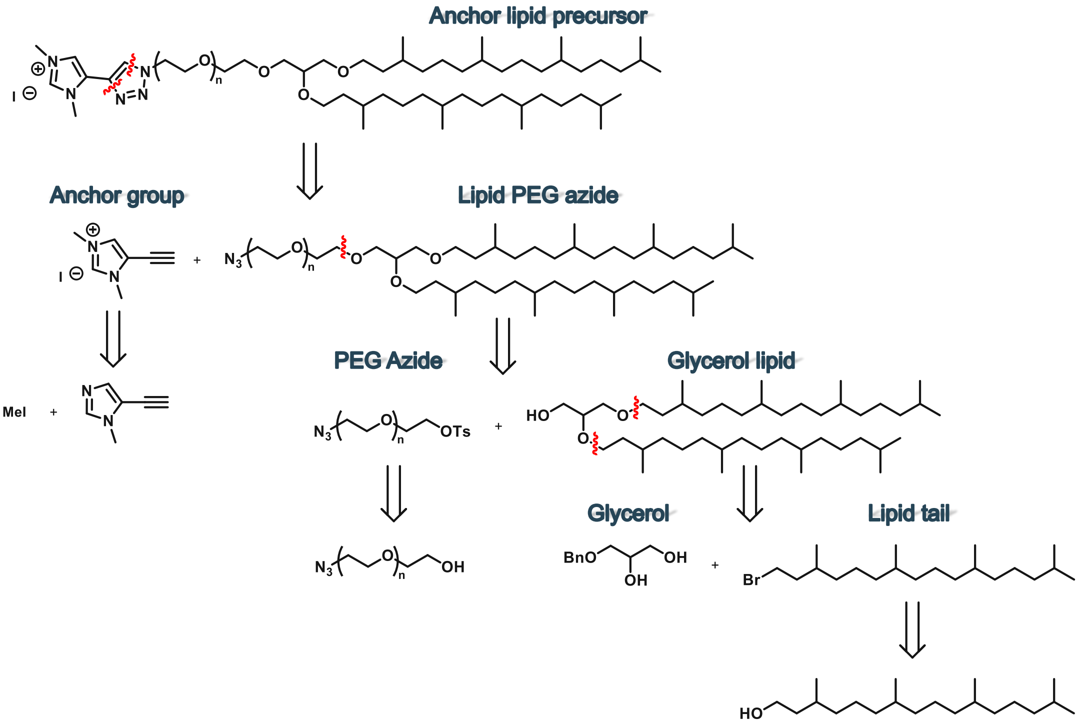

Scheme 1: Retrosynthetic approach towards the synthesis of the anchor lipids

3.1.1.1 Synthesis of the glycerol lipid

The first synthetic modification towards diphytanly-glycerol (DPG **5**) was performing a nucleophilic substitution of the OH-group of **1** in an Appel type reaction, as shown in Scheme 2, to install a bromide as leaving group on the phytanyl chain to obtain compound **2** 97 % yield. Next, a benzyl-protected glycerol unit **3** was introduced *via* another nucleophilic substitution to obtain the disubstituted glycerol molecule **4**. Although diphytanylether was observed as a side product, this step yielded in 70 %. Finally, the benzyl-protected OH-group of the glycerol had to be deprotected using H_2 gas in a Pd-catalyzed reduction to yield 85 % of compound **5**.

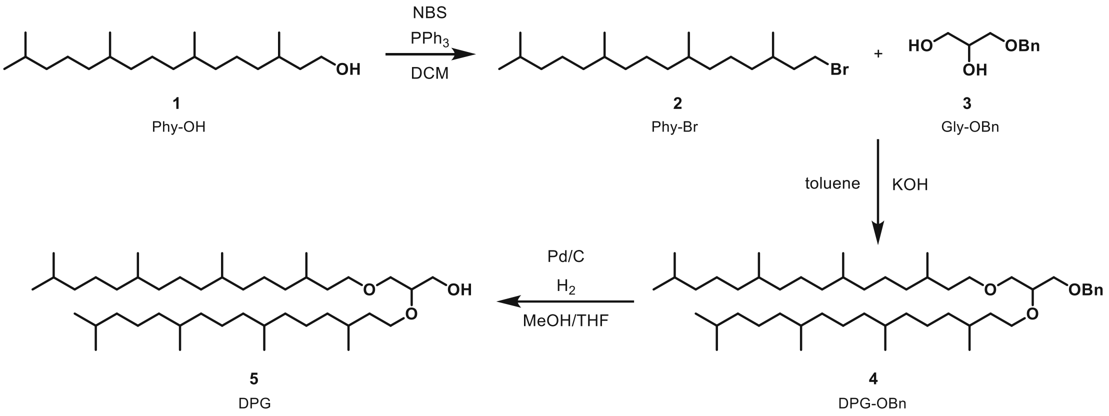

Scheme 2: Synthetic steps towards DPG

The same synthetic steps were also applied to obtain dihexadecyl-glycerol (DHDG **11)** as depicted in Scheme 3. Commercially available bromo-substituted starting material **9** was used in the first step. The substitution of **3** and deprotection of the benzyl-group were performed in the same way as mentioned above yielding in 85 % of **10**. Further deprotection of the benzyl group to the corresponding alcohol **11** was realized quantitatively.

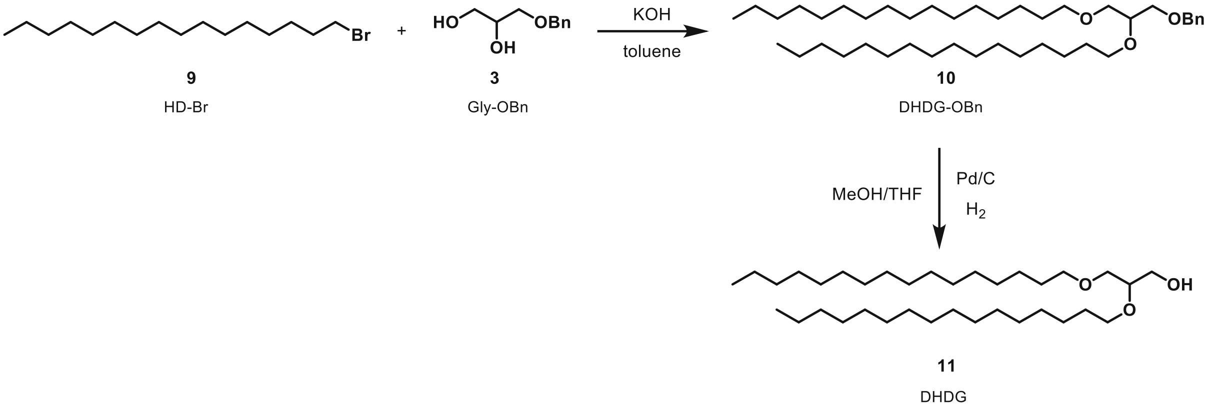

Scheme 3: Synthetic steps towards DHDG

3.1.1.2 Synthesis of the PEG azides

In order to connect the PEG-tether with the glycerol lipids, leaving groups had to be installed on the tether-precursors. Three different PEG lengths were chosen, namely PEG_3, PEG_4 and PEG_5.

For the PEG_3-tether **7a**, the starting material was the corresponding bistosylated PEG **6a** in which one tosylat-group was converted into an azide moiety as shown in Scheme 4 using NaN_3. The reaction yielded 36 %.

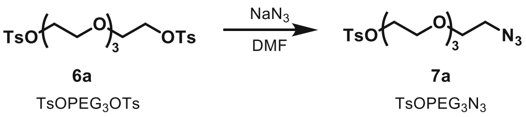

Scheme 4: Synthesis of $TsOPEG_3N_3$

For both PEG$_4$ **7b** and PEG$_5$ **7c**, a substitution reaction was performed, to convert the OH-group into a tosylat leaving group using *p*TsCl and NEt$_3$ as a base as depicted in Scheme 5. It can be noted that this method led to a significantly higher yield (96 % for **7b** and 70 % for **7c**) than the previously mentioned reaction.

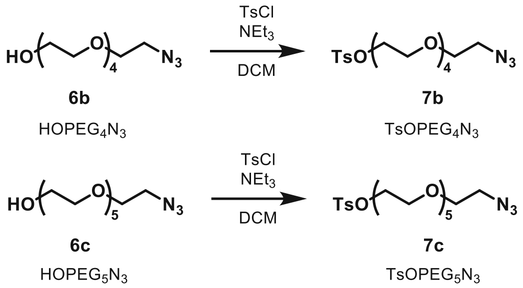

Scheme 5: Synthesis of TsOPEG$_4$N$_3$ and TsOPEG$_5$N$_3$

3.1.1.3 Synthesis of the lipid PEG azides

In the next step, the glycerol lipids **5** and **11** could be linked with the tether by applying another substitution reaction, following Scheme 5 using NaH to deprotonate the OH-group of the glycerol lipids. Performing these reactions for several times showed that a better yield was obtained at reaction times of several days. The long reaction time may be explained due to the severe difference in polarity of the glycerol lipids and the PEG-tethers. Generally, the synthesis of **IV** showed higher yields (82-95 %) than those of **I** (53-82 %). Since DPG **5** is less polar than the corresponding hexadecyl analogue **11**, conversion rates may be slower and more starting material is left.

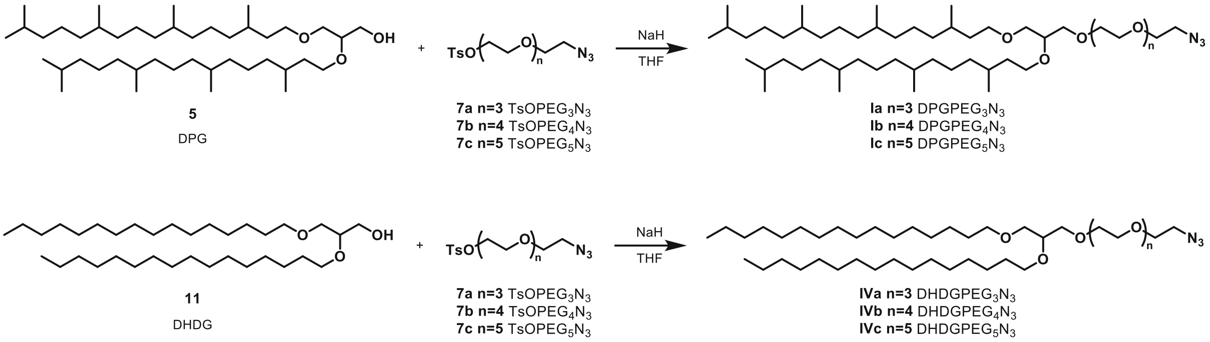

Scheme 6: Synthesis of DPGPEG$_n$N$_3$ and DHDGPEG$_n$N$_3$

3.1.1.4 Synthesis of (benz)imidazolium-based and multidentate anchor groups

In order to form membranes, NHC-based anchor groups had to be connected with lipid tails that could then be further used as inner leaflet. To get an efficient surface coverage different approaches were chosen, namely a variation of the NHC-system (imidazolium- or benzimidazolium-based) and *N,N*-dimethylation of *N,N*-diisopropylation. Additionally, first experiments towards the synthesis of multidentate NHC-systems were done.

To synthesize the imidazolium-based anchor group **8**, the commercially available starting material **15** was methylated in position 5 using MeI, as shown in Scheme 7.

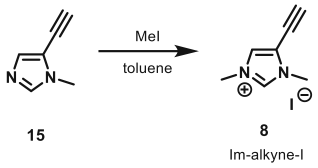

Scheme 7: Synthesis of *N,N*-dimethylated Im-alkyne-I

The synthetic route towards the *N,N*-diisopropylated benzimidazolium-based anchor group **X** can be seen in Scheme 8. First, a Sonogashira coupling of **16** with TMS-acetylene was performed to obtain **17** (22 %). The poor yield of this reaction may be explained by its high air sensitivity. Then, two subsequent substitution reactions were performed with 2-bromopropane and Cs_2CO_3 as a base to first get the mono-isopropylated (**Xa**) with a yield of 81 %. During workup of **Xa**, the TMS-group was deprotected. In the second substitution reaction the *N,N*-diisopropylated anchor group **X** was synthesized by adding 2-iodopropane and K_2CO_3 to a solution of **Xa**. The product precipitated out of solution yielding 61 % of **X**.

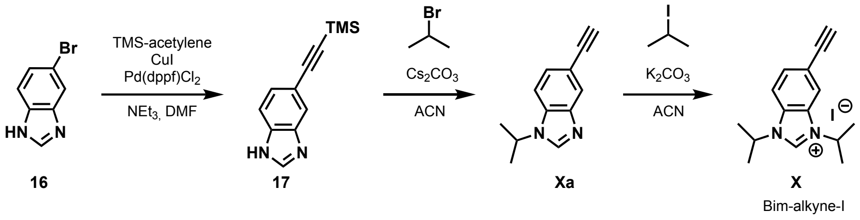

Scheme 8: Synthesis of *N,N*-diisopropylated Bim-alkyne-I

To optimize surface density of the formed SAM, multidentate NHC-precursors may be interesting. First experiments towards the formation of a multidentate anchor group have been made. Following Scheme 9, a Sonogashira coupling of **16** with TMS-acetylene was performed. Then, a substitution reaction of **17** using NaH in the presence of **22** was done. After workup and purification, the TMS-deprotected product **XVI** was obtained with a yield of 67 %. An additional deprotection reaction was therefore not needed. **XVI** is a mixture of three products, namely two symmetric products with both alkyne moieties symmetric in 4 or 5 position of the corresponding benzimidazolium-subunit and one asymmetric product with one alkyne moiety in position 4 and one in position 5 (Figure 19). The rather low yield may be explained, that monosubstituted may be formed, since 22 was added in excess. In the last synthetic step, a second 1,2-dibromo-*o*-xylene group was introduced. First experiments showed traces of product after stirring the reaction for about 40 days. However, product could not be verified after workup and purification.

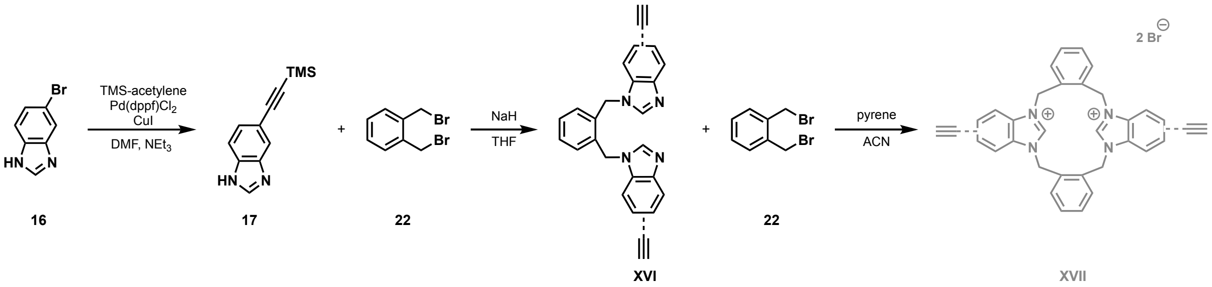

Scheme 9: Synthetic steps towards a multidentate NHC-based anchor group

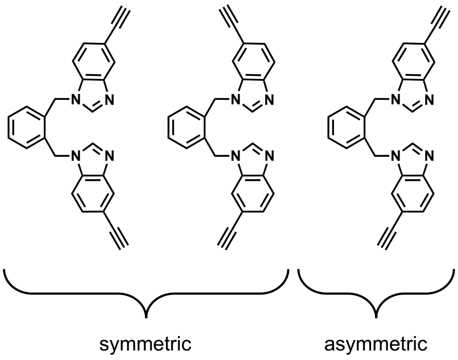

Figure 19: **XVI** was obtained as a mixture of three products

Guo et al. previously reported a method to synthesize tetracationic cyclophanes, where the target molecules were synthesized in the presence of 6 eq. pyrene as a template, with 30 mol% of tetrabutylammonium iodide (TBAI) as a catalyst.[46] Furthermore, Fang et al. reported a study on template-directed strategies to obtain macrocycles in high yields. They reported that imidazolium groups display flexible conformation and an ability to alter ring shape to accommodate different template molecules.[47] The pyrene-template method was applied to our system as well. Adding pyrene to the reaction, showed first product formation after 30 minutes, which was observed *via* LC/MS. After 12 h, no starting material could be detected. However, the product could not be purified due to solubility issues and separation problems resulting from the used excess of pyrene. A conformation of the product *via* crude NMR was not possible since the product is a mixture of three different isomers.

3.1.1.5 Click reaction and ion exchanges

The last synthetic step that had to be performed was a copper catalyzed azide alkyne cycloaddition (CuAAC) in which the azide moiety of the lipid PEG azide is connected with the alkyne moiety of the anchor group to form a triazolium subunit. For uncatalyzed 1,3-dipolar cycloadditions, 1,4- or 1,5-regiochemistries as shown in Scheme 10 are possible. However, for copper catalyzed cycloadditions only the 1,4-regiochemistry is obtained.

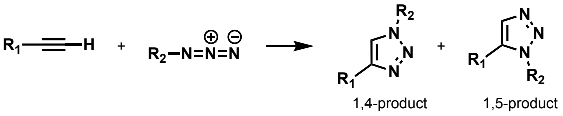

Scheme 10: Regioselectivity of uncatalyzed cycloaddition towards 1,4- and 1,5-product

The click reactions of *N,N*-dimethyl-substituted imidazolium alkyne were performed with all six previously synthesized lipid PEG azides as depicted in Scheme 11. The rather low yields (13-48 %) may as well be explained due to the significant difference in polarities of both reagents.

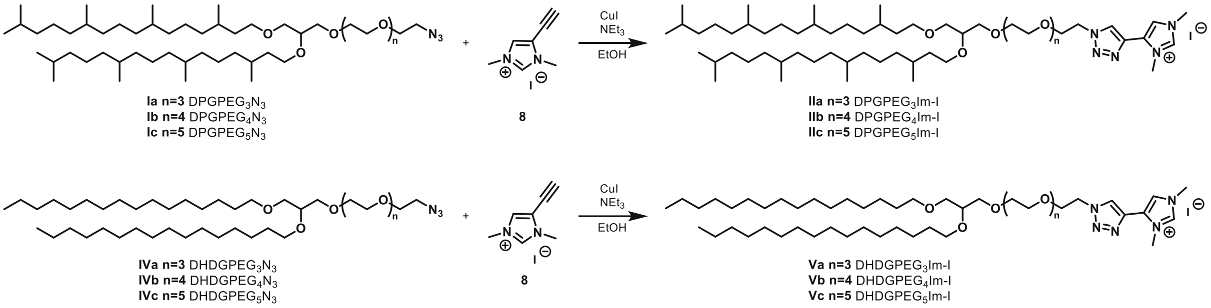

Scheme 11: Synthesis of DPGPEG$_n$Im-I and DHDGPEG$_n$Im-I

According to Crudden et al.[29] it is assumed, that anchor lipids with smaller *N,N*-substituents (**IIIa-c** and **VIa-c**) form a more dense SAM than anchor lipids with larger *N,N*-substituents (**XIIa**). As published in Bakker et al. *N,N*-dimethyl and *N,N*-diisopropyl NHC-based SAMs form monolayers, that are facing away from the surface.[35] One test system **XIa** with a *N,N*-diisopropylated benzimidazolium anchor group was synthesized, as shown in Scheme 12 according to the general CuAAC protocol, to gain further information about the influence of the anchor group on the membrane properties.

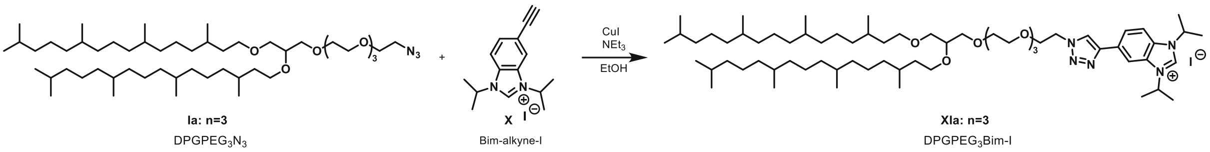

Scheme 12: Synthesis of DPGPEG$_3$-Bim-I

Halide-based NHC precursors can only be immobilized on gold surfaces using strong bases and inert conditions as already mentioned in chapter 2.4.2. To bypass harsh conditions, an ion exchange from the halide to a mild base such as triflate is necessary. Triflate masked NHC can undergo SAM formation in presence of a mild base in a concerted mechanism where the mild base, the imidazolium salt and the substrate react subsequently with each other without the involvement of a free carbene.[37]

An ion exchange of the halide precursors **IIa-c** and **Va-c** was performed to obtain the corresponding triflate salts **IIIa-c** and **VIa-c** as shown in Scheme 13. Therefore, AgOTf was added to the dissolved halide which led to the formation of unsolvable AgI (solubility of AgI in

MeOH: 1.923 · 10^{-7} g/100 g MeOH[48]) that precipitates from the methanolic solution. For the DHD-system, acetone was chosen as a solvent since **Va-c** is not fully soluble in methanol. The solubility of AgI in acetone is 3.2 · 10^{-10} g/100 g acetone.[48] Further application of these compounds will be described in chapter 3.1.5.1.

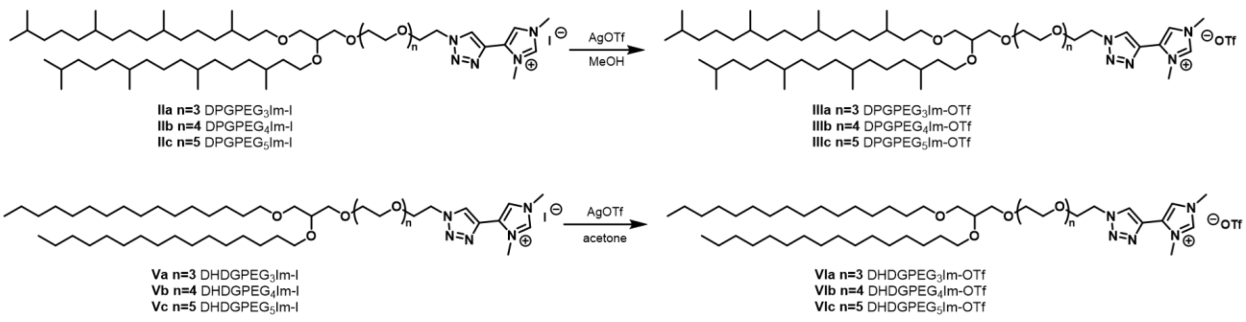

Scheme 13: Synthesis of DPGPEG$_n$Im-OTf and DHDGPEG$_n$Im-OTf

As shown in Scheme 14 an ion exchange of the benzimidazolium-based halide precursor was performed in analogy to the previously described imidazolium-based precursors using AgOTf in a methanolic solution of **XIa**.

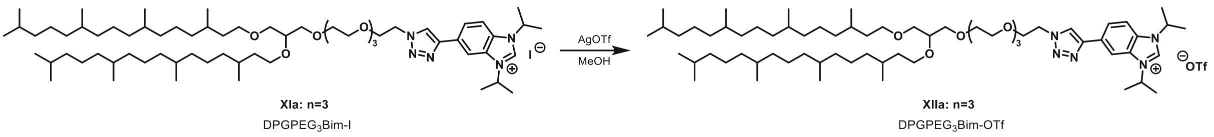

Scheme 14: Synthesis of DPGPEG$_3$-Bim-OTf

Generally, the ion exchange reactions towards the triflate precursors gave good to excellent yields (80-99 %). Losses of product may be caused due to filtration over the celite plug and subsequent syringe filter filtration. However, observation of the completeness of the reaction is difficult. To circumvent incomplete conversion of the halide precursor, which may be hindering the following immobilization process, the reactions were stirred over a longer time period (up to three hours) even though precipitation of AgI was observed after several minutes. Formation of the triflate was confirmed *via* ^{19}F-NMR.

3.1.2 Synthesis of an NHC-based spacer molecule

Besides changing the size of the *N,N*-disubstituents, another strategy to decrease the packing density of the SAM and increase the submembrane hydration of the lipid bilayer[17] sparsely tethered bilayer lipid membranes are an option. Therefore, an NHC-based spacer molecule was synthesized as depicted in Scheme 15.

First, the tosylat-group of **18** was substituted with an azide moiety using NaN_3. The click reaction was performed in analogy to the previously described (benz)imidazolium-based anchor lipids yielding 36 %. The rather low yield may be explained due to the fact, that **19** was used without further purification in that case due to safety reasons. Lastly, to obtain an [OTf] masked NHC, an ion exchange using AgOTf in methanolic solution was performed in the same manner as described in chapter 3.1.1.5. **XIV** was obtained quantitively.

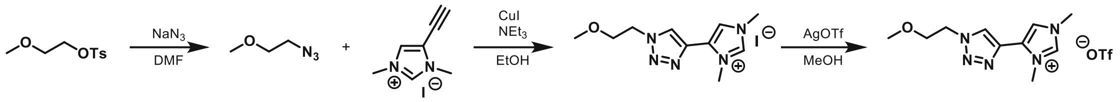

18

19

8
Im-alkyne-I

XIII
MeOIm-I

XIV
MeOIm-OTf

Scheme 15: Synthesis towards MeOIm-OTf

3.1.3 Synthesis of an NHC-based outer leaflet

In a further approach, the aim was to build a full synthetic membrane by implementing an NHC-based lipid as outer leaflet structure instead of using usually employed phospholipids.[14,17] Therefore, DPG was modified in a two-step synthetic process towards an azide-substituted lipid analogue as depicted in Scheme 16.

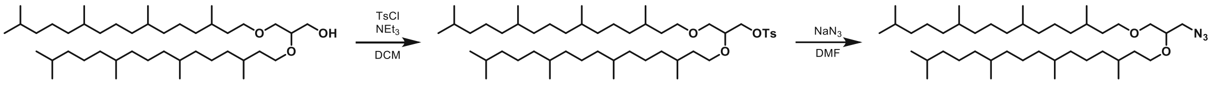

5
DPG

20
DPG-OTs

21
DPG-N$_3$

Scheme 16: Synthesis of DPG-N$_3$

Finally, a CuAAC reaction was performed (Scheme 17) to obtain an analogue of the previously synthesized lipid anchor groups, that can be implemented in tBLMs as outer leaflet structures.

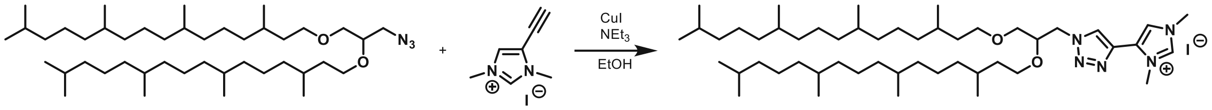

21
DPG-N$_3$

8
Im-alkyne-I

XV
DPGIm-I

Scheme 17: Synthesis of DPGIm-I

Due to solubility issues, a purification of **XV** was not possible yet. Impurities could not be removed with filtration or flash column chromatography. However, the formation of the target molecule could be confirmed *via* NMR.

3.1.4 Synthesis of thiol-based anchor lipids

To synthesize thiol-based anchor lipids with longer PEG chains, the OH-moiety of the PEG-precursors **12a** and **12b** had to be modified by a tosylat-leaving group as depicted in Scheme 18 to obtain **13a** and **13b**.

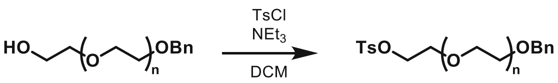

12a: n=5 HOPEG$_5$OBn
12b: n=7 HOPEG$_7$OBn

13a: n=5 TsOPEG$_5$OBn
13b: n=7 TsOPEG$_7$OBn

Scheme 18: Synthesis of TsOPEG$_5$OBn and TsOPEG$_7$OBn

The modification of DHDG **11** with the tethers was carried out in the same manner as for the previously explained NHC-anchor lipids (chapter 3.1.1.3). However, a complete separation of **13** and **VII** *via* normal phase column chromatography was not possible, which may explain the relatively fair yields (**VIIa**: 42 %, **VIIb:** 46 %) of these reactions. The benzyl group was then again reduced, as shown Scheme 19 using H_2 in presence of a Pd-catalyst to obtain **VIIIa** and **VIIIb** almost quantitatively. For the last step, an EDC-coupling reaction of lipoic acid **14** and the respective deprotected PEG-lipid was applied to successfully obtain **IXa** (45 %) and **IXb** (40%). The rather low yields of the coupling may be explained due to the small scale and therefore weighing errors of these reactions.

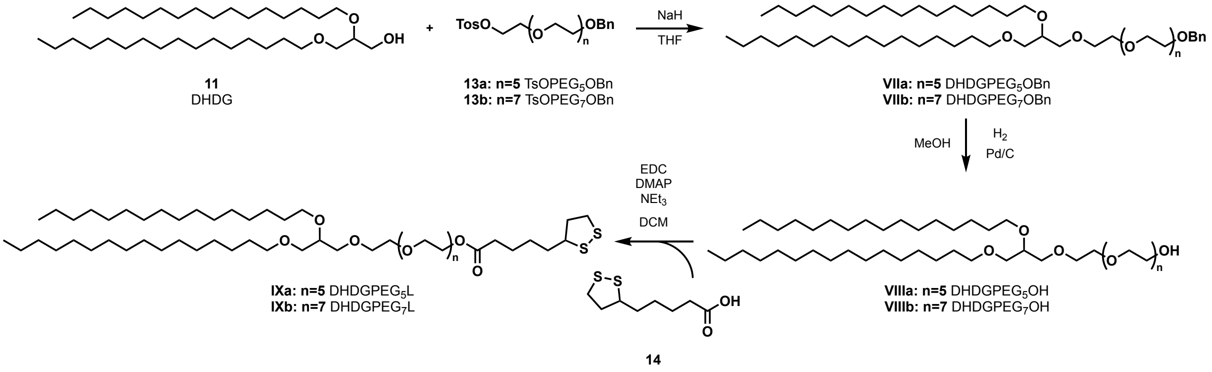

Scheme 19: Synthesis of $DHDGPEG_5L$ and $DHDGPEG_7L$

3.1.5 SAM formation and analysis of the monolayer

By applying the mild SAM formation method mentioned in chapter 2.4.2, the synthesized triflate masked NHCs can be immobilized on gold substrates. In this context, the general immobilization method described by the Crudden group[33,36] was applied, where a methanolic solution of the NHC-precursor was prepared and a gold slide was immersed in the solution upon addition of a mild base such as $KHCO_3$.

3.1.5.1 SAM formation

For the SAM formation, methanolic solutions of triflate precursors **IIIa-c** or **VIa-c** were prepared, as shown in Figure 20. Different concentrations (10 mM and 0.5 mM) were tested to gain further insights in the formation process. Gold slides were cleaned using a piranha solution (H_2SO_4/H_2O_2, 3:1 v/v) for 10 min, washing by immersion in HPLC water for 10 min and UV/ozone surface cleaning for 15 min. After addition of 1 eq. $KHCO_3$ a dry, precleaned gold slide was immersed in the solution for 24 h under ambient conditions. After the incubation time, the slide was rinsed with MeOH and dried under Argon gas.

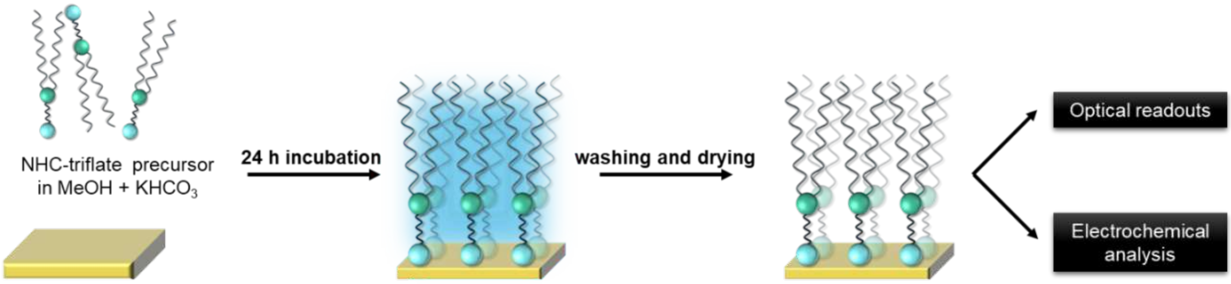

Figure 20: Schematic illustration of the SAM formation process

In order to obtain a high-quality bilayer, the quality of the SAM is crucial. Therefore, several methods to analyze the monolayer properties, such as packing density as well as stability under ambient conditions and electrochemical stability, have been applied.

3.1.5.2 Contact angle measurements

After the SAM formation of **IIIa** on a gold slide, the contact angle (CA) of the functionalized substrate was measured. In reference to a clean gold substrate, which has a contact angle of about 65°,[49] contact angles between 72° and 93° were obtained for the functionalized substrate, leading to the conclusion that there is indeed a thin layer on the surface.

For each functionalized substrate, three representative contact angles were measured to give average contact angles listed in Table 1. It is assumed that a denser packed SAM has a higher CA than less dense SAMs. DPGPEG$_4$Im functionalized gold showed the highest CA of 93°, leading to the conclusion that this anchor lipid has the best ability to build dense monolayers on gold surfaces. Exemplary pictures of the contact angles can be seen in Figure 21.

Table 1: Contact angles of functionalized gold coated Kapton

SAM	Average contact angle (°)
DPGPEG3Bim	81.9 ± 1.2
DPGPEG3Im	83.1
DPGPEG4Im	92.7 ± 4.6
DPGPEG5Im	65.8 ± 6.1
DHDGPEG3Im	76.2 ± 5.0
DHDGPEG4Im	72.6 ± 3.8
DHDGPEG5Im	83.9 ± 1.5

For the measurement of the contact angles, gold coated Kapton was used as a substrate. Due to the flexibility and low thickness of the substrate, it was difficult to obtain a flat surface during CA measurements.

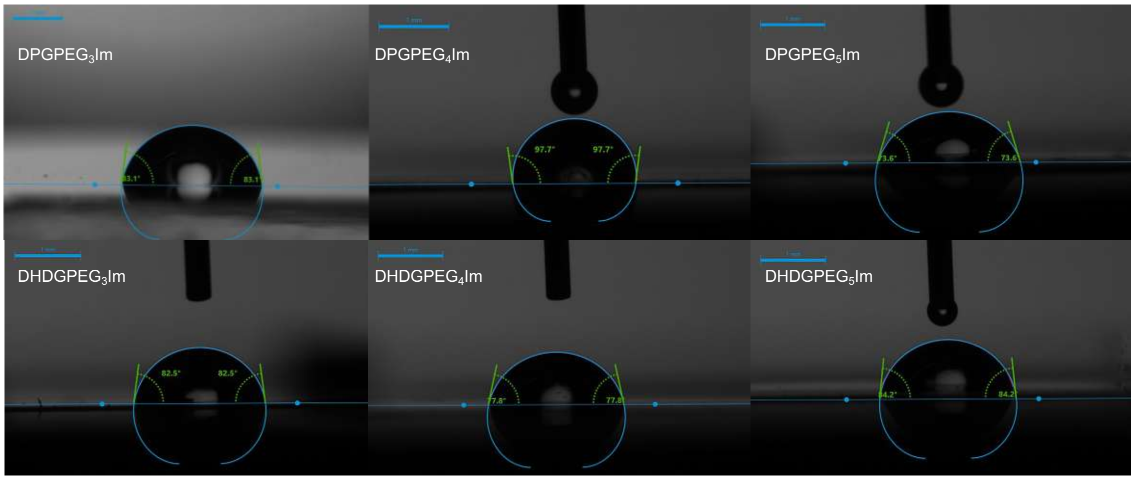

Figure 21: Contact angle measurements of gold coated Kapton functionalized with imidazolium-based anchor lipids

Andersson et al. found, that a SAM with a contact angle of less than 100° appears to have insufficient surface energy to promote the fusion of vesicles into a continuous lipid bilayer.[21] Additionally, it has been reported, that due to a lower degree of surface ordering, CAs of NHC-based SAMs are typically lower than those of comparable thiol-based monolayers.[50]

3.1.5.3 XPS measurements

XPS analysis was performed to characterize the surface composition of the formed SAM and to show the successful immobilization on gold substrates. An XPS survey scan (Figure 22) of the SAM of DPGPEG$_3$-Im **IIIa** anchored on a gold substrate that has been immersed for 24 hours in 10 mM of a methanolic solution in presence of $KHCO_3$ as mild base, shows the elements Au, C, N and O which represent the elemental composition of DPGPEG$_3$-Im ($C_{58}H_{112}N_5O_6$). The analysis of the shape of the background of the spectra, which is caused by inelastic scattered electrons at near-surface structures, clearly shows the formation of a thin layer on the gold surface.[51]

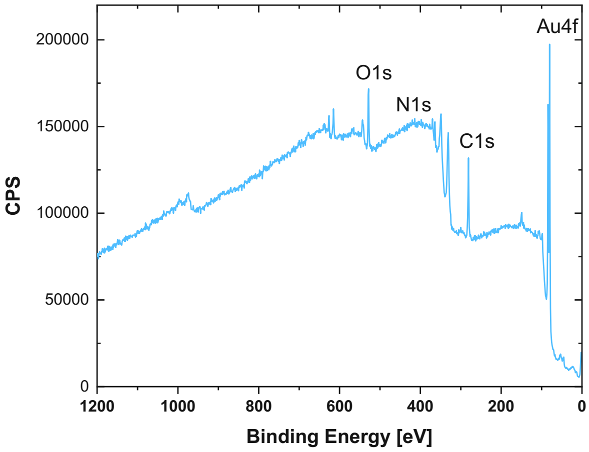

Figure 22: XPS survey scan of **IIIa** immobilized on a gold surface

Figure 23 shows the high resolution XPS spectra of the core elements analyzing a SAM of **IIIa** on a gold substrate. The corresponding average binding energies of the respective elements are listed in Table 2.

Table 2: Average binding energies from high resolution XPS spectra of core elements

	Binding energy (eV)		
C-C*	284.8	±	0.21
N-C*	286.2	±	0.02
O-C*	287.4	±	0.17
C-O*	532.5	±	0.04
C-N*	401.0	±	0.10
triazole*	399.7	±	0.24
triazole*	402.3	±	0.00
Au*	83.7	±	0.09
	87.3	±	0.07

Figure 23 A shows the high resolution XPS spectrum of the C1s signal. The obtained data (black) was modeled with three components resulting in the fit (dark green). The energy scale is calibrated to the main carbon peak at 284.8 eV. The main C peak (purple), which is the largest contribution comes from the C1s (C-C).[52] The second peak (light blue) at 286.2 eV can be attributed to N-C*.[45] Lastly, the weak contribution at 287.4 eV can be attributed to the O-C* bond.[45]

Figure 23 B displays the high resolution XPS spectrum of the N1s signal. Two components were required to fit (dark green) the measured data (black). The peak at 401.0 eV (light green) is shown to contain a contribution of C-N*.[45] The two peaks at 399.7 eV (light blue) and 402.3 eV (purple) may be attributed to the triazolium group.[45]

Figure 23 C shows the high resolution XPS spectrum of the O1s signal. The obtained data (black) was fitted (dark green) using two components. The major peak at 532.5 eV is shown to contain a contribution of C-O*-C bonds.[52]

Lastly, Figure 23 D shows the high resolution XPS spectrum of the Au4f signal. In the case of well-ordered SAMs, a doublet is observed with the Au 4f components at binding energies of Au4f$_{5/2}$ 83.7 eV (light blue) and Au4f$_{7/2}$ 87.3 eV (purple) as expected.[52]

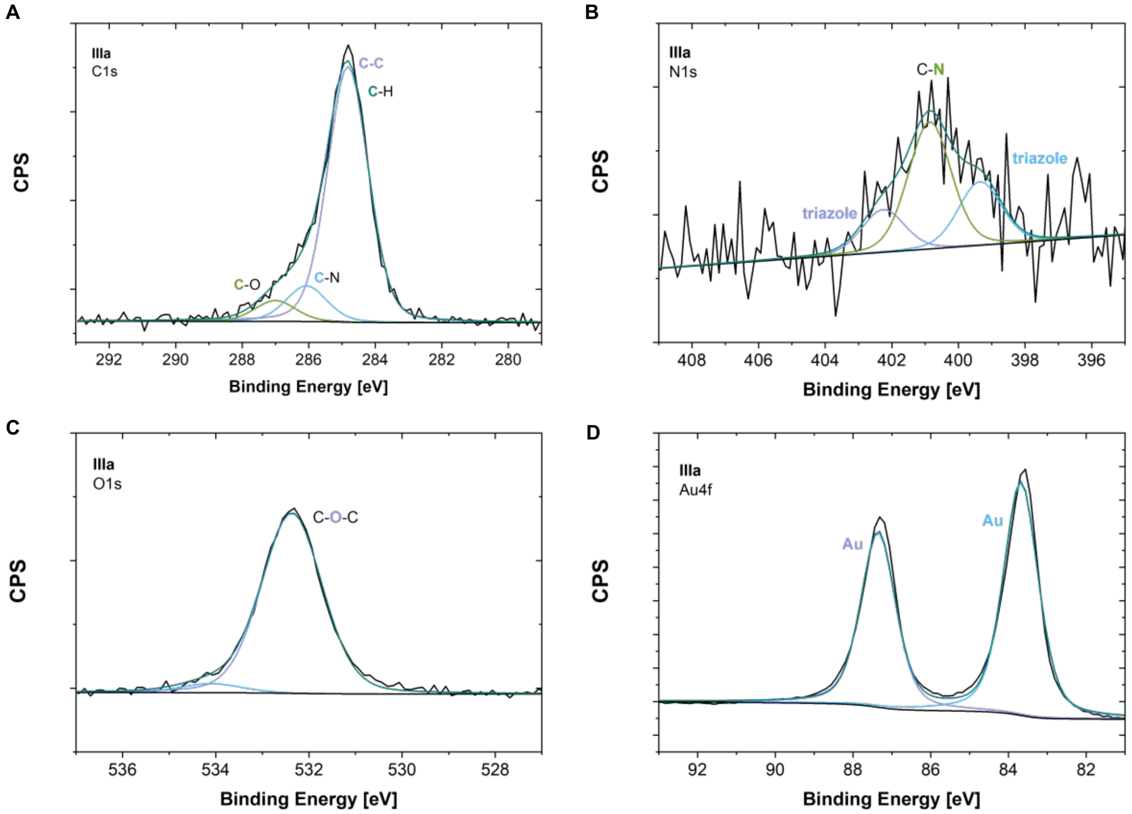

Figure 23: High resolution XPS spectra of the core elements occur on the SAMs of **IIIa** on gold substrate (immersed for 24 hours in methanol solution). Regions of the high resolution XPS spectra: (**A**) C1s, (**B**) N1s, (**C**) O1s, (**D**) Au4f

3.1.5.4 Stability of monolayers

To gain further insights of the electrochemical stability of the formed NHC-based SAMs, cyclovoltammetry was performed. Four different gold slides were analyzed, namely a bare gold slide, **IIb** immobilized without $KHCO_3$, **IIb** immobilized in presence of $KHCO_3$ and **VIb** immobilized in presence of $KHCO_3$. Experiments with and without base were done, to show that a mild base is crucial for the SAM formation process. Cyclic voltammograms were measured in a three-electrode set-up using the gold substrate as a working electrode, a platin wire as the counter electrode and an Ag/AgCl reference electrode in aqueous media of the redox probe $K_4[Fe(CN)_6 \cdot 3\ H_2O]$ and 0.1 M KCl. The cyclic voltammograms at different scan rates (10, 20, 50 and 100 mV/s) can be seen in Figure 24. The cyclic voltammograms have an effect on the scan rates, in which the oxidation and reduction signals are higher with a higher scan rate. According to Randles-Sevcik equation,[53] faster scan rates lead to a decrease in the size of the diffusion layer. Therefore, higher currents are observed.

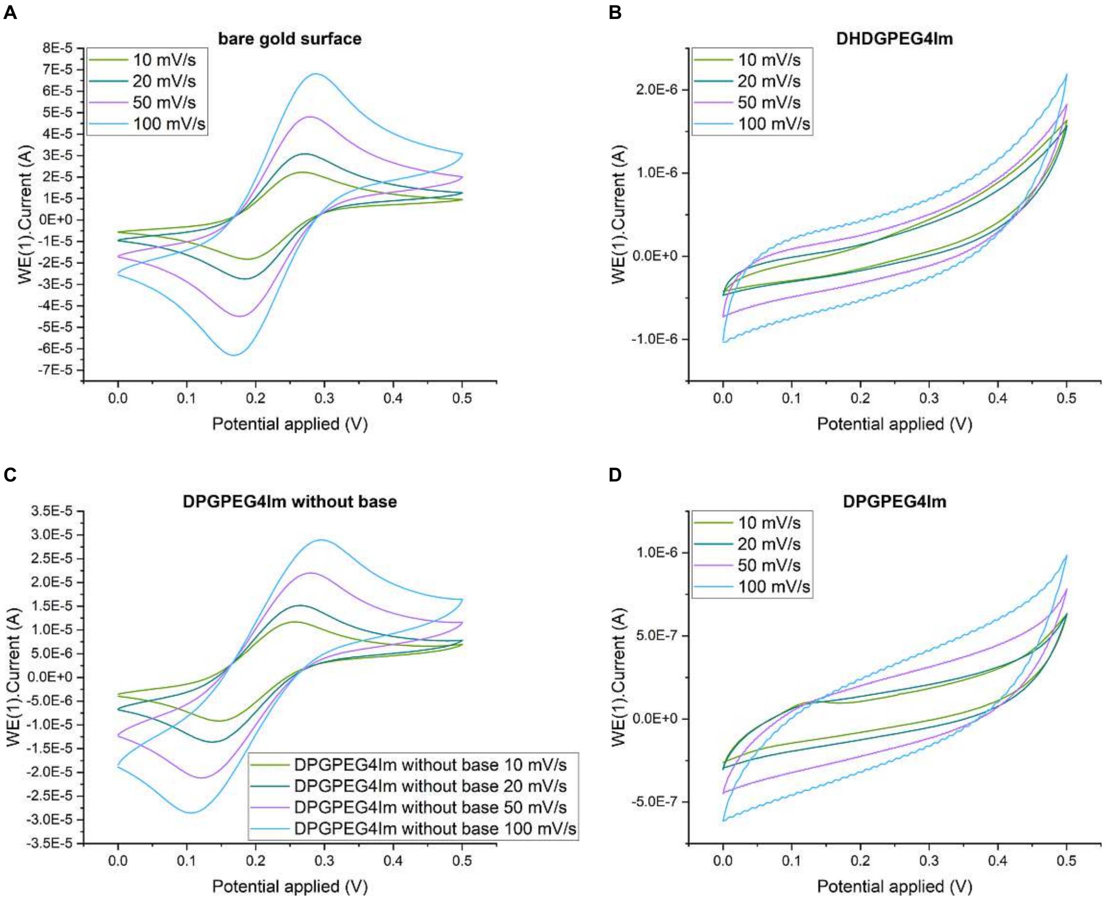

Figure 24: Cyclic voltammograms of **A** bare gold surface, **B** DHDGPEG$_4$Im with KHCO$_3$ **C** DPGPEG$_4$Im without presence KHCO$_3$ and **C** DPGPEG$_4$Im in presence on gold surface at different scan rates. The measurements were carried out in 1 mM K$_4$[Fe(CN)$_6$] and 0.1 M KCl aqueous solution. NHCs were immobilized in 10 mM methanolic solution of NHC.

The cyclic voltammogram of the clean gold slide clearly shows the reduction and oxidation of $Fe(CN)_6^{3-}/Fe(CN)_6^{4-}$ (Figure 25 **A**) while no reduction or oxidation processes could be observed for the functionalized gold slides with a base. However, when the NHC-precursor is functionalized without the use of a base, oxidation and reduction of $Fe(CN)_6^{3-}/Fe(CN)_6^{4-}$ can be observed. This indicates that the addition of a mild base such as KHCO$_3$ is crucial for the successful formation of a SAM on gold when using [OTf] masked NHCs. The decreased oxidation/reduction signal compared to the clean gold slide may be explained due to nonspecific adsorption on the surface.

Comparing the immobilization of **IIIb** and **VIb** with KHCO$_3$ (Figure 25 **B**) shows no significant difference in oxidation and reduction processes. However, DPGPEG$_4$Im shows a slightly better surface coverage than DHDGPEG$_4$Im.

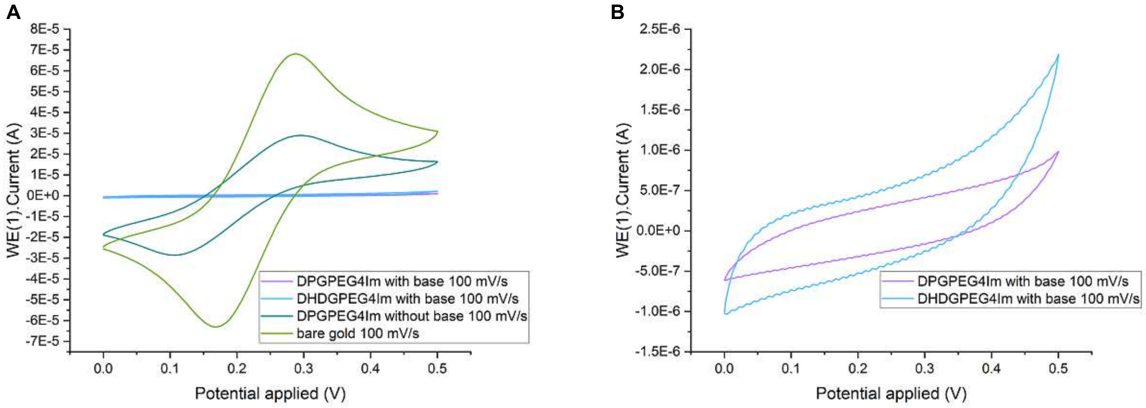

Figure 25: Cyclic voltammograms of a bare gold slide (light green), **IIIb** immobilized without $KHCO_3$ (dark green), **IIIb** immobilized in presence of $KHCO_3$ (purple) and **VIb** immobilized in presence of $KHCO_3$ (blue). The measurements were carried out in 1 mM $K_4[Fe(CN)_6]$ and 0.1 M KCl aqueous solution. NHCs were prior immobilized in 10 mM methanolic solution of NHC.

In the case of thiol-based SAMs, instability of the thin film under repeated electrochemical cycling is a limitation for their application in some electrochemical processes.[29] Cycling experiments of **IIIb** and **VIb** was performed to confirm the electrochemical stability of the NHC-based SAMs. Figure 26 clearly shows, that the formed film is indeed stable after at least 100 electrochemical cycles under ambient conditions.

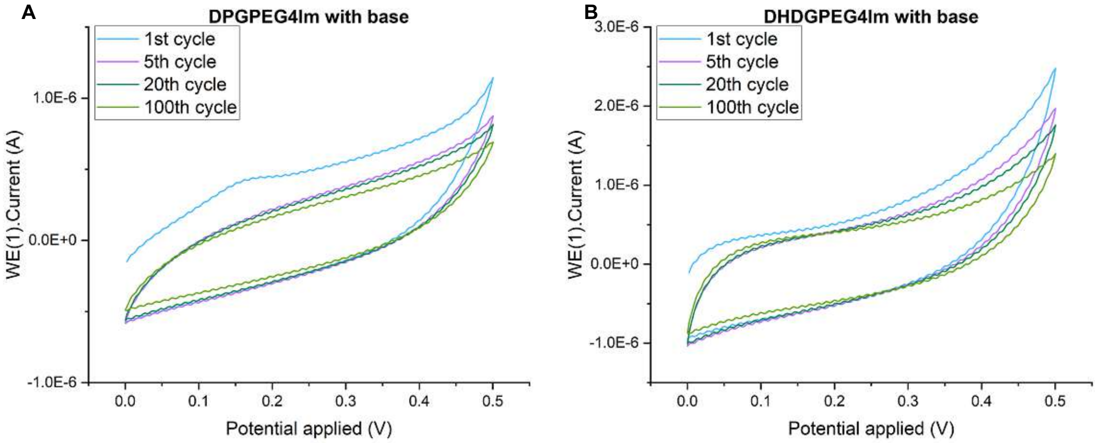

Figure 26: Electrochemical cycling experiments of NHC-based films on gold immobilized in presence of a base: **A IIIb**, **B VIb**

3.1.6 Bilayer formation and analysis of the bilayer

As already mentioned in chapter 2.3, rapid solvent exchange and vesicle fusion are commonly used for the formation of lipid bilayers. The bilayer can then be analyzed *via* electrochemical and optical methods.

To obtain bilayers formed *via* rapid solvent exchange, the formed monolayer is incubated under 1,2-dipalmitoyl-sn-glycero-3-phosphocholine (DPPC) in ethanol (5 mg/ml) for 15 min and then rinsed rapidly with 100 mM NaCl. Vesicle fusion was achieved by adding 20 µl of vesicles generated *via* extrusion in an Avanti mini-extruder (Figure 27 **A**) of 2 mg/ml DPPC in Milli-Q through 50 nm filters to the monolayer under 100 mM NaCl and incubating overnight at 25 °C. The setup of the filtering system can be seen in Figure 27 **C**.

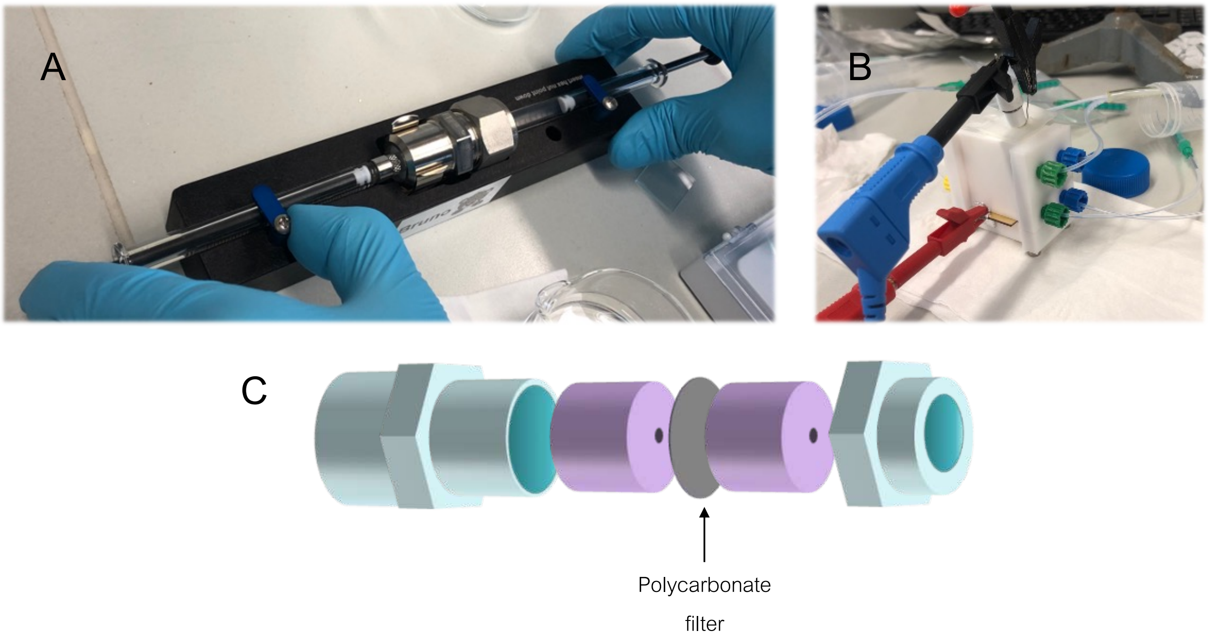

Figure 27: **A**: setup of the mini extruder to form vesicles, **B**: cell setup for EIS measurements with working electrode (red), counter electrode (black) and reference electrode (blue), **C**: setup of the polycarbonate filter (50 nm) in the mini-extruder

Depending on the solid substrate, different analytical methods for the determination of membrane properties are possible. For tBLMs, the usual substrate of choice is gold due to its stability and wide range of applicable analytical methods.[17] In this work, template striped gold was used as source of ultraflat gold-substrate.

Generally, the monolayer properties have a severe effect on the formed bilayer. Various sensitive techniques that are specific to the solid−liquid interface can be used to characterize the formed SAM. Surface characterization of the obtained functionalized gold substrates are realized using different techniques gaining chemical (X-ray photoelectron spectroscopy), structural (grazing incident X-ray diffraction, angle dependent X-ray photoelectron spectroscopy), topographical (AFM, scanning tunneling microscopy STM), electrochemical (CV, EIS) and kinetic (SPR) information.

For bilayers, electrochemical impedance spectroscopy is a tool for investigation of functions, physical and mechanical properties of the model membrane.[11]

3.1.6.1 Electrochemical impedance spectroscopy

Electrochemical impedance spectroscopy (EIS), an alternating current (AC) method, is a commonly used tool to study a planar bilayer and to obtain a characterization of electric properties of these model membrane systems.[11] EIS probes surface electrodynamics in the frequency scale spanning typically from 10^{-3} to 10^{6} Hz.[54] Measurements are usually conducted in a three-electrode set-up with the substrate as the working electrode.[19] The applied cell setup can be seen in Figure 27 **B**.

Some physical properties like capacitance or solution resistance can be obtained from the corresponding impedance spectra. Bode plots are often used for the presentation of EIS data. For detailed information it is necessary to model the spectra by a so-called equivalent electrochemical circuit (EEC).[11,54] Depending on the complexity of the membrane, different EECs are suitable, some examples are shown in Figure 28. EEC models are typically constructed on electrical components, such as resistors, capacitors and occasionally other special elements.[54] Typically, the lipid bilayer can be modeled by an RC element and the tether region can often be modeled by a single capacitor.[19]

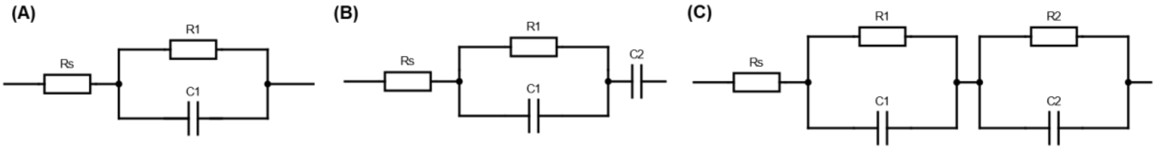

Figure 28: Exemplary equivalent electrical circuits to model EIS spectra

First EIS experiments of synthesized NHC-based tBLMs were performed. The main goal of this work was to prove the stability of the formed tBLM.

Figure 29 shows the EIS spectra and fitted data of a tBLM with **IIIb** as inner leaflet. The bilayer was formed by rapid solvent exchange of 1,2-dipalmitoyl-sn-glycero-3-phosphocholine (DPPC). Figure 29 clearly show that a stable bilayer was formed by applying a fully tethered tBLM with an NHC based inner leaflet. The spectra do not change significantly within 60 h under ambient conditions. In Table 3 the corresponding resistance and capacitance data are listed. The resistances are consistently high, implementing a high-quality bilayer.

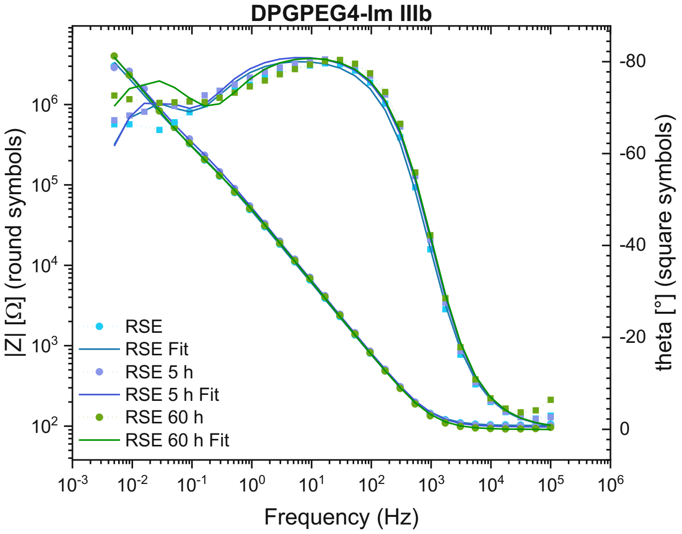

Figure 29: EIS spectra and fitted data of a bilayer of DPGPEG4Im (inner leaflet) and 1,2-dipalmitoyl-sn-glycero-3-phosphocholine (DPPC, outer leaflet) formed by RSE

Table 3: Area normalized impedance and capacitance data for fully tethered tBLM formed *via* RSE of **IIIb** as a function of the electrolyte composition

	resistance (MΩ)	**capacity (µF)**
after RSE	11	6.2
5 h after RSE	12	5.7
60 h after RSE	20	5.8

For comparison purposes, tBLMs were formed with the same system (**IIIb**) by vesicle fusion of DPPC lipids. The measured EIS spectra as well as the fitted data can be seen in Figure 30. Figure 30 **A** shows data a double layer formed by vesicle fusion of a monolayer that consists of 100 % DPGPEG$_4$-Im whereas Figure 30 **B** shows data obtained from a monolayer that was diluted with 20 % of an NHC-based spacer **XIV**. Table 4 shows the corresponding resistance and capacitance data of the formed bilayer. Compared to the data obtained from RSE, the capacity is about ten times higher, and resistance is lower by 10^{-2}-10^{-3} for both, the fully tethered and the sparsely tethered system. According to the obtained data it cannot surely be said that the formation of a bilayer was successful. Fundamental parameters for a successful application of tBLMs in a concept of biosensing is the incorporation of functional membrane proteins and the formation of pores. The effects of interaction of membrane and pore can then be detected by changes in the electrical properties using EIS.[11] Despite the low resistance values, valinomycin was integrated in the system as a potassium-ion transporter.

Valinomycin is a cyclic peptide (Figure 18), that can selectively transport alkali metal ions through membranes. The size of the cavity is suitable to K^+ ions, but too large for Na^+ or Li^+ ions including the hydration shell.

With valinomycin incorporated in the membrane, the resistance should be significantly lower in presence of a KCl electrolyte. When exchanging the electrolyte back to NaCl the resistance and capacity should be regenerated back to the original values. However, this was not the case for the fully or sparsely tethered system, indicating that ether the bilayer formation was not successful on firsthand or only a partial bilayer was formed *via* vesicle fusion.

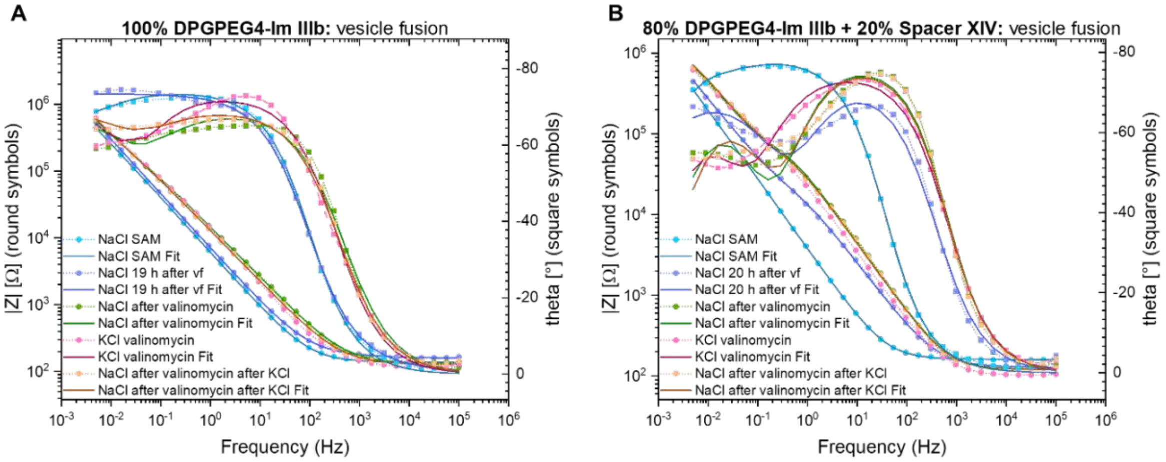

Figure 30: EIS spectra and fitted data of a bilayer of DPGPEG4Im (inner leaflet) and 1,2-dipalmitoyl-sn-glycero-3-phosphocholine (DPPC, outer leaflet) formed by vesicle fusion

Table 4: Area normalized impedance and capacitance data for fully tethered tBLM formed *via* vesicle fusion of **IIIb** as a function of the electrolyte composition

	100% DPGPEG$_4$Im		**80% DPGPEG$_4$Im + 20 %Spacer**	
	R$_1$ (MΩ)	CPE (µF)	R$_1$ (MΩ)	CPE (µF)
SAM	0.30	88	1.94	71
bilayer (NaCl)	0.04	7	4.73	31
valinomycin (NaCl)	0.05	48	1.78	27
valinomycin (KCl)	0.07	43	1.72	21
valinomycin (NaCl after KCl)	0.04	79	0.24	3

3.2 Conclusion and outlook

In conclusion, a synthetic route towards the formation of NHC-based precursors for the formation of monolayers on gold substrates was successfully designed. As a first step, two different glycerol lipids, namely DPG and DHDG, were prepared to then connect the OH-moiety with three different tethers (PEG$_3$, PEG$_4$ and PEG$_5$). With a set of six azide-precursors in hand, CuAAC reactions were performed with an imidazolium-based anchor group. Subsequent ion exchange towards the [OTf] masked NHCs gave the target molecules which were confirmed by NMR.

All six precursors were immobilized on gold surfaces using a mild base in methanolic solution under ambient conditions and analyzed *via* contact angle measurements. Additionally, a benzimidazolium-based NHC-precursor with *N,N*-diisopropyl groups was successfully synthesized and immobilized on a gold surface as well.

Contact angle measurements were performed and compared with CAs in literature. DPGPEG$_4$Im gave the highest CA of 93°, rendering this compound an interesting artificial lipid for surface modification. This immobilized molecule was analyzed on gold *via* further methods such as cyclic voltammetry and first EIS experiments. Gold coated Kapton was used as a substrate which made the reproducibility of the measurements difficult due to the low thickness and flexibility of the substrate. In further studies, these experiments need to be repeated using different substrates, for example gold coated glass slides or template stripped gold to obtain reliable results.

The elemental composition of a DPGPEG$_3$Im functionalized gold slide was confirmed *via* XPS measurements. The survey scan shows the elements Au, C, N and O which represents the elemental composition of DPGPEG$_3$Im. Additionally, an increase of the baseline can be observed in the survey scan, which is caused by inelastic scattered electrons at near-surface structures. That indicates the successful formation of a thin layer on the gold surface. The binding energies of the corresponding core elements C, N, O and Au, which were obtained from the respective high resolution XPS spectra, were similar to comparable compounds in literature.

Stability of the monolayers was tested *via* cyclic voltammetry. Compared to thiol-based SAMs, which show instability of the film under repeated electrochemical cycling,[29] the NHC-based SAMs were stable after 100 cycles and more. To further confirm the formation of a thin layer, cyclic voltammetry was applied to a clean gold slide which clearly showed reduction and oxidation of the applied redox probe $Fe(CN)_6^{3-}/Fe(CN)_6^{4-}$. For the functionalized substrate, no oxidation or reduction processes were observed, which shows that there is indeed a thin film on the surface. To show the importance of $KHCO_3$ as a mild base for the SAM formation process, another experiment without base was performed. In that case, a reduction and oxidation processes were observed as expected, indicating that a monolayer cannot be formed without presence of $KHCO_3$ and that NHCs are not physically adsorbed on the gold surface.

Furthermore, bilayers were formed using RSE and vesicle fusion with DPGPEG$_4$Im as inner leaflet. First EIS experiments of those bilayers were performed. EIS data of the bilayer formation *via* RSE gave consistently high resistances of up to 20 MΩ and a capacitance of about 6 µF which indicates the formation of a high-quality bilayer. It was also shown that the formed bilayer was stable under ambient conditions over several days. To confirm the formation of a bilayer further experiments such as AFM measurements of neutron scattering experiments have to be performed. However, bilayers formed *via* vesicle fusion did not give good results regarding resistance and capacity. Additionally, the incorporation of valinomycin did not show the expected effect of the reversible exchange of electrolyte. Since EIS is an error prone analytical method, further experiments are crucial in order to confirm the reliability of the previously presented results.

To prepare sparsely tethered bilayers, an NHC-based spacer molecule was successfully synthesized in a three-step protocol. Further experiments of sparsely tethered bilayers using different mixtures of the prepared anchor lipids and spacer molecule need to be done, to show the influence of the surface density of the monolayer on the membrane properties.

In addition to the presented NHC-based anchor lipids, two thiol-based reference systems with two different tether lengths (PEG_6 and PEG_8) were synthesized. These systems can either be used as reference system the designed NHC-based anchor lipids and for the integration of odorant binding proteins. In future projects, these systems can be used in addition to the presented reference DPTL to show further influence of the PEG-chain length for the formation of a high-quality bilayer.

Additionally, it is necessary to confirm the formation of a bilayer *via* other analytical methods besides EIS such as AFM measurements or neutron scattering. If the formation of an artificial membrane can be confirmed, optimization can be done for EIS measurements. In addition to that, surface plasmon resonance (SPR) fluorescence flow cell experiments will be performed by incorporating Nile red, which is a dye that is strongly fluorescent in lipid environment (Figure 31).

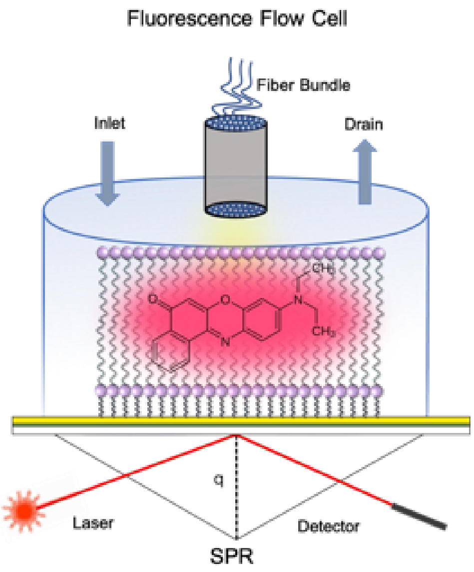

Figure 31: SPR-flow cell experiments by incorporating Nile red into the formed membrane.

4 Experimental part

4.1 Materials and Solvents

4.1.1 Reactants and Solvents

Chemicals were commercially purchased and used without any purification unless otherwise stated. Synthesized compounds were tested for purity with NMR.

Anhydrous solvents were purified on PURESOLV-system (it-innovative technology inc.).

4.1.2 Chromatographic methods

Thin layer chromatography was performed using TLC plates on aluminum support (Merck, silica gel 60, fluorescence indicator F254).

Column Chromatography was performed on *Büchi Sepacore TM Flash System* using silica gel from Merck (40-63 µm) and distilled or redistilled solvents were used.

4.1.3 GC/MS

For GC/MS analysis a GC/MS coupling from Thermo Finnigan was used. The device was equipped with a Focus gas chromatograph including a BGB5 column *(l = 30 m,* d_i *= 0.25 mm, 0.25 µm film, achiral)* and a DSQ II quadrupol mass spectrometer.

4.1.4 LC/MS

LCMS experiments were conducted on the following system: Shimadzu Nexera UHPLC/MS System (2x Nexera LC-30AD Solvent Delivery Unit, Shimadzu SIL-30AC UHPLC Autosampler, Shimadzu DGU-20A3R/DGU-20A5R HPLC Degassing Unit, Shimadzu CBM-20A HPLC System Controller, Shimadzu CTO-20AC Prominence HPLC Column Oven, Shimadzu SPD-20A Prominence HPLC UV-Vis Detector, Shimadzu RF-20Axs Fluorescence Detector, Shimadzu LCMS-2020 Single Quadrupole Liquid Chromatograph Mass Spectrometer (LC/MS)).

4.1.5 NMR-spectroscopy

Nuclear magnetic resonance (NMR) spectra were obtained by using a Bruker Avance III HD 600 MHz with cryo probe or Avance III HD 400 MHz Fourier transform spectrometer operating at the following frequencies: Avance III HD 600 MHz: 600.2 MHz (^{1}H), 150.9 MHz (^{13}C) and 565 MHz (^{19}F); Avance III HD 400 MHz: 400.1 MHz (^{1}H), 100.6 MHz (^{13}C) and 376 MHz (^{19}F). The ^{1}H and ^{13}C shifts are reported in d units, parts per million (ppm) downfield from tetramethylsilane by using residual solvent signals for calibration. Coupling constants are reported in Hertz; multiplicity of signals is indicated by using following abbreviations: s=singlet, d=doublet, t=triplet, q=quartet, quin=quintet. The multiplicity of the ^{13}C signals were obtained by measuring JMOD spectra.

4.1.6 Mono- and bilayer formation

Gold slides were cleaned using a piranha solution (H_2SO_4/H_2O_2, 3:1 v/v) for 10 min, washing by immersion in HPLC water for 10 min and UV/ozone surface cleaning for 15 min. Precleaned gold slides were rinsed with MeOH, dried under Ar gas and immersed in a 10 mM methanolic solution of lipid upon addition of 1 eq. $KHCO_3$ for 24 h, rinsed thoroughly with 100% methanol, and dried under a stream of Ar. Bilayers were formed *via* rapid solvent exchange or vesicle fusion. For the first process, the monolayer is incubated under DPPC in ethanol (5 mg/mL) for 15 min and then rinsed rapidly with 100 mM NaCl. Vesicle fusion was achieved by adding 20 µL of vesicles generated *via* extrusion (Avanti mini-extruder) of 2 mg/mL DPPC in Milli-Q through 50 nm filters to the monolayer under 100 mM NaCl and incubating overnight at 25 °C.

4.1.7 XPS

X-ray photoelectron spectroscopy analyses were performed with a Versa Probe II Scanning XPS Microprobe spectrometer (Physical Electronics GmbH). The measurements were done in Large Area mode with a 100 µm Al X-ray spot rasterized over a 1400 × 200 µm area, at a power of 100 W. Wide scans and detailed spectra were acquired in fixed analyzer transmission mode with a pass energy of 117.40 and 46.95 eV, respectively. An electron gun was used for charge compensation (1.0 V 20.0 µA). Data processing was performed using the MultiPak software v. 9.5.0.8.

4.1.8 Contact angle

Contact angles and surface/interface tensions were measured on a Krüss DSA 30 contact angle goniometer equipped with a CCD video camera (resolution 780 × 582 pixel, speed 60 fps). Static contact angles were measured by putting a drop of water onto the sample surface, recording the drop image, and determining the contact angle using the Young–Laplace method ($\theta > 10°$) of the instrument software.

4.1.9 Electrochemical Characterization

Cyclic voltammetry of functionalized gold substrates was performed with an Autolab potentiostat (PGSTAT204) and a three-electrode set-up using the gold substrate as a working electrode, a platin wire (37 · 0.5 mm) as the counter electrode and an Ag/AgCl reference electrode (35 · 0.5 mm). The electrochemical cycling experiments were performed in aqueous media of 1 mM · 3 H_2O $K_4[Fe(CN)_6]$ (Sigma Aldrich, 98.5%) and 0.1 M KCl (Fluka, puriss p.a.). All electrolyte solutions were degassed with an Ar balloon for 20 min prior usage. Details of the applied electrochemical parameters are described in the corresponding experiment.

Electrochemical impedance spectroscopy was performed with an Autolab potentiostat (PGSTAT204) and a FRA32M module. Data were recorded between 3 mHz and 100 kHz with 0 V potential versus Ag/AgCl at a 10 mV AC modulation amplitude. Raw data were analyzed using ZView (version3.3B by Scribner Associates) and fitted to an equivalent circuit comprising resistors and constant phase elements with final values normalized to an electrode area of 0.283 cm^2. All measurements were taken under 100 mM NaCl or 100 mM KCl solution. To exchange the electrolyte, the cell was rinsed with 5 cell volumes of the new electrolyte.

4.2 Synthesis of NHC-based lipid tails

4.2.1 1-Bromo-3,7,11,15-tetramethylhexadecane (**2**)

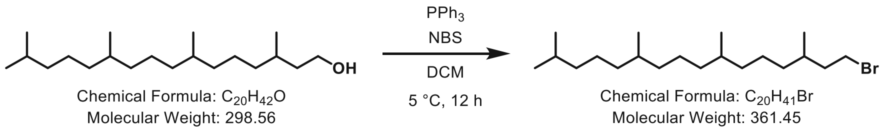

1 **2**

Scheme 20: Synthesis of **2**

1 (3.013 g, 10 mmol, 1 eq.) was dissolved in 40 ml anh. DCM and flushed with Ar. PPh_3 (3.441 g, 13 mmol, 1.3 eq.) was added and the mixture was cooled to 5 °C. NBS (3.592 g, 20 mmol, 2 eq.) was added in portions. After the completed addition, the reaction mixture was allowed to warm to room temperature and stirred for 12 h. The mixture was poured to PE (350 ml) and the precipitate was removed by filtration. After removal of the solvent, the crude product was filtered over a silica plug using PE as a solvent yielding 3.523 g (97 %) of **2** as a clear oil.

^{1}H NMR (400 MHz, $CDCl_3$) δ 3.52 – 3.35 (m, 2H), 1.74 – 1.57 (m, 2H), 1.57 – 1.47 (m, 2H), 1.42 – 1.01 (m, 20H), 0.92 – 0.81 (m, 15H).

4.2.2 ((2,3-Bis((3,7,11,15-tetramethylhexadecyl)oxy)propoxy)methyl)benzene (**4**)

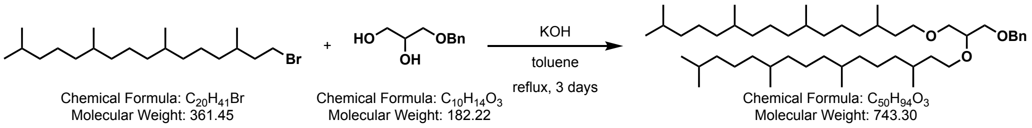

2 **3** **4**

Scheme 21: Synthesis of **4**

2 (1.807 g, 5 mmol, 5.8 eq.) was dissolved in 45 ml toluene, **3** (157 mg, 0.86 mmol, 1 eq.) and predried KOH (425 mg, 7.58 mmol, 8.8 eq.) was added in a Dean Stark apparatus. The reaction was refluxed for 3 days. After cooling to room temperature, the reaction mixture was diluted with hexanes and washed twice with H_2O. The combined aqueous solutions were then extracted with PE, dried over sodium sulfate, and dried in vacuo. The crude product was purified over column chromatography yielding 447 mg (70 %) of **4** as a colorless oil.

^{1}H NMR (600 MHz, $CDCl_3$) δ 7.37 – 7.30 (m, 5H), 4.55 (s, 2H), 3.66 – 3.42 (m, 9H), 1.56 – 1.47 (m, 4H), 1.42 – 0.99 (m, 42H), 0.91 – 0.81 (m, 30H).

4.2.3 2,3-Bis((3,7,11,15-tetramethylhexadecyl)oxy)propan-1-ol (**5**)

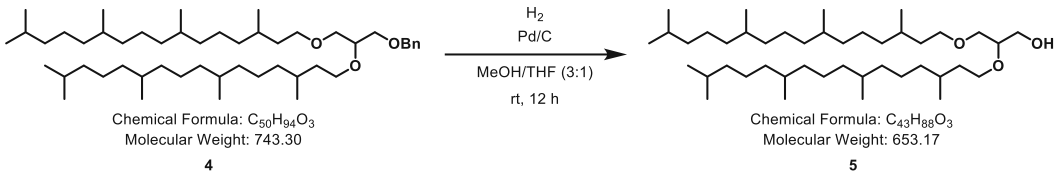

Scheme 22: Synthesis of **5**

4 (365 mg, 0.49 mmol, 1 eq.) was added to a flame dried vial, flushed with Ar, and dissolved in a 3:1 mixture of anh. MeOH/THF (2 ml). A spatula tip of Pd/C (10 %) was added, and the Ar balloon was exchanged with a H_2 balloon. The reaction was stirred at room temperature for 12 h. After completeness of the reaction the catalyst was removed through celite filtration. The solvent was then removed in vacuo yielding 273 mg (85 %) of **5** as a colorless oil.

^{1}H NMR (400 MHz, $CDCl_3$) δ 3.78 – 3.39 (m, 9H), 2.17 – 2.13 (t, 1H), 1.70 – 1.44 (m, 4H), 1.44 – 0.98 (m, 44H), 0.94 – 0.75 (m, 30H).

4.2.4 ((2,3-Bis(hexadecyloxy)propoxy)methyl)benzene (**10**)

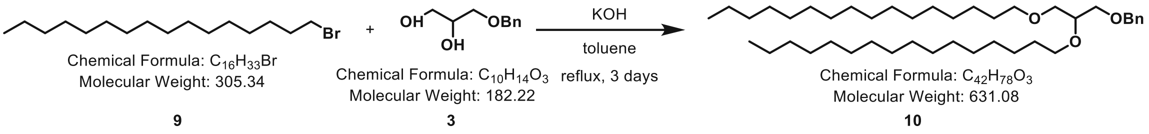

Scheme 23: Synthesis of **10**

9 (10 g, 33 mmol, 5.8 eq.) was dissolved in 80 ml toluene, **3** (1.029 g, 5.6 mmol, 1 eq.) and predried KOH (2.788 g, 50 mmol, 8.8 eq.) was added in a Dean Stark apparatus. The reaction was refluxed for 3 days. After cooling to room temperature, the reaction mixture was diluted with hexanes and washed twice with H_2O. The combined aqueous solutions were then extracted with PE, dried over sodium sulfate, and dried in vacuo. The crude product was purified over column chromatography yielding 3.020 g (85 %) of a colorless oil.

^{1}H NMR (400 MHz, $CDCl_3$) δ 7.37 – 7.27 (m, 5H), 4.55 (s, 2H), 3.63 – 3.35 (m, 9H), 1.60 – 1.51 (m, 4H), 1.35 – 1.22 (m, 52H), 0.91 – 0.85 (m, 6H).

4.2.5 2,3-Bis(hexadecyloxy)propan-1-ol (**11**)

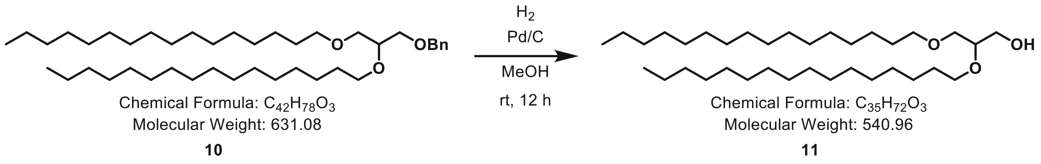

Scheme 24: Synthesis of **11**

10 (3.020 g, 4.8 mmol, 1 eq.) was added to a flame dried vial, flushed with Ar, and dissolved in 25 ml of EtOAc. A 300 mg Pd/C (10 %) was added, and the Ar balloon was exchanged with a H_2 balloon. The reaction was stirred at room temperature for 12 h. After completeness of the reaction the catalyst was removed through celite filtration. The crude product was purified over column chromatography (PE/EtOAc 10-20 %) yielding 2.392 mg (92 %) of a white solid.

^{1}**H NMR** (400 MHz, $CDCl_3$) δ 3.76 – 3.38 (m, 9H), 1.87 (bs, 1H), 1.63 – 1.50 (m, 4H), 1.32 – 1.21 (m, 52H), 0.94 – 0.83 (m, 6H).

4.3 Synthesis of tethers

4.3.1 2-(2-(2-(2-Azidoethoxy)ethoxy)ethoxy)ethyl 4-methylbenzenesulfonate (**7a**)

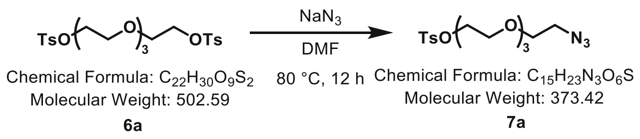

Scheme 25: Synthesis of **7a**

6a (3.559 g, 7.08 mmol, 1 eq.) and NaN_3 (495 mg, 7.612 mmol, 1.07 eq.) were added to a flask, dissolved in 45 ml EtOH, and stirred at 80 °C for 12 h. After completeness of the reaction, the mixture was poured on ice and was then extracted with EtOAc three times. The combined organic layers were washed with brine and dried over Na_2SO_4 The crude product was purified *via* column chromatography (PE/acetone 15 %) to yield 1.00 g (34 %) of a colorless oil.

^{1}**H NMR** (600 MHz, $CDCl_3$) δ 7.77 (d, *J* = 8.3 Hz, 2H), 7.32 (d, *J* = 8.3 Hz, 2H), 4.14 (t, *J* = 5.0 Hz, 1H), 3.69 – 3.54 (m, 12H), 3.36 (t, *J* = 5.1 Hz, 2H), 2.43 (s, 3H).

4.3.2 14-Azido-3,6,9,12-tetraoxatetradecyl 4-methylbenzenesulfonate (**7b**)

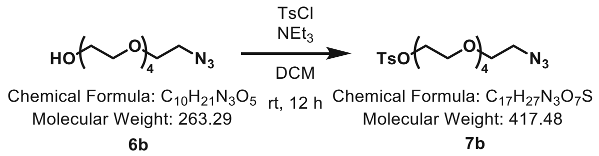

Scheme 26: Synthesis of **7b**

6b (500 mg, 1.90 mmol, 1 eq.) was dissolved in 6 ml anh. DCM and the vial was flushed with Ar. The solution was cooled to 0 °C and *p*TsCl (724 mg, 3.80 mmol, 2 eq.), Ag_2O (880 mg, 3.80 mmol, 2 eq.) and KI (62 mg, 0.374 mmol, 0.2 eq.) were added. The reaction was allowed to warm to room temperature and stirred for 12 h. The mixture was filtered over celite and the crude product was then purified over flash column chromatography (DCM/MeOH 0-50 %) to yield 760 mg (96 %) of pure product.

^{1}**H NMR** (600 MHz, $CDCl_3$) δ 7.79 (d, *J* = 8.3, 2H), 7.33 (d, *J* = 8.3 Hz, 2H), 4.17 – 4.11 (m, 2H), 3.67 – 3.54 (m, 16H), 3.40 – 3.30 (m, 2H), 2.44 (s, 3H).

4.3.3 17-Azido-3,6,9,12,15-pentaoxaheptadecyl 4-methylbenzenesulfonate (**7c**)

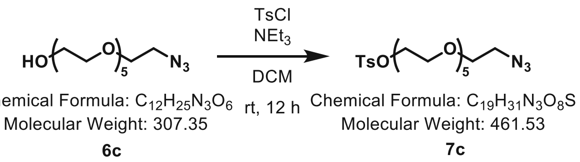

Scheme 27: Synthesis of **7c**

6c (806 mg, 2.62 mmol, 1 eq.) was dissolved in 10 ml anh. DCM and the vial was flushed with Ar. The solution was cooled to 0 °C and pTsCl (1 g, 5.25 mmol, 2 eq.), Ag_2O (1.215 g, 5.2 mmol, 2 eq.) and KI (87 mg, 0.525 mmol, 0.2 eq.) were added. The reaction was allowed to warm to room temperature and stirred for 12 h. The mixture was filtered over celite and the crude product was then purified over flash column chromatography (DCM/MeOH 0-50 %) to yield 846 mg (70 %) of pure product.

^{1}H NMR (400 MHz, $CDCl_3$) δ 7.77 (d, *J* = 8.3 Hz, 2H), 7.32 (d, *J* = 8.3 Hz, 2H), 4.18 – 4.08 (m, 2H), 3.69 – 3.49 (m, 20H), 3.35 (t, *J* = 5.1 Hz, 2H), 2.42 (s, 3H).

4.4 Introduction of lipid tails to tether molecules

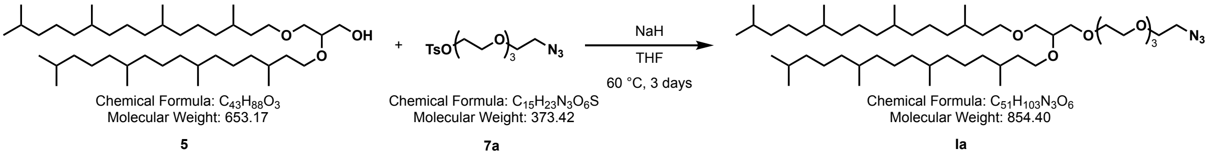

Scheme 28: Synthesis of **Ia**

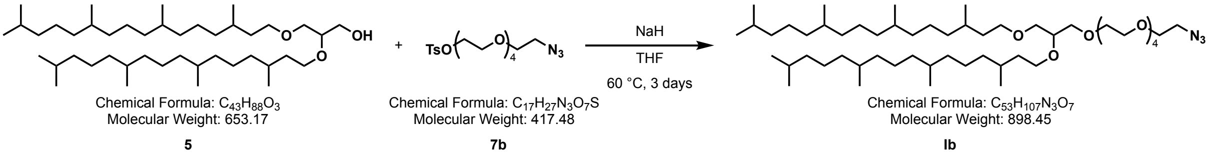

Scheme 29: Synthesis of **Ib**

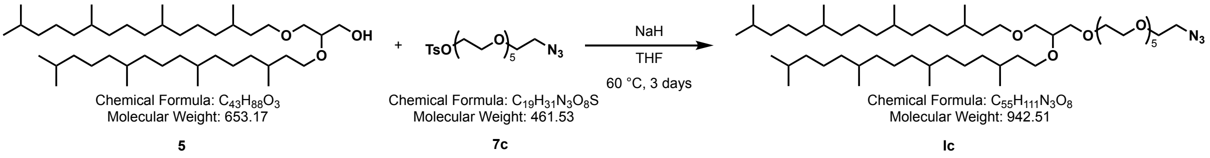

Scheme 30: Synthesis of **Ic**

NaH 60 % dispersion in mineral oil (0.8 mmol, 2 eq.) was dispersed in 2 ml anh. THF in a flame dried vial. **5** (0.4 mmol, 1 eq.) was dissolved in 1 ml THF and added dropwise to the suspension. The mixture was then stirred at room temperature for about 90 minutes. 7 (0.64 mmol, 1.6 eq.) was dissolved in 500 µl THF and slowly added to the mixture. The reaction was stirred for 3 days at 60 °C. After completeness of the reaction, die solvent was removed by evaporation. The residue was taken up in water and DCM and added to a separation funnel. The aqueous phase was extracted with DCM six times. Combined organic layers were then washed with brine, dried over sodium sulfate and solvent was evaporated. The crude product was purified over column chromatography (DCM/MeOH 0-15 %).

1-Azido-19,23,27,31-tetramethyl-14-((3,7,11,15-tetramethylhexadecyl)oxy)-3,6,9,12,16-pentaoxadotriacontane (**Ia**): 220 mg (77 %) of a colorless oil

^{1}H NMR (400 MHz, $CDCl_3$) δ 3.71 – 3.42 (m, 23H), 3.38 (t, *J* = 5.1 Hz, 2H), 1.56 – 1.47 (m, 4H), 1.40 – 0.98 (m, 44H), 0.89 – 0.81 (m, 30H).

1-Azido-22,26,30,34-tetramethyl-17-((3,7,11,15-tetramethylhexadecyl)oxy)-3,6,9,12,15,19-hexaoxapentatriacontane (**Ib**): 200 mg (53%) of a colorless oil

^{1}H NMR (400 MHz, $CDCl_3$) δ 3.70 – 3.42 (m, 29H), 3.39 (d, *J* = 4.7 Hz, 2H), 1.52 (p, *J* = 6.6 Hz, 4H), 1.40 – 0.97 (m, 44H), 0.92 – 0.81 (m, 30H).

1-Azido-25,29,33,37-tetramethyl-20-((3,7,11,15-tetramethylhexadecyl)oxy)-3,6,9,12,15,18,22-heptaoxaoctatriacontane (**Ic**): 260 mg (82%) of a colorless oil

^{1}H NMR (400 MHz, $CDCl_3$) δ 3.69 – 3.43 (m, 31H), 3.38 (t, *J* = 5.1 Hz, 2H), 1.56 – 1.47 (m, 4H), 1.42 – 1.01 (m, 44H), 0.88 – 0.81 (m, 30H).

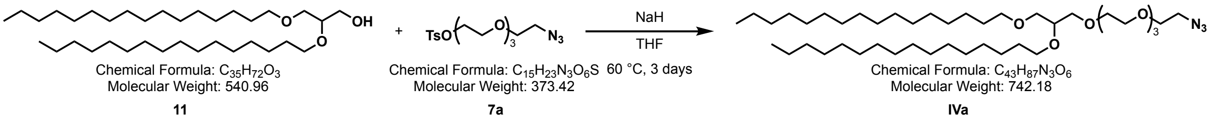

Scheme 31: Synthesis of **IVa**

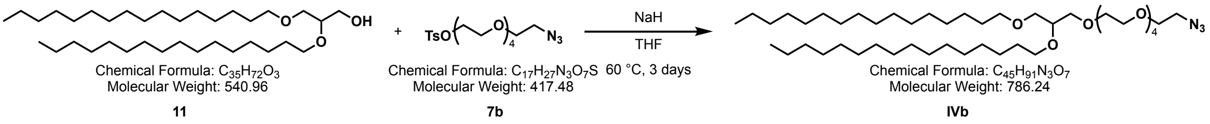

Scheme 32: Synthesis of **IVb**

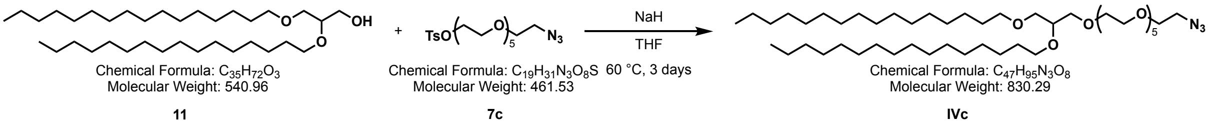

Scheme 33: Synthesis of **IVc**

NaH 60 % dispersion in mineral oil (0.8 mmol, 2 eq.) was dispersed in 2 ml anh. THF in a flame dried vial. **11** (0.4 mmol, 1 eq.) was dissolved in 1 ml THF and added dropwise to the suspension. The mixture was then stirred at room temperature for about 90 minutes. **7** (0.64 mmol, 1.6 eq.) was dissolved in 500 µl THF and slowly added to the mixture. The reaction was stirred for 3 days at 60 °C. After completeness of the reaction, die solvent was removed by evaporation. The residue was taken up in water and DCM and added to a separation funnel. The aqueous phase was extracted with DCM six times. Combined organic layers were then washed with brine, dried over sodium sulfate and solvent was evaporated. The crude product was purified over column chromatography (DCM/MeOH 0-15 %).

1-Azido-14-(hexadecyloxy)-3,6,9,12,16-pentaoxadotriacontane (**IVa**): 283 mg (95 %) of a white waxy solid

^{1}H NMR (400 MHz, $CDCl_3$) δ 3.78 – 3.26 (m, 25H), 1.58 – 1.44 (m, 4H), 1.35 – 1.15 (m, 52H), 1.01 – 0.73 (m, 6H).

1-Azido-17-(hexadecyloxy)-3,6,9,12,15,19-hexaoxapentatriacontane (**IVb**): 316 mg (90 %) of a white waxy solid

^{1}H NMR (400 MHz, $CDCl_3$) δ 3.72 – 3.27 (m, 33H), 1.54 (t, *J* = 7.0 Hz, 4H), 1.30 – 1.12 (m, 52H), 0.91 – 0.78 (m, 6H).

1-Azido-20-(hexadecyloxy)-3,6,9,12,15,18,22-heptaoxaoctatriacontane (**IVc**): 271 mg (82 %) of a white waxy solid

^{1}H NMR (400 MHz, $CDCl_3$) δ 3.70 – 3.34 (m, 33H), 1.61 – 1.49 (m, 4H), 1.32 – 1.14 (m, 52H), 0.94 – 0.82 (m, 6H).

4.5 Synthesis of the anchor groups

4.5.1 Imidazolium based anchor group

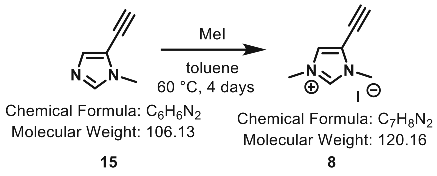

Scheme 34: Synthesis of **8**

15 (915 mg, 8.86 mmol, 1 eq.) was dissolved in 22 ml degassed toluene and flushed with Ar. MeI (1.895 g, 13.35 mmol, 1.55 eq.) was added and the reaction was heated to 60 °C. After completeness of the reaction, the precipitate was separated *via* filtration and washed with cold toluene. The residue yielded in 2.125 mg (99 %) product.

^{1}H NMR (400 MHz, $CDCl_3$) δ 10.44 (s, 1H), 7.46 (s, 1H), 4.12 (s, 3H), 4.03 (s, 3H), 3.70 (s, 1H).

4.5.2 Benzimidazolium based anchor group

4.5.2.1 5-((Trimethylsilyl)ethynyl)-1*H*-benzo[*d*]imidazole (**17**)

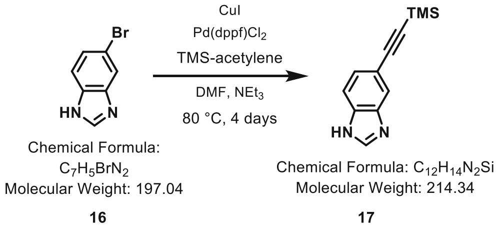

Scheme 35: Synthesis of **17**

16 (500 mg, 2.5 mmol, 1 eq.), NEt$_3$ (1.669 g, 16.5 mmol, 6.5 eq.) and DMF (2.3 ml) was added to a vial and degassed with Ar gas. CuI (38 mg, 0.2 mmol, 0.08 eq.), Pd(dppf)Cl$_2$ (37 mg, 0.05 mmol, 0.02 eq.) and TMS-acetylene (498 mg, 5 mmol, 2 eq.) was added. The reaction was stirred at room temperature for 12 h. On the next day, the reaction was heated to 80 °C and stirred for 4 days. After completeness of the reaction the mixture war poured on ice and pH was adjusted to 6 using 2 N HCl. Phases were separated in a separatory funnel and the aqueous phase was extracted three times with DCM. The combined organic layers were washed with brine and dried over Na$_2$SO$_4$. Solvent was evaporated and the crude product was purified *via* column chromatography (DCM/MeOH 0-10 %). The product was then recrystallized from hexane yielding 118 mg (22 %) as a brown solid.

^{1}H NMR (400 MHz, CDCl$_3$) δ 8.14 (s, 1H), 7.80 (s, 1H), 7.59 (s, 1H), 7.42 (d, *J* = 8.0 Hz, 1H), 0.31 – 0.21 (m, 9H).

4.5.2.2 5-Ethynyl-1-isopropyl-1*H*-benzo[*d*]imidazole (**Xa**)

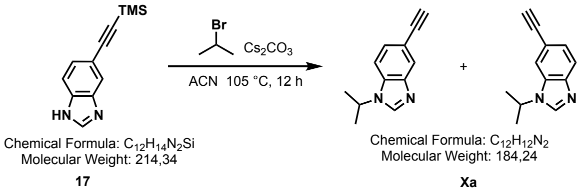

Scheme 36: Synthesis of **Xa**

17 (200 mg, 0.93 mmol, 1 eq.) was dissolved in 7 ml ACN and flushed with Ar. Cs$_2$CO$_3$ (493 mg, 1.51 mmol, 1.62 eq.) was added and 2-bromopropane (324 mg, 2.64 mmol, 2.83 mmol) was added dropwise. The reaction was stirred at 105 °C for 12 h. The mixture was filtered over a celite plug and solvent was evaporated. The crude product was purified *via* column chromatography (DCM/MeOH 2-5 %) to yield 140 mg (81 %) of a yellow solid.

The TMS group was deprotected during workup of the reaction to obtain **Xa**.

^{1}**H NMR** (400 MHz, $CDCl_3$) δ 8.09 (d, *J* = 5.8 Hz, 2H), 7.98 (t, *J* = 1.0 Hz, 1H), 7.75 (dd, *J* = 8.4, 0.7 Hz, 1H), 7.61 (t, *J* = 1.0 Hz, 1H), 7.47 – 7.32 (m, 2H), 3.09 (s, 1H), 3.05 (s, 1H), 1.63 (dd, *J* = 6.8, 1.7 Hz, 12H).

4.5.2.3 5-Ethynyl-1,3-diisopropyl-1*H*-3‘4-benzo[*d*]imidazole iodide (**X**)

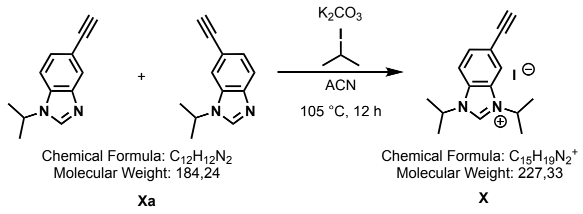

Scheme 37: Synthesis of **X**

Xa (56 mg, 0.30 mmol, 1 eq.) and K_2CO_3 (46 mg, 0.33 mmol, 1.1 eq.) were added to a vial, dissolved in 2 ml ACN and flushed with Ar. The, 2-iodopropane (206 mg, 1.21 mmol, 4 eq.) was added dropwise and the reaction was stirred at 90 °C for 12 h. The reaction was extracted with DCM and water. Combined organic layers were washed with brine and dried over Na_2SO_4. The crude product was purified *via* column chromatography (DCM/MeOH 5 %) to yield 65 mg (61 %) of pure product.

^{1}**H NMR** (400 MHz, $CDCl_3$) δ 10.90 (s, 1H), 7.89 – 7.77 (m, 2H), 7.75 – 7.67 (m, 1H), 5.20 (m, 2H), 1.85 (dd, *J* = 6.8, 1.1 Hz, 12H).

4.5.3 Multidentate anchor group

4.5.3.1 1,2-Bis((5-ethynyl-1*H*-benzo[*d*]imidazol-1-yl)methyl)benzene (**XVI**)

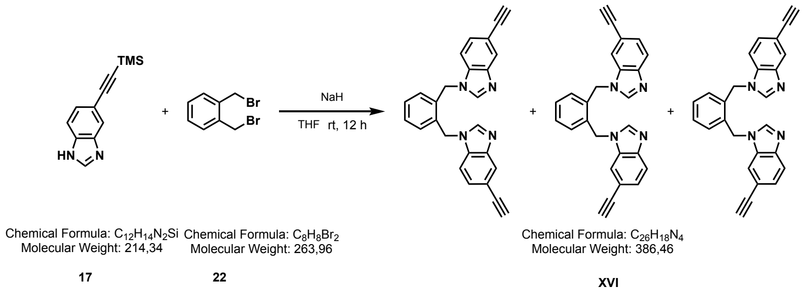

Scheme 38: Synthesis of **XVI**

17 (118 mg, 0.55 mmol, 2 eq.) was dissolved in 3.5 ml THF and flushed with Ar. NaH 60 % dispersion in mineral oil (17 mg, 0.72 mmol, 2.6 eq.) was added and stirred for 20 min, until no gas formation was observed. **22** (73 mg, 0.28 mmol, 1 eq.) was dissolved in 500 µl THF and added dropwise. The reaction was stirred at room temperature for 12 h. Upon completeness of the reaction, the solvent was evaporated. The residue was transferred in a separatory funnel using H_2O and EtOAc. The aqueous layer was extracted with EtOAc three times. Combined organic layers were washed with brine and dried over Na_2SO_4. After evaporation, the crude product was purified *via* column chromatography (DCM/MeOH 1-20 %) to yield 73 mg (67 %) of the pure product.

^{1}H NMR (400 MHz, $CDCl_3$) δ 8.00 (s, 1H), 7.80 (m, 2H), 7.48 – 7.28 (m, 4H), 7.10 – 6.98 (m, 2H), 5.29 (s, 3H), 5.27 (s, 1H), 3.09 – 3.01 (m, 1H), 2.03 (s, 1H).

4.6 Connection of anchor groups with lipid-PEG azides *via* CuAAC

4.6.1 DPG based anchor lipids

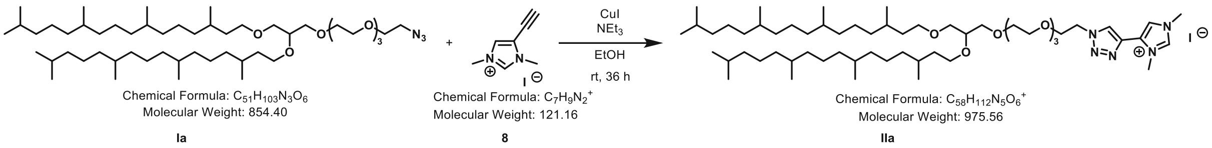

Scheme 39: Synthesis of **IIa**

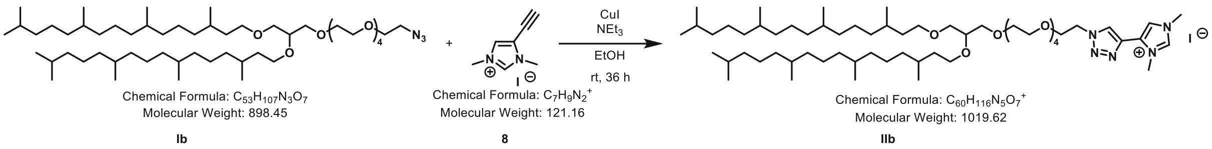

Scheme 40: Synthesis of **IIb**

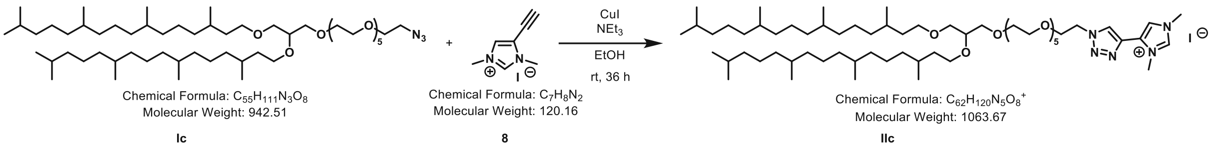

Scheme 41: Synthesis of **IIc**

Ia-c (0.1 mmol, 1 eq.) was dissolved in 1 ml degassed EtOH. CuI (6 mg, 0.03 mmol, 0.3 eq.) was added. **8** (13 mg, 0.11 mmol, 1.1 eq.) was dissolved in 1 ml degassed EtOH and added to the mixture. NEt_3 (12 mg, 0.12 mmol, 1.2 eq.) was added *via* a septum and the reaction was stirred at rt for 36 h. After completeness of the reaction, the solvent was evaporated. The residue was taken up in MeOH and filtered over a silica plug. After evaporation of the solvent, the crude product was purified *via* column chromatography (DCM/MeOH 1-9%) to yield the product as yellow oil.

1,3-Dimethyl-4-(1-(19,23,27,31-tetramethyl-14-((3,7,11,15-tetramethylhexadecyl)oxy)-3,6,9,12,16-pentaoxadotriacontyl)-1*H*-1,2,3-triazol-4-yl)-1*H*-imidazol-3-ium iodide (**IIa**): 20 mg (16 %)

^{1}H NMR (600 MHz, $CDCl_3$) δ 10.03 (s, 1H), 8.80 (s, 1H), 7.98 (s, 1H), 4.72 – 4.66 (m, 2H), 4.22 (s, 3H), 4.10 (s, 3H), 4.00 – 3.94 (m, 2H), 3.67 – 3.38 (m, 19H), 1.52 – 1.45 (m, 4H), 1.37 – 0.95 (m, 44H), 0.86 – 0.79 (m, 30H).

1,3-Dimethyl-4-(1-(22,26,30,34-tetramethyl-17-((3,7,11,15-tetramethylhexadecyl)oxy)-3,6,9,12,15,19-hexaoxapentatriacontyl)-1*H*-1,2,3-triazol-4-yl)-1*H*-imidazol-3-ium iodide (**IIb**): Yield: 25 mg (25 %)

^{1}H NMR (400 MHz, $CDCl_3$) δ 10.08 (s, 1H), 8.62 (s, 1H), 7.83 (s, 1H), 4.71 – 4.65 (m, 2H), 4.23 (s, 3H), 4.11 (s, 3H), 3.95 (t, *J* = 4.9 Hz, 2H), 3.74 – 3.33 (m, 25H), 1.59 – 1.43 (m, 4H), 1.35 – 1.01 (m, 44H), 0.94 – 0.73 (m, 30H).

1,3-Dimethyl-4-(1-(25,29,33,37-tetramethyl-20-((3,7,11,15-tetramethylhexadecyl)oxy)-3,6,9,12,15,18,22-heptaoxaoctatriacontyl)-1*H*-1,2,3-triazol-4-yl)-1*H*-imidazol-3-ium iodide (**IIc**): Yield: 57 mg (48 %)

^{1}H NMR (400 MHz, $CDCl_3$) δ 10.06 (s, 1H), 8.48 (s, 1H), 7.74 (s, 1H), 4.71 – 4.61 (m, 2H), 4.21 (s, 3H), 4.11 (s, 3H), 3.92 (d, *J* = 5.1 Hz, 2H), 3.70 – 3.37 (m, 29H), 1.56 – 1.45 (m, 4H), 1.40 – 1.00 (m, 44H), 0.91 – 0.81 (m, 30H).

4.6.2 DHDG based anchor lipids

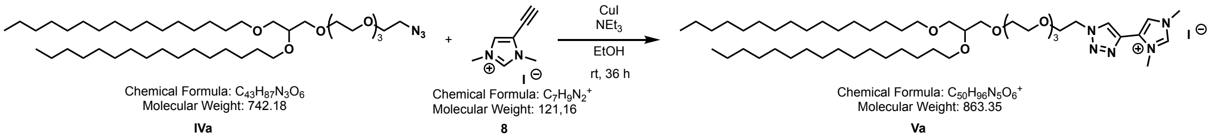

Scheme 42: Synthesis of **Va**

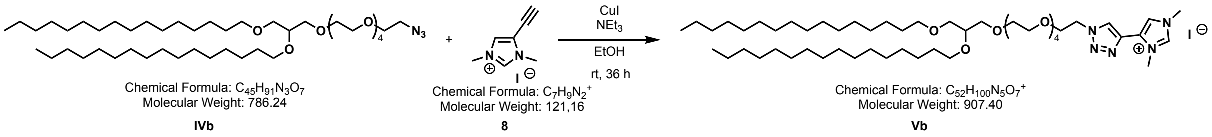

Scheme 43: Synthesis of **Vb**

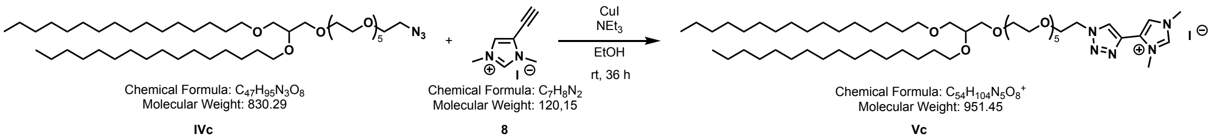

Scheme 44: Synthesis of **Vc**

IVa-c (0.1 mmol, 1 eq.) was dissolved in 1 ml degassed EtOH. CuI (6 mg, 0.03 mmol, 0.3 eq.) was added. **8** (13 mg, 0.11 mmol, 1.1 eq.) was dissolved in 1 ml degassed EtOH and added to the mixture. NEt_3 (12 mg, 0.12 mmol, 1.2 eq.) was added *via* a septum and the reaction was stirred at rt for 36 h. After completeness of the reaction, the solvent was evaporated. The residue was taken up in MeOH and filtered over a silica plug. After evaporation of the solvent, the crude product was purified *via* column chromatography (DCM/MeOH 1-9%) to yield the product as yellow oil.

4-(1-(14-(Hexadecyloxy)-3,6,9,12,16-pentaoxadotriacontyl)-1*H*-1,2,3-triazol-4-yl)-1,3-dimethyl-1*H*-imidazol-3-ium iodide (**Va**): Yield: 11 mg (13 %)

^{1}H NMR (400 MHz, $CDCl_3$) δ 9.91 (s, 1H), 8.50 (s, 1H), 7.82 (s, 1H), 4.65 (t, *J* = 5.6 Hz, 2H), 4.21 (s, 3H), 4.17 (s, 3H), 4.00 (t, *J* = 5.6 Hz, 2H), 3.71 – 3.33 (m, 21H), 1.57 – 1.49 (m, 4H), 1.33 – 1.10 (m, 52H), 0.97 – 0.76 (m, 6H).

4-(1-(17-(Hexadecyloxy)-3,6,9,12,15,19-hexaoxapentatriacontyl)-1*H*-1,2,3-triazol-4-yl)-1,3-dimethyl-1*H*-imidazol-3-ium iodide (**Vb**): Yield: 36 mg (35 %)

^{1}H NMR (400 MHz, $CDCl_3$) δ 10.06 (s, 1H), 8.50 (s, 1H), 7.79 (s, 1H), 4.66 (t, *J* = 5.0 Hz, 2H), 4.21 (s, 3H), 4.11 (s, 3H), 3.93 (d, *J* = 4.6 Hz, 2H), 3.70 – 3.28 (m, 24H), 1.56 – 1.47 (m, 5H), 1.33 – 1.17 (m, 54H), 0.92 – 0.80 (m, 6H).

4-(1-(20-(Hexadecyloxy)-3,6,9,12,15,18,22-heptaoxaoctatriacontyl)-1*H*-1,2,3-triazol-4-yl)-1,3-dimethyl-1*H*-imidazol-3-ium iodide (**Vc**): Yield: 26 mg (24 %)

^{1}H NMR (600 MHz, $CDCl_3$) δ 10.07 (s, 1H), 8.56 (s, 1H), 7.82 (s, 1H), 4.67 (t, *J* = 4.9 Hz, 2H), 4.22 (s, 3H), 4.11 (s, 3H), 3.94 (t, *J* = 4.9 Hz, 2H), 3.67 – 3.35 (m, 29H), 1.55 – 1.49 (m, 4H), 1.30 – 1.22 (m, 52H), 0.90 – 0.83 (m, 6H).

4.6.3 DPG based anchor lipids with benzimidazolium anchor group

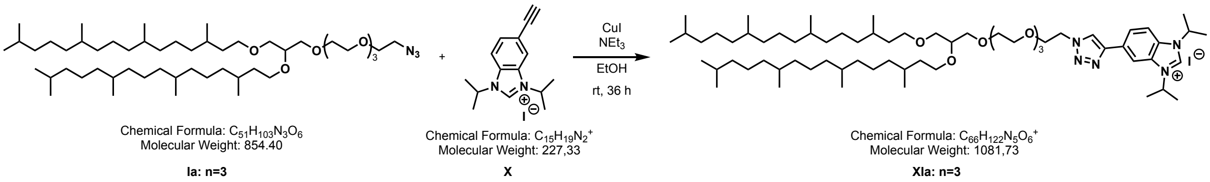

Scheme 45: Synthesis of **XIa**

Ia (59 mg, 0.069 mmol, 1 eq.) was dissolved in 1 ml degassed EtOH. CuI (4 mg, 0.2 mmol, 0.3 eq.) was added. **X** (27 mg, 0.076 mmol, 1.1 eq.) was dissolved in 500 µl degassed EtOH and added to the mixture. NEt_3 (8 mg, 0.080 mmol, 1.2 eq.) was added *via* a septum and the reaction was stirred at rt for 36 h. After completeness of the reaction, the solvent was evaporated. The residue was taken up in MeOH and filtered over a silica plug. After evaporation of the solvent, the crude product was purified twice *via* column chromatography (DCM/MeOH 1-9%) to yield 20 mg (24 %) the product as yellow oil.

1,3-Diisopropyl-5-(1-(19,23,27,31-tetramethyl-14-((3,7,11,15-tetramethylhexadecyl)oxy)-3,6,9,12,16-pentaoxadotriacontyl)-1*H*-1,2,3-triazol-4-yl)-1*H*-benzo[*d*]imidazol-3-ium iodide (**XIa**):

^{1}H NMR (400 MHz, $CDCl_3$) δ 10.95 (s, 1H), 8.44 (s, 1H), 8.29 (s, 1H), 8.03 (dd, *J* = 8.8, 1.4 Hz, 1H), 7.81 (dd, *J* = 8.7, 0.7 Hz, 1H), 5.23 (m, 2H), 4.64 (t, *J* = 4.4 Hz, 2H), 3.96 (t, *J* = 4.3 Hz, 2H), 3.70 – 3.34 (m, 21H), 1.90 (t, *J* = 6.9 Hz, 12H), 1.55 – 1.45 (m, 4H), 1.37 – 0.99 (m, 44H), 0.90 – 0.77 (m, 30H).

^{13}C NMR (100 MHz, CDCl$_3$) δ 145.70, 140.14, 131.81, 130.85, 130.28, 125.18, 122.39, 114.32, 110.49, 78.07, 77.36, 71.65, 71.01, 70.71, 70.69, 70.65, 70.15, 69.48, 69.04, 52.86, 52.66, 50.76, 39.50, 37.65, 37.60, 37.55, 37.52, 37.50, 37.42, 36.89, 36.81, 32.93, 32.91, 30.06, 29.98, 29.95, 28.11, 24.93, 24.62, 24.51, 22.86, 22.76, 22.55, 22.43, 19.89, 19.82, 19.75.

4.7 Ion exchanges

4.7.1 DPG based anchor lipids

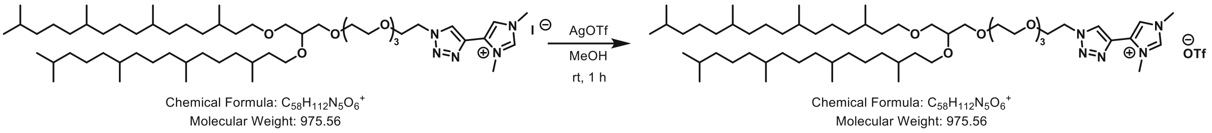

IIa **IIIa**

Scheme 46: Synthesis of **IIIa**

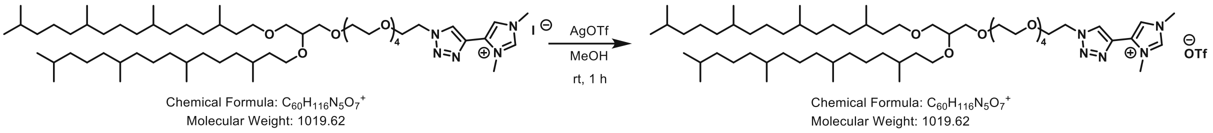

IIb **IIIb**

Scheme 47: Synthesis of **IIIb**

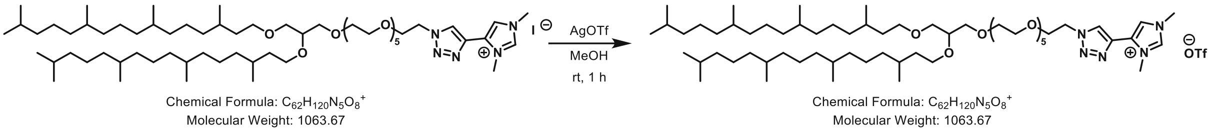

IIc **IIIc**

Scheme 48: Synthesis of **IIIc**

II (**a:** 20 mg, 0.019 mmol, 1 eq., **b:** 84 mg, 0.073 mmol, 1 eq., **c:** 52 mg, 0.043 mmol, 1 eq.) was dissolved in 1 ml MeOH, AgOTf (**a:** 5 mg, 0.019 mmol, 1 eq., **b:** 19 mg, 0.073 mmol, 1 eq., **c:** 11 mg, 0.043 mmol, 1 eq.) was added in 1 ml methanolic solution. The reaction was stirred at rt for 60-90 minutes. The precipitate was removed by filtration over a celite plug and then the solution was again filtered over a syringe filter. Evaporation of the solvent yielded the product as an oil.

1,3-Dimethyl-4-(1-(19,23,27,31-tetramethyl-14-((3,7,11,15-tetramethylhexadecyl)oxy)-3,6,9,12,16-pentaoxadotriacontyl)-1*H*-1,2,3-triazol-4-yl)-1*H*-imidazol-3-ium trifluoromethanesulfonate (**IIIa**): Yield: 21 mg (99 %)

^{1}H NMR (400 MHz, CDCl$_3$) δ 9.12 (s, 1H), 8.41 (s, 1H), 7.68 (s, 1H), 4.60 (t, *J* = 5.0 Hz, 2H), 4.08 (s, 3H), 3.93 (s, 3H), 3.87 (t, *J* = 5.0 Hz, 2H), 3.61 – 3.32 (m, 21H), 1.48 – 1.39 (m, 4H), 1.33 – 0.92 (m, 44H), 0.85 – 0.69 (m, 30H).

^{19}F NMR (376 MHz, CDCl$_3$) δ -78.51.

1,3-Dimethyl-4-(1-(22,26,30,34-tetramethyl-17-((3,7,11,15-tetramethylhexadecyl)oxy)-3,6,9,12,15,19-hexaoxapentatriacontyl)-1*H*-1,2,3-triazol-4-yl)-1*H*-imidazol-3-ium trifluoromethanesulfonate (**IIIb**): Yield: 69 mg (81 %)

^{1}H NMR (600 MHz, MeOD) δ 8.53 (s, 1H), 7.90 (s, 1H), 4.70 (t, *J* = 4.6 Hz, 2H), 4.08 (s, 3H), 3.98 (s, 3H), 3.96 – 3.92 (m, 2H), 3.66 – 3.40 (m, 29H), 1.56 – 1.50 (m, 4H), 1.42 – 1.04 (m, 44H), 0.91 – 0.86 (m, 30H). Singulet around 9 ppm is missing.

^{13}C NMR (151 MHz, MeOD) δ 134.99, 126.60, 122.71, 72.22, 72.08, 72.04, 71.99, 71.92, 71.58, 71.51, 71.48, 71.41, 71.39, 70.78, 70.15, 69.75, 69.73, 69.57, 51.75, 49.85, 40.57, 38.65, 38.59, 38.55, 38.50, 38.45, 38.41, 38.37, 38.31, 38.25, 37.96, 37.94, 37.90, 37.88, 36.64, 36.23, 33.96, 33.92, 30.96, 30.94, 30.90, 30.86, 30.81, 29.17, 25.94, 25.53, 25.52, 23.14, 23.06, 20.33, 20.26, 20.20, 20.13.

^{19}F NMR (565 MHz, MeOD) δ -80.13.

1,3-Dimethyl-4-(1-(25,29,33,37-tetramethyl-20-((3,7,11,15-tetramethylhexadecyl)oxy)-3,6,9,12,15,18,22-heptaoxaoctatriacontyl)-1*H*-1,2,3-triazol-4-yl)-1*H*-imidazol-3-ium trifluoromethanesulfonate (**IIIc**): Yield: 43 mg (81 %)

^{1}H NMR (600 MHz, MeOD) δ 9.00 (s, 1H), 8.54 (s, 1H), 7.91 (s, 1H), 4.70 (d, *J* = 4.7 Hz, 2H), 4.08 (s, 3H), 3.98 (s, 3H), 3.94 (d, *J* = 4.8 Hz, 2H), 3.66 – 3.39 (m, 31H), 1.56 – 1.51 (m, 4H), 1.43 – 1.04 (m, 44H), 0.91 – 0.82 (m, 30H).

^{13}C NMR (151 MHz, MeOD) δ 138.13, 133.57, 126.73, 125.23, 121.34, 119.33, 77.98, 77.90, 70.83, 70.67, 70.52, 70.20, 70.12, 70.08, 70.05, 70.03, 69.99, 69.98, 69.37, 68.72, 68.33, 68.16, 50.34, 48.44, 48.16, 39.16, 37.24, 37.18, 37.14, 37.09, 37.07, 37.05, 37.00, 36.90, 36.84, 36.53, 36.47, 35.27, 34.86, 34.83, 32.56, 32.54, 32.51, 29.56, 29.53, 29.45, 27.77, 24.53, 24.52, 24.13, 24.10, 21.73, 21.65, 18.92, 18.87, 18.85, 18.83, 18.81, 18.79, 18.77, 18.75, 18.72.

^{19}F NMR (565 MHz, MeOD) δ -80.14.

4.7.2 DHDG based anchor lipids

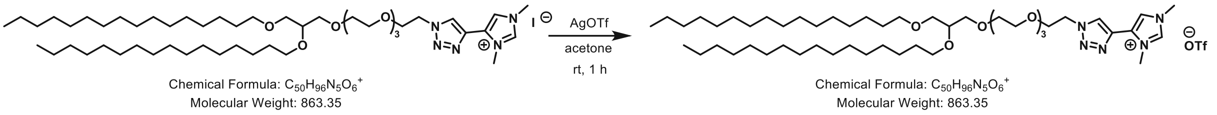

Va **VIa**

Scheme 49: Synthesis of **VIa**

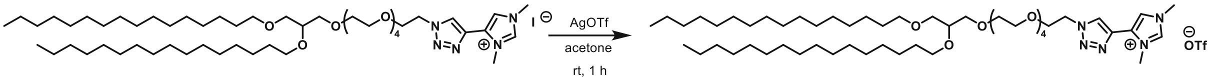

Chemical Formula: $C_{52}H_{100}N_5O_7^+$
Molecular Weight: 907.40
Vb

Chemical Formula: $C_{52}H_{100}N_5O_7^+$
Molecular Weight: 907.40
VIb

Scheme 50: Synthesis of **VIb**

Chemical Formula: $C_{54}H_{104}N_5O_8^+$
Molecular Weight: 951.45
Vc

Chemical Formula: $C_{54}H_{104}N_5O_8^+$
Molecular Weight: 951.45
VIc

Scheme 51: Synthesis of **VIc**

V (**a:** 11 mg, 0.011 mmol, 1 eq., **b:** 45 mg, 0.043 mmol, 1 eq., **c:** 29 mg, 0.026 mmol, 1 eq.) was dissolved in 1 ml acetone, AgOTf (**a:** 3 mg, 0.011 mmol, 1 eq., **b:** 11 mg, 0.043 mmol, 1 eq., **c:** 7 mg, 0.026 mmol, 1 eq.) was dissolved in 1 ml acetone and added to the solution. The reaction was stirred at rt for 60-90 minutes. The precipitate was removed by filtration over a celite plug and then the solution was again filtered over a syringe filter. Evaporation of the solvent yielded the product as an oil.

4-(1-(14-(Hexadecyloxy)-3,6,9,12,16-pentaoxadotriacontyl)-1*H*-1,2,3-triazol-4-yl)-1,3-dimethyl-1*H*-imidazol-3-ium trifluoromethanesulfonate (**VIa**): Yield: 11 mg (99 %) as a mixture of 1,4- and 1,5-isomer.

^{1}H NMR (400 MHz, MeOD) δ 8.95 (s, 1H), 8.89 (s, 1H), 8.59 (s, 1H), 8.44 (s, 1H), 7.99 (d, *J* = 1.6 Hz, 1H), 7.80 (d, *J* = 1.8 Hz, 1H), 4.67 – 4.56 (m, 4H), 3.99 – 3.87 (m, 12H), 3.86 – 3.81 (m, 2H), 3.58 – 3.30 (m, 43H), 1.49 – 1.39 (m, 8H), 1.19 (s, 104H), 0.82 – 0.77 (m, 12H).

^{19}F NMR (376 MHz, MeOD) δ -80.09.

4-(1-(17-(Hexadecyloxy)-3,6,9,12,15,19-hexaoxapentatriacontyl)-1*H*-1,2,3-triazol-4-yl)-1,3-dimethyl-1*H*-imidazol-3-ium trifluoromethanesulfonate (**VIb**): Yield: 36 mg (78 %)

^{1}H NMR (600 MHz, MeOD) δ 8.99 (s, 1H), 8.54 (s, 1H), 7.91 (s, 1H), 4.70 (t, *J* = 5.2 Hz, 2H), 4.07 (s, 3H), 3.98 (s, 3H), 3.95 (t, *J* = 4.9 Hz, 2H), 3.67 – 3.40 (m, 25H), 1.58 – 1.48 (m, 4H), 1.37 – 1.24 (m, 52H), 0.92 – 0.87 (m, 6H).

^{13}C NMR (151 MHz, MeOD) δ 139.49, 135.04, 126.65, 122.80, 79.26, 72.55, 72.15, 71.90, 71.87, 71.56, 71.49, 71.48, 71.42, 71.39, 71.37, 70.15, 51.80, 36.68, 36.25, 33.10, 31.17, 30.83, 30.80, 30.77, 30.62, 30.60, 30.51, 27.33, 27.26, 23.76, 14.47.

^{19}F NMR (565 MHz, MeOD) δ -80.12.

4-(1-(20-(Hexadecyloxy)-3,6,9,12,15,18,22-heptaoxaoctatriacontyl)-1*H*-1,2,3-triazol-4-yl)-1,3-dimethyl-1*H*-imidazol-3-ium trifluoromethanesulfonate (**VIc**): Yield: 30 mg (99 %)

^{1}H NMR (400 MHz, MeOD) δ 9.00 (s, 1H), 8.61 (s, 1H), 7.94 (d, *J* = 1.7 Hz, 1H), 4.79 – 4.70 (m, 2H), 4.06 (s, 3H), 3.98 (s, 3H), 3.97 – 3.92 (m, 2H), 3.70 – 3.40 (m, 29H), 1.58 – 1.51 (m, 4H), 1.35 – 1.21 (m, 52H), 0.94 – 0.85 (m, 6H).

^{19}F NMR (376 MHz, MeOD) δ -80.04.

4.7.3 DPG based anchor lipids with benzimidazolium anchor group

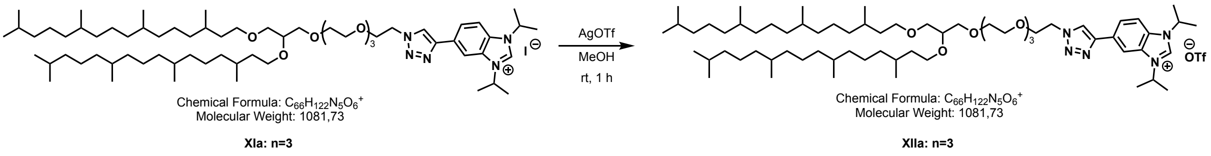

Scheme 52: Synthesis of **XIa**

XIa (20 mg, 0.016 mmol, 1 eq.) was dissolved in 1 ml MeOH, AgOTf (4 mg, 0.016 mmol, 1 eq.) was dissolved in 1 ml MeOH and added to the solution. The reaction was stirred at rt for 60 minutes. The precipitate was removed by filtration over a celite plug and then the solution was again filtered over a syringe filter. Evaporation of the solvent yielded 18 mg (95 %) of the product as an oil. The product was obtained as a mixture if 1,4- and 1,5-isomer.

^{1}H NMR (400 MHz, MeOD) δ 8.65 (s, 1H), 8.50 (s, 1H), 8.22 (d, *J* = 1.4 Hz, 1H), 8.13 (s, 1H), 5.18 – 5.04 (m, 2H), 4.70 (d, *J* = 5.0 Hz, 2H), 3.98 (t, *J* = 5.3 Hz, 2H), 3.70 – 3.56 (m, 13H), 3.54 – 3.39 (m, 5H), 1.80 – 1.73 (m, 12H), 1.61 – 1.46 (m, 4H), 1.43 – 1.03 (m, 42H), 0.90 – 0.83 (m, 30H).

^{13}C NMR (101 MHz, MeOD) δ 147.22, 133.25, 132.25, 131.43, 126.12, 124.41, 115.70, 111.28, 72.24, 71.92, 71.55, 71.49, 71.44, 70.33, 53.05, 52.91, 51.89, 40.56, 38.49, 38.40, 33.95, 33.91, 30.96, 29.16, 25.92, 25.52, 23.14, 23.05, 22.21, 22.16, 20.33, 20.26, 20.20.

^{19}F NMR (376 MHz, MeOD) δ -80.08.

4.8 Synthesis of NHC-based spacer molecule

4.8.1 4-(1-(2-Methoxyethyl)-1*H*-1,2,3-triazol-4-yl)-1,3-dimethyl-1*H*-imidazol-3-ium iodide (**XIII**)

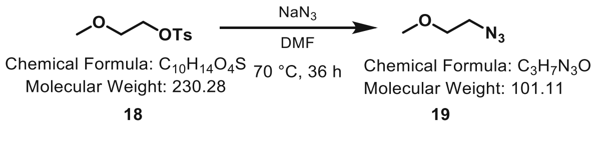

Scheme 53: Synthesis of **19**

18 (100 mg, 0.43 mmol, 1.1 eq.) was dissolved in 10 ml degassed EtOH. After the addition of NaN$_3$ (26 mg, 0.39 mmol, 1 eq.), the reaction was stirred at rt for 12 h. On the next day, the reaction was heated to 70 °C and stirred for another 24 h. The product formation was characterized *via* LC/MS. Upon formation of **19** the synthesis of **XIII** was performed without further workup or purification.

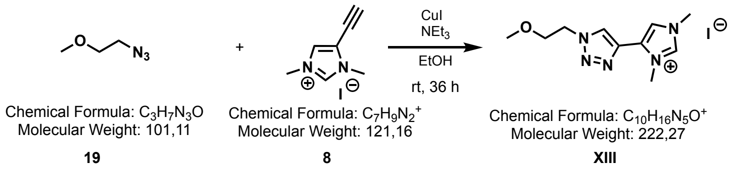

Scheme 54: Synthesis of **XIII**

CuI (22 mg, 0.12 mmol, 0.3 eq.) was added to the reaction solution of **19** (maximum yield 40 mg, 0.39 mmol, 1 eq.) and the vial was flushed with Ar. Then, **8** (107 mg, 0.43 mmol, 1.1 eq.) was added in a 1 ml EtOH (degassed) solution dropwise. NEt_3 (48 mg, 0.47 mmol, 1.2 eq.) was added and the reaction was stirred at room temperature for 36 h. After completeness of the reaction, the mixture was filtered over a celite plug. After removal of the solvent, the crude product was purified over silica gel (DCM/MeOH 10-15 %) to yield the 52 mg (36 %) product as yellow solid.

^{1}H NMR (400 MHz, MeOD) δ 8.55 (s, 1H), 7.91 (s, 1H), 7.71 (m, 1H), 7.26 – 7.22 (m, 1H), 4.70 (d, *J* = 4.9 Hz, 2H), 4.08 (s, 3H), 4.00 (s, 3H), 3.86 (d, *J* = 5.2 Hz, 2H), 3.36 (s, 3H).

4.8.2 4-(1-(2-Methoxyethyl)-1*H*-1,2,3-triazol-4-yl)-1,3-dimethyl-1*H*-imidazol-3-ium trifluoromethanesulfonate (**XIV**)

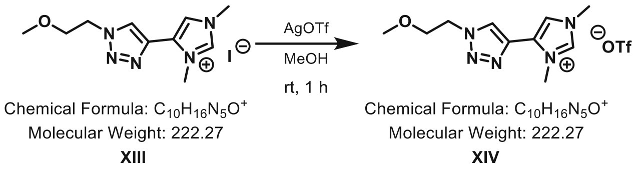

Scheme 55: Synthesis of **XIV**

XIII (52 mg, 0.15 mmol, 1 eq.) was dissolved in 1 ml MeOH, AgOTf (38 mg, 0.15 mmol, 1 eq.) was dissolved in 1 ml MeOH and added to the solution. The reaction was stirred at rt for 1 h. The precipitate was removed by filtration over a celite plug and then the solution was again filtered over a syringe filter. Evaporation of the solvent yielded to 43 mg (78 %) of the product as an orange solid. The product was obtained as a mixture of 1,4- and 1,5-isomers.

^{1}H NMR (400 MHz, MeOD) δ 8.45 (s, 1H), 7.87 (s, 1H), 7.71 (d, *J* = 8.2 Hz, 4H), 7.24 (d, *J* = 8.3 Hz, 4H), 4.06 (s, 3H), 3.97 (s, 3H), 3.88 (d, *J* = 7.9 Hz, 2H), 3.60 (s, 1H), 2.37 (s, 6H).

^{19}F NMR (376 MHz, MeOD) δ -80.13.

4.9 Synthesis of NHC-based outer leaflet

4.9.1 2,3-Bis((3,7,11,15-tetramethylhexadecyl)oxy)propyl 4-methylbenzenesulfonate (**20**)

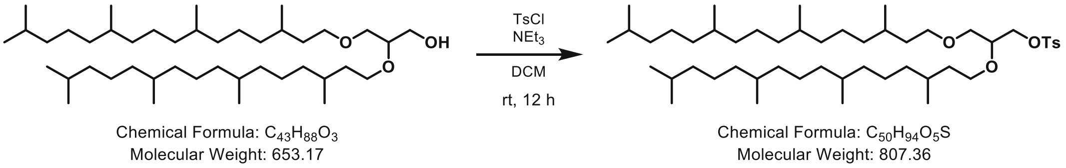

5 **20**

Scheme 56: Synthesis of **20**

5 (150 mg, 0.23 mmol, 1 eq.) was added to a vial, flushed with Ar, and dissolved in 1 ml anhydrous DCM. NEt_3 (42 mg, 0.41 mmol, 1.8 eq.) was added through a septum. *p*TsCl (65 mg, 0.34 mmol. 1.5 eq.) was dissolved in 1 ml anhydrous DCM and added dropwise. The reaction was stirred at rt for 12 h. After completeness of the reaction, the mixture was extracted with saturated NH_4Cl-solution. The organic layer was then extracted three times with saturated $NaHCO_3$-solution and dried over Na_2SO_4. Solvent was evaporated and the product was used for further steps without further purification (Yield: 185 mg (99 %)).

^{1}H NMR (400 MHz, $CDCl_3$) δ 7.80 (d, *J* = 8.3 Hz, 2H), 7.33 (d, *J* = 7.9 Hz, 2H), 3.64 – 3.29 (m, 5H), 2.44 (s, 3H), 1.57 – 1.43 (m, 4H), 1.39 – 0.96 (m, 44H), 0.90 – 0.79 (m, 30H).

4.9.2 1-(3-Azido-2-((3,7,11,15-tetramethylhexadecyl)oxy)propoxy)-3,7,11,15-tetramethylhexadecane (**21**)

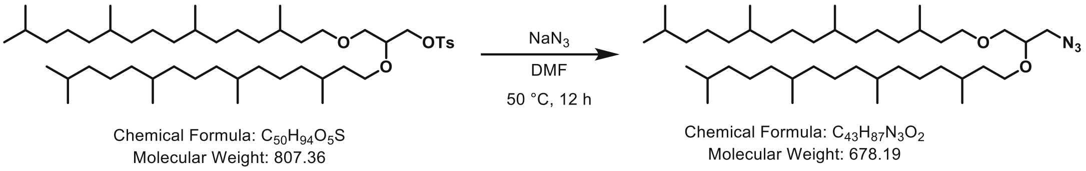

20 **21**

Scheme 57: Synthesis of **21**

20 (173 mg, 0.24 mmol, 1 eq.) was dissolved in 1.5 ml DMF. After the addition of NaN_3 (23 mg, 0.36 mmol, 1.5 eq.), the reaction was stirred at 50 °C for 12 h. Upon completeness of the reaction, the mixture was filtered over a celite plug and the solvent was removed *via* evaporation. The crude product was purified *via* flash column chromatography (PE) to yield 106 mg (64 %) of the purified product.

^{1}H NMR (400 MHz, $CDCl_3$) δ 3.67 – 3.40 (m, 5H), 3.36 – 3.22 (m, 2H), 1.68 – 1.47 (m, 8H), 1.42 – 1.01 (m, 44H), 0.91 – 0.83 (m, 30H).

4.9.3 4-(1-(2,3-Bis((3,7,11,15-tetramethylhexadecyl)oxy)propyl)-1H-1,2,3-triazol-4-yl)-1,3-dimethyl-1H-imidazol-3-ium iodide (**XV**)

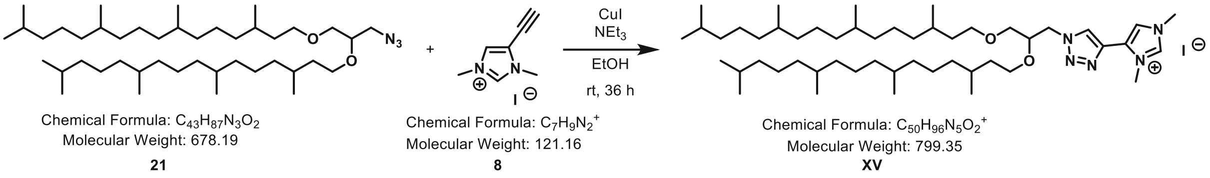

Scheme 58: Synthesis of **XV**

21 (97 mg, 0.14 mmol, 1 eq.) was dissolved in 1 ml degassed EtOH and CuI (8 mg, 0.04 mmol, 0.3 eq.) was added and the vial was flushed with Ar. Then, **8** (39 mg, 0.16 mmol, 1.1 eq.) was added in a 1 ml EtOH (degassed) solution dropwise. EtN_3 (17 mg, 0.17 mmol, 1.2 eq.) was added and the reaction was stirred at room temperature for 36 h. After completeness of the reaction, solvent was evaporated. The residue was taken up in MeOH was filtered over a celite plug. Impurities could not be fully removed.

4.10 Synthesis of thiol-based anchor lipids

4.10.1 1-Phenyl-2,5,8,11,14,17-hexaoxanonadecan-19-yl 4-methylbenzenesulfonate (**13a**) and 1-phenyl-2,5,8,11,14,17,20,23-octaoxapentacosan-25-yl 4-methylbenzenesulfonate (**13b**)

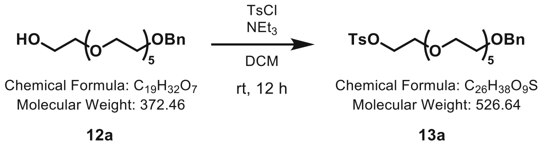

Scheme 59: Synthesis of **13a**

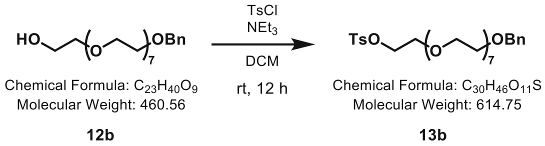

Scheme 60: Synthesis of **13b**

12 (**a**: 500 mg, 1.34 mmol, 1 eq., **b**: 500 mg, 1.1 mmol, 1 eq.) was added to a vial, flushed with Ar, and dissolved in 1 ml anhydrous DCM. NEt_3 (**a**: 244 mg, 2.41 mmol, 1.8 eq., **b**: 198 mg, 1.95 mmol, 1.8 eq.) was added through a septum. TsCl (**a**: 383 mg, 2.01 mmol. 1.5 eq., **b**: 310 mg, 1.63 mmol. 1.5 eq.) was dissolved in 1.2 ml anhydrous DCM and added dropwise. The reaction was stirred at rt for 12 h. After completeness of the reaction, the mixture was extracted with saturated NH_4Cl-solution. The organic layer was then extracted with saturated $NaHCO_3$-solution and dried over Na_2SO_4. Solvent was evaporated and an aliquot of the crude product was purified *via* column chromatography (DCM/MeOH 0-5%) to yield 307 mg (**13a**) and 237 mg (**13b**) of a colorless oil.

13a: **^{1}H NMR** (400 MHz, $CDCl_3$) δ 7.79 (d, *J* = 8.4 Hz, 2H), 7.41 – 7.29 (m, 7H), 4.56 (s, 2H), 4.15 (d, *J* = 4.7 Hz, 2H), 3.82 – 3.49 (m, 24H), 2.44 (s, 3H).

13b: **^{1}H NMR** (400 MHz, $CDCl_3$) δ 7.79 (d, *J* = 8.3 Hz, 2H), 7.37 – 7.27 (m, 7H), 4.56 (s, 2H), 4.15 (d, *J* = 4.8 Hz, 2H), 3.77 – 3.50 (m, 32H), 2.44 (s, 3H).

4.10.2 22-(Hexadecyloxy)-1-phenyl-2,5,8,11,14,17,20,24-octaoxatetracontane (**VIIa**) and 28-(hexadecyloxy)-1-phenyl-2,5,8,11,14,17,20,23,26,30-decaoxahexatetracontane (**VIIb**)

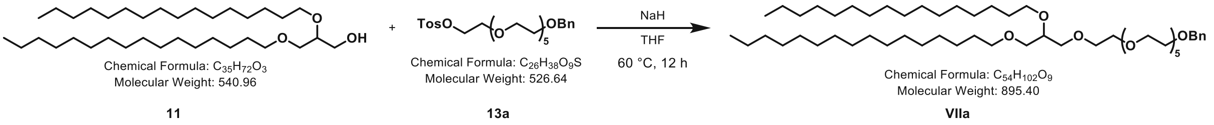

Scheme 61: Synthesis of **VIIa**

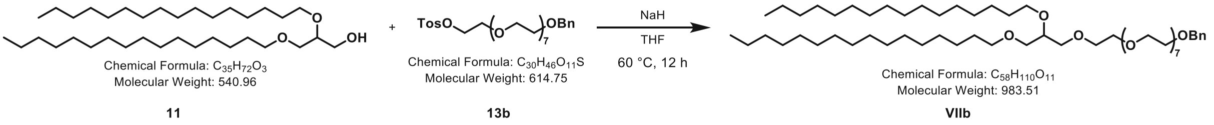

Scheme 62: Synthesis of **VIIb**

500 µl THF was added to a flame dried vial and NaH (60 % dispersion in mineral oil) (**a**: 20 mg, 0.51 mmol, 2 eq., **b**: 17 mg, 0.44 mmol, 2 eq.) was added. **11** (**a**: 140 mg, 0.25 mmol, 1 eq., **b**: 120 mg, 0.24 mmol, 1 eq.) was dissolved in 1 ml THF and added dropwise. The mixture was stirred at rt until completeness of gas formation. **13** (**a**: 150 mg, 0.28 mmol, 1.1 eq., **b**: 150 mg, 0.22 mmol, 1.1 eq.) was dissolved in 300 µl THF and added to the reaction. The mixture was heated to 60 °C and stirred for 12 h. The reaction was allowed to cool to rt and the solvent was removed in vacuo. The residue was transferred to a separatory funnel with H_2O and DCM. After separation of the layers, the aqueous phase was extracted with DCM four times. Combined organic layers were washed with brine, dried over Na_2SO_4 and the solvent was evaporated. The crude product was purified *via* column chromatography (DCM/EtOAc 10-20%) yielding a slightly waxy solid.

VIIa: Yield: 99 mg (42 %)

^{1}H NMR (400 MHz, $CDCl_3$) δ 7.45 – 7.28 (m, 5H), 4.57 (s, 2H), 3.80 – 3.30 (m, 33H), 1.65 – 1.46 (m, 4H), 1.36 – 1.11 (m, 52H), 1.00 – 0.67 (m, 6H).

VIIb: Yield: 100 mg (46 %)

^{1}H NMR (400 MHz, $CDCl_3$) δ 7.43 – 7.27 (m, 5H), 4.57 (s, 2H), 3.75 – 3.34 (m, 41H), 1.59 – 1.50 (m, 4H), 1.36 – 1.13 (m, 52H), 1.00 – 0.80 (m, 6H).

4.10.3 20-(Hexadecyloxy)-3,6,9,12,15,18,22-heptaoxaoctatriacontan-1-ol (**VIIIa**) and 26-(hexadecyloxy)-3,6,9,12,15,18,21,24,28-nonaoxatetratetracontan-1-ol (**VIIIb**)

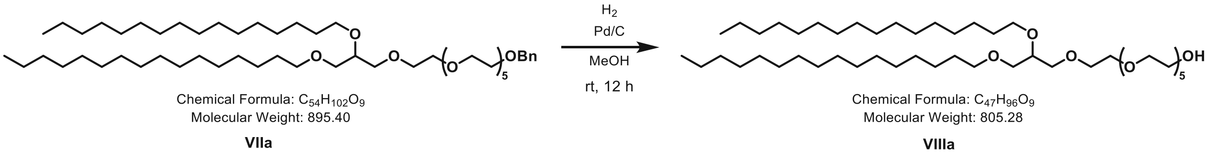

Scheme 63: Synthesis of **VIIIa**

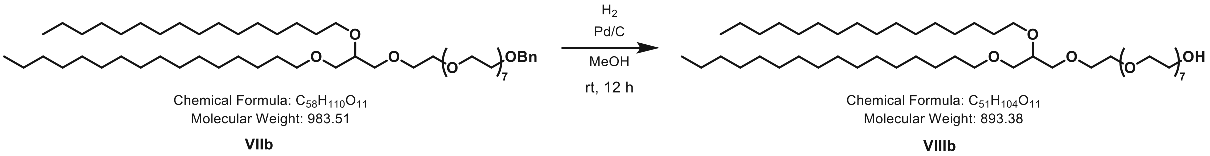

Scheme 64: Synthesis of **VIIIb**

VII (**a**: 99 mg, 0.11 mmol, 1 eq., **b**: 100 mg, 0.10 mmol, 1 eq.) was added to a flame dried vial and dissolved in 1 ml anh. MeOH and flushed with Ar. A spatula tip of Pd/C was added in Ar atmosphere. Then, the Ar balloon was exchanged with a H_2 balloon. The reaction was stirred at rt for 12 h. Upon completeness of the reaction, the mixture was filtered over a Celite plug and then again filtered through a syringe filter. The solvent was evaporated to yield the product as colorless oil.

VIIIa: Yield: 88 mg (99 %)

^{1}H NMR (400 MHz, $CDCl_3$) δ 3.77 – 3.37 (m, 33H), 1.59 – 1.51 (m, 4H), 1.35 – 1.20 (m, 52H), 0.92 – 0.83 (m, 6H).

VIIIb: Yield: 85 mg (95 %)

^{1}H NMR (400 MHz, $CDCl_3$) δ 3.74 – 3.36 (m, 41H), 1.61 – 1.49 (m, 4H), 1.34 – 1.17 (m, 52H), 0.92 – 0.84 (m, 6H).

4.10.4 20-(Hexadecyloxy)-3,6,9,12,15,18,22-heptaoxaoctatriacontyl 5-(1,2-dithiolan-3-yl)pentanoate (**IXa**) and 26-(hexadecyloxy)-3,6,9,12,15,18,21,24,28-nonaoxatetratetracontyl 5-(1,2-dithiolan-3-yl)pentanoate (**IXb**)

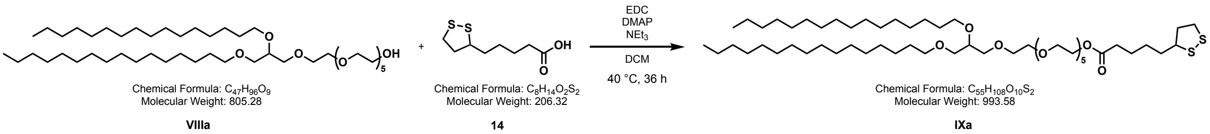

Scheme 65: Synthesis of **IXa**

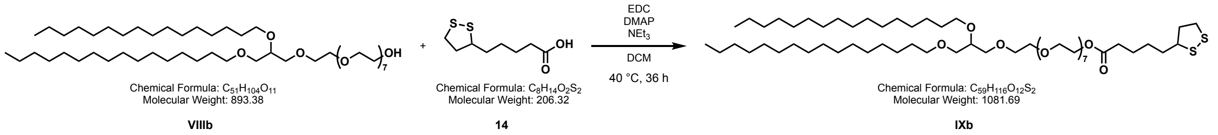

Scheme 66: Synthesis of **IXb**

14 (**a**: 13 mg, 0.064 mmol, 1.3 eq., **b**: 12 mg, 0.058 mmol, 1.3 eq.), DMAP (**a**: 500 µg, 0.003 mmol, 0.075 eq., **b**: 400 µg, 0.003 mmol, 0.075 eq.) and EDC · HCl (**a**: 13 mg, 0.069 mmol, 1.4 eq., **b**: 12 mg, 0.062 mmol, 1.4 eq.) were added to a flame dried vial, flushed with Ar and dissolved in 400 µl anhydrous DCM. The mixture was stirred at rt for 2 h. Then a mixture of **VIII** (**a**: 40 mg, 0.049 mmol, 1 eq., **b**: 40 mg, 0.045 mmol, 1 eq.) and NEt_3 (**a**: 8 mg, 0.074 mmol, 1.5 eq., **b**: 7 mg, 0.067 mmol, 1.5 eq.) was prepared and added dropwise to the previously prepared mixture. The reaction was stirred for 12 h at rt. On the next day, the reaction was heated to 40 °C and stirred for another 24 h. Upon completeness of the reaction, the mixture was transferred to a separatory funnel with saturated NH_4Cl-solution and extracted with DCM. The organic layer was washed with saturated $NaHCO_3$-solution. Then, the $NaHCO_3$-layer was extracted three times with DCM. Combined organic layers were dried over Na_2SO_4 and solvent was evaporated. The crude product was then purified *via* column chromatography (DCM/MeOH 1-5%) to yield the product as a slightly yellow oil.

IXa: Yield: 22 mg (45 %)

^{1}H NMR (600 MHz, $CDCl_3$) δ 4.22 (t, *J* = 4.8 Hz, 2H), 3.71 – 3.37 (m, 33H), 3.21 – 3.06 (m, 1H), 3.14 – 3.08 (m, 1H), 2.46 (h, *J* = 5.3 Hz, 1H), 2.35 (t, *J* = 7.5 Hz, 2H), 1.91 (h, *J* = 7.0 Hz, 1H), 1.73 – 1.61 (m, 4H), 1.58 – 1.51 (m, 4H), 1.51 – 1.39 (m, 2H), 1.25 (s, 52H), 0.88 (t, *J* = 7.0 Hz, 6H).

^{13}C NMR (151 MHz, $CDCl_3$) δ 173.60, 77.99, 71.81, 71.55, 70.99, 70.94, 70.76, 70.74, 70.73, 70.70, 70.68, 69.32, 63.62, 56.47, 40.36, 38.62, 34.74, 34.08, 32.07, 30.25, 29.86, 29.81, 29.67, 29.51, 28.89, 26.28, 26.24, 24.75, 22.84, 14.28.

IXb: Yield: 19 mg (40%)

^{1}H NMR (600 MHz, $CDCl_3$) δ 4.22 (t, *J* = 4.8 Hz, 2H), 3.69 (t, *J* = 4.8 Hz, 2H), 3.67 – 3.39 (m, 39H), 3.20 – 3.15 (m, 1H), 3.14 – 3.08 (m, 1H), 2.50 – 2.41 (m, 1H), 2.35 (t, *J* = 7.5 Hz, 2H), 1.94 – 1.86 (m, 1H), 1.73 – 1.61 (m, 4H), 1.58 – 1.38 (m, 4H), 1.33 – 1.21 (m, 52H), 0.90 – 0.84 (m, 6H).

^{13}C NMR (151 MHz, $CDCl_3$) δ 173.60, 77.99, 71.81, 71.55, 70.99, 70.94, 70.76, 70.74, 70.72, 70.68, 69.32, 63.62, 56.47, 53.58, 40.36, 38.63, 34.74, 34.08, 32.07, 30.25, 29.86, 29.81, 29.67, 29.51, 28.89, 26.28, 26.24, 24.75, 22.84, 21.21, 14.28.

5 Figures

6 Schemes

7 Tables

8 Supplementary Figures

9 References

(1) Saboe, P. O.; Conte, E.; Farell, M.; Bazan, G. C.; Kumar, M. Biomimetic and Bioinspired Approaches for Wiring Enzymes to Electrode Interfaces. *Energy Environ. Sci.* **2017**, *10* (1), 14–42. https://doi.org/10.1039/C6EE02801B.

(2) Ghaed-Sharaf, T.; Yang, D.-S.; Baldelli, S.; Ghatee, M. H. From Micelles to Vesicle and Membrane Structures of Double-Strand Ionic Liquids in Water: Molecular Dynamics Simulation. *Langmuir* **2019**, *35* (7), 2780–2791. https://doi.org/10.1021/acs.langmuir.8b03773.

(3) Schlenoff, J. B.; Li, M.; Ly, H. Stability and Self-Exchange in Alkanethiol Monolayers. *J. Am. Chem. Soc.* **1995**, *117* (50), 12528–12536. https://doi.org/10.1021/ja00155a016.

(4) Schoenfisch, M. H.; Pemberton, J. E. Air Stability of Alkanethiol Self-Assembled Monolayers on Silver and Gold Surfaces. *J. Am. Chem. Soc.* **1998**, *120* (18), 4502–4513. https://doi.org/10.1021/ja974301t.

(5) Flynn, N. T.; Tran, T. N. T.; Cima, M. J.; Langer, R. Long-Term Stability of Self-Assembled Monolayers in Biological Media. *Langmuir* **2003**, *19* (26), 10909–10915. https://doi.org/10.1021/la035331e.

(6) Wegner, T.; Laskar, R.; Glorius, F. Lipid Mimetics: A Versatile Toolbox for Lipid Biology and Beyond. *Current Opinion in Chemical Biology* **2022**, *71*, 102209. https://doi.org/10.1016/j.cbpa.2022.102209.

(7) Lee, T.-H.; Hirst, D. J.; Kulkarni, K.; Del Borgo, M. P.; Aguilar, M.-I. Exploring Molecular-Biomembrane Interactions with Surface Plasmon Resonance and Dual Polarization Interferometry Technology: Expanding the Spotlight onto Biomembrane Structure. *Chem. Rev.* **2018**, *118* (11), 5392–5487. https://doi.org/10.1021/acs.chemrev.7b00729.

(8) Cournia, Z.; Allen, T. W.; Andricioaei, I.; Antonny, B.; Baum, D.; Brannigan, G.; Buchete, N.-V.; Deckman, J. T.; Delemotte, L.; del Val, C.; Friedman, R.; Gkeka, P.; Hege, H.-C.; Hénin, J.; Kasimova, M. A.; Kolocouris, A.; Klein, M. L.; Khalid, S.; Lemieux, M. J.; Lindow, N.; Roy, M.; Selent, J.; Tarek, M.; Tofoleanu, F.; Vanni, S.; Urban, S.; Wales, D. J.; Smith, J. C.; Bondar, A.-N. Membrane Protein Structure, Function and Dynamics: A Perspective from Experiments and Theory. *J Membr Biol* **2015**, *248* (4), 611–640. https://doi.org/10.1007/s00232-015-9802-0.

(9) Watson, H. Biological Membranes. *Essays Biochem* **2015**, *59*, 43–69. https://doi.org/10.1042/bse0590043.

(10) Singer, S. J.; Nicolson, G. L. The Fluid Mosaic Model of the Structure of Cell Membranes. *Science* **1972**, *175* (4023), 720–731. https://doi.org/10.1126/science.175.4023.720.

(11) Skalová, Š.; Vyskočil, V.; Barek, J.; Navrátil, T. Model Biological Membranes and Possibilities

of Application of Electrochemical Impedance Spectroscopy for Their Characterization. *Electroanalysis* **2018**, *30* (2), 207–219. https://doi.org/10.1002/elan.201700649.

(12) Chan, Y.-H. M.; Boxer, S. G. Model Membrane Systems and Their Applications. *Curr Opin Chem Biol* **2007**, *11* (6), 581–587. https://doi.org/10.1016/j.cbpa.2007.09.020.

(13) Penkauskas, T.; Preta, G. Biological Applications of Tethered Bilayer Lipid Membranes. *Biochimie* **2019**, *157*, 131–141. https://doi.org/10.1016/j.biochi.2018.11.011.

(14) Andersson, J.; Köper, I. Tethered and Polymer Supported Bilayer Lipid Membranes: Structure and Function. *Membranes* **2016**, *6* (2), 30. https://doi.org/10.3390/membranes6020030.

(15) Aleknavičienė, I.; Talaikis, M.; Budvytyte, R.; Valincius, G. The Impact of an Anchoring Layer on the Formation of Tethered Bilayer Lipid Membranes on Silver Substrates. *Molecules* **2021**, *26* (22), 6878. https://doi.org/10.3390/molecules26226878.

(16) Knobloch, J.; Suhendro, D. K.; Zieleniecki, J. L.; Shapter, J. G.; Köper, I. Membrane–Drug Interactions Studied Using Model Membrane Systems. *Saudi Journal of Biological Sciences* **2015**, *22* (6), 714–718. https://doi.org/10.1016/j.sjbs.2015.03.007.

(17) Andersson, J.; Köper, I.; Knoll, W. Tethered Membrane Architectures—Design and Applications. *Frontiers in Materials* **2018**, *5*.

(18) Winterhalter, M. Black Lipid Membranes. *Current Opinion in Colloid & Interface Science* **2000**, *5* (3), 250–255. https://doi.org/10.1016/S1359-0294(00)00063-7.

(19) Köper, I. Insulating Tethered Bilayer Lipid Membranes to Study Membrane Proteins. *Mol. BioSyst.* **2007**, *3* (10), 651–657. https://doi.org/10.1039/B707168J.

(20) McGillivray, D. J.; Valincius, G.; Vanderah, D. J.; Febo-Ayala, W.; Woodward, J. T.; Heinrich, F.; Kasianowicz, J. J.; Lösche, M. Molecular-Scale Structural and Functional Characterization of Sparsely Tethered Bilayer Lipid Membranes. *Biointerphases* **2007**, *2* (1), 21–33. https://doi.org/10.1116/1.2709308.

(21) Andersson, J.; Knobloch, J. J.; Perkins, M. V.; Holt, S. A.; Köper, I. Synthesis and Characterization of Novel Anchorlipids for Tethered Bilayer Lipid Membranes. *Langmuir* **2017**, *33* (18), 4444–4451. https://doi.org/10.1021/acs.langmuir.7b00778.

(22) Junghans, A.; Köper, I. Structural Analysis of Tethered Bilayer Lipid Membranes. *Langmuir* **2010**, *26* (13), 11035–11040. https://doi.org/10.1021/la100342k.

(23) Forbrig, E.; Staffa, J. K.; Salewski, J.; Mroginski, M. A.; Hildebrandt, P.; Kozuch, J. Monitoring the Orientational Changes of Alamethicin during Incorporation into Bilayer Lipid Membranes. *Langmuir* **2018**, *34* (6), 2373–2385. https://doi.org/10.1021/acs.langmuir.7b04265.

(24) Rakovska, B.; Ragaliauskas, T.; Mickevicius, M.; Jankunec, M.; Niaura, G.; Vanderah, D. J.; Valincius, G. Structure and Function of the Membrane Anchoring Self-Assembled Monolayers. *Langmuir* **2015**, *31* (2), 846–857. https://doi.org/10.1021/la503715b.

(25) Ragaliauskas, T.; Mickevicius, M.; Rakovska, B.; Penkauskas, T.; Vanderah, D. J.; Heinrich, F.; Valincius, G. Fast Formation of Low-Defect-Density Tethered Bilayers by Fusion of Multilamellar Vesicles. *Biochimica et Biophysica Acta (BBA) - Biomembranes* **2017**, *1859* (5), 669–678. https://doi.org/10.1016/j.bbamem.2017.01.015.

(26) Harder, P.; Grunze, M.; Dahint, R.; Whitesides, G. M.; Laibinis, P. E. Molecular Conformation in Oligo(Ethylene Glycol)-Terminated Self-Assembled Monolayers on Gold and Silver Surfaces Determines Their Ability To Resist Protein Adsorption. *J. Phys. Chem. B* **1998**, *102* (2), 426–436. https://doi.org/10.1021/jp972635z.

(27) Cerruti, M.; Fissolo, S.; Carraro, C.; Ricciardi, C.; Majumdar, A.; Maboudian, R. Poly(Ethylene Glycol) Monolayer Formation and Stability on Gold and Silicon Nitride Substrates. *Langmuir* **2008**, *24* (19), 10646–10653. https://doi.org/10.1021/la801357v.

(28) Schiller, S. M.; Naumann, R.; Lovejoy, K.; Kunz, H.; Knoll, W. Archaea Analogue Thiolipids for Tethered Bilayer Lipid Membranes on Ultrasmooth Gold Surfaces. *Angewandte Chemie International Edition* **2003**, *42* (2), 208–211. https://doi.org/10.1002/anie.200390080.

(29) Crudden, C. M.; Horton, J. H.; Ebralidze, I. I.; Zenkina, O. V.; McLean, A. B.; Drevniok, B.; She, Z.; Kraatz, H.-B.; Mosey, N. J.; Seki, T.; Keske, E. C.; Leake, J. D.; Rousina-Webb, A.; Wu, G. Ultra Stable Self-Assembled Monolayers of N-Heterocyclic Carbenes on Gold. *Nature Chemistry* **2014**, *6* (5), 409–414. https://doi.org/10.1038/nchem.1891.

(30) Häkkinen, H. The Gold–Sulfur Interface at the Nanoscale. *Nature Chem* **2012**, *4* (6), 443–455. https://doi.org/10.1038/nchem.1352.

(31) Bürgi, T. Properties of the Gold–Sulphur Interface: From Self-Assembled Monolayers to Clusters. *Nanoscale* **2015**, *7* (38), 15553–15567. https://doi.org/10.1039/C5NR03497C.

(32) Vericat, C.; Vela, M. E.; Benitez, G.; Carro, P.; Salvarezza, R. C. Self-Assembled Monolayers of Thiols and Dithiols on Gold: New Challenges for a Well-Known System. *Chem. Soc. Rev.* **2010**, *39* (5), 1805–1834. https://doi.org/10.1039/B907301A.

(33) Choi, Y.; Park, C. S.; Tran, H.-V.; Li, C.-H.; Crudden, C. M.; Lee, T. R. Functionalized N-Heterocyclic Carbene Monolayers on Gold for Surface-Initiated Polymerizations. *ACS Appl. Mater. Interfaces* **2022**, *14* (39), 44969–44980. https://doi.org/10.1021/acsami.2c10985.

(34) Kim, H. K.; Hyla, A. S.; Winget, P.; Li, H.; Wyss, C. M.; Jordan, A. J.; Larrain, F. A.; Sadighi, J. P.; Fuentes-Hernandez, C.; Kippelen, B.; Brédas, J.-L.; Barlow, S.; Marder, S. R. Reduction of the

Work Function of Gold by N-Heterocyclic Carbenes. *Chem. Mater.* **2017**, *29* (8), 3403–3411. https://doi.org/10.1021/acs.chemmater.6b04213.

(35) Bakker, A.; Timmer, A.; Kolodzeiski, E.; Freitag, M.; Gao, H. Y.; Mönig, H.; Amirjalayer, S.; Glorius, F.; Fuchs, H. Elucidating the Binding Modes of N-Heterocyclic Carbenes on a Gold Surface. *J. Am. Chem. Soc.* **2018**, *140* (38), 11889–11892. https://doi.org/10.1021/jacs.8b06180.

(36) Crudden, C. M.; Horton, J. H.; Narouz, M. R.; Li, Z.; Smith, C. A.; Munro, K.; Baddeley, C. J.; Larrea, C. R.; Drevniok, B.; Thanabalasingam, B.; McLean, A. B.; Zenkina, O. V.; Ebralidze, I. I.; She, Z.; Kraatz, H.-B.; Mosey, N. J.; Saunders, L. N.; Yagi, A. Simple Direct Formation of Self-Assembled N-Heterocyclic Carbene Monolayers on Gold and Their Application in Biosensing. *Nat Commun* **2016**, *7* (1), 12654. https://doi.org/10.1038/ncomms12654.

(37) Martynova, E. A.; Tzouras, N. V.; Pisanò, G.; Cazin, C. S. J.; Nolan, S. P. The “Weak Base Route” Leading to Transition Metal–N-Heterocyclic Carbene Complexes. *Chem. Commun.* **2021**, *57* (32), 3836–3856. https://doi.org/10.1039/D0CC08149C.

(38) Wang, G.; Rühling, A.; Amirjalayer, S.; Knor, M.; Ernst, J. B.; Richter, C.; Gao, H.-J.; Timmer, A.; Gao, H.-Y.; Doltsinis, N. L.; Glorius, F.; Fuchs, H. Ballbot-Type Motion of N-Heterocyclic Carbenes on Gold Surfaces. *Nature Chemistry* **2017**, *9* (2), 152–156. https://doi.org/10.1038/nchem.2622.

(39) Gonzalez, A.; Kengmana, E. S.; Fonseca, M. V.; Han, G. G. D. Solid-State Photoswitching Molecules: Structural Design for Isomerization in Condensed Phase. *Materials Today Advances* **2020**, *6*, 100058. https://doi.org/10.1016/j.mtadv.2020.100058.

(40) Nguyen, D. T.; Freitag, M.; Gutheil, C.; Sotthewes, K.; Tyler, B. J.; Böckmann, M.; Das, M.; Schlüter, F.; Doltsinis, N. L.; Arlinghaus, H. F.; Ravoo, B. J.; Glorius, F. An Arylazopyrazole-Based N-Heterocyclic Carbene as a Photoswitch on Gold Surfaces: Light-Switchable Wettability, Work Function, and Conductance. *Angewandte Chemie International Edition* **2020**, *59* (32), 13651–13656. https://doi.org/10.1002/anie.202003523.

(41) Wang, D.; Richter, C.; Rühling, A.; Drücker, P.; Siegmund, D.; Metzler-Nolte, N.; Glorius, F.; Galla, H.-J. A Remarkably Simple Class of Imidazolium-Based Lipids and Their Biological Properties. *Chemistry – A European Journal* **2015**, *21* (43), 15123–15126. https://doi.org/10.1002/chem.201502333.

(42) Wang, D.; de Jong, D. H.; Rühling, A.; Lesch, V.; Shimizu, K.; Wulff, S.; Heuer, A.; Glorius, F.; Galla, H.-J. Imidazolium-Based Lipid Analogues and Their Interaction with Phosphatidylcholine Membranes. *Langmuir* **2016**, *32* (48), 12579–12592. https://doi.org/10.1021/acs.langmuir.6b02496.

(43) Drücker, P.; Rühling, A.; Grill, D.; Wang, D.; Draeger, A.; Gerke, V.; Glorius, F.; Galla, H.-J.

Imidazolium Salts Mimicking the Structure of Natural Lipids Exploit Remarkable Properties Forming Lamellar Phases and Giant Vesicles. *Langmuir* **2017**, *33* (6), 1333–1342. https://doi.org/10.1021/acs.langmuir.6b03182.

(44) Matos, A. L. L.; Keller, F.; Wegner, T.; del Castillo, C. E. C.; Grill, D.; Kudruk, S.; Spang, A.; Glorius, F.; Heuer, A.; Gerke, V. CHIMs Are Versatile Cholesterol Analogs Mimicking and Visualizing Cholesterol Behavior in Lipid Bilayers and Cells. *Commun Biol* **2021**, *4* (1), 1–11. https://doi.org/10.1038/s42003-021-02252-5.

(45) Nguyen, D. T.; Freitag, M.; Körsgen, M.; Lamping, S.; Rühling, A.; Schäfer, A. H.; Siekman, M. H.; Arlinghaus, H. F.; van der Wiel, W. G.; Glorius, F.; Ravoo, B. J. Versatile Micropatterns of N-Heterocyclic Carbenes on Gold Surfaces: Increased Thermal and Pattern Stability with Enhanced Conductivity. *Angewandte Chemie International Edition* **2018**, *57* (35), 11465–11469. https://doi.org/10.1002/anie.201807197.

(46) Guo, Q.-H.; Zhou, J.; Mao, H.; Qiu, Y.; Nguyen, M. T.; Feng, Y.; Liang, J.; Shen, D.; Li, P.; Liu, Z.; Wasielewski, M. R.; Stoddart, J. F. TetrazineBox: A Structurally Transformative Toolbox. *J. Am. Chem. Soc.* **2020**, *142* (11), 5419–5428. https://doi.org/10.1021/jacs.0c01114.

(47) Fang, Q.-S.; Chen, L.; Liu, Q.-Y. Template-Directed Synthesis of Pyridazine-Containing Tetracationic Cyclophane for Construction of [2]Rotaxane. *Chinese Chemical Letters* **2017**, *28* (5), 1013–1017. https://doi.org/10.1016/j.cclet.2016.12.002.

(48) Solubilities of Inorganic and Organic Compounds. A Compilation of Quantitative Solubility Data from the Periodical Literature. In *Journal of the American Medical Association*; 1928; Vol. 91, p 1131. https://doi.org/10.1001/jama.1928.02700150057034.

(49) Erb, R. A. Wettability of Gold. *The Journal of Physical Chemistry* **1968**, *72* (7).

(50) Mayall, R. M.; Smith, C. A.; Hyla, A. S.; Lee, D. S.; Crudden, C. M.; Birss, V. I. Ultrasensitive and Label-Free Detection of the Measles Virus Using an N-Heterocyclic Carbene-Based Electrochemical Biosensor. *ACS Sens.* **2020**, *5* (9), 2747–2752. https://doi.org/10.1021/acssensors.0c01250.

(51) Bubert, H. Practical Surface Analysis A2, Vol. 1. Auger and X-Ray Photoelectron Spectroscopy. 2. Auflage. Herausgegeben von D. Briggs Und M. P. Seah. Wiley, Chichester, Salle + Sauerländer, Aarau, 1994. 649 S., Broschur 49.95 £. – ISBN 0-471-9540-7. *Angewandte Chemie* **1995**, *107* (11), 1367–1367. https://doi.org/10.1002/ange.19951071133.

(52) Alharbi, A. R. M.; Andersson, J. M.; Köper, I.; Andersson, G. G. Investigating the Structure of Self-Assembled Monolayers Related to Biological Cell Membranes. *Langmuir* **2019**, *35* (44), 14213–14221. https://doi.org/10.1021/acs.langmuir.9b02553.

(53) Elgrishi, N.; Rountree, K. J.; McCarthy, B. D.; Rountree, E. S.; Eisenhart, T. T.; Dempsey, J. L. A Practical Beginner's Guide to Cyclic Voltammetry. *J. Chem. Educ.* **2018**, *95* (2), 197–206. https://doi.org/10.1021/acs.jchemed.7b00361.

(54) Valincius, G.; Meškauskas, T.; Ivanauskas, F. Electrochemical Impedance Spectroscopy of Tethered Bilayer Membranes. *Langmuir* **2012**, *28* (1), 977–990. https://doi.org/10.1021/la204054g.

10 Appendix

10.1 NMR

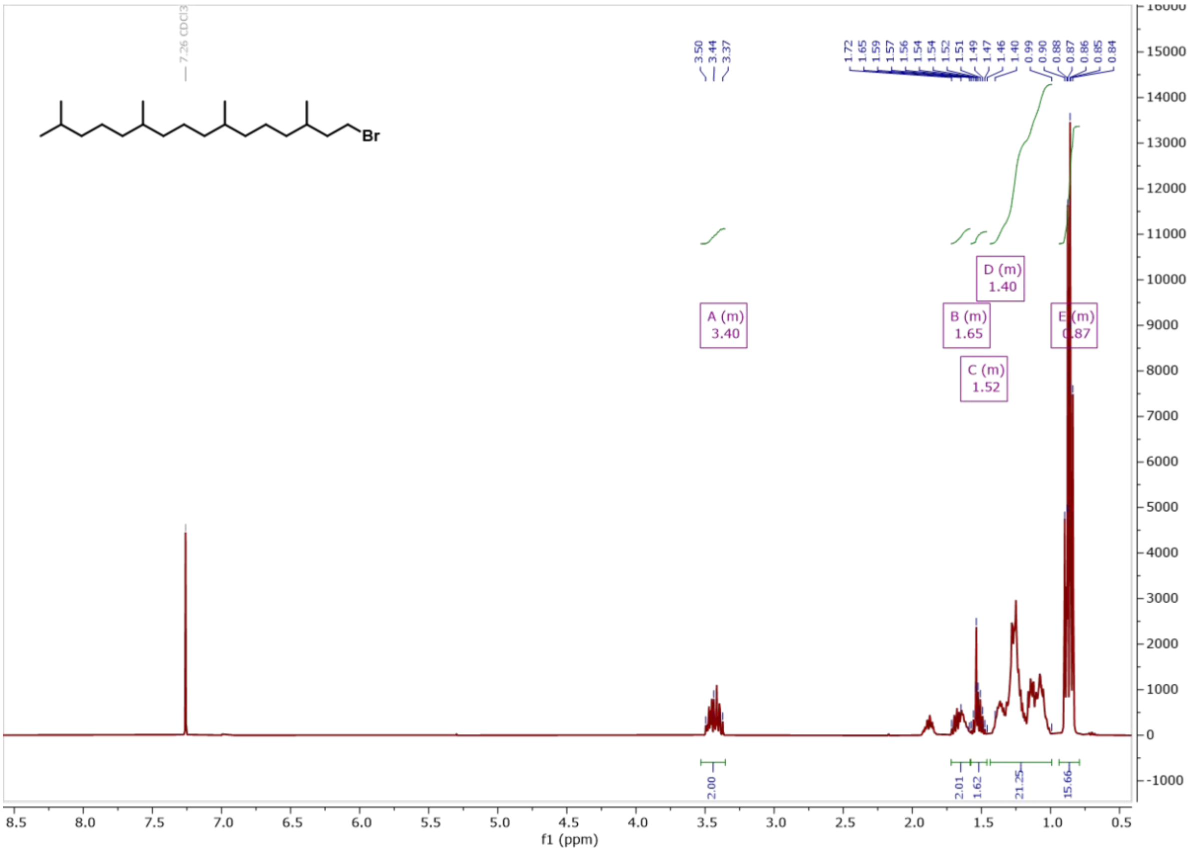

Supplementary Figure 1: ^{1}H-NMR of **2**

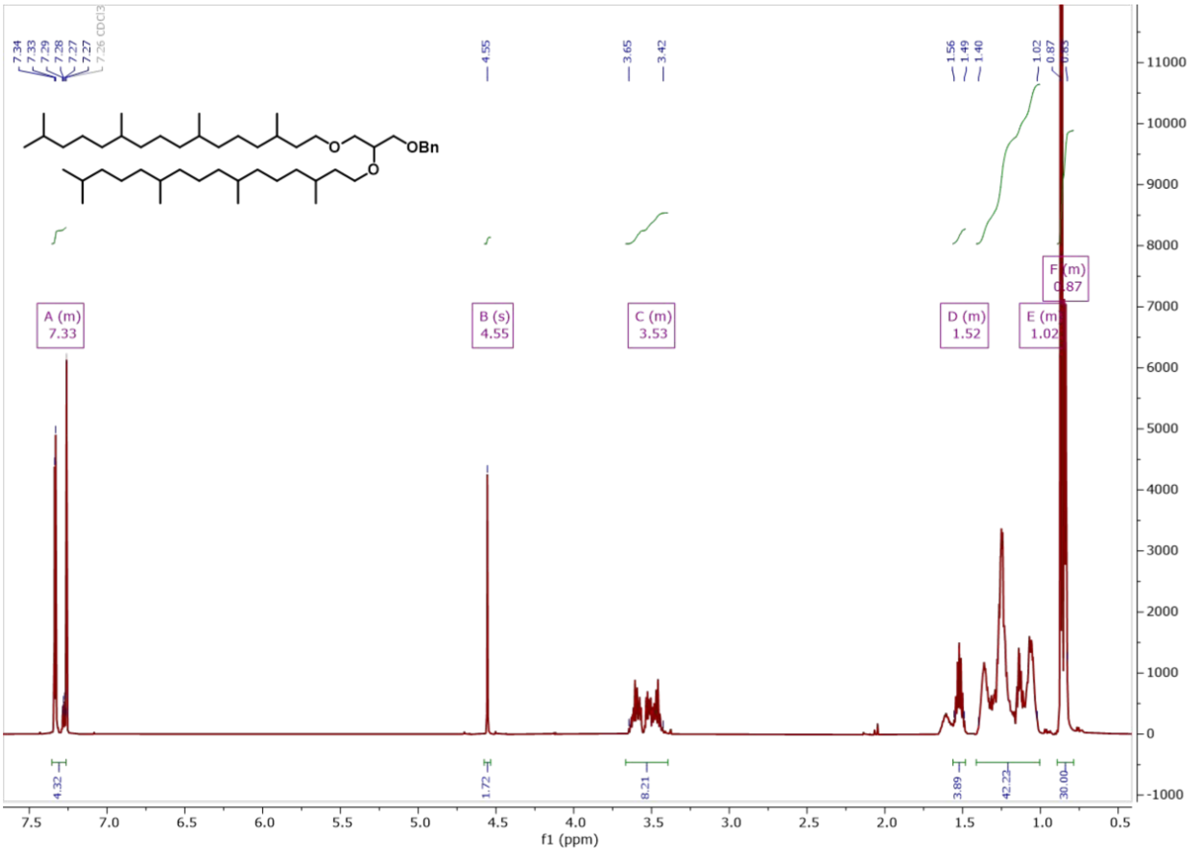

Supplementary Figure 2: ^{1}H-NMR of **4**

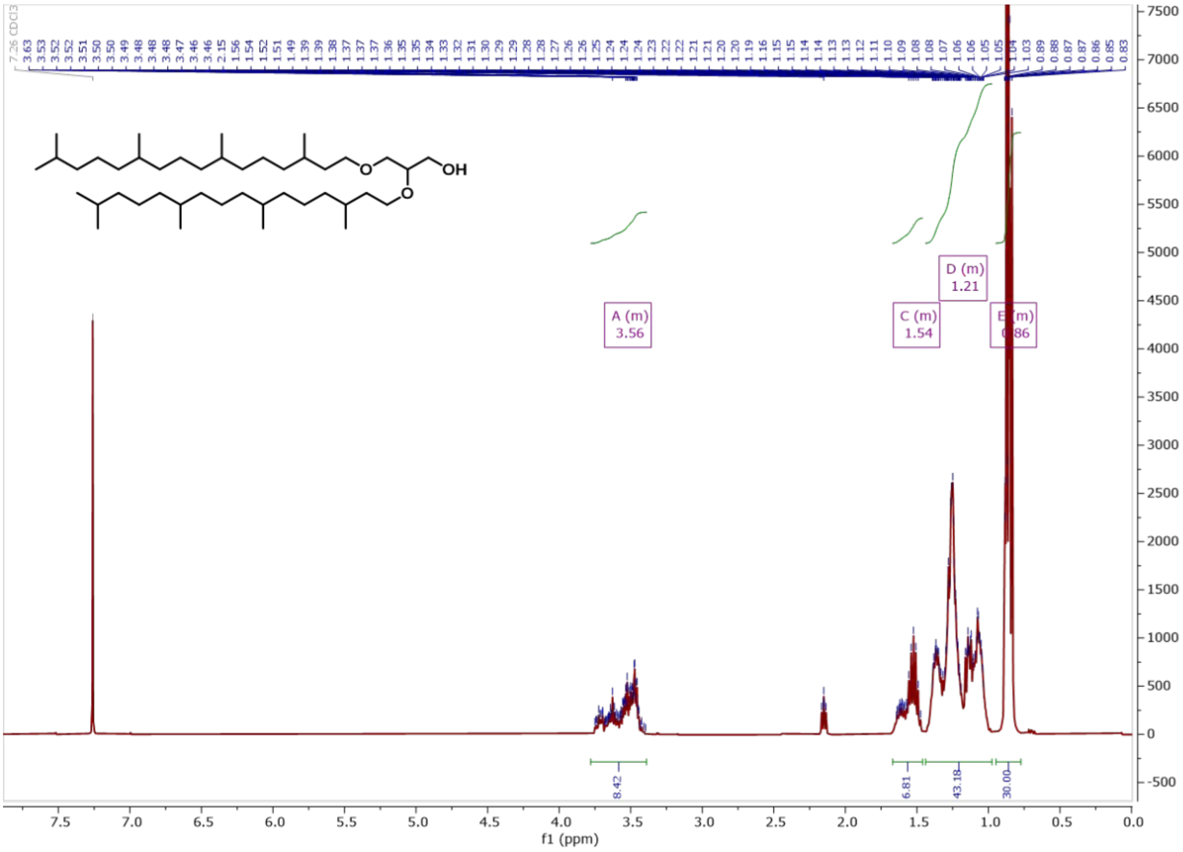

Supplementary Figure 3: ^{1}H-NMR of **5**

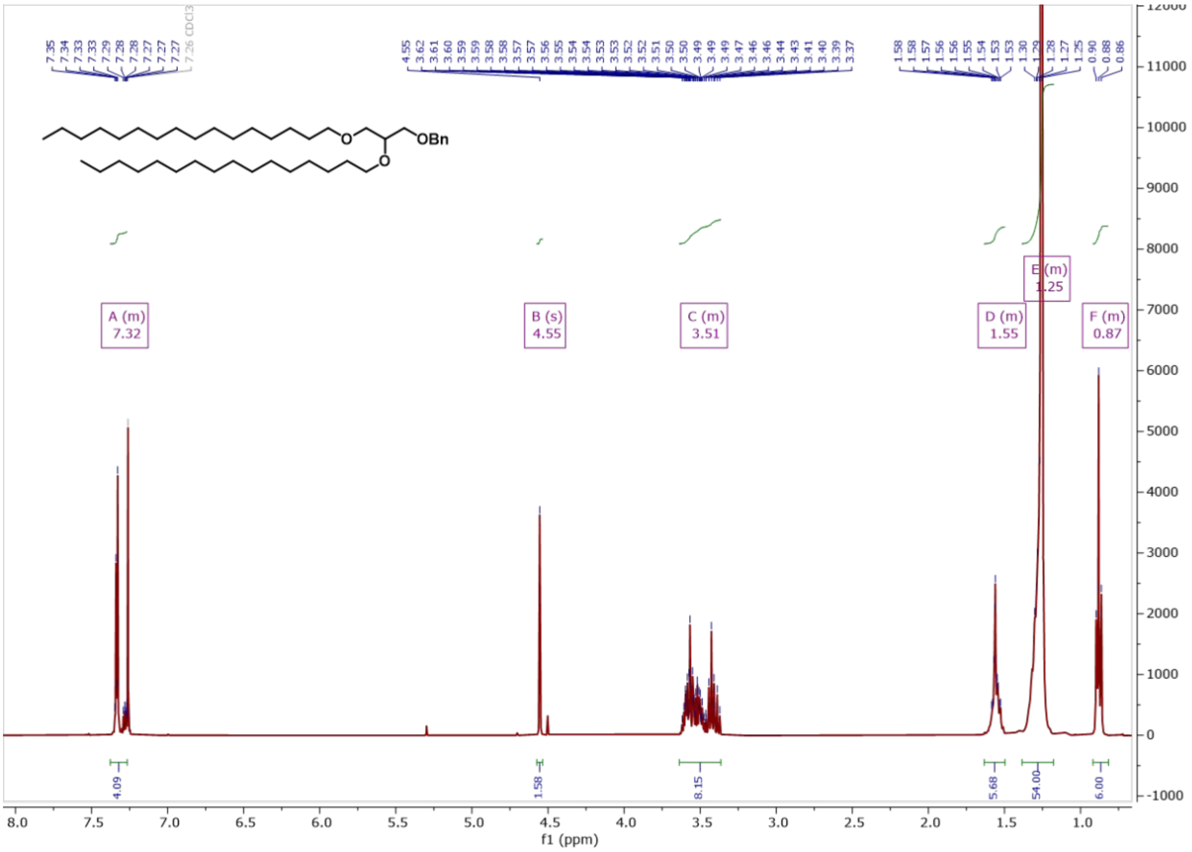

Supplementary Figure 4: ^{1}H-NMR of **10**

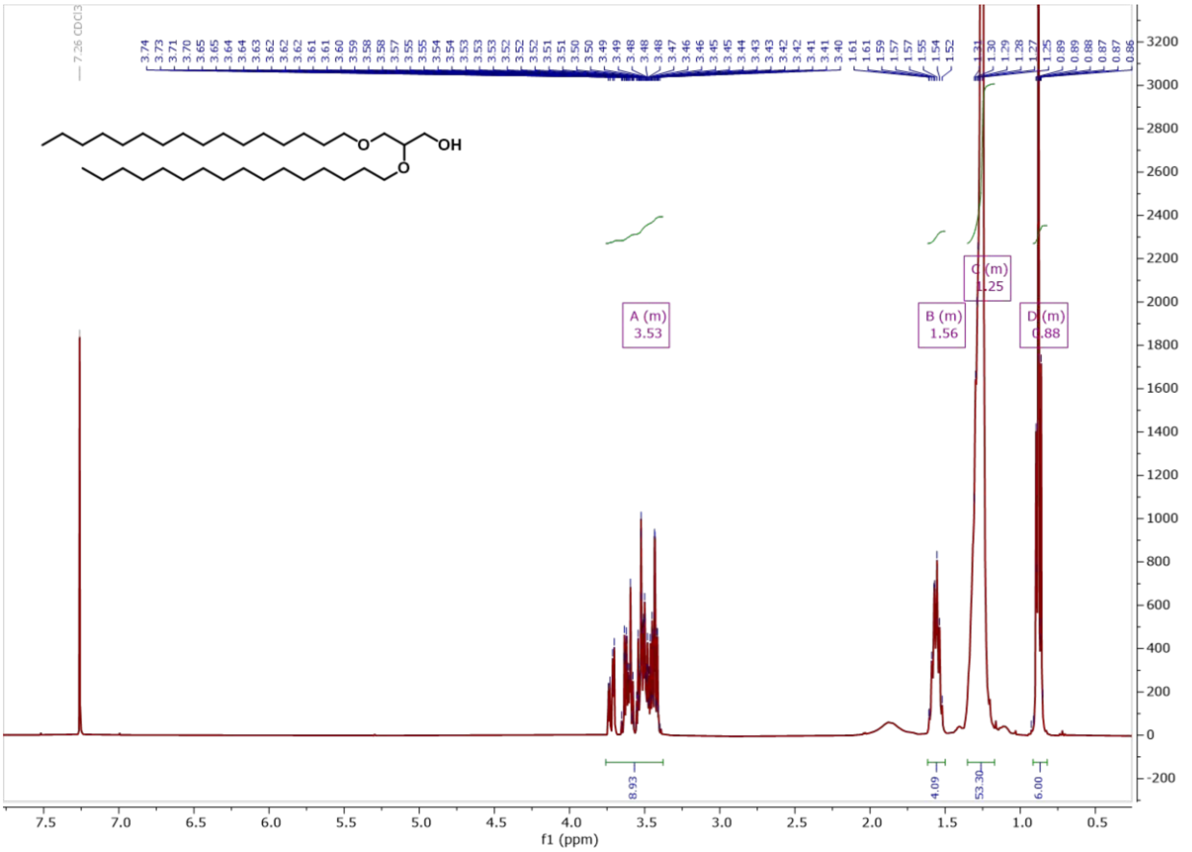

Supplementary Figure 5: ^{1}H-NMR of **11**

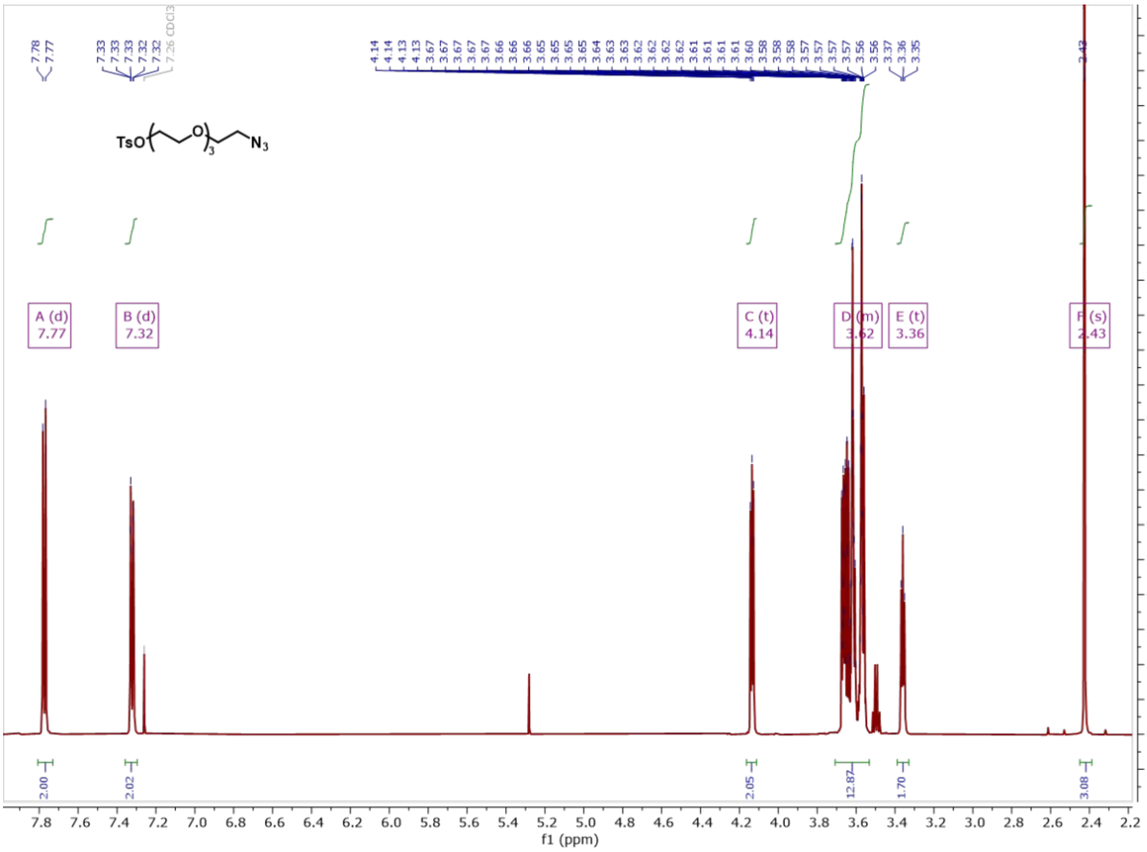

Supplementary Figure 6: ^{1}H-NMR of **7a**

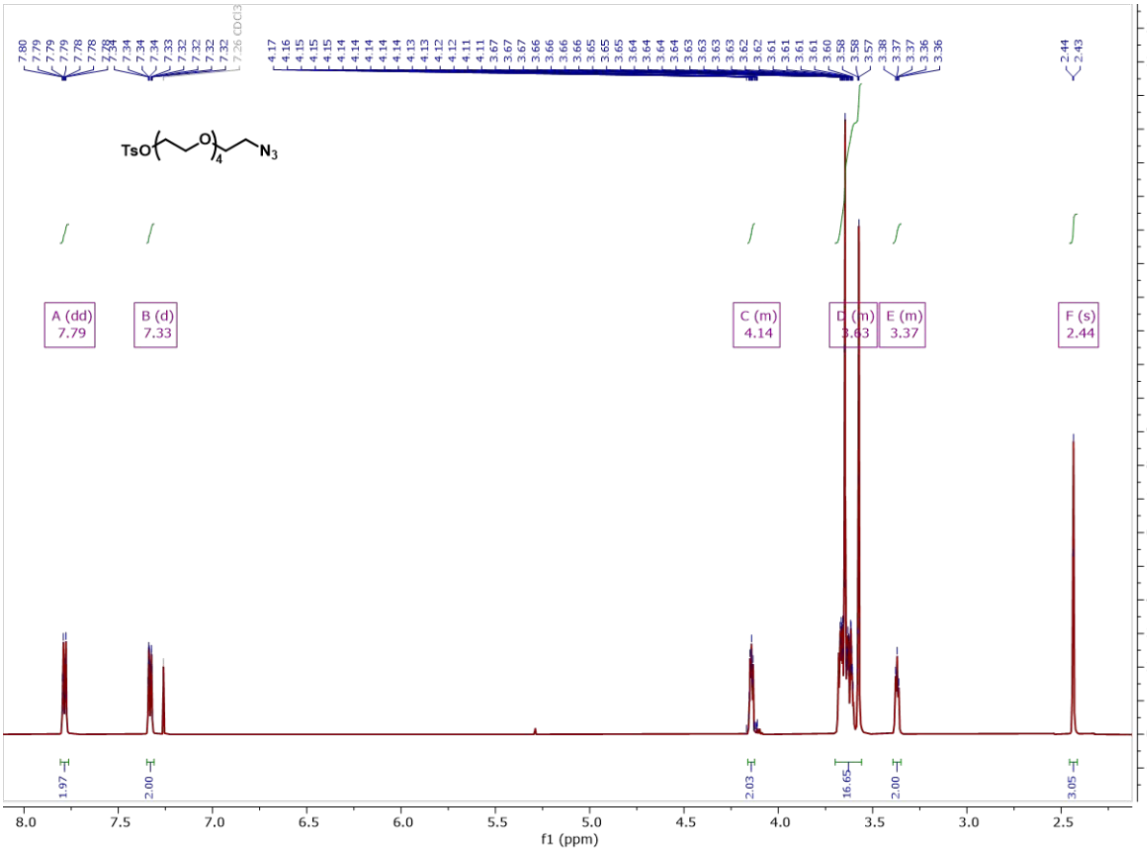

Supplementary Figure 7: ^{1}H-NMR of **7b**

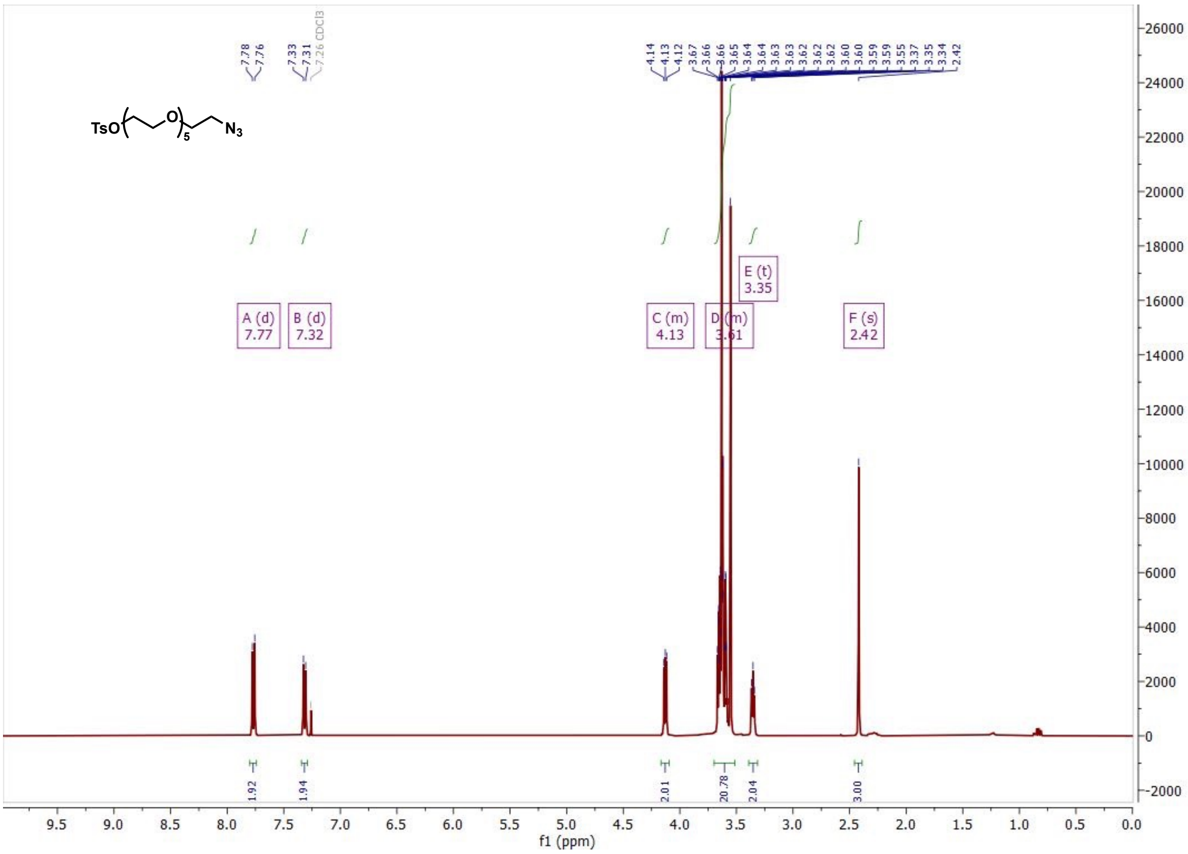

Supplementary Figure 8: ^{1}H-NMR of **7c**

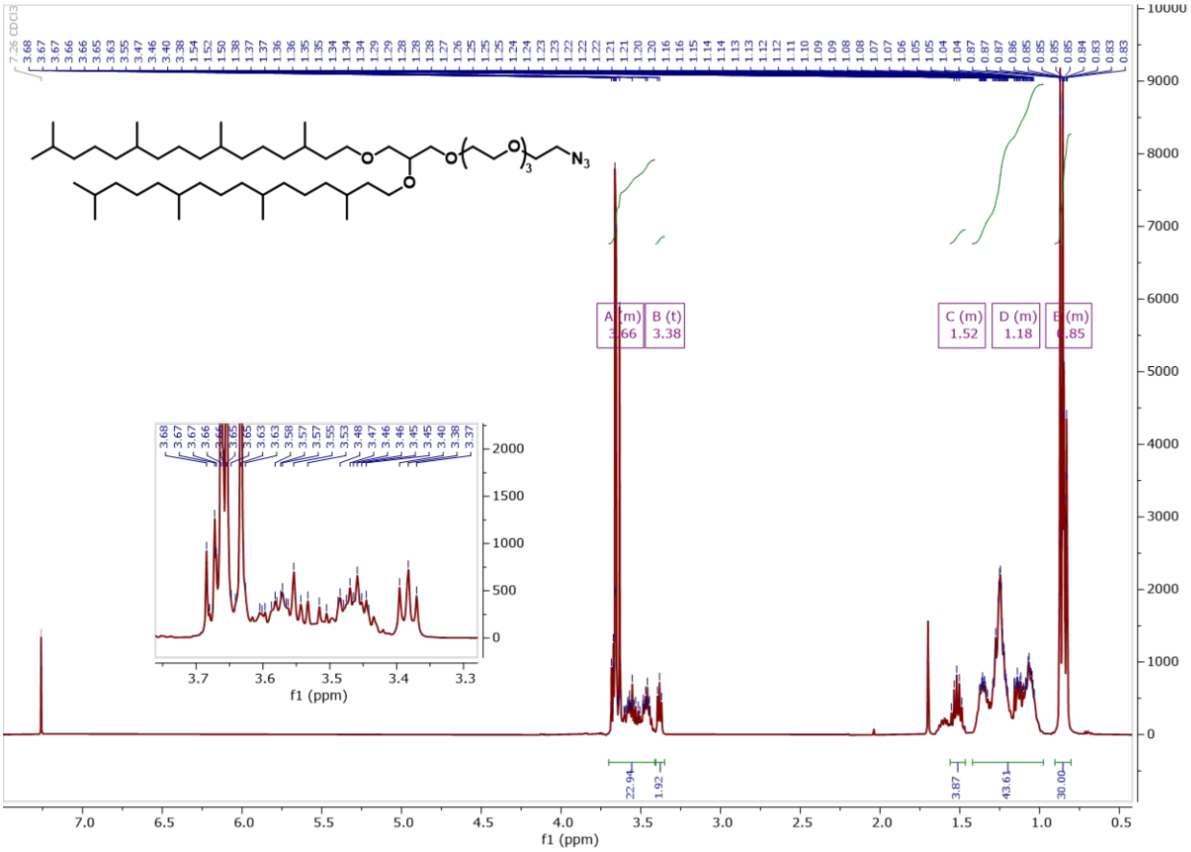

Supplementary Figure 9: ^{1}H-NMR of **Ia**

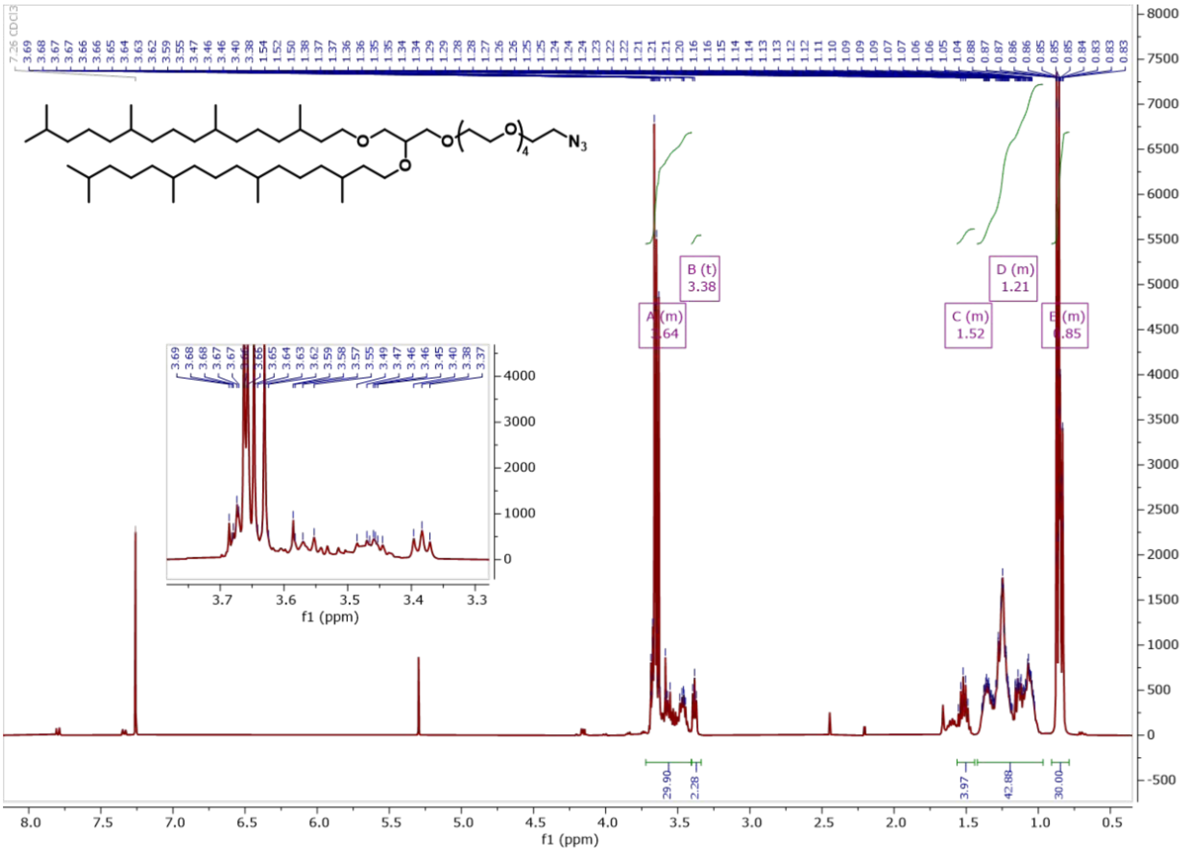

Supplementary Figure 10: ^{1}H-NMR of **Ib**

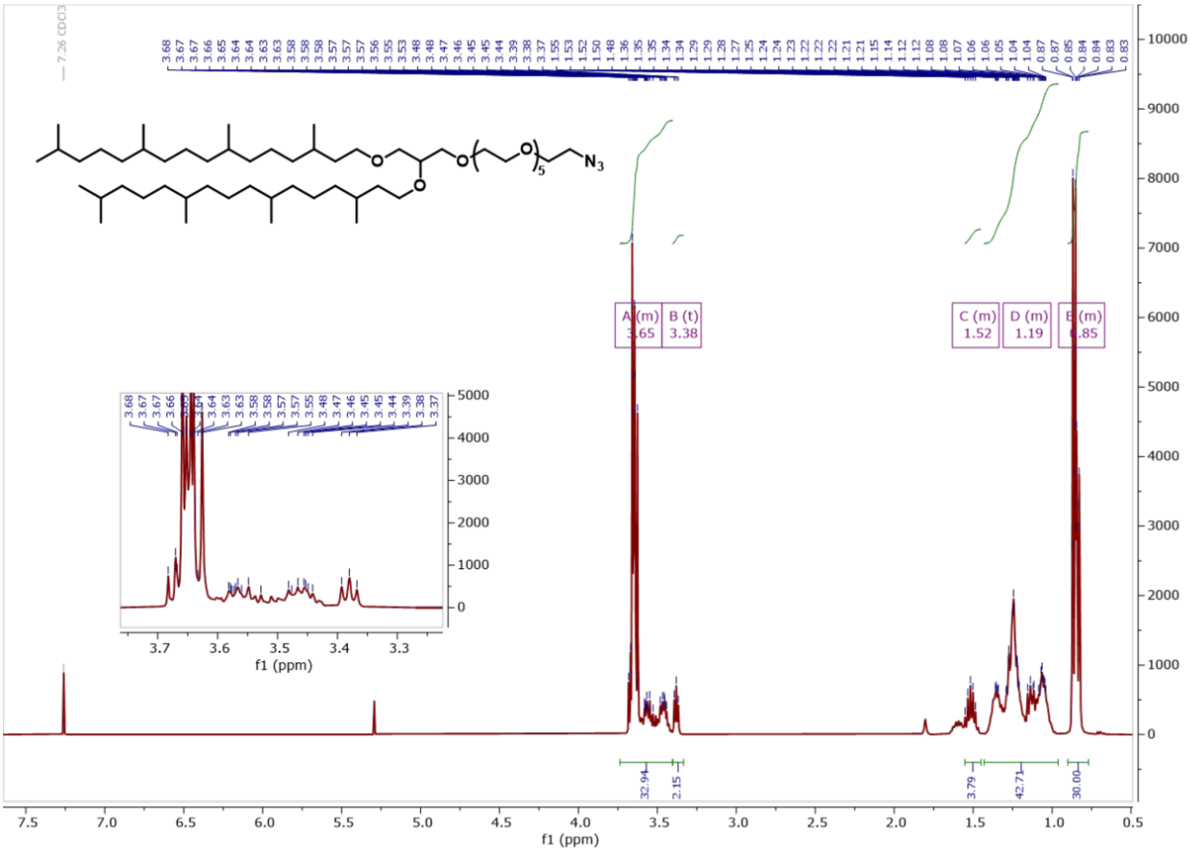

Supplementary Figure 11: ^{1}H-NMR of **Ic**

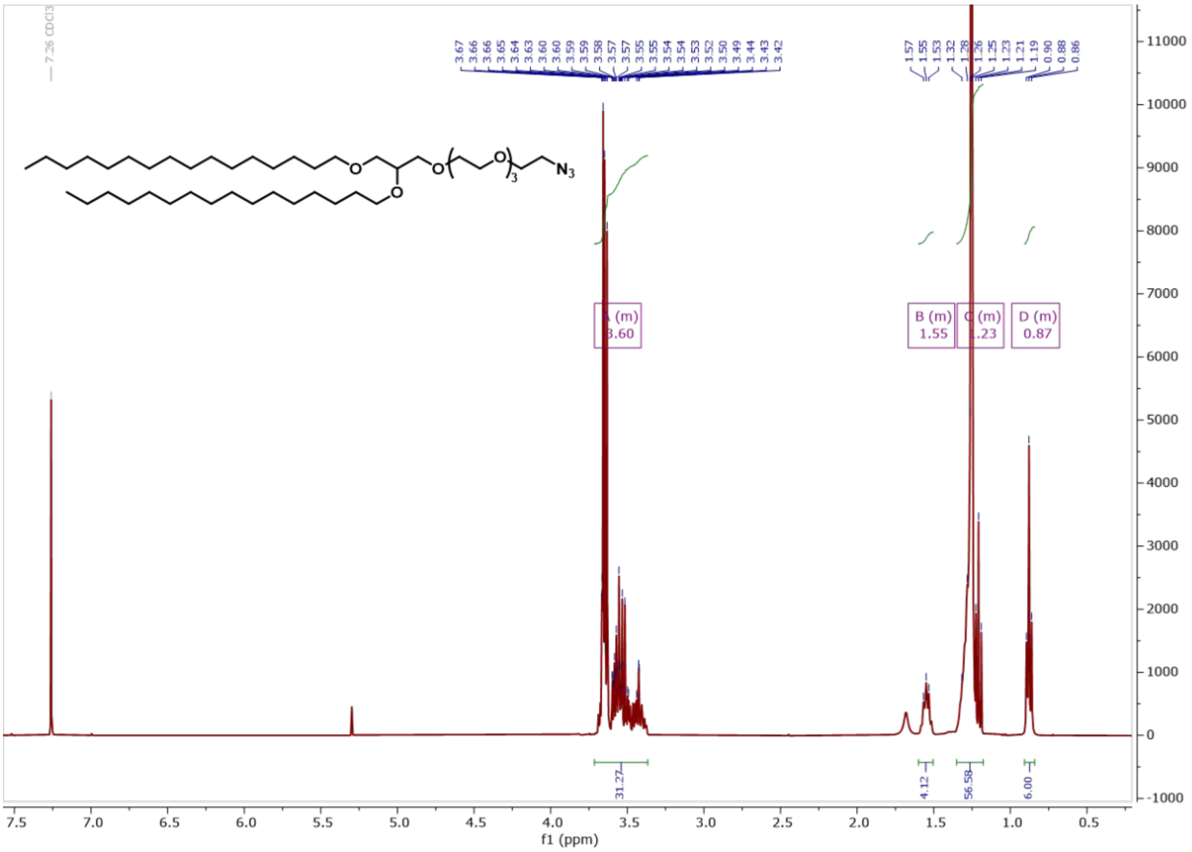

Supplementary Figure 12: ^{1}H-NMR of **IVa**

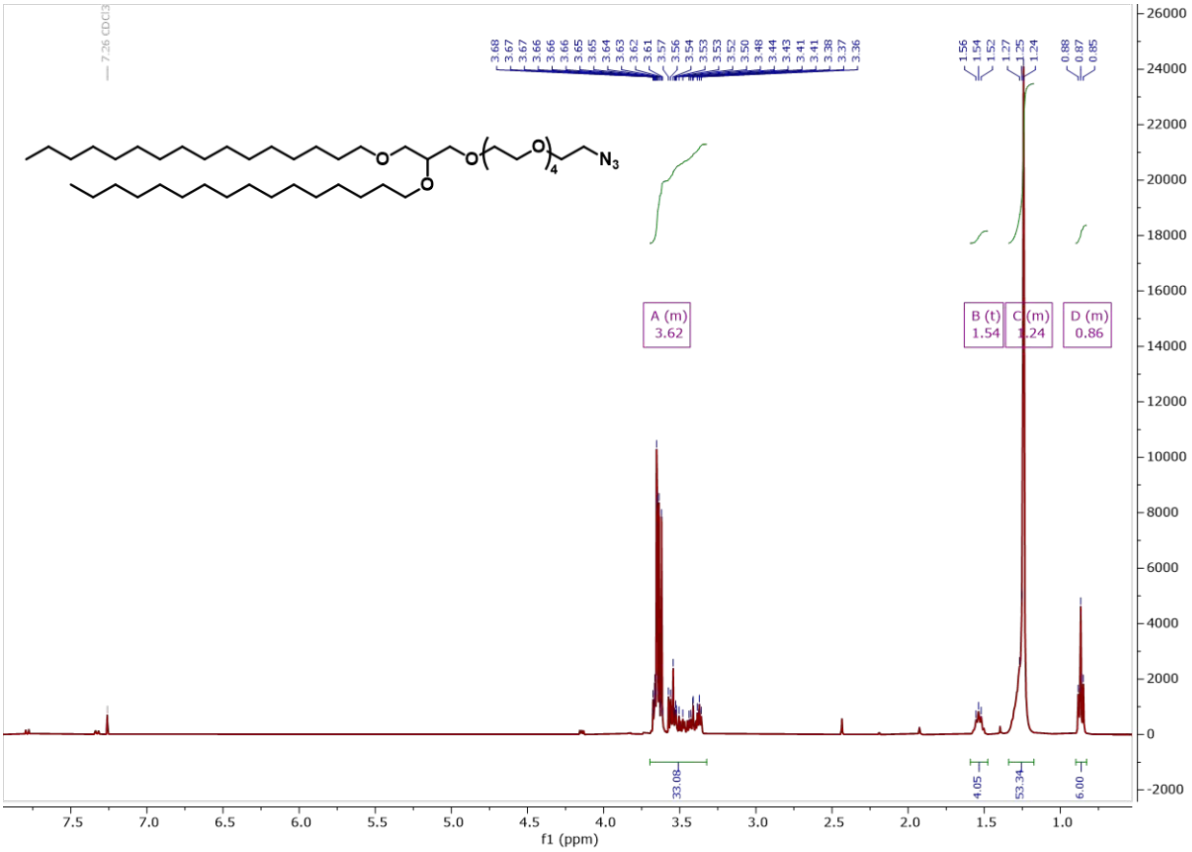

Supplementary Figure 13: ^{1}H-NMR of **IVb**

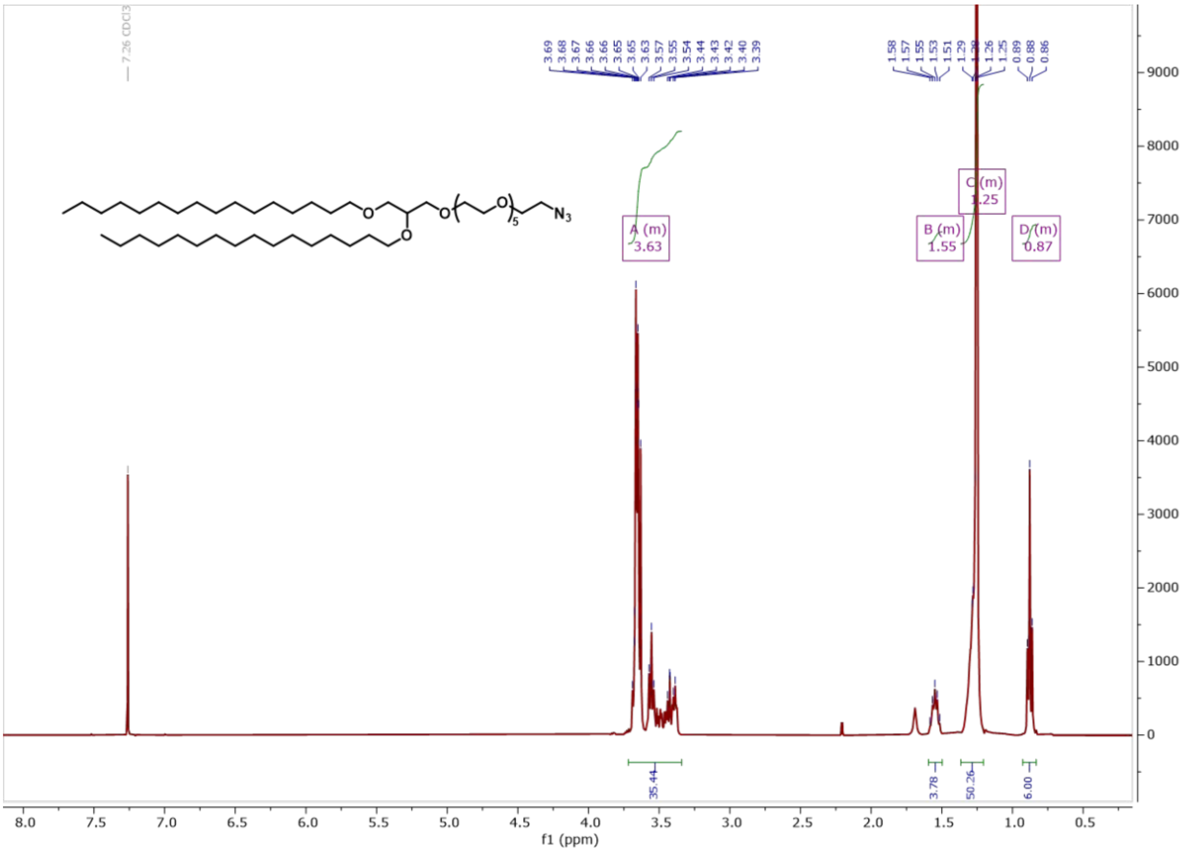

Supplementary Figure 14: ^{1}H-NMR of **IVc**

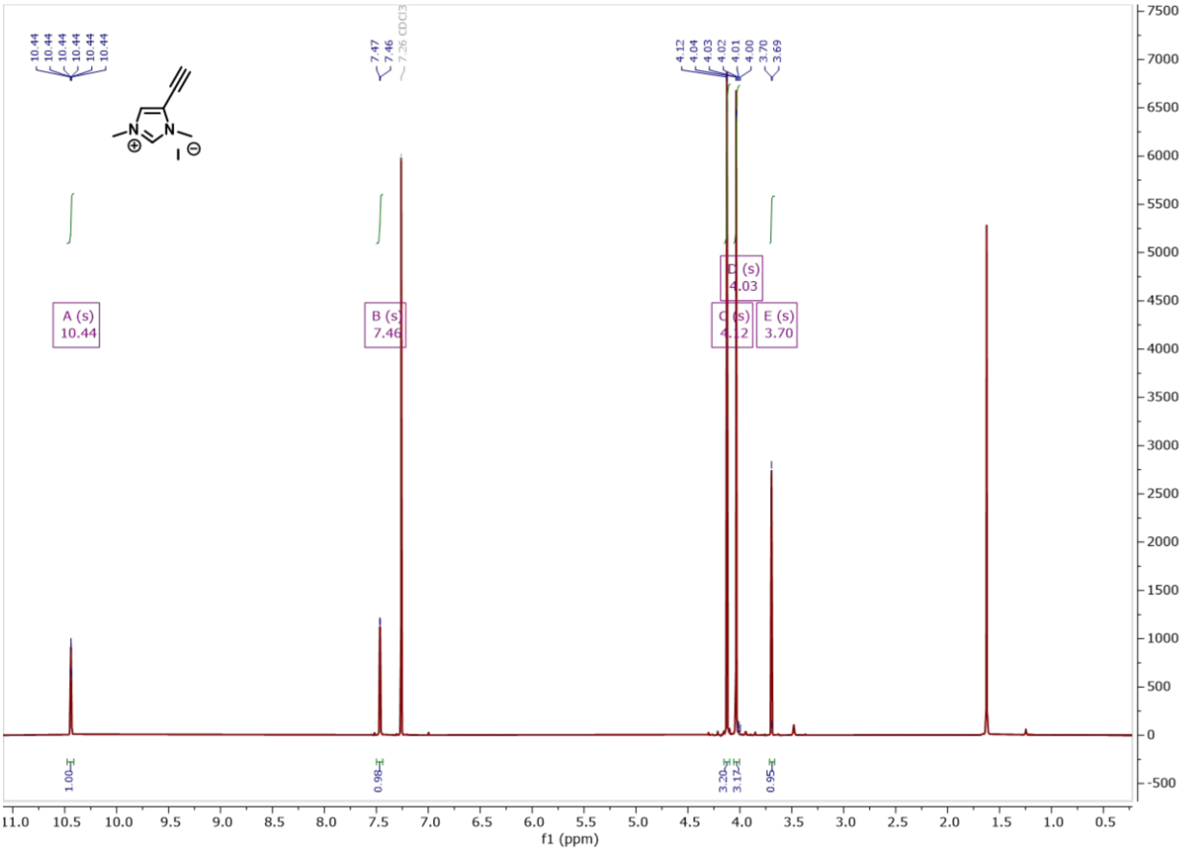

Supplementary Figure 15: ^{1}H-NMR of **8**

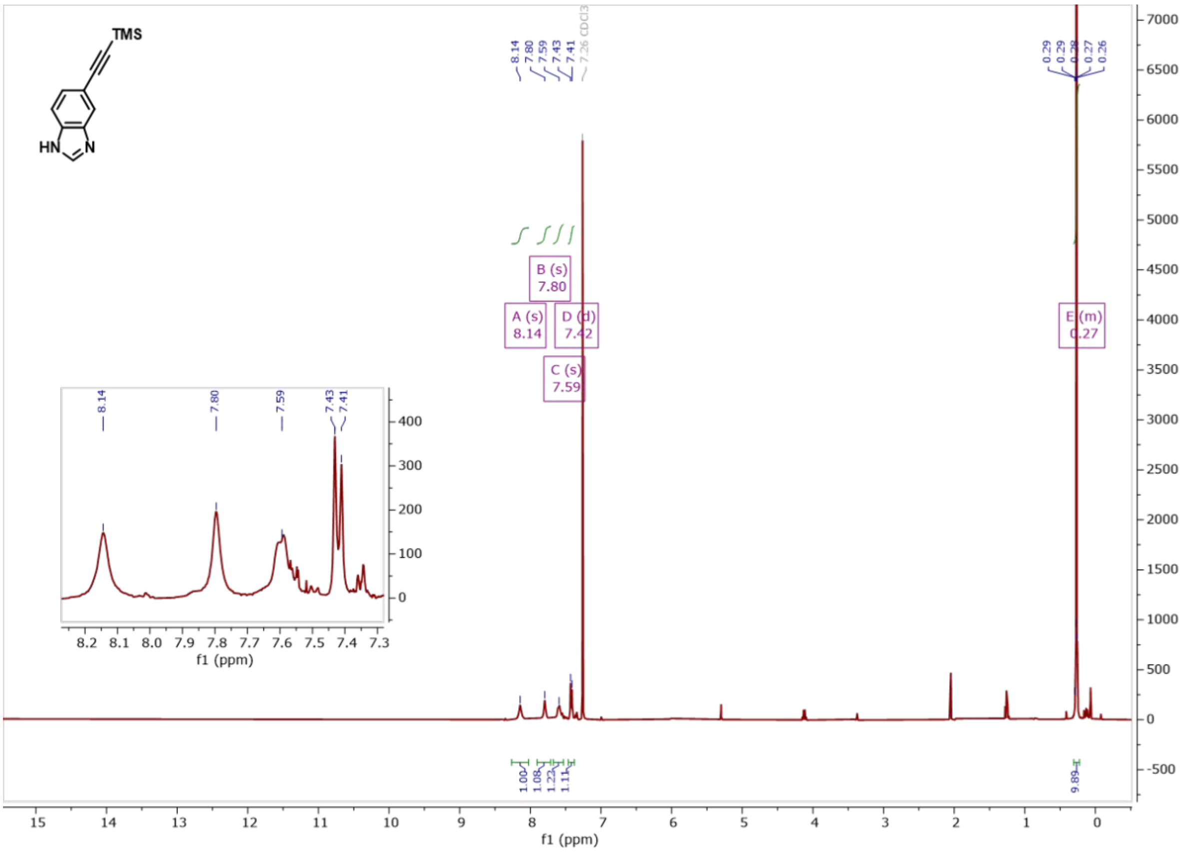

Supplementary Figure 16: ^{1}H-NMR of **17**

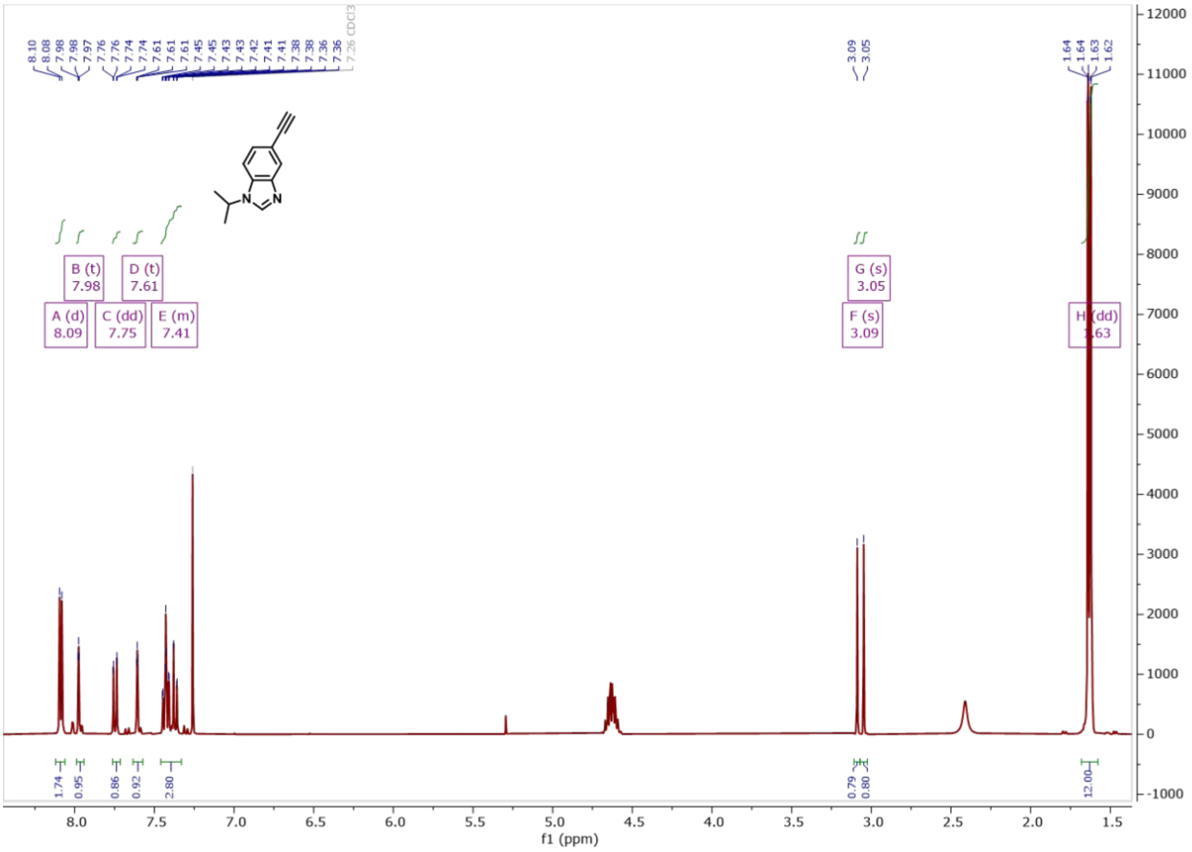

Supplementary Figure 17: ^{1}H-NMR of **Xa**

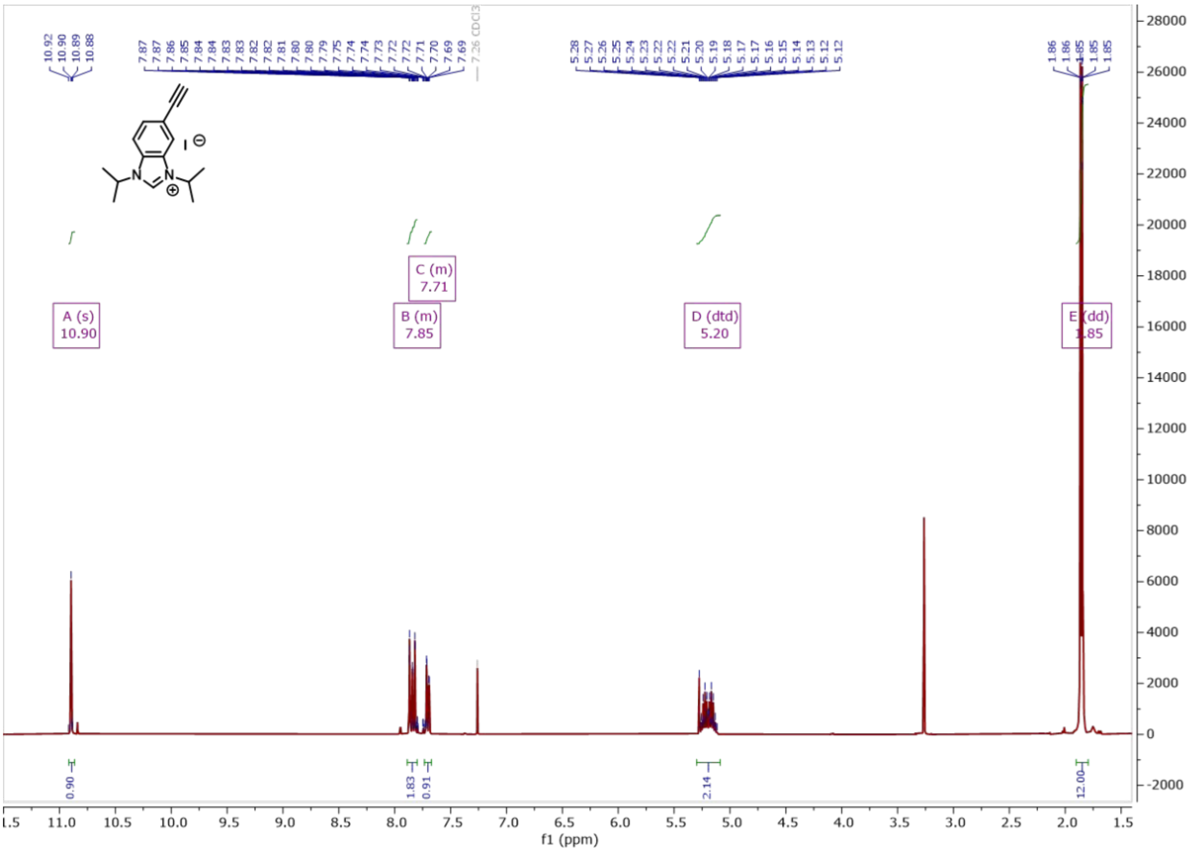

Supplementary Figure 18: ^{1}H-NMR of **X**

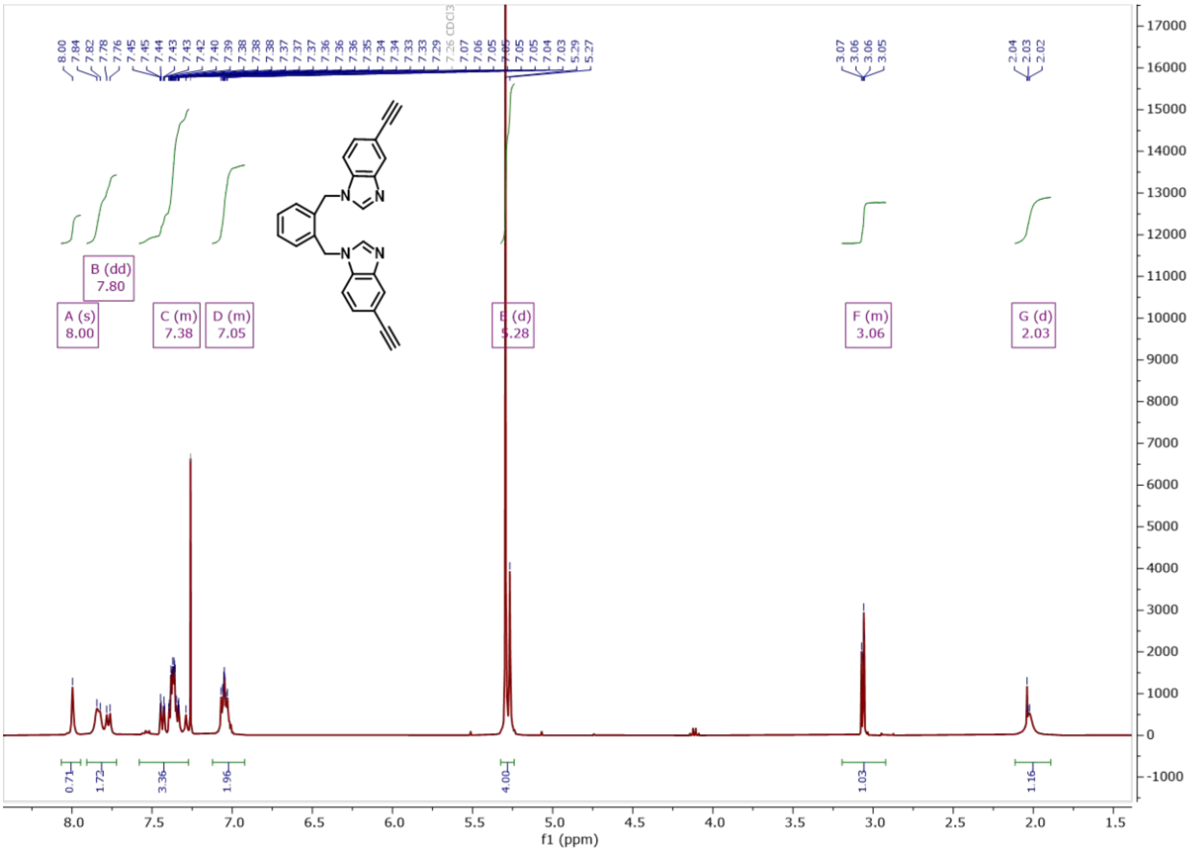

Supplementary Figure 19: ^{1}H-NMR of **XVI**

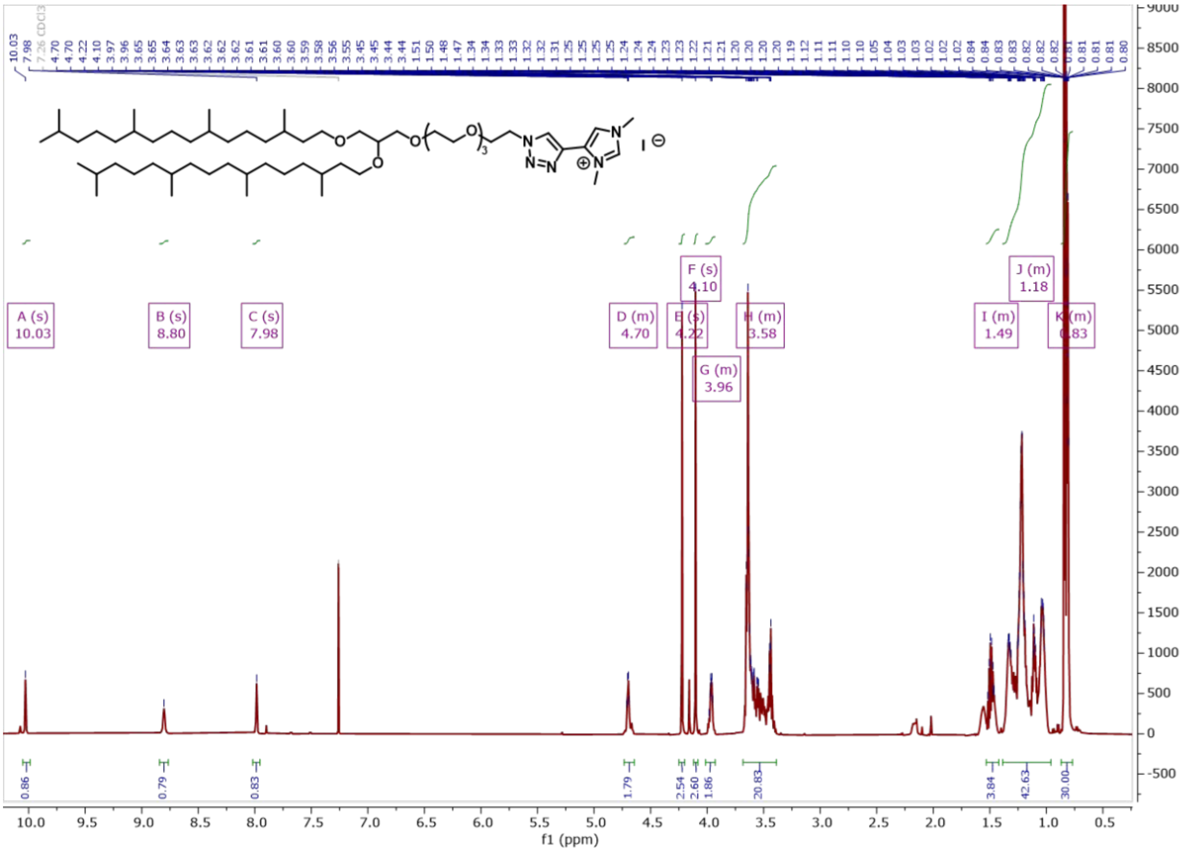

Supplementary Figure 20: ^{1}H-NMR of **IIa**

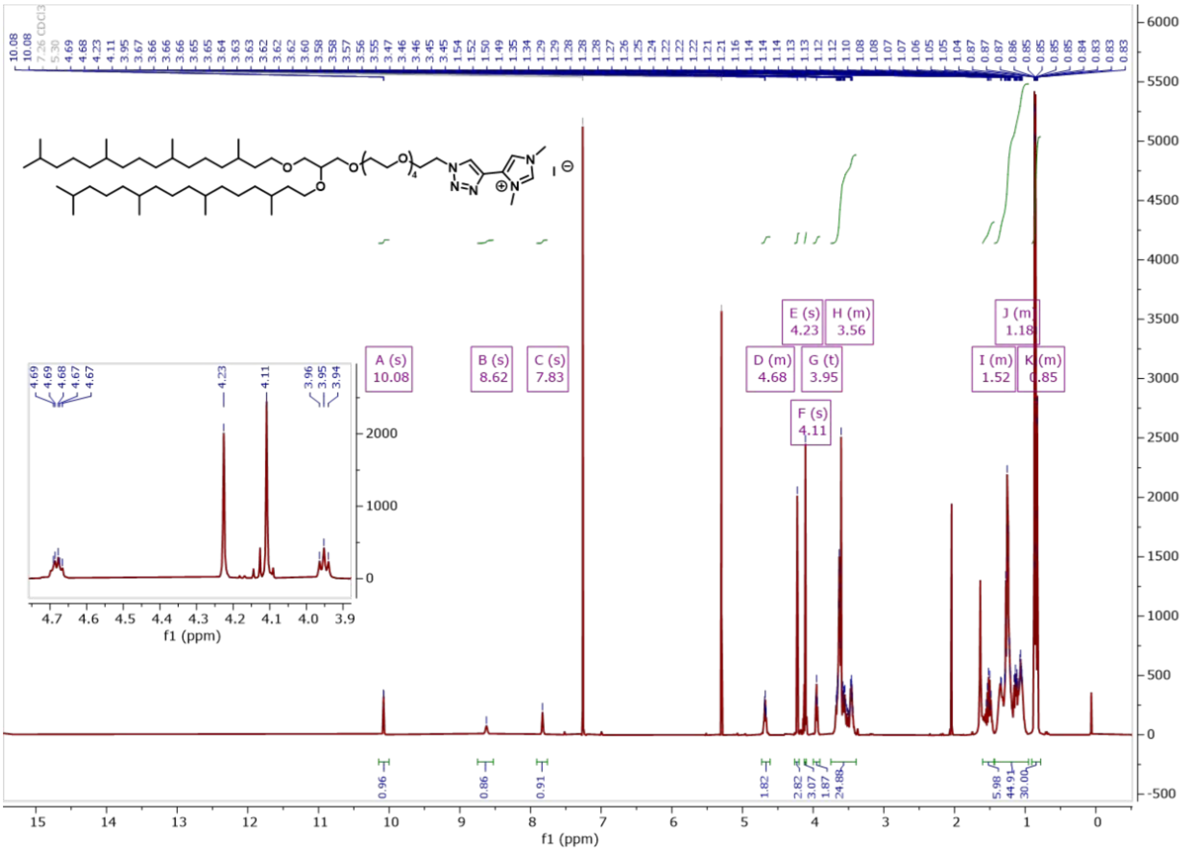

Supplementary Figure 21: ^{1}H-NMR of **IIb**

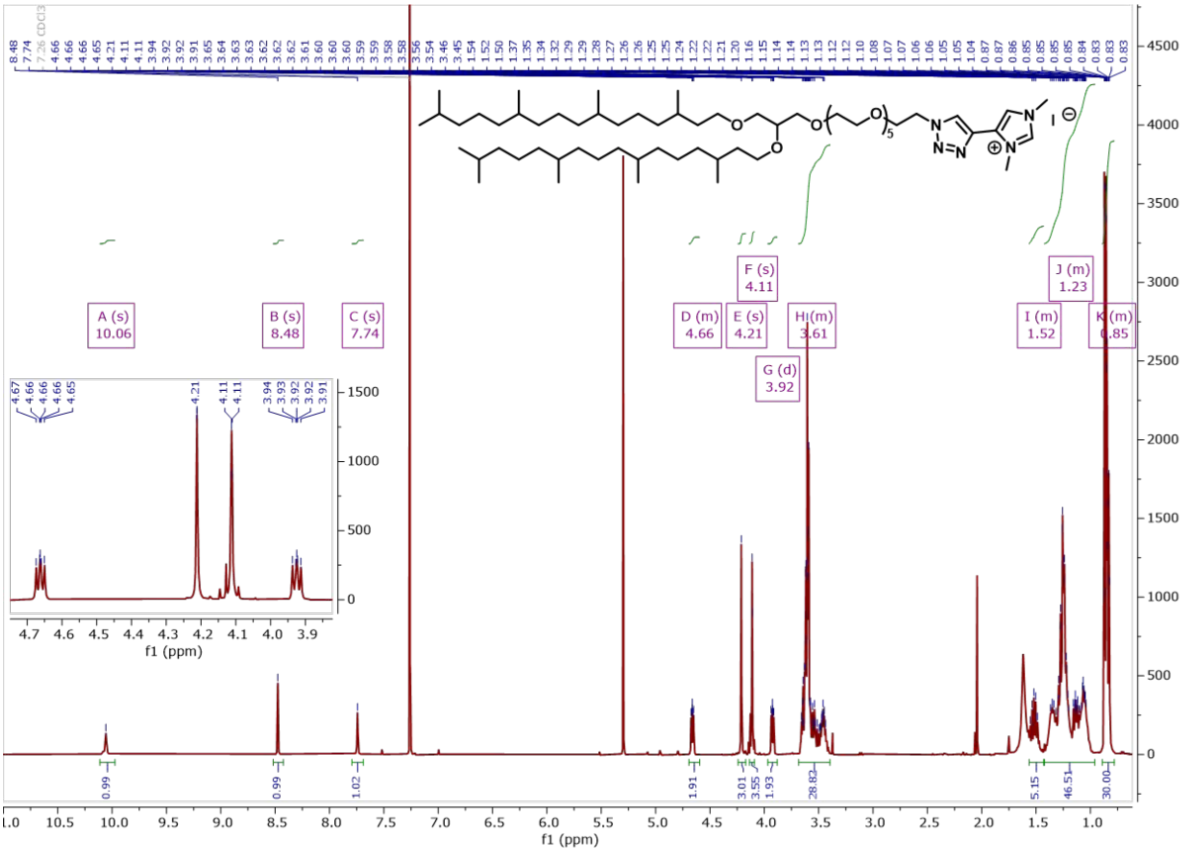

Supplementary Figure 22: ^{1}H-NMR of **IIc**

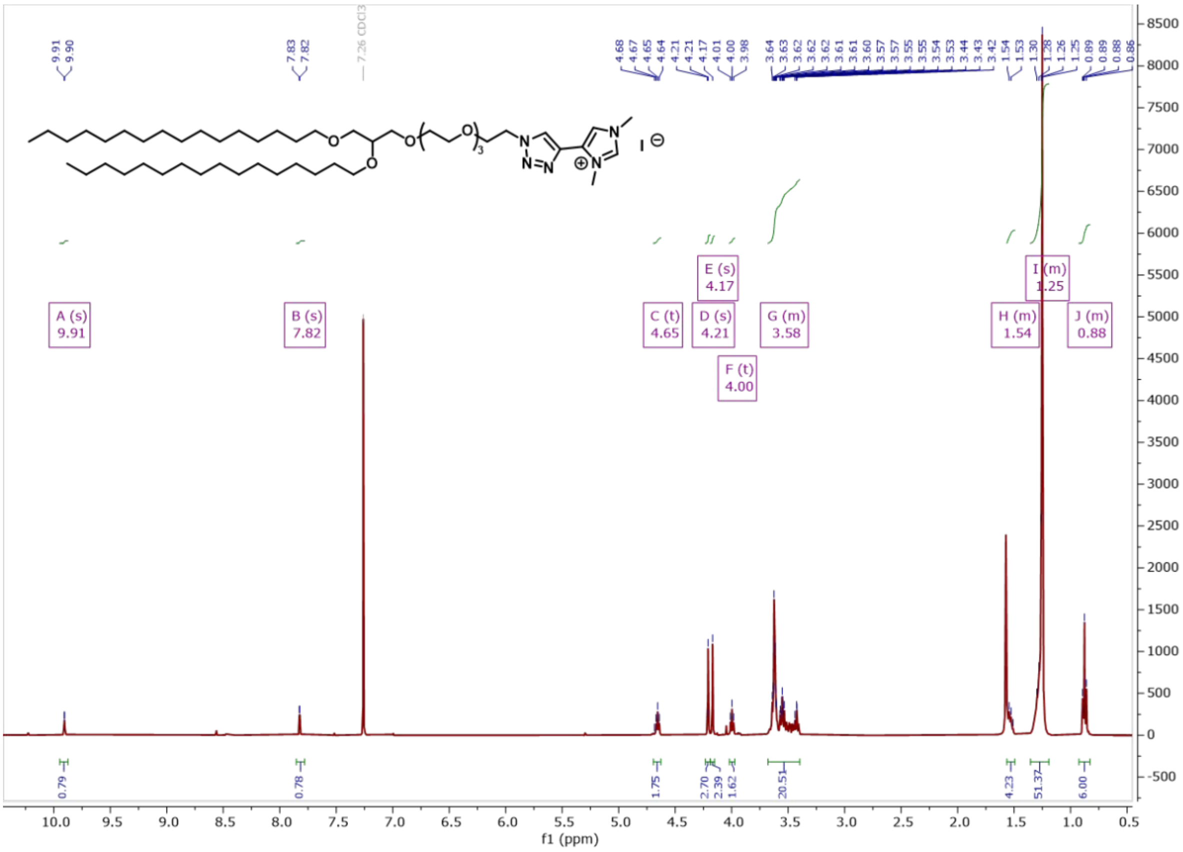

Supplementary Figure 23: ^{1}H-NMR of **Va**

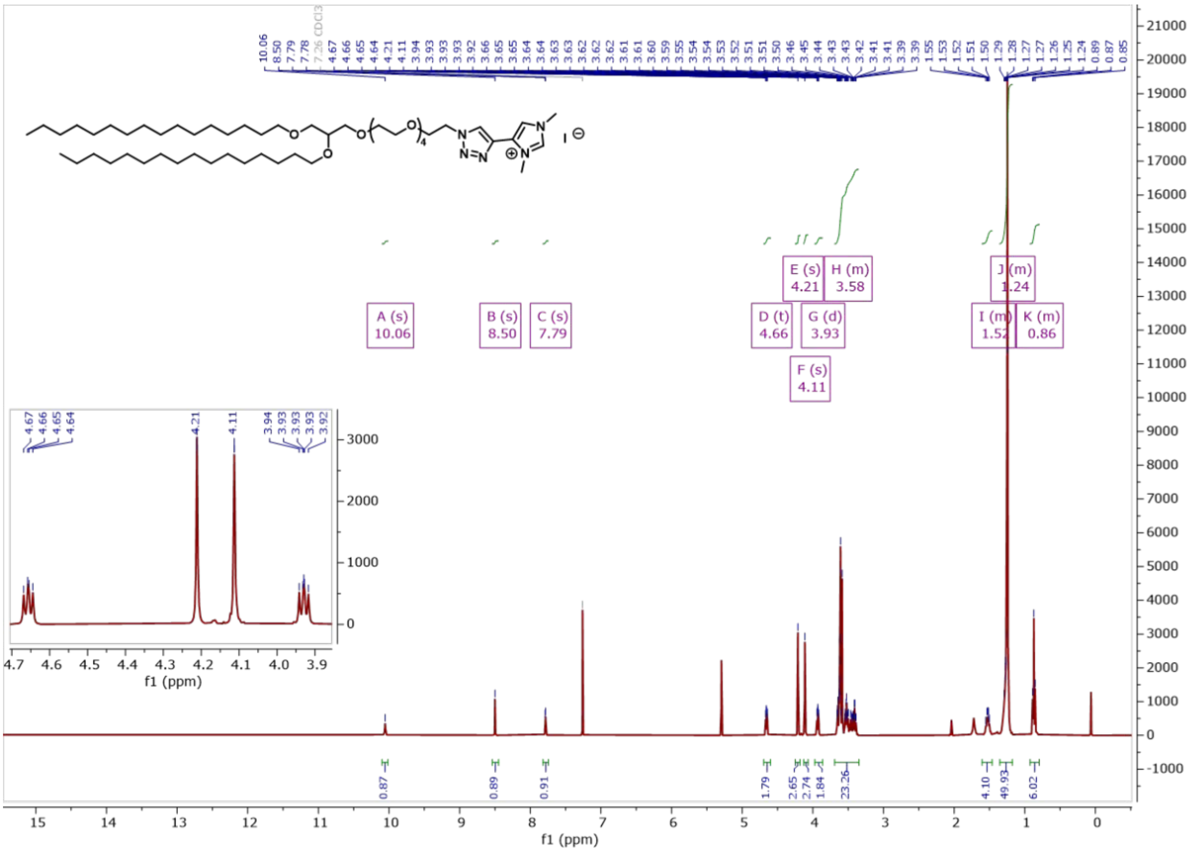

Supplementary Figure 24: ^{1}H-NMR of **Vb**

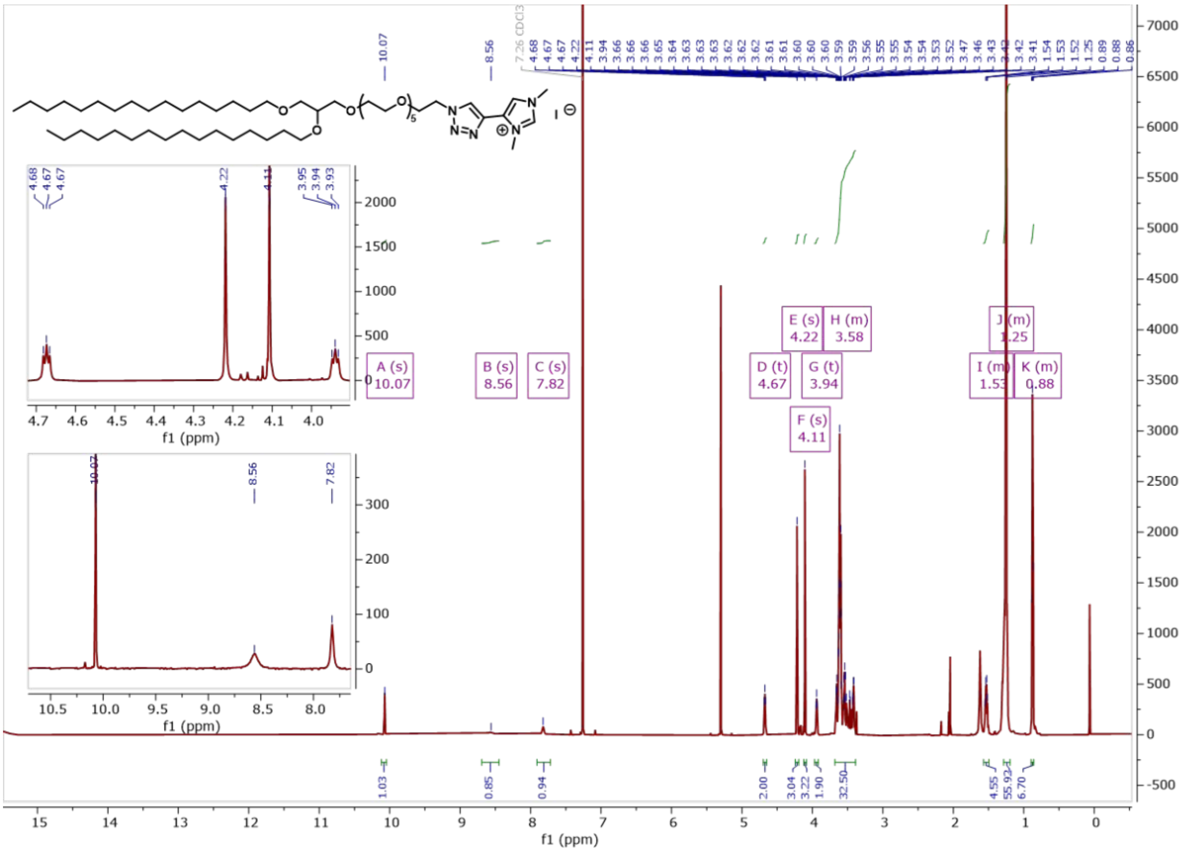

Supplementary Figure 25: ^{1}H-NMR of **Vc**

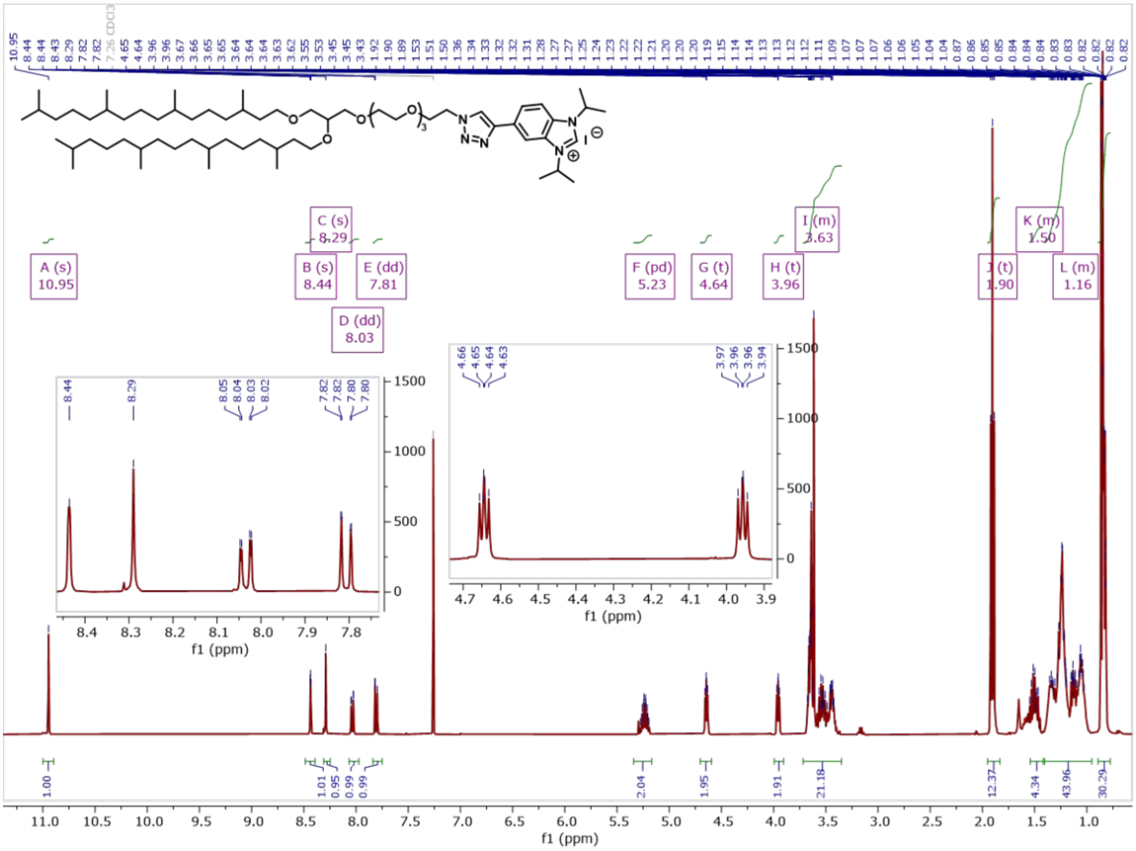

Supplementary Figure 26: ^{1}H-NMR of **XIa**

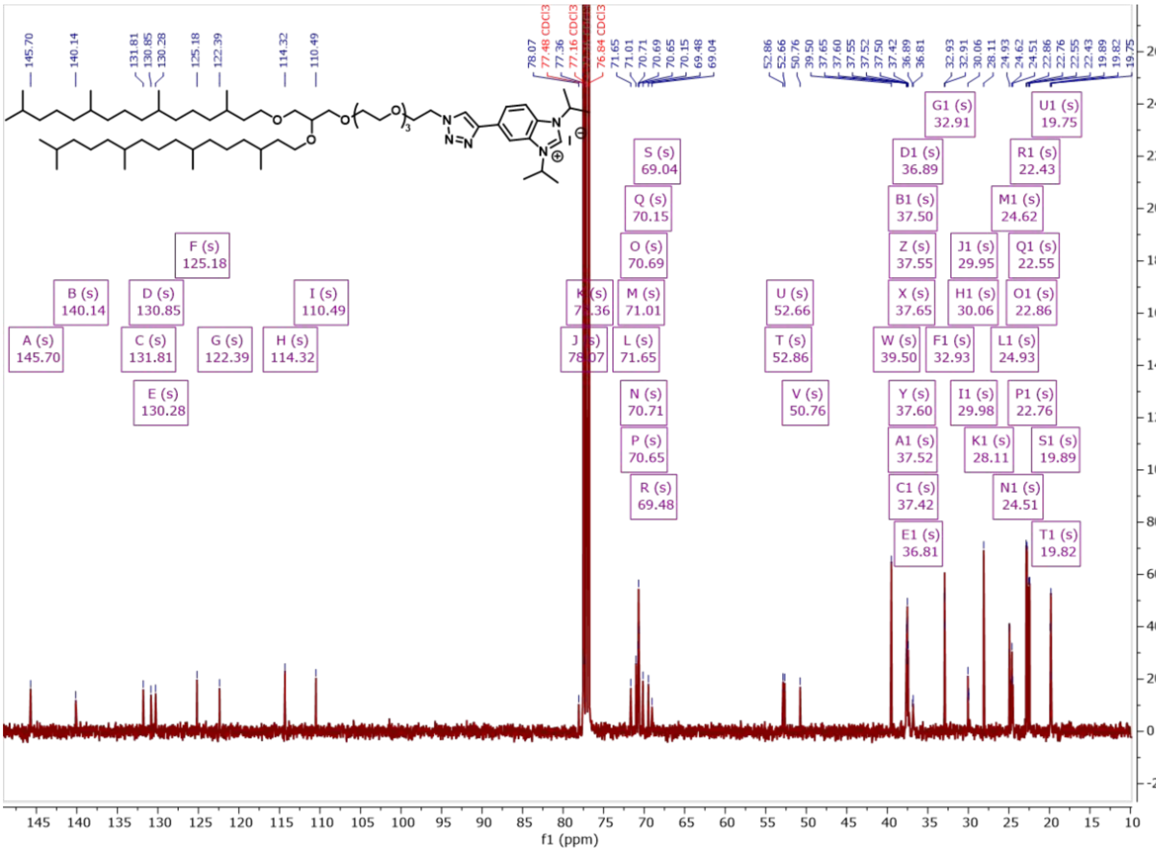

Supplementary Figure 27: ^{13}C-NMR of **XIa**

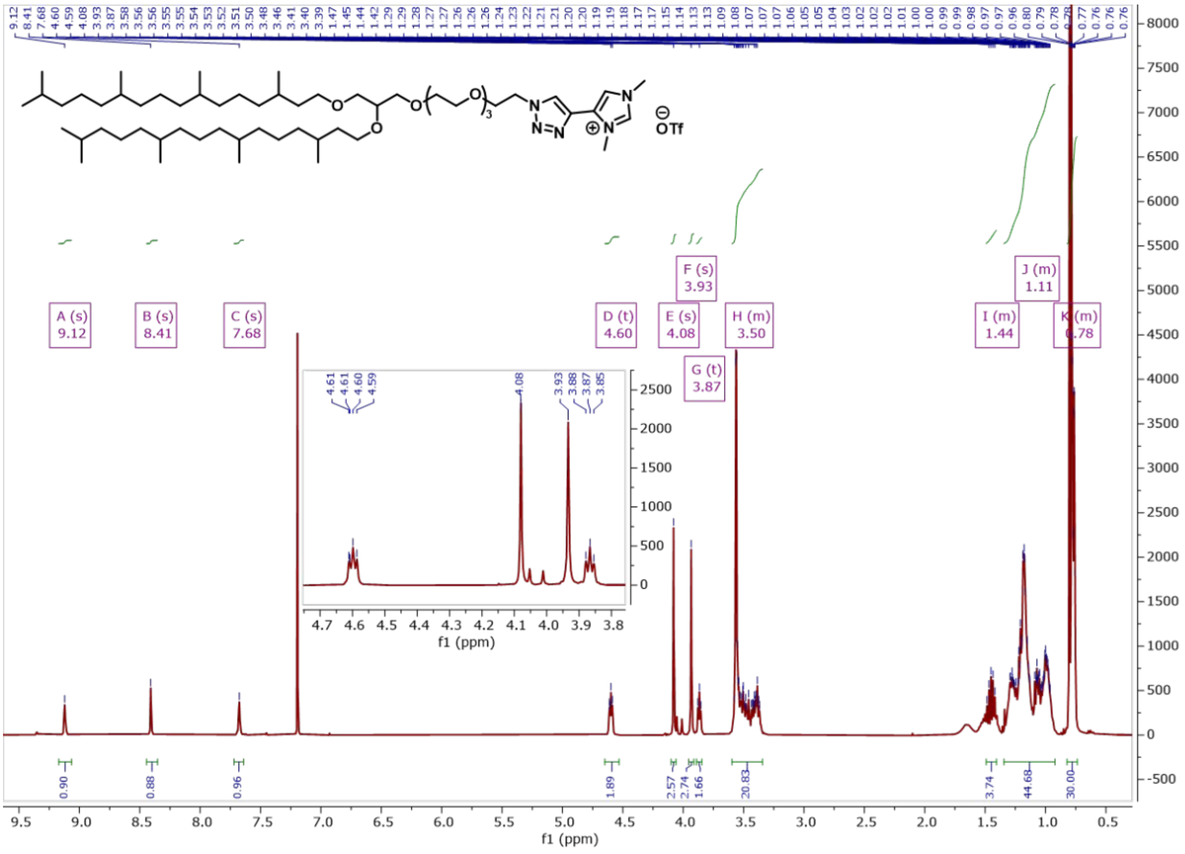

Supplementary Figure 28: ^{1}H-NMR of **IIIa**

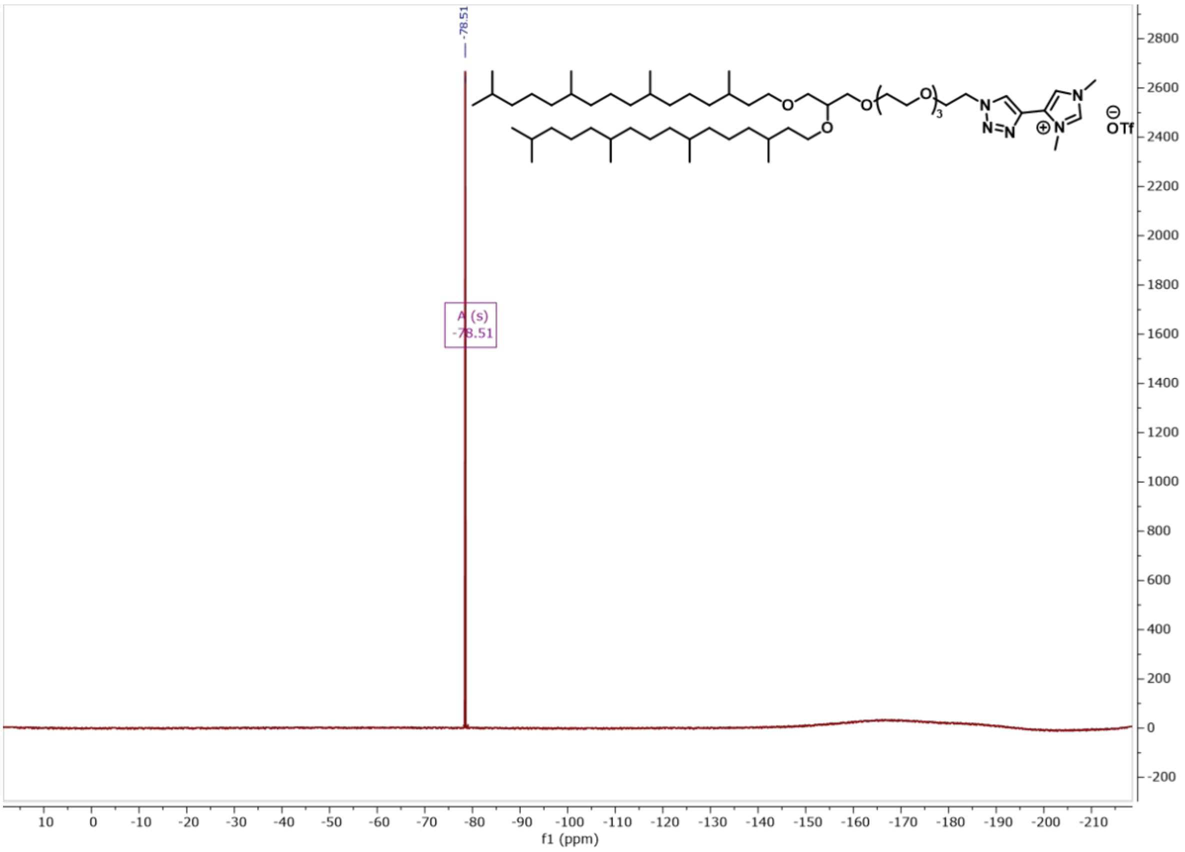

Supplementary Figure 29: ^{19}F-NMR of **IIIa**

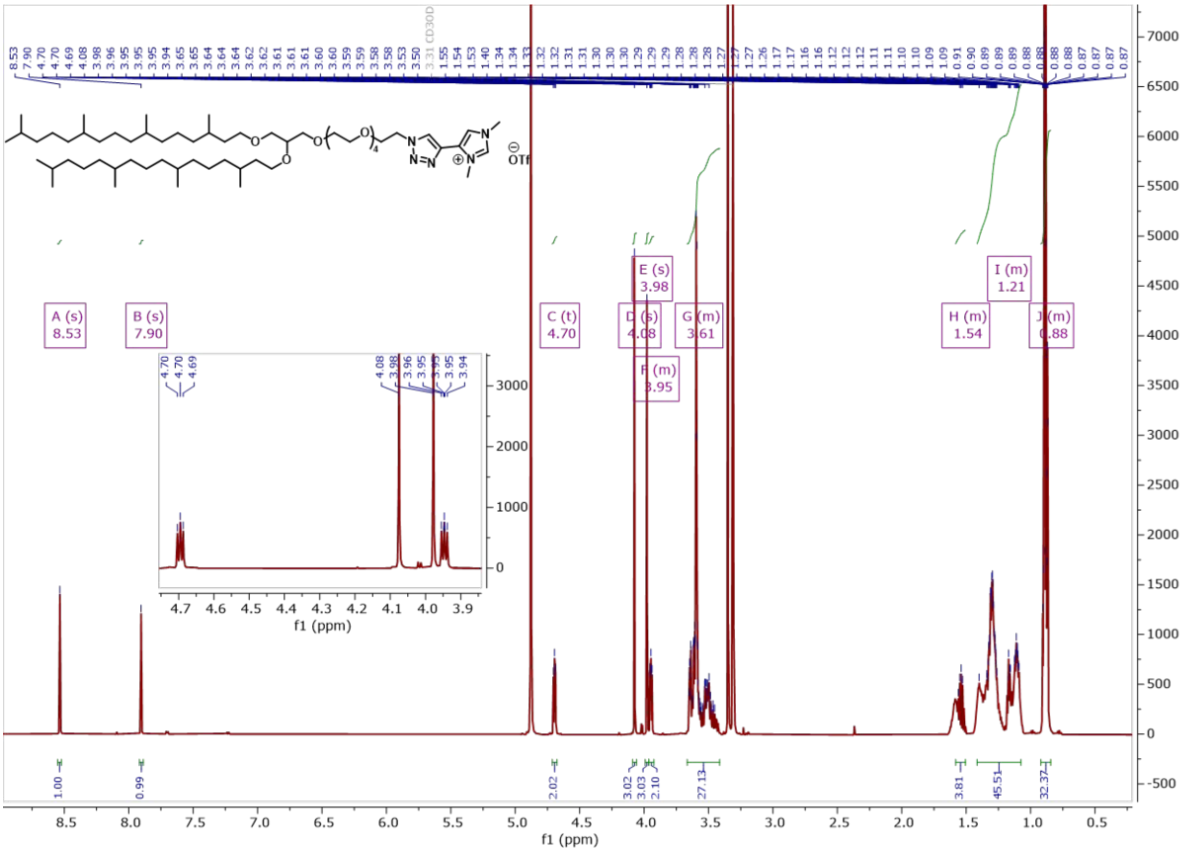

Supplementary Figure 30: ^{1}H-NMR of **IIIb**

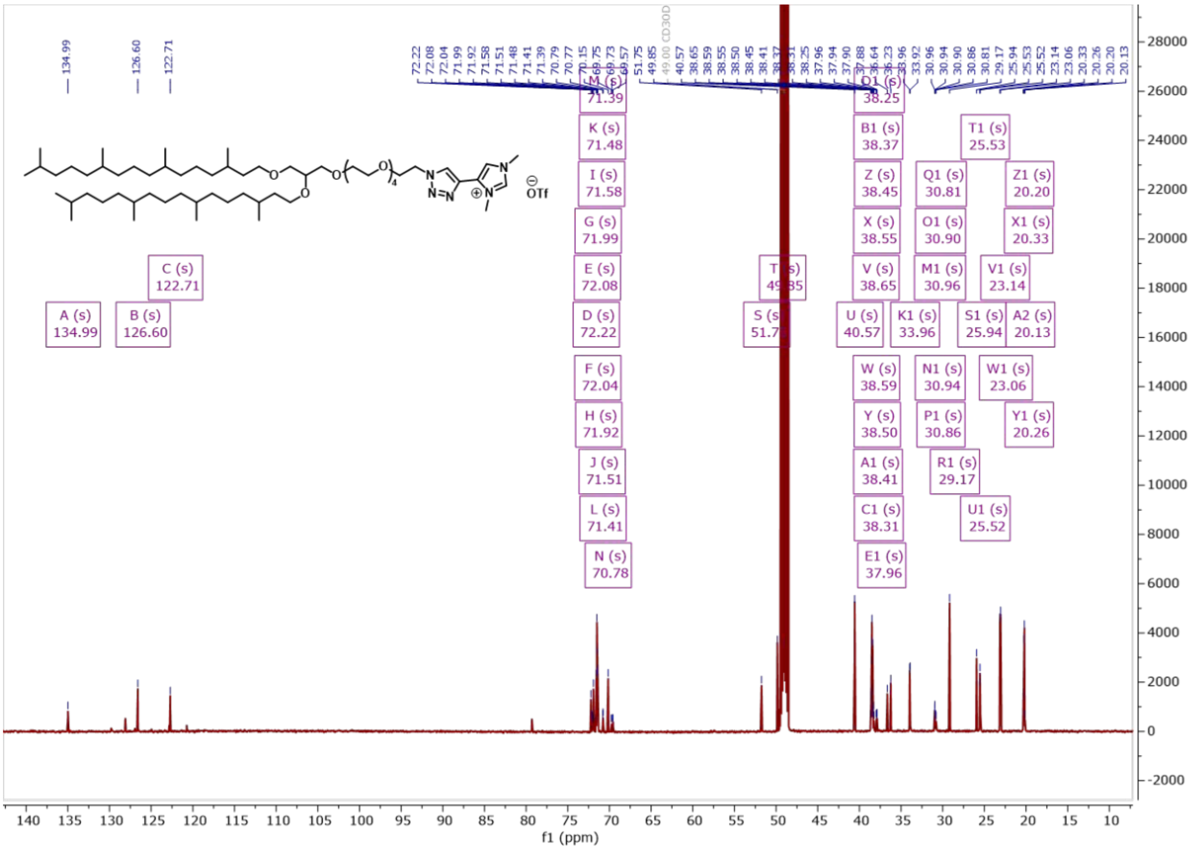

Supplementary Figure 31: ^{13}C-NMR of **IIIb**

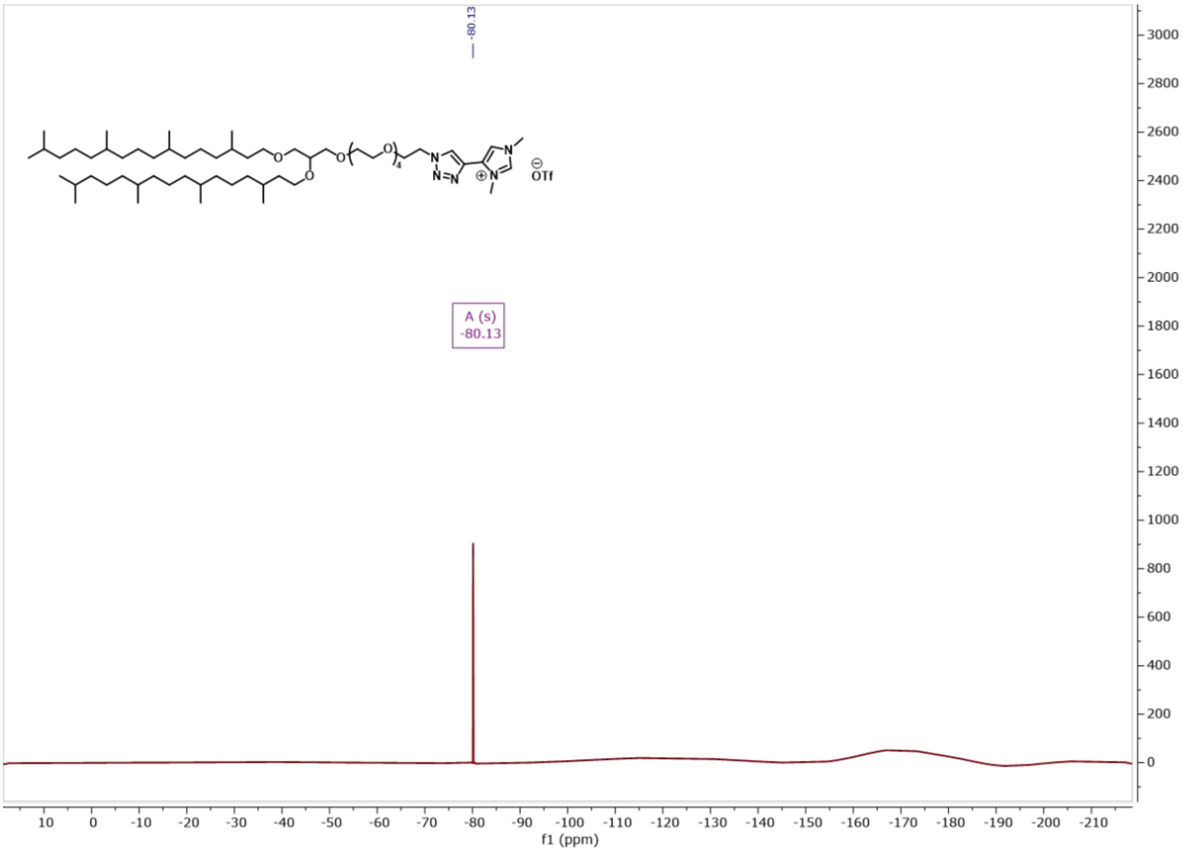

Supplementary Figure 32: ^{19}F-NMR of **IIIb**

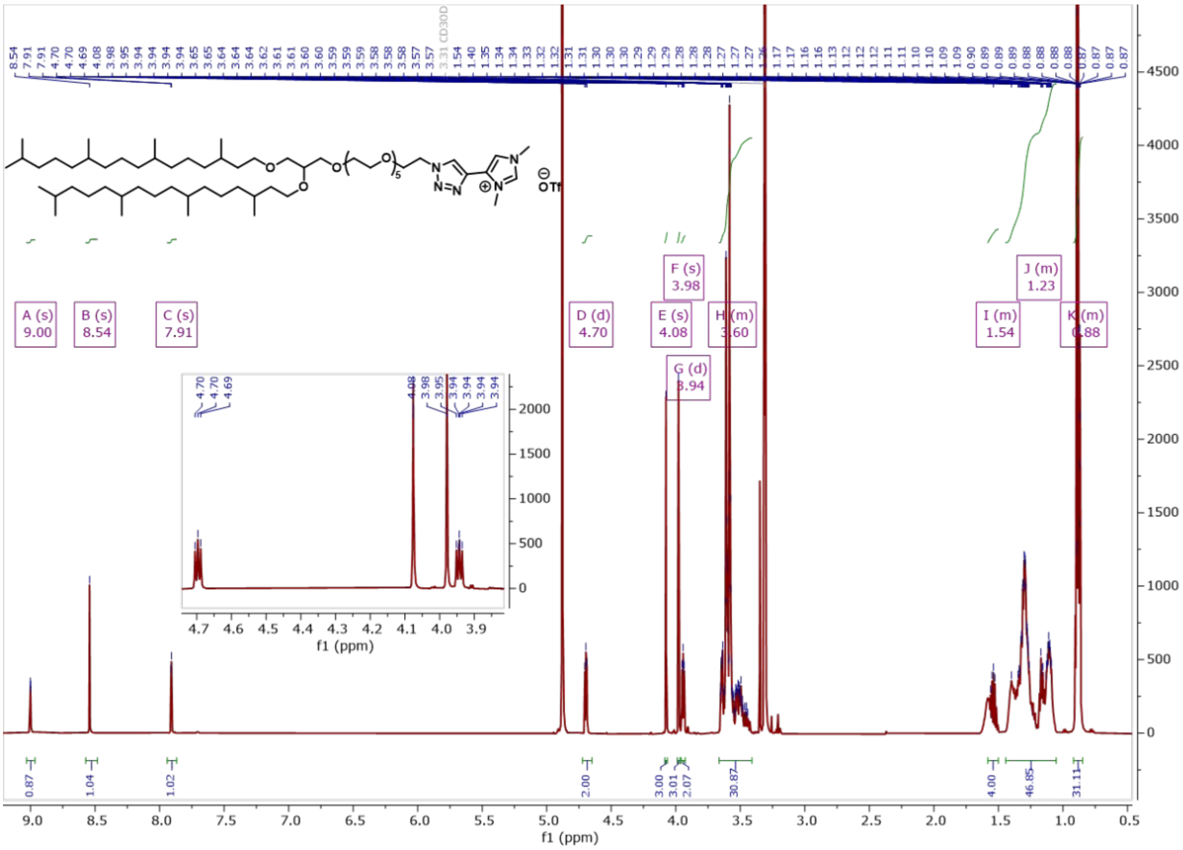

Supplementary Figure 33: ^{1}H-NMR of **IIIc**

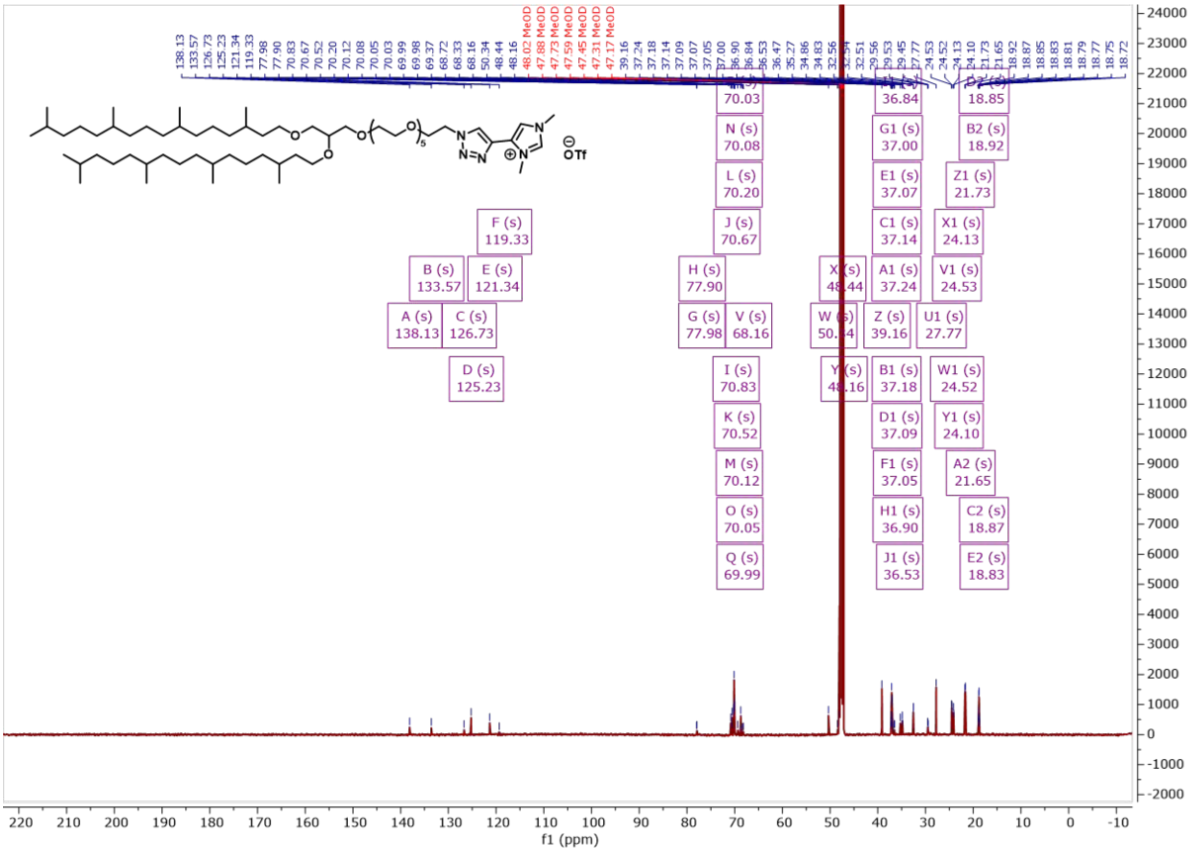

Supplementary Figure 34: ^{13}C-NMR of **IIIc**

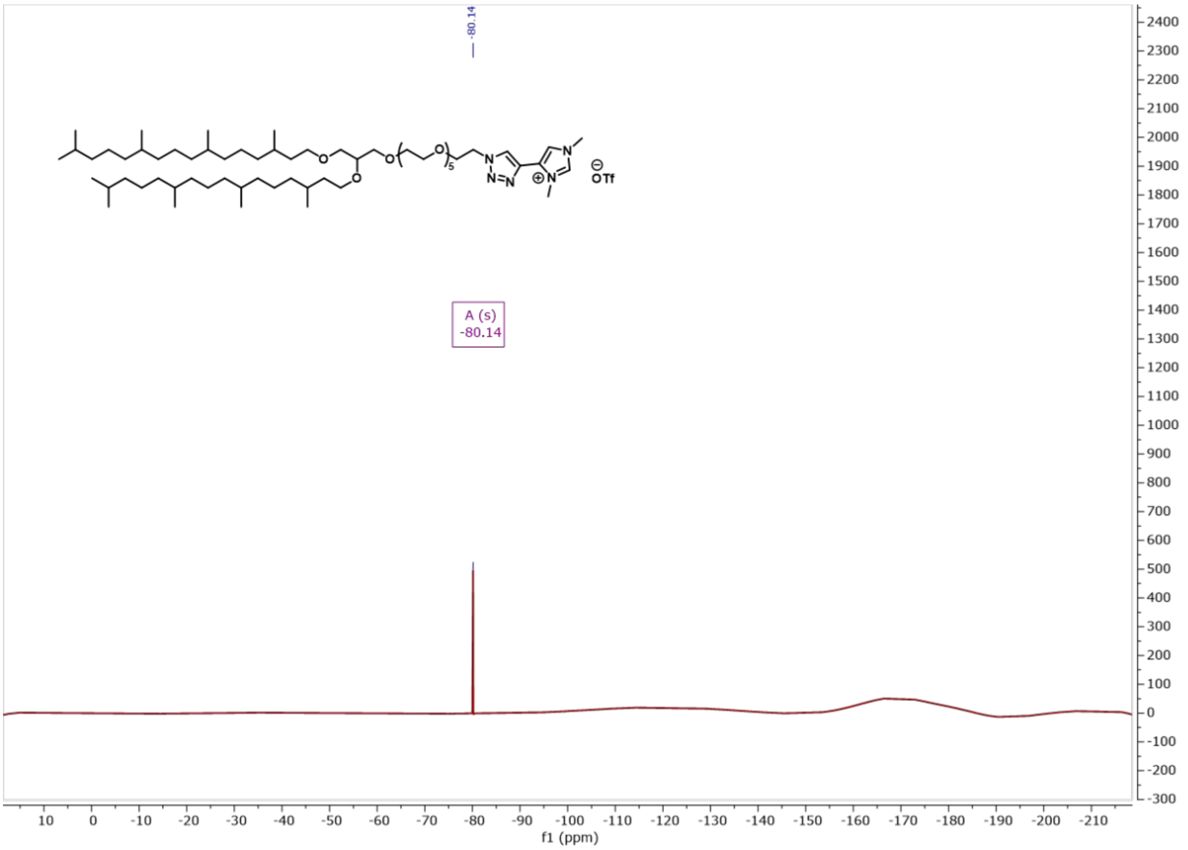

Supplementary Figure 35: ^{19}F-NMR of **IIIc**

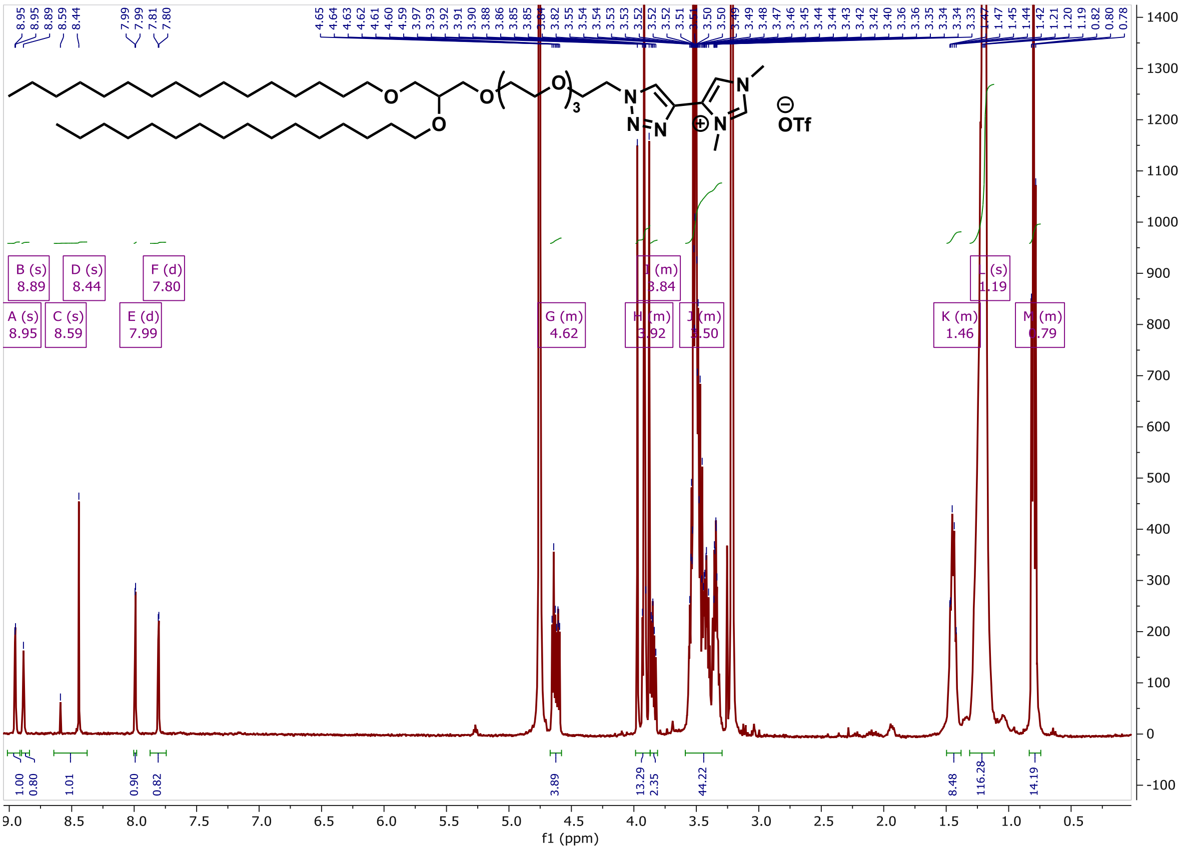

Supplementary Figure 36: ^{1}H-NMR of **VIa**

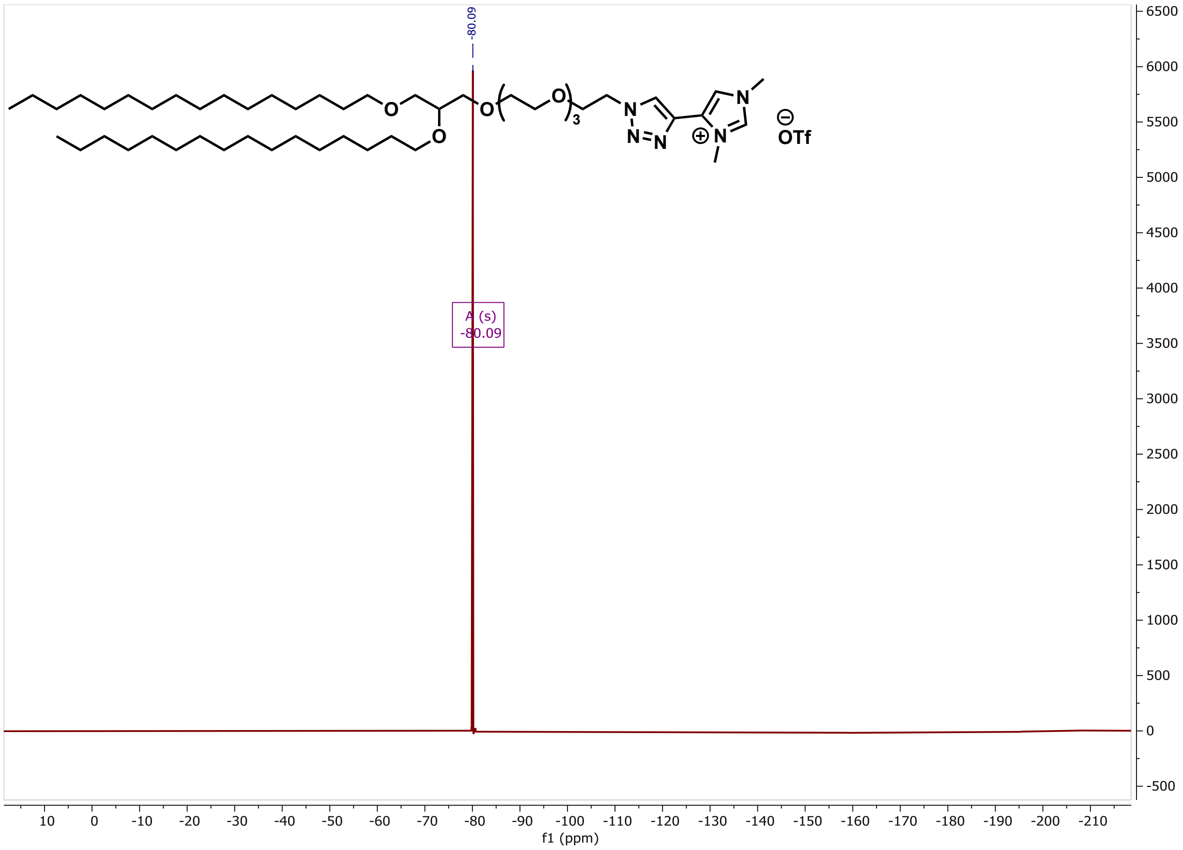

Supplementary Figure 37: ^{19}F-NMR of **VIa**

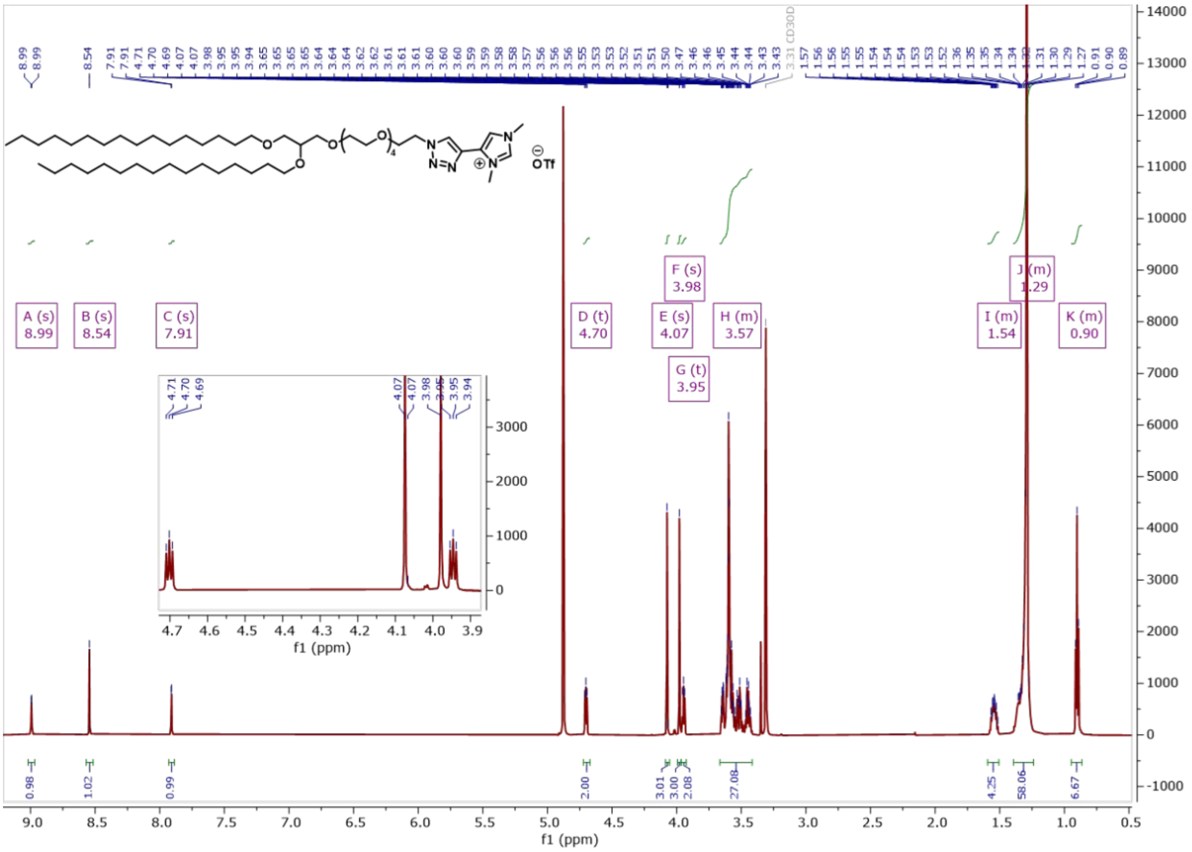

Supplementary Figure 38: ^{1}H-NMR of **VIb**

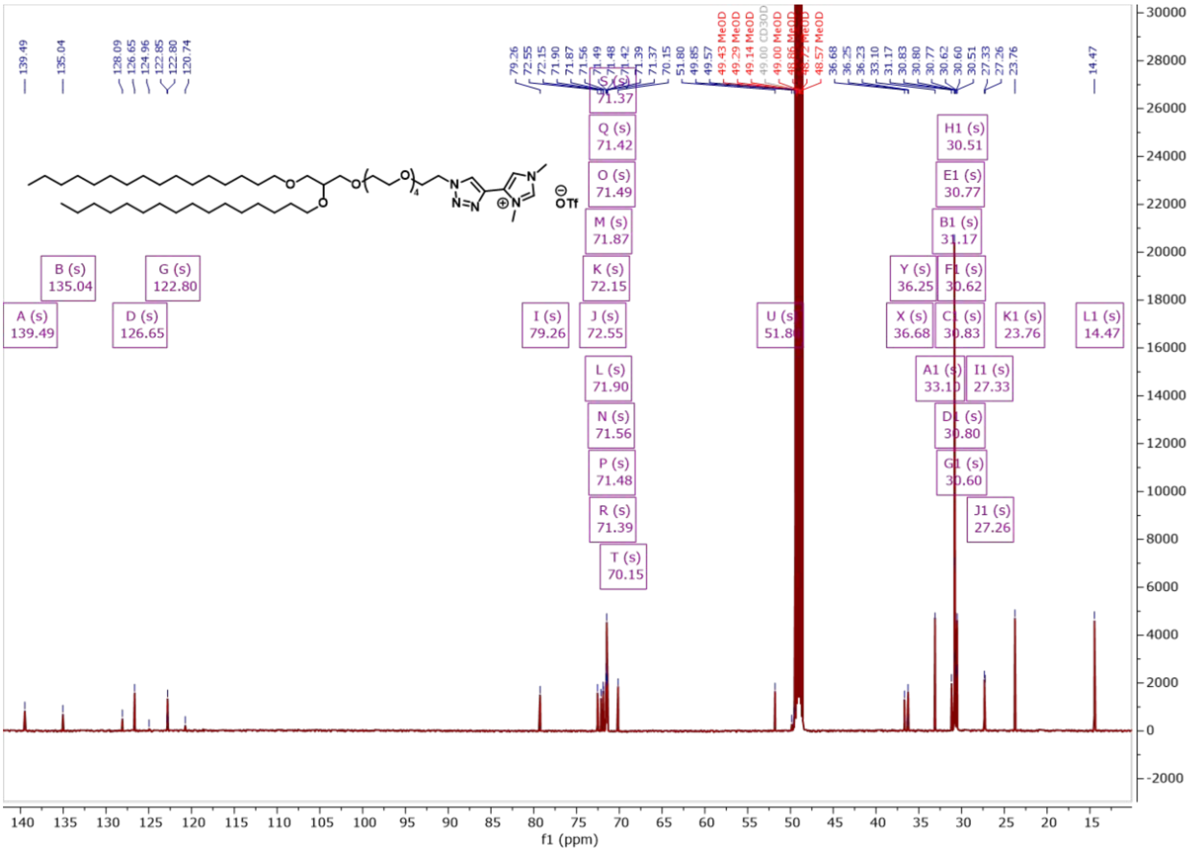

Supplementary Figure 39: ^{13}C-NMR of **VIb**

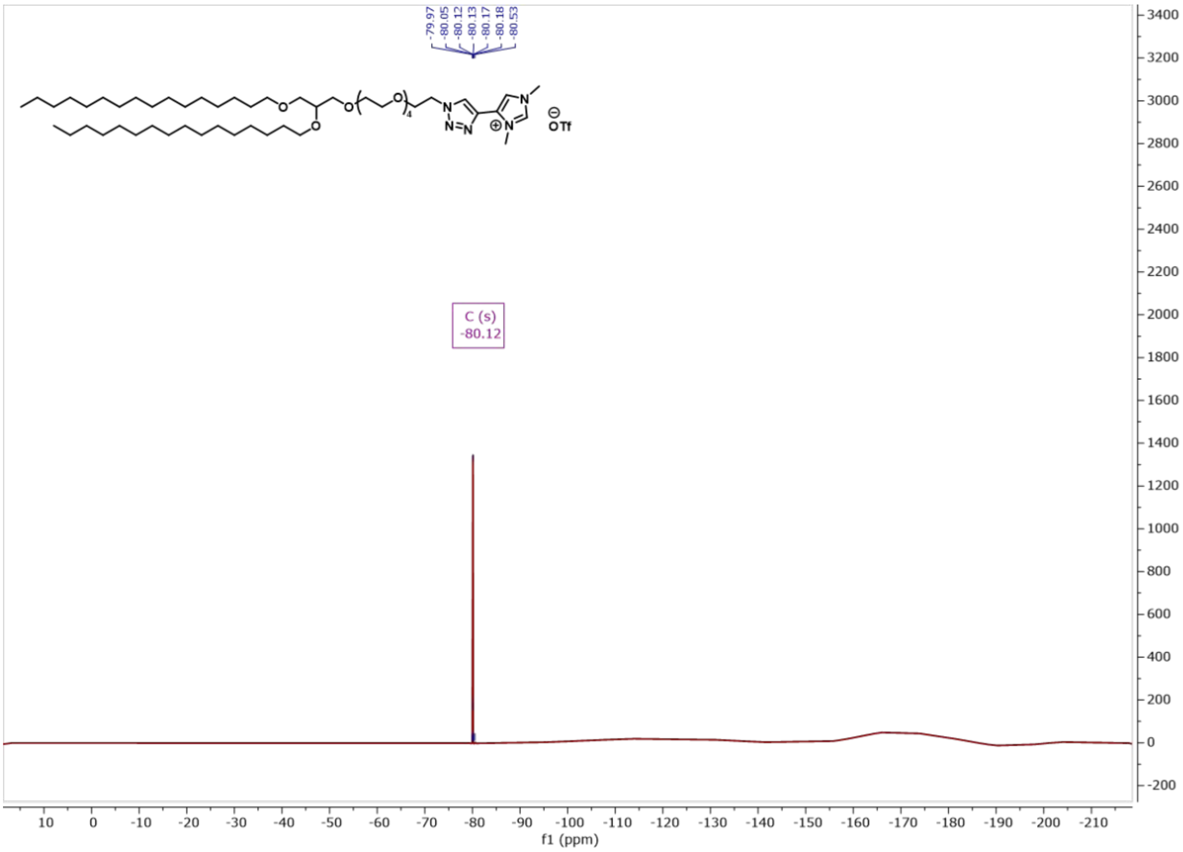

Supplementary Figure 40: ^{19}F-NMR of **VIb**

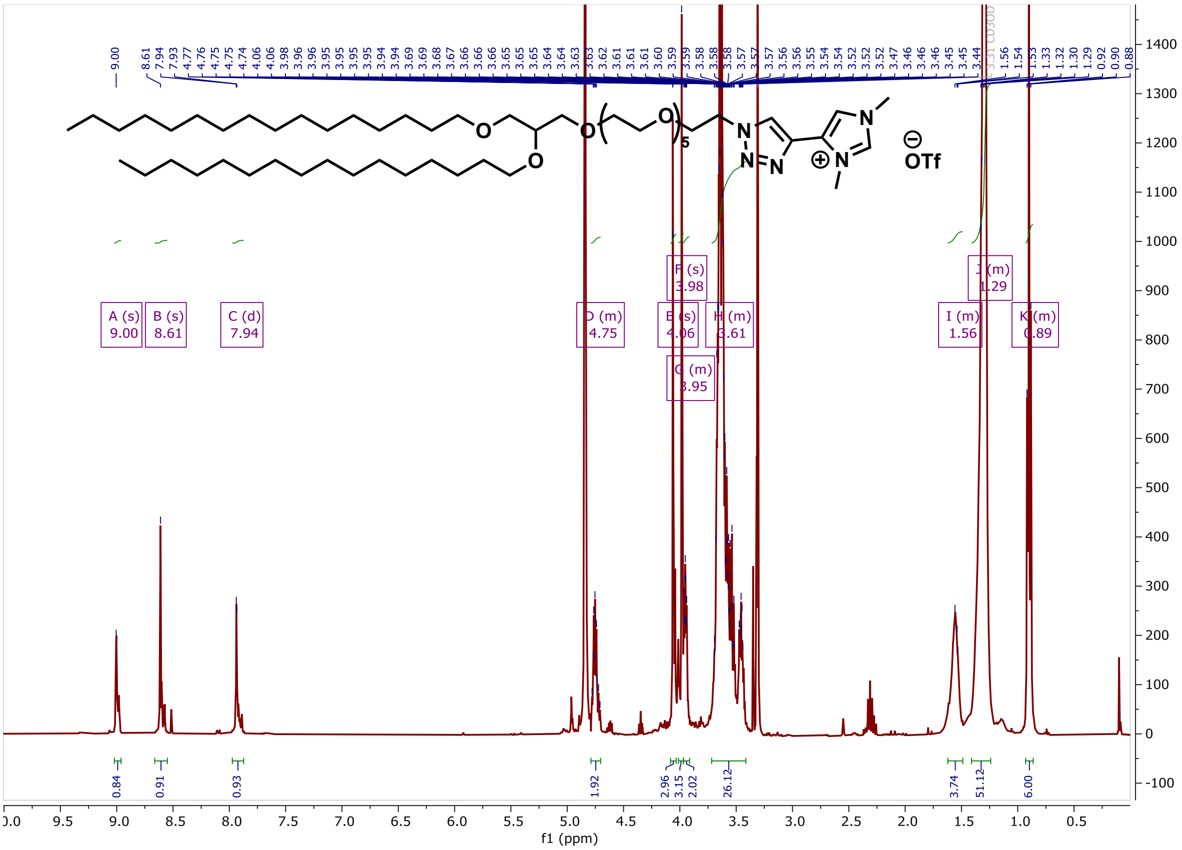

Supplementary Figure 41: ^{1}H-NMR of **VIc**

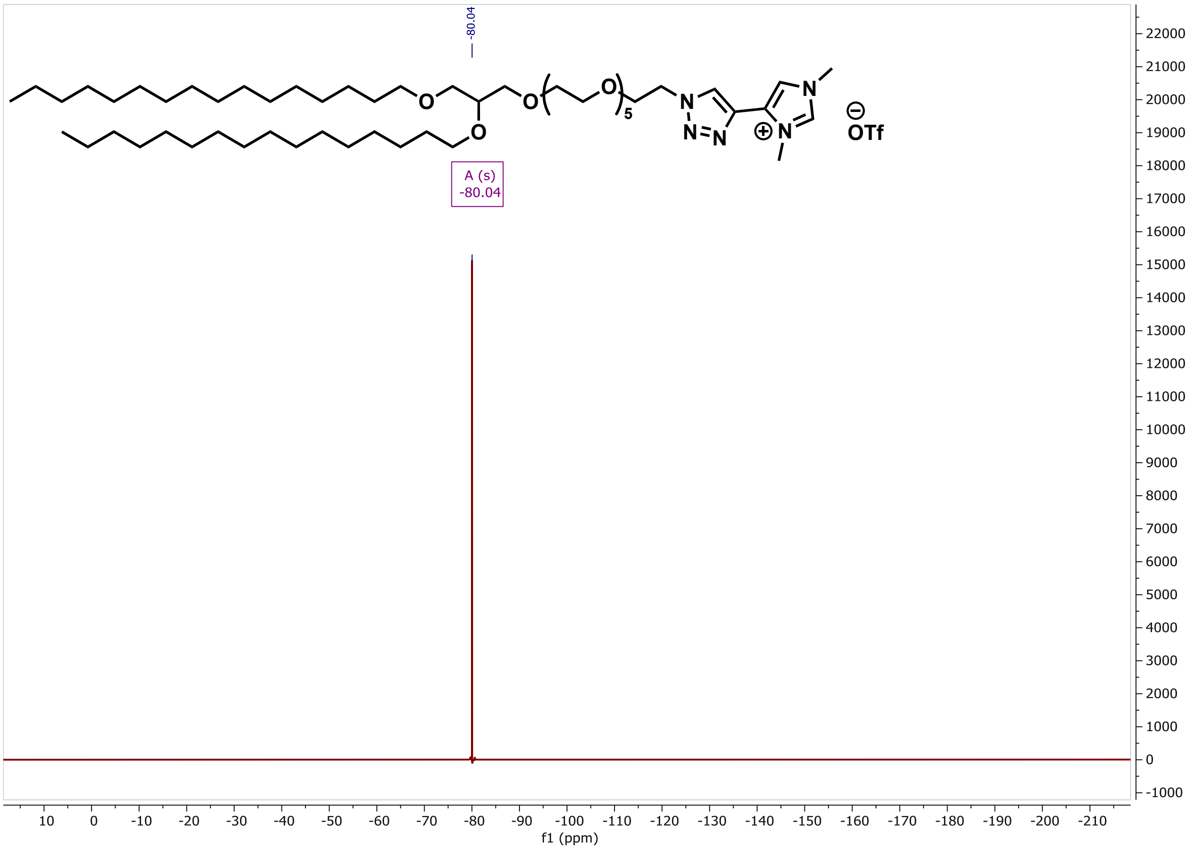

Supplementary Figure 42: ^{19}F-NMR of **Vic**

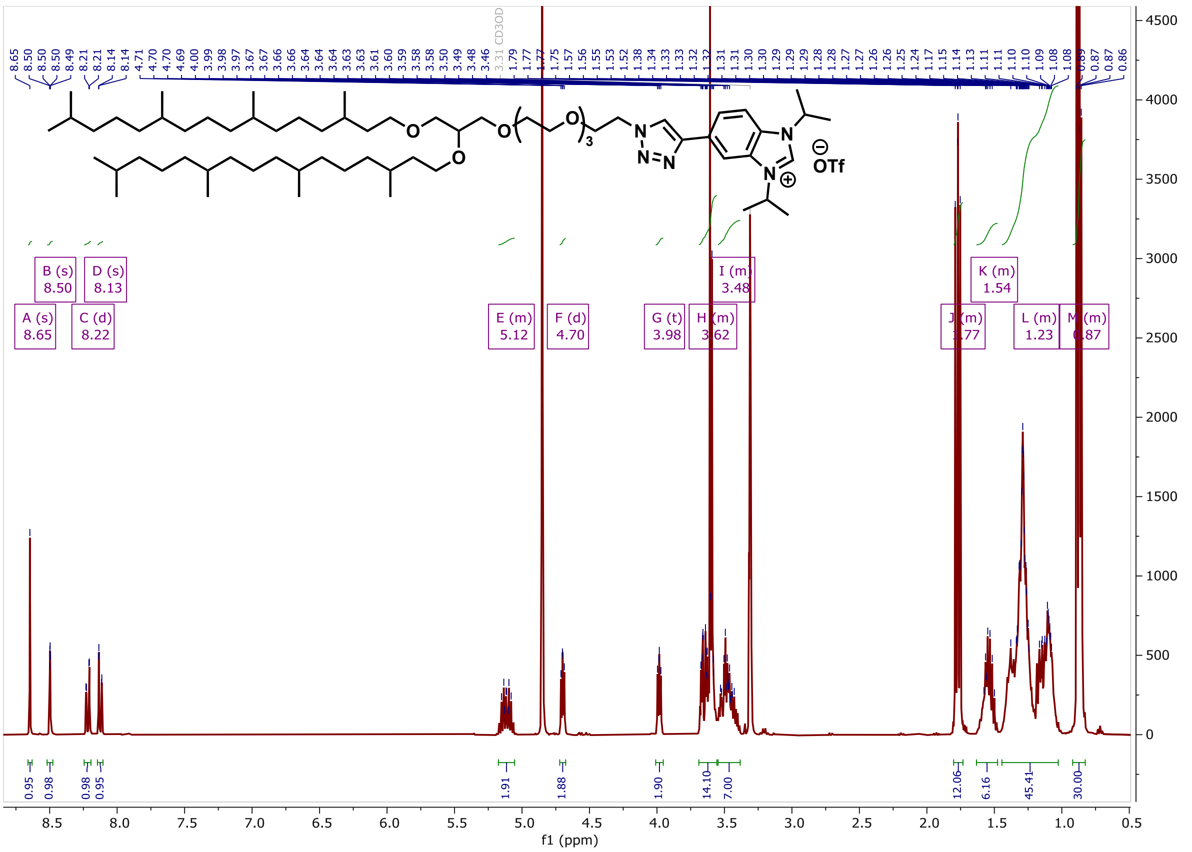

Supplementary Figure 43: ^{1}H-NMR of **XIIa**

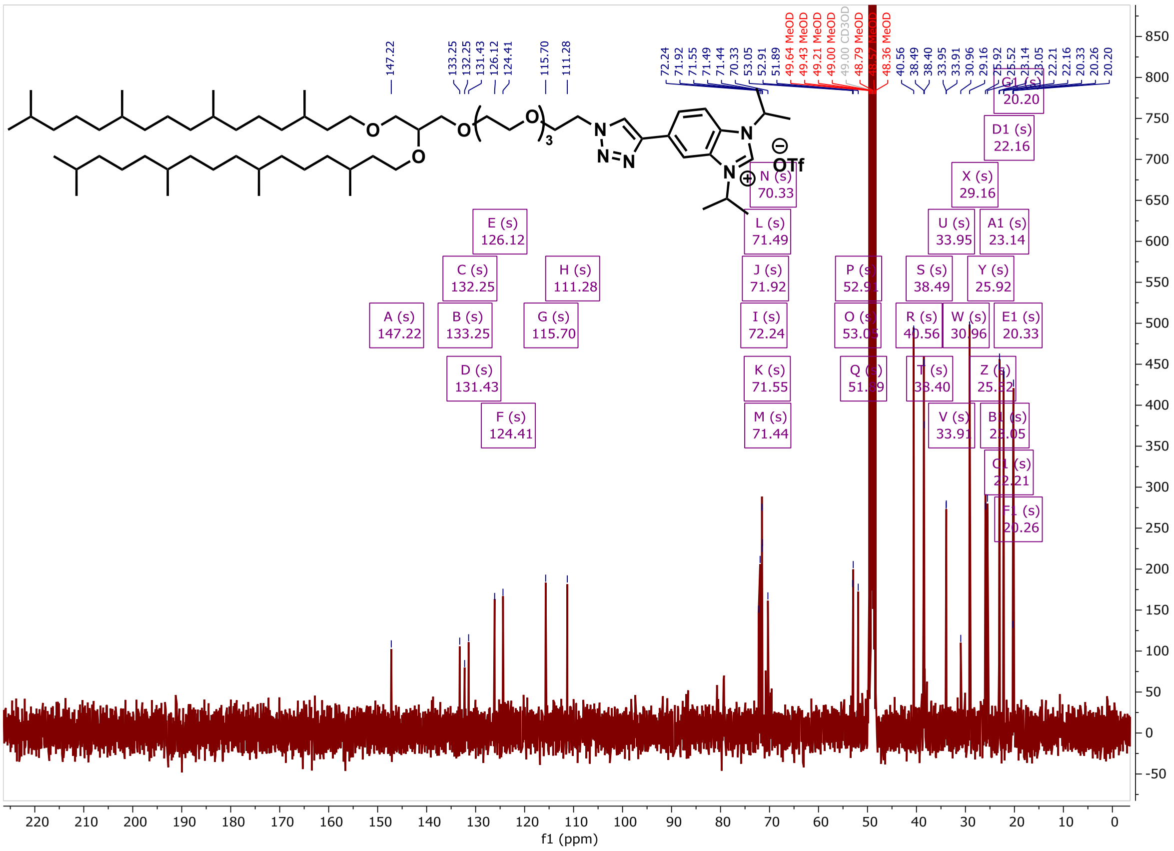

Supplementary Figure 44: ^{13}C-NMR of **XIIa**

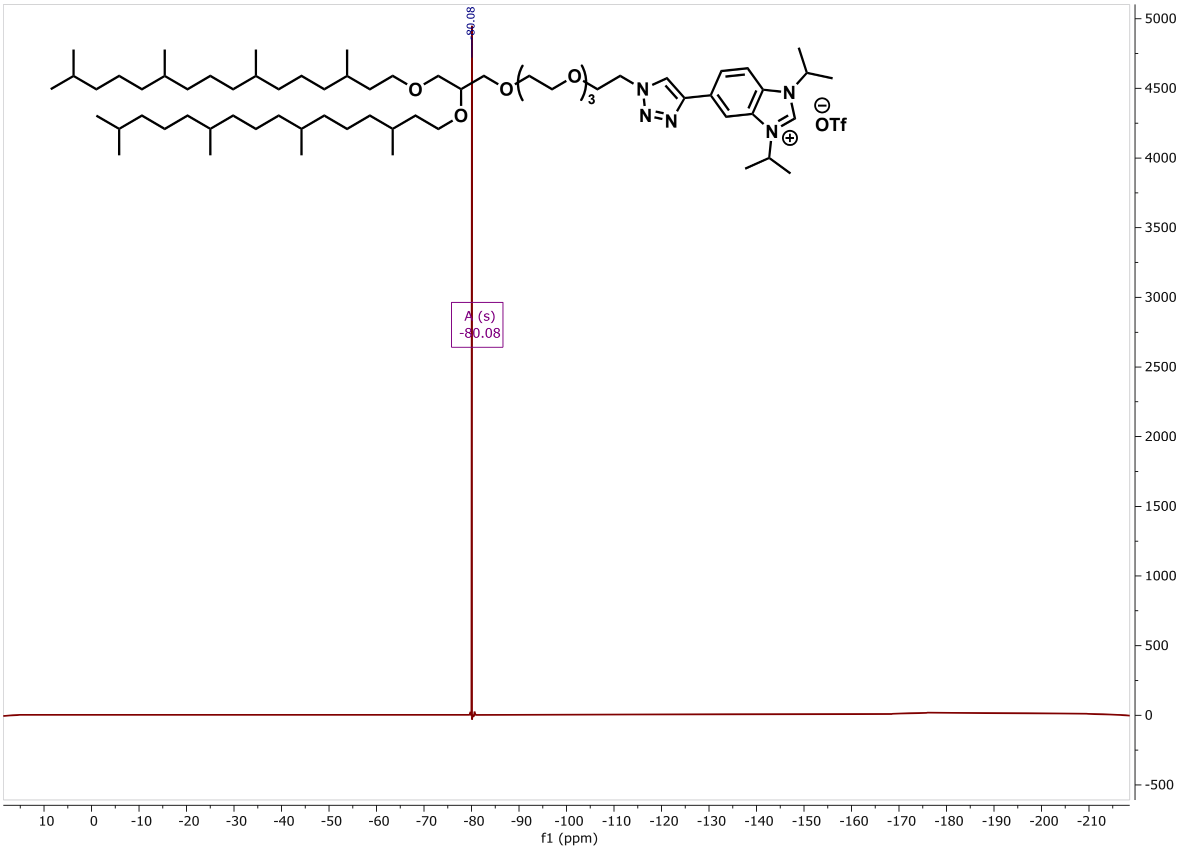

Supplementary Figure 45: ^{19}F-NMR of **XIIa**

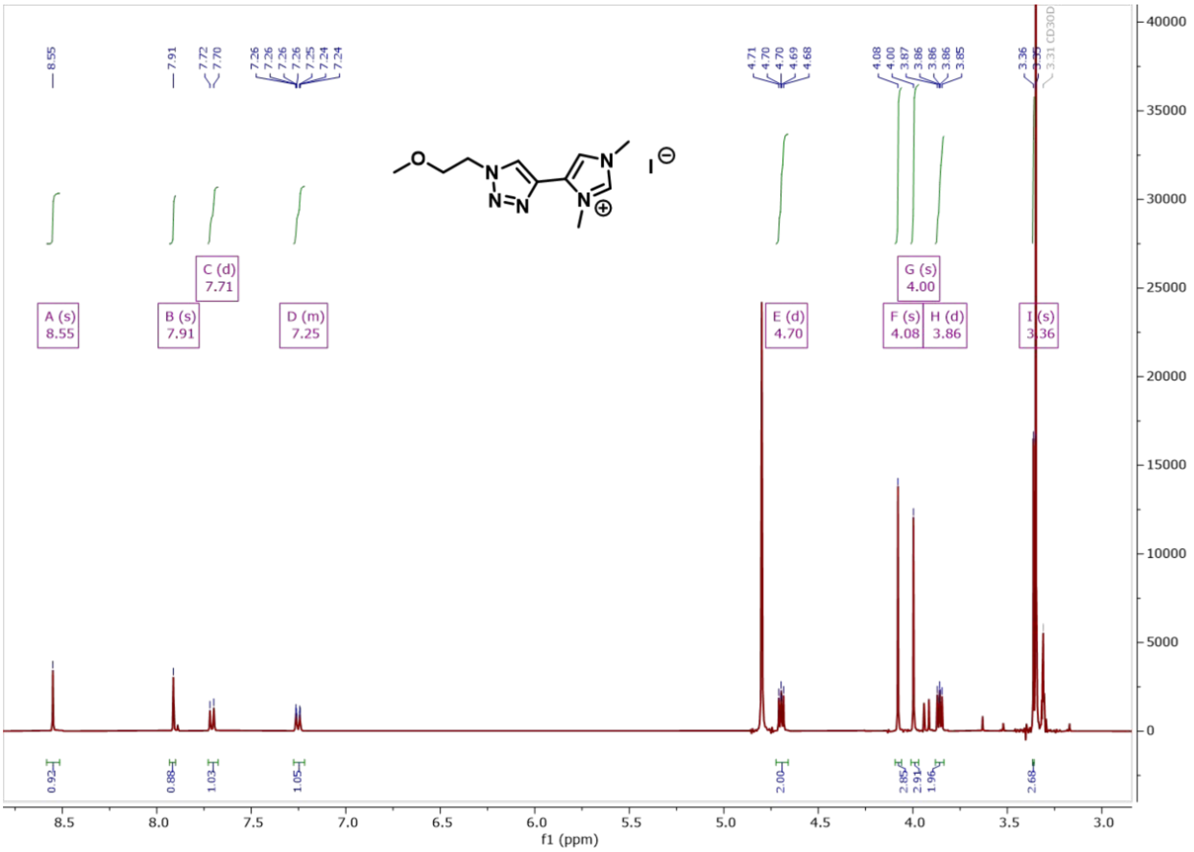

Supplementary Figure 46: ^{1}H-NMR of **XIII**

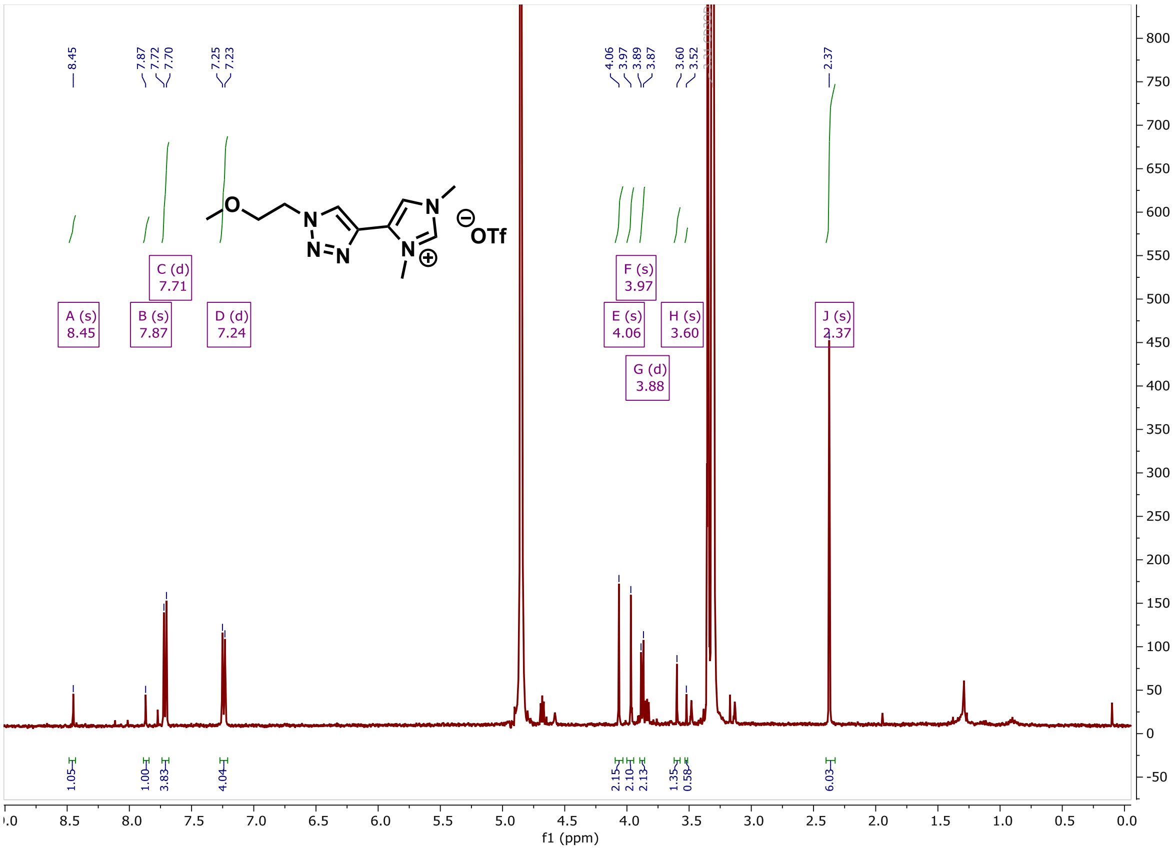

Supplementary Figure 47: ^{1}H-NMR **XIV**

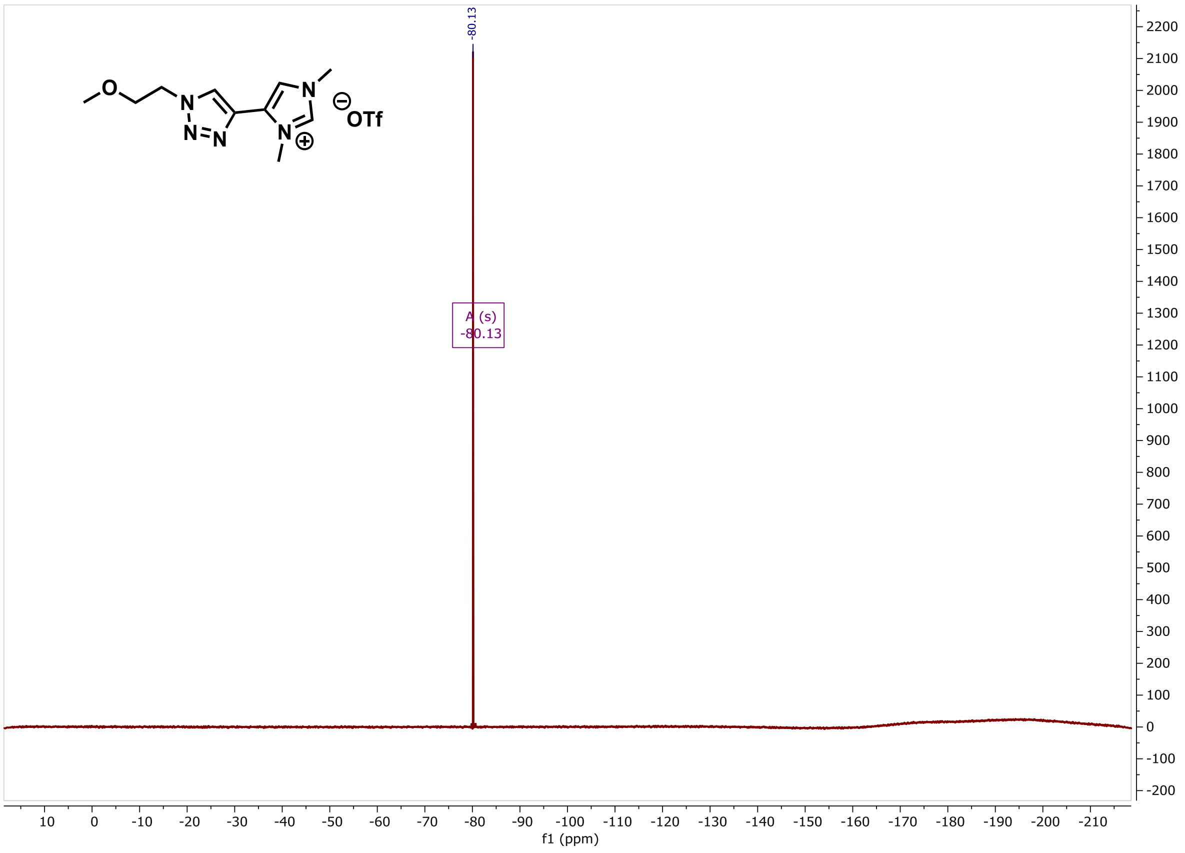

Supplementary Figure 48: ^{19}F-NMR of **XIV**

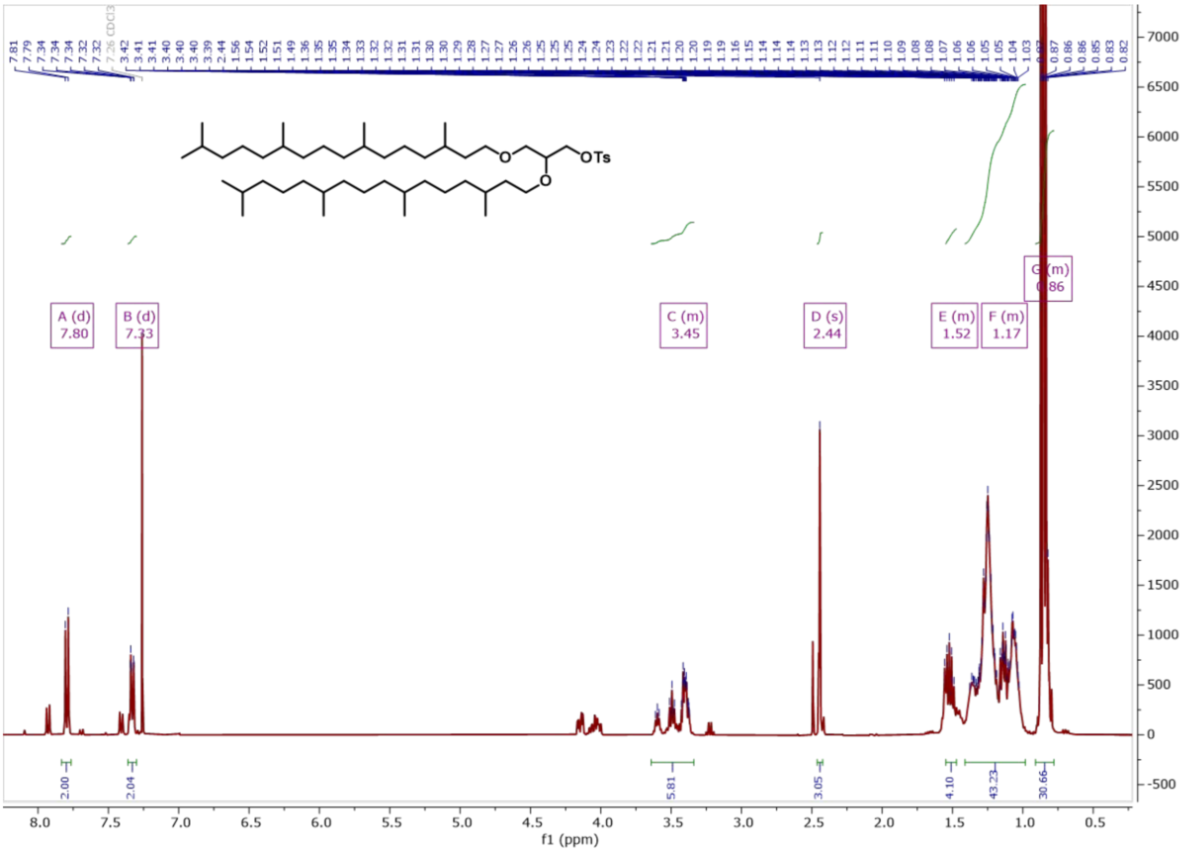

Supplementary Figure 49: ^{1}H-NMR of **20**

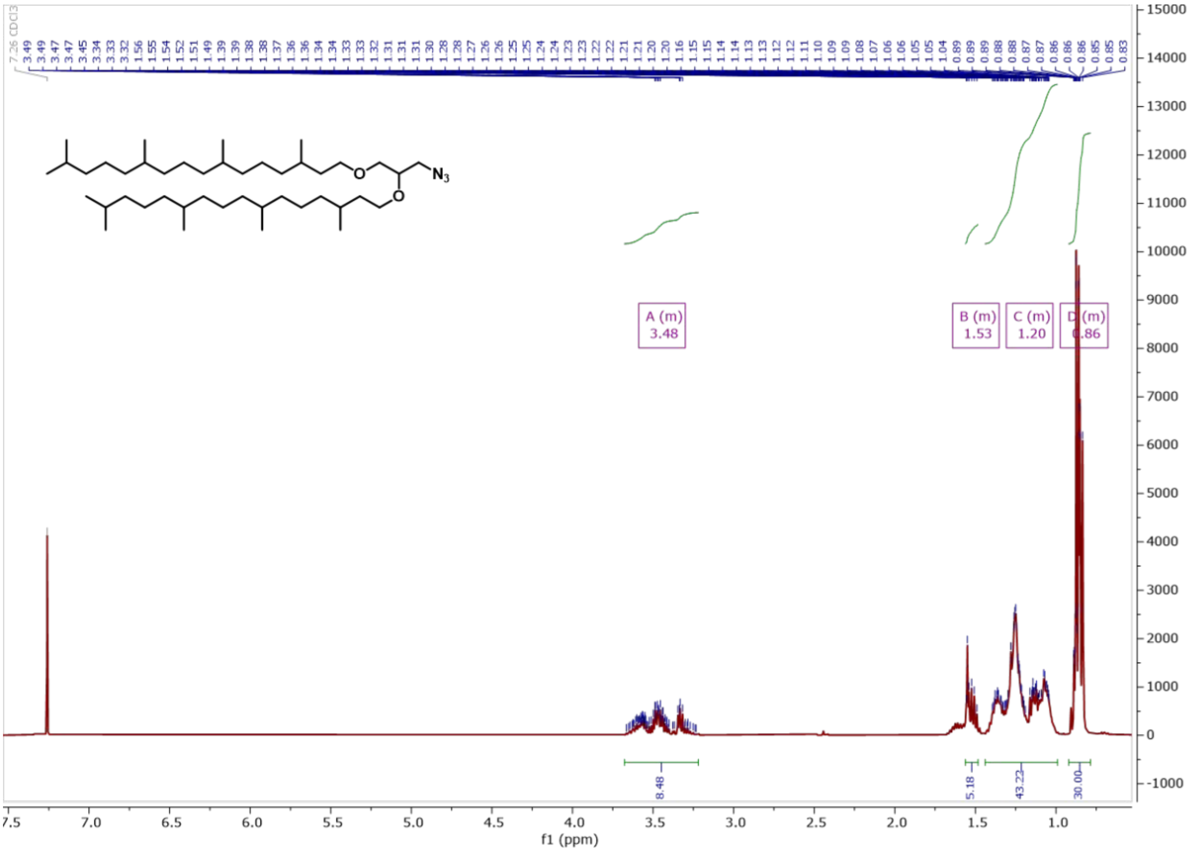

Supplementary Figure 50: ^{1}H-NMR of **21**

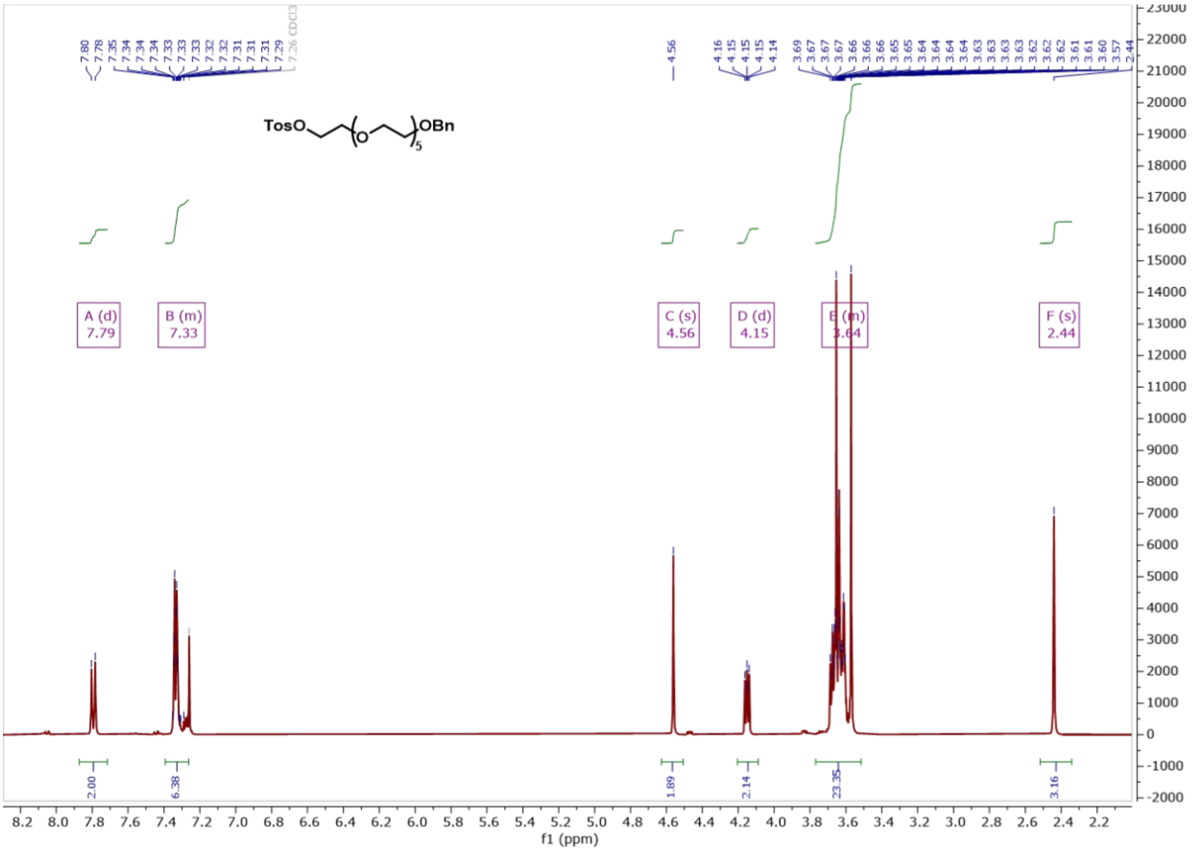

Supplementary Figure 51: ^{1}H-NMR of **13a**

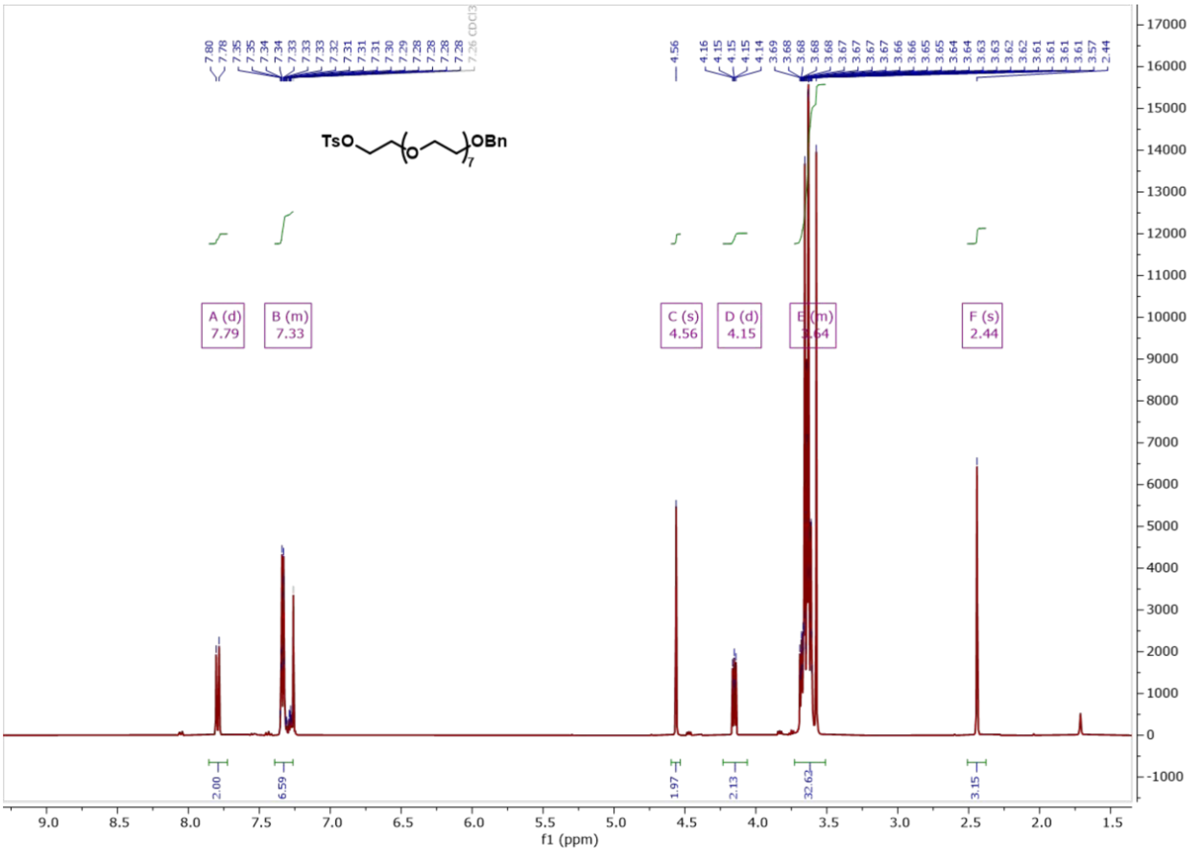

Supplementary Figure 52: ¹H-NMR of **13b**

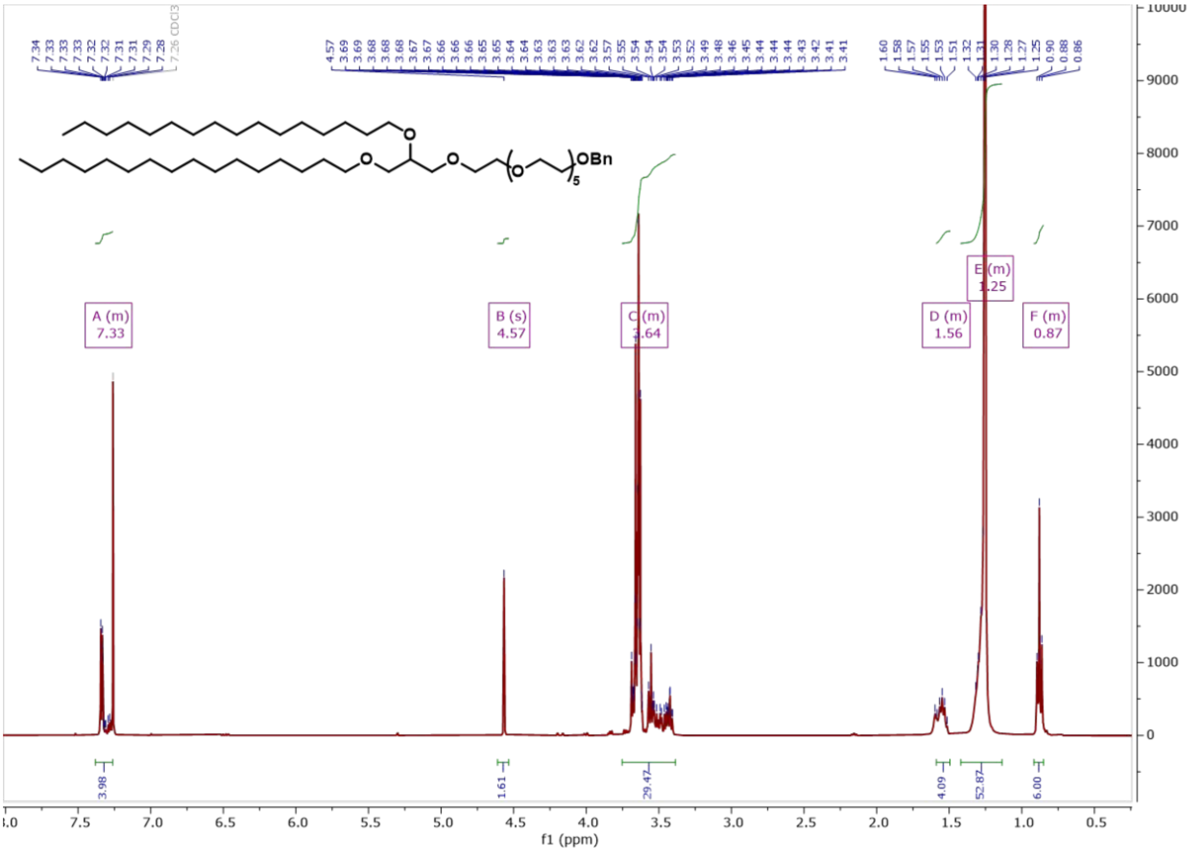

Supplementary Figure 53: ¹H-NMR of **VIIa**

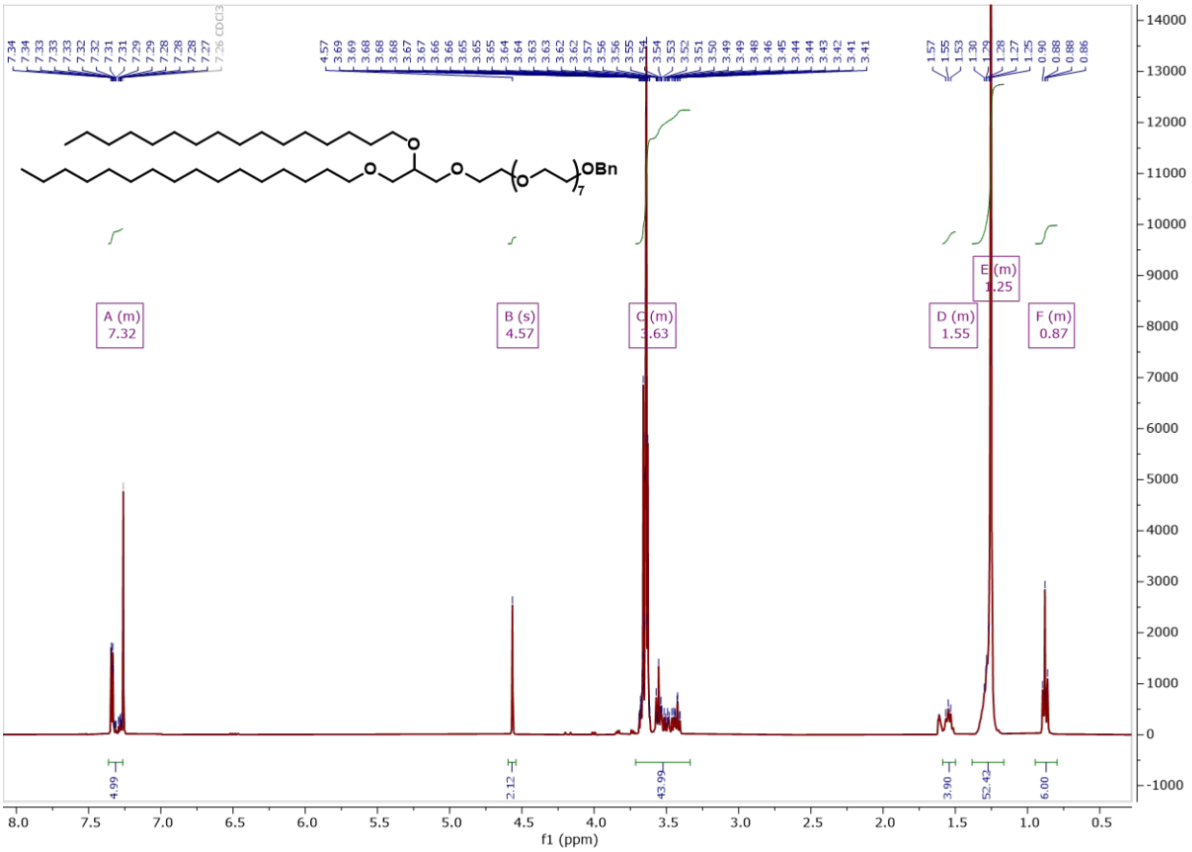

Supplementary Figure 54: ^{1}H-NMR of **VIIb**

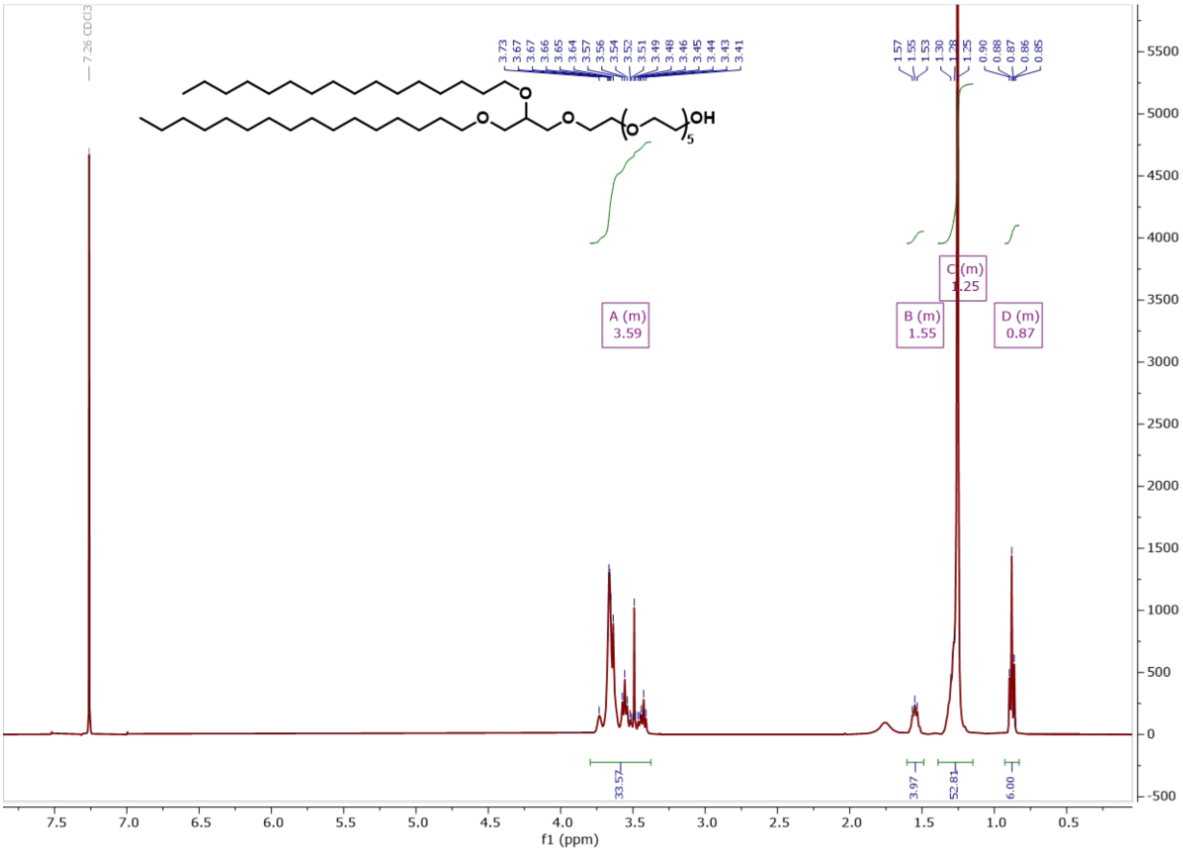

Supplementary Figure 55: ^{1}H-NMR of **VIIIa**

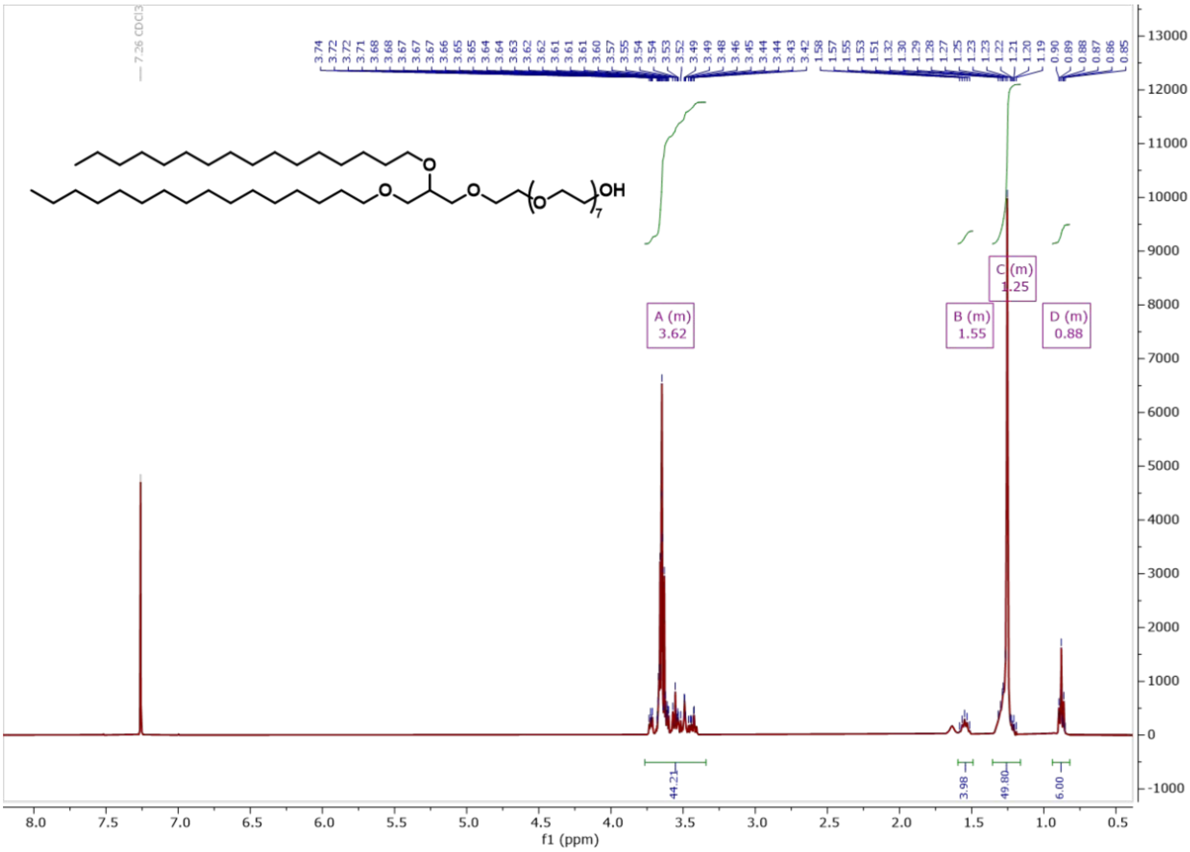

Supplementary Figure 56: ^{1}H-NMR of **VIIIb**

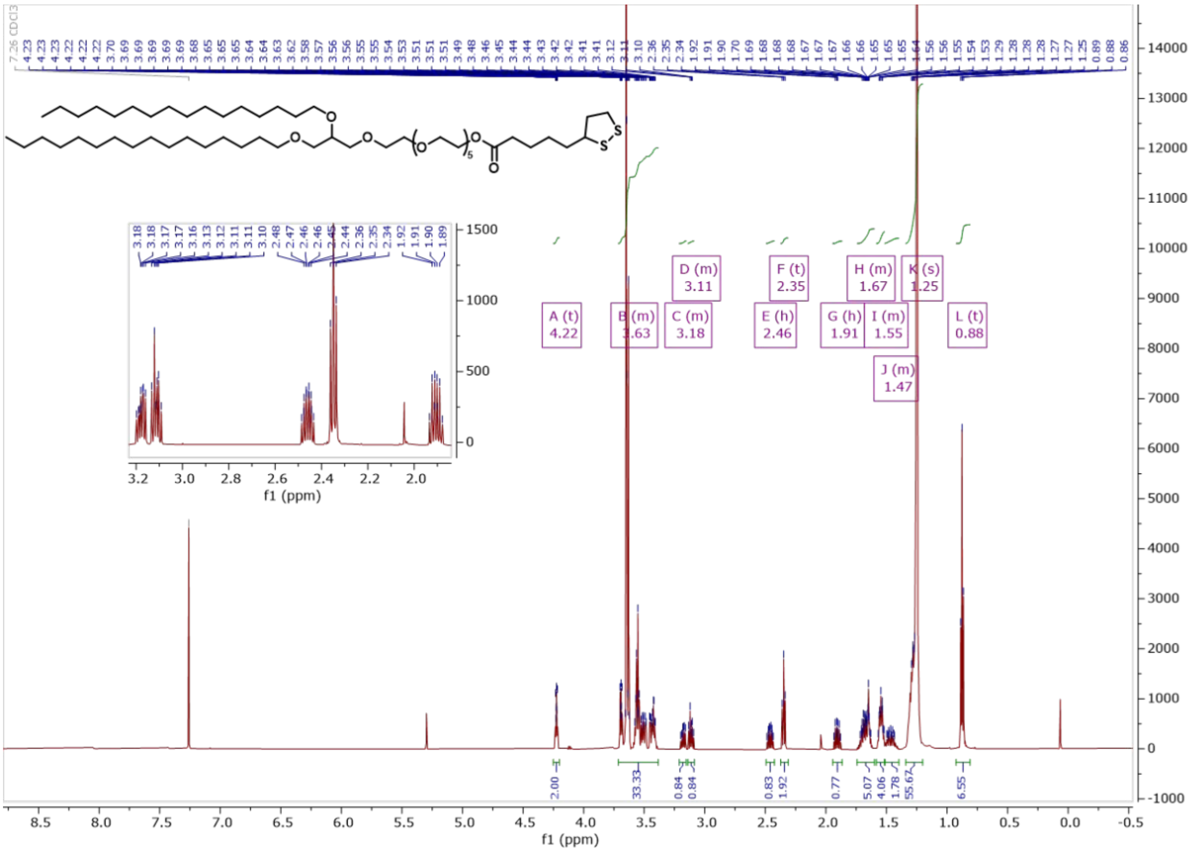

Supplementary Figure 57: ^{1}H-NMR of **IXa**

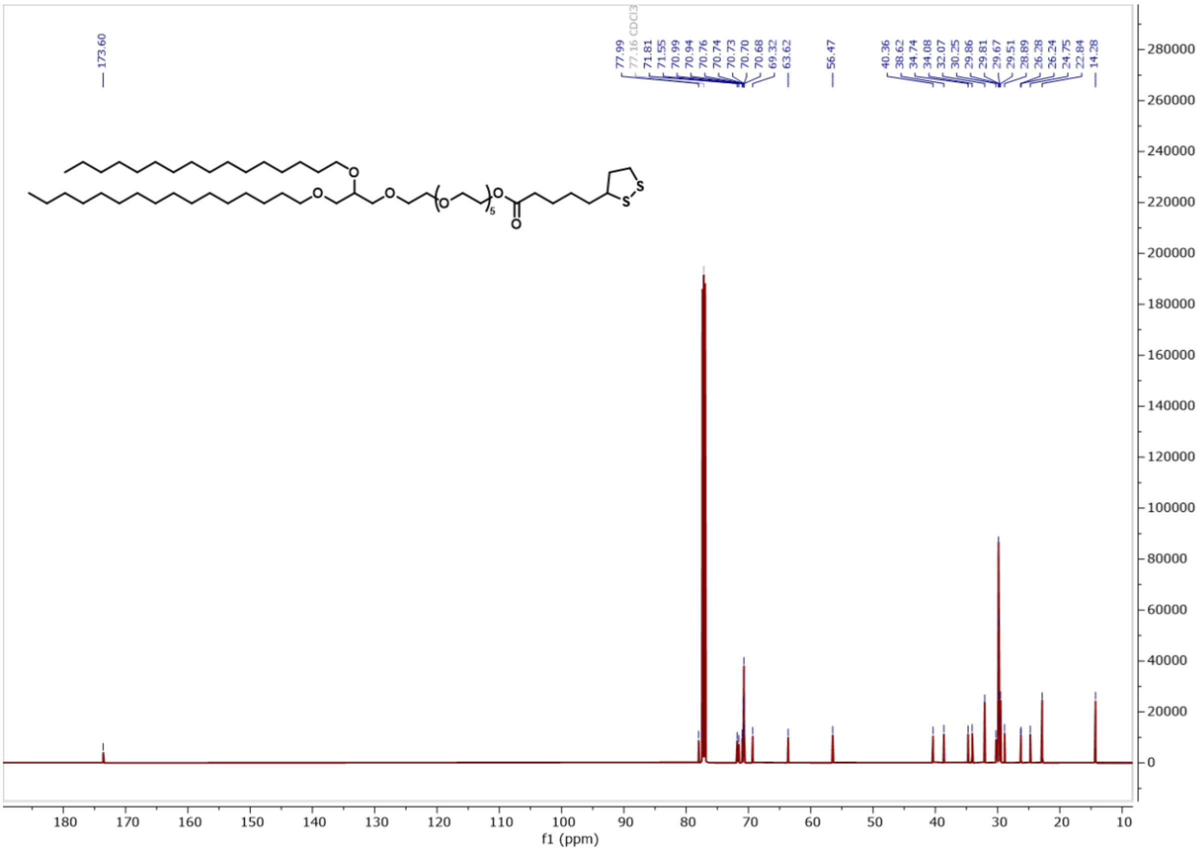

Supplementary Figure 58: ^{13}C-NMR of **IXa**

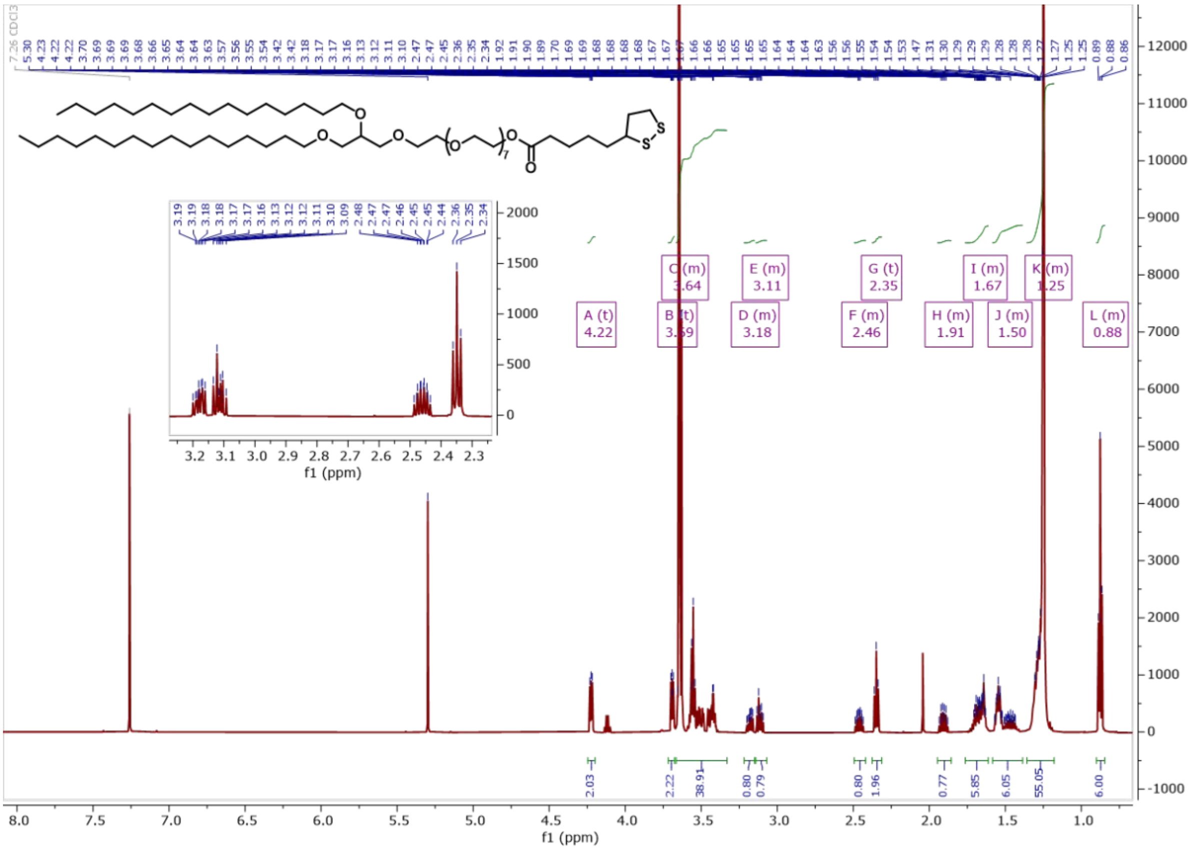

Supplementary Figure 59: ^{1}H-NMR of **IXb**

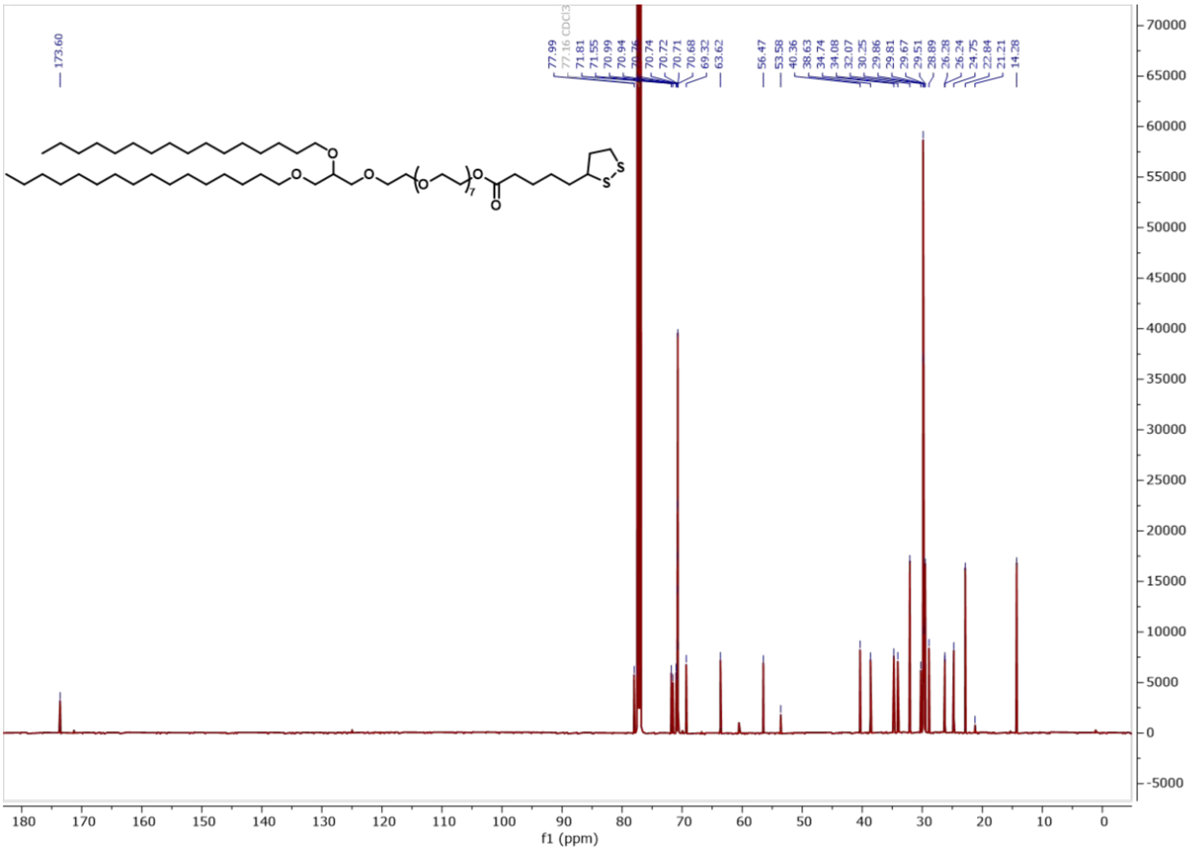

Supplementary Figure 60: ^{13}C-NMR of **IXb**